SUB-SURFACE MIGRATION OF AN OIL POLLUTANT INTO AQUIFERS.

By

LOUISE ANN MACDONALD

A thesis submitted to the University of Plymouth in partial fulfilment for the degree of

DOCTOR OF PHILOSOPHY

Department of Environmental Science
Faculty of Science

Funded by

Plymouth Environmental Research Centre (PERC)

and

The National Grid Company plc (NGC)

February 2000

Abstract

SUB-SURFACE MIGRATION OF AN OIL POLLUTANT INTO AQUIFERS.

Louise Ann MacDonald

The risk to groundwater quality following a sub-surface spillage of immiscible pollutants such as oil, petroleum and other organic chemicals is an increasingly potent threat, through escalating industrial application of such pollutants.

This study significantly enhances the understanding of the flow of immiscible pollutants within soil, through field scale investigations to define the spatial variability and extent of a contaminated area and the development of a comprehensive framework for the analysis of oil pollutant migration. This study represents a first attempt by researchers to analyse oil pollutant migration on a wide range of scales, from pore- to field-level.

The research shows that quantity of pollutant is a critical factor in determining the extent of oil migration. Permeability and porosity of the sample material are also important secondary factors. High permeability assists the migration of oil pollutants. Soils with a high porosity allow the pollutant to migrate vertically under the influence of gravity, whereas soils with low porosity induce lateral oil migration, as the oil spreads from the point of injection. A full scale field study using contrasting soil types determines that oil migration is approximately symmetrical about the point of injection.

Experimental data is used to establish modelling capabilities for the characterisation of pollutant migration. Modelling is undertaken at two levels. The first consists of the development of simple Gaussian equations based upon observations of oil glomuses. The glomus approach, newly developed in this work, can be compared to a fractal model, with the glomuses observed in each of the different scales studied.

The second stage involves the use of Pore-Cor to determine the pore scale movement of pollutants. This suggests that during the early stages of pollutant migration, oil is often located in larger stagnant pores, enabling smaller pores to continue to carry water. Consequently there is little impact on permeability. Where greater concentration occurs, oil contaminates both larger and smaller pores, reducing permeability significantly. In addition, Pore-Cor also realistically reproduces the capillary fingering of oil.

Contents

List of Figures

List of Tables

Acknowledgements

I would like to thank my supervisors, Dr Peter Matthews and Dr Dax Patel for their support and encouragement throughout this project.

I would also like to acknowledge the assistance of all of the University's staff who have aided me in this work and those at the University of Cranfield and BHR Group where much of the field analysis for this study was conducted.

Thank you to my post-graduate colleagues in the department especially Cathy, Toby, Darren, Paul and Anthony. I would also like to thank Yolande for all her help, particularly during my time at Cranfield.

Finally, I would like to say thank you very much to Neil for all his inspiration and to my parents without whom, none of this would have been possible.

Author's Declaration

At no time during the registration for the degree of Doctor of Philosophy has the author been registered for any other University award.

This study was financed with the aid of a studentship from the Plymouth Environmental Research Council and funding from the National Grid Company plc.

Seminars and conferences were attended throughout the period of study at which work was regularly presented. Consultation with other institutions and industrial contacts took place and several publications have been prepared.

Signed.LAMacDonald.....

Louise A. MacDonald, February 2000

Publications

The following papers are in the process of being prepared for publication:

MacDonald, L. A., Matthews, G. P., and Patel, D. (1999a), Metre-Scale Migration of Cable Oil in Sand and Soil, *Water Resources Research*, **in preparation**, pp

MacDonald, L. A., Matthews, G. P., and Patel, D. (1999b), Migration of Cable Oil in a Half-Metre Scale Grid Lysimeter, *European Journal of Soil Science*, **in preparation**, pp

MacDonald, L. A., Matthews, G. P., and Patel, D. (1999c), Simulation of Cable Oil Migration in Sand and Soil Using a Three-Dimensional Network, *European Journal of Soil Science*, **in preparation**, pp

MacDonald, L. A., Matthews, G. P., Patel, D., and Rowland, S. J. (1999d), *Analysis and Migration of Cable Oil in Sand Columns*, Environmental Technology, ***to be submitted, pp***

Conferences, Presentations and Training

Characterisation Of Porous Solids IV Conference, September 1996, University of Bath – Attended

Geo Fluids II Conference, March 1997, Waterfront Centre, Belfast – Attended

Environmental Technology Conference, September 1997, Manchester - Presented poster

National Grid Update, October 1997, Kelvin House, Leatherhead - Presentation

NERC Environmental Diagnostics Conference, January 1998, The Great Western Hotel, London – Presented two posters

Environmental Technology Conference, June 1998, National Exhibition Centre, Birmingham – Presented Poster

New Analytical Technology & Biotechnology Conference, September 1998, SCI, London - Attended.

National Grid Update, November 1998, Kelvin House, Leatherhead - Presentation

NERC Environmental Diagnostics, January 1999, London – Attended.

1. Introduction

1.1 Overview

The ability to make reliable predictions of the multiphase flow of hydrocarbon fluids in natural underground reservoirs has long been the subject of intense research and development activity in the oil industry. More recently, as a result of the widespread use of oil, petroleum and other industrial organic chemicals, contamination of groundwater reservoirs has drawn the attention of hydrologists to the analysis of such flow problems. Their interest is motivated by the need to evaluate the risk to groundwater quality following a subsurface spill, (Butts and Jensen, 1996). To ensure the continued supply of potable groundwater, scientists and engineers must strive to understand the processes that lead to groundwater contamination and develop methods to remediate existing problems, (Thomson et al., 1992).

The physical principles of solute transport in porous media are fairly well established, (Porter, 1968a). Often the source of contamination is an immiscible liquid (a liquid that can not be mixed with water) located beneath the ground surface. The solubilities of these often very toxic compounds are low, but non-zero. Once in the soil they may provide a long-term supply of contamination to local groundwater and infiltrating rainfall, (Thomson et al., 1992).

Much work has been performed on the properties of non-aqueous phase liquids by the petroleum industry. The flow characteristics of hydrocarbons in porous media such as sandstone are well understood. Much less is known about the flow of hydrocarbons, as pollutants, within soil. Consequently much research in this area is still required. Such research includes being able to define the spatial variability and extent of a contaminated area, thus producing better predictive capabilities. These predictive capabilities are

required to assist in the pollutant migration risk assessment, and implementation of remediation techniques. This thesis goes some way to addressing these issues.

1.2 Timeliness of this Project

The current state of knowledge of sub-surface oil migration is reviewed later in this chapter. Further work in this area is timely for the following reasons:

(i) The increasingly stringent environmental legislation with regard to the possible contamination of aquifers by oil pollutants;

(ii) The availability at Plymouth of a half-meter scale precision lysimeter and rainfall simulator, and a newly developed software package called 'Pore-Cor' for the modelling of fluid behaviour in porous media;

(iii) The ready availability of very fast computers, with con-current development of powerful data-handling packages;

(iv) An interest in, and funding provision from, an end-user, namely the National Grid Company plc, who are interested in studying the effect of possible oil leaks in joint bays.

1.3 Applicability of the Project

The National Grid Company plc (NGC) owns and operates the high-voltage electricity transmission system in England and Wales. This system consists of both overhead power lines and underground power cables for the transmission of electricity at 275kV and 400kV. The 650km of underground cables in England and Wales mainly use a paper-oil insulation system. Layers of paper surround the copper conductor and are impregnated with 'cable oil', a term used for the mixture of dodecylbenzenes (DDB) and mineral oil, commonly termed either as DDB or cable oil. Cable oil is also contained within the central oil duct. Figure 1.1 shows a cross-section of a 275kV cable. Damage to the sheathing around the cable and/or failure at the joints could cause a leakage of the cable oil into the surrounding soil. Such damage requires excavation to make repairs and removal of the soil

containing the oil. The latter can be costly, particularly if the cable has to be taken out of service.

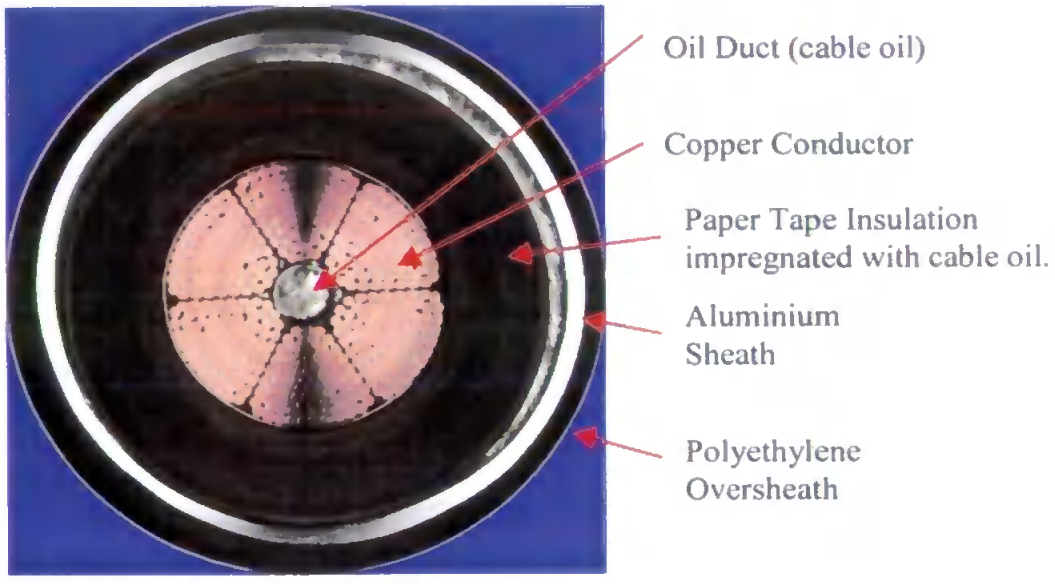

Figure 1.1 Cross-section through a 275kV Cable.

Although the cables are buried in the ground, they are subject to accidental damage by third parties or occasional joint failure due to ground movement, which can cause leakage of cable oil. The joints are situated in bays approximately 10m x 3m x 2m (34ft x 10ft x 6ft) in dimension, Figure 1.2.

The cables and joints are encompassed by a sand:cement backfill at a ratio of 20:1, (Cheston, 1997). This acts as a protective shield against some damage, whilst allowing adequate levels of thermal transmissivity, (Nichols, 1996). A concrete slab is placed into the bay below the cable that supports the joints, see Figure 1.3. The diagram shows a cross-section of cables R, Y and B carrying the three phases of the electricity supply. When a joint is located at the lowest point in the hydraulic gradient, accumulation of cable oil may occur, acting as a sub-surface point source.

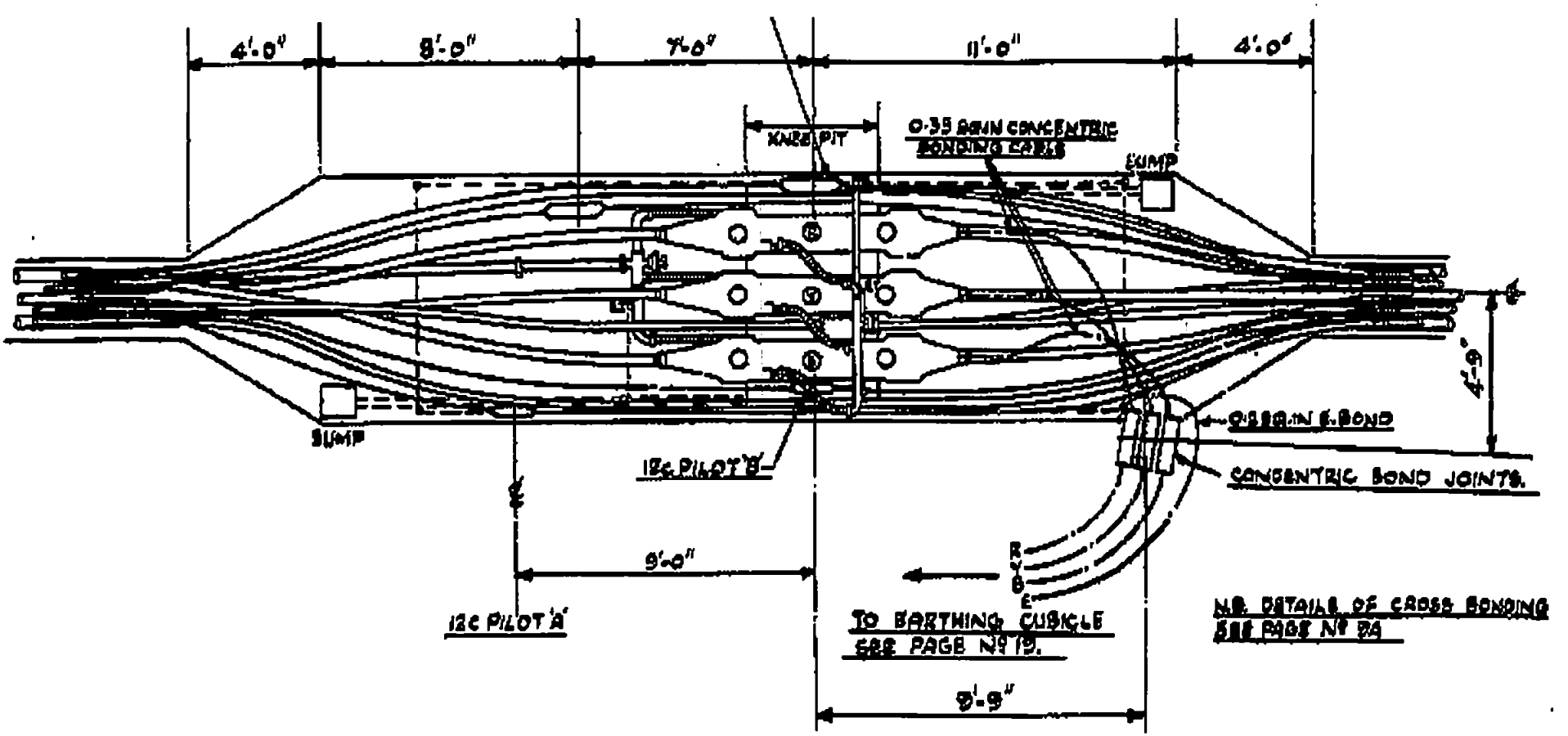

Figure 1.2 Plan of a joint bay for a self-contained oil-filled cable.

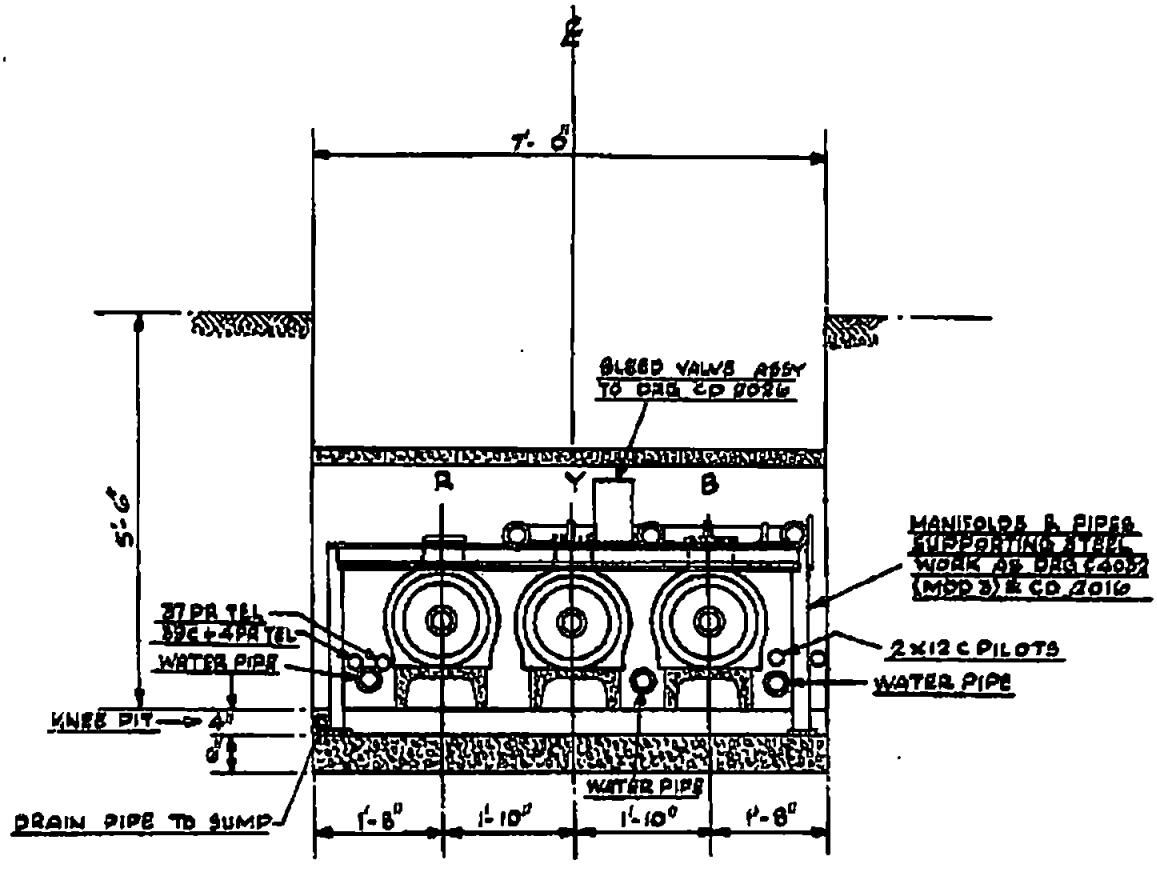

Figure 1.3 Joint bay cross-section for a self-contained oil-filled cable.

The cable oil is stored along the length of the cables in oil-feed tanks. The oil pressures within the cables range from 0 to 6.25 bar in the central oil duct. Any leaks of cable oil are therefore compensated for by an inflow from the oil tanks, that ensures an adequate level of pressure is maintained. Where a leak occurs, losses varying between 20 litres a week and 100 litres a day have been recorded.

1.3.1 Other National Grid Funded Projects

The NGC are currently undertaking research to determine the toxicity of cable oil and to develop possible remediation strategies that could be employed following a leak. No work in either area has been undertaken as part of this project.

1.4 Chemical Characteristics of Cable Oil

Linear alkylbenzenes (LABs) have been produced industrially since the 1960's as the precursor for linear alkylbenzene sulphonates, an anionic surfactant most commonly used in commercial detergents. They are also used in the paper, flooring and functional fluid industries, (Gledhill et al., 1991). This production of LAB from benzene and petroleum or natural gas based feedstocks results in a mixture of homologues with various alkyl chain lengths depending on the type of feedstock used. Each of the alkyl homologues consists of a mixture of isomers in which the phenyl group may be attached to any of the carbon atoms except the terminal one.

The form of linear alkylbenzene used for cable oils is commonly known as dodecylbenzene, which although not being strictly C_{12}, is composed of various lengths of both linear and branched alkylbenzene chains in the C_{10} to C_{13} range, giving it the overall properties of a C_{12} LAB. Linear alkylbenzene has been in use by the NGC since 1990 and has a homologue distribution as shown in Table 1.1. It is composed of approximately 90% linear alkylbenzene and 10% branched alkylbenzene.

Alkylbenzene Chain Length	% Linear Alkylbenzene	% Branched Alkylbenzene	% Total Alkylbenzene
$<C_{10}$	0.4	0.5	0.9
C_{10}	9.0	2.6	11.6
C_{11}	32.0	2.5	34.5
C_{12}	24.7	1.3	26.0
C_{13}	24.6	0.9	25.5
C_{14}	0.9	0.4	1.3
$>C_{14}$	<0.1	0.2	0.2
Total	**91.6**	**8.4**	**100.0**

Table 1.1 Pirelli PG6000D cable oil alkylbenzene homologue distribution

Dodecylbenzene, the C_{12} homologue has five possible phenyl isomers because the benzene ring may be attached to any of the carbons between C_2 and C_7. The 1-phenyl isomers are not formed, (Swisher et al., 1961) due to the instability of the intermediate carbonium ion.

S. Rowland (PEP Research and Consultancy) carried out a chemical characterisation of DDB cable oil. Initial elemental analysis revealed the presence of only hydrogen and carbon, with an average atomic H/C ratio of 2.6.

A GC-MS (Gas Chromatography – Mass Spectropectry), analysis revealed 18 major components. The mass spectra of each component were obtained and compared with the best-fit US National Bureau of Standards library spectra. It was used to classify the 18 components into four groups, the decyl-(C_{10}), undecyl-(C_{11}), dodecyl-(C_{12}) and tridecyl-(C_{13}) benzenes. The 1-phenyl isomer was absent, as predicted by (Swisher et al., 1961). The resultant GC-MS of DDB cable oil can be seen in Figure 1.4.

The environmental distribution of high molecular weight organic compounds such as LAB's is substantially affected by their physical and chemical properties. The physical and chemical properties of the cable oil supplied by Pirelli, PG6000D are summarised in Table 1.2.

Property	**PG6000D linear alkybenzene**	**Water**
Appearance	Clear liquid, no suspended matter	Clear liquid
Density at 20°C (kgl^{-1})	0.86	0.9978
Boiling Range (°C)	726	100
Kinematic Viscosity (mm^2s^{-1} at 20°C)	8.1	1.01
Flashpoint (°C)	150	-
Aqueous Solubility	Not miscible, $0.01mgl^{-1}$ $0.041\ mgl^{-1(1)}$	-
Vapour Pressure (25 °C)	4.9×10^{-4} (1) mm Hg	-
Henry's Law Constant	7.1×102 torr $^{-1}$ mol^{-1} (1)	-
Soil Partition Coefficient, K_{oc}	2.2×10^{4} (1)	-
Log Octanol : Water Partition Coefficient, K_{ow}	5.72 – 5.75 (1)	-

Table 1.2 Comparison of the physical and chemical properties of PG6000D Linear Alkybenzene and water. Source: All PG6000D linear alkybenzene data from Shell Health, Safety & environment data sheets with the exception of: (1) (Gledhill et al., 1991).

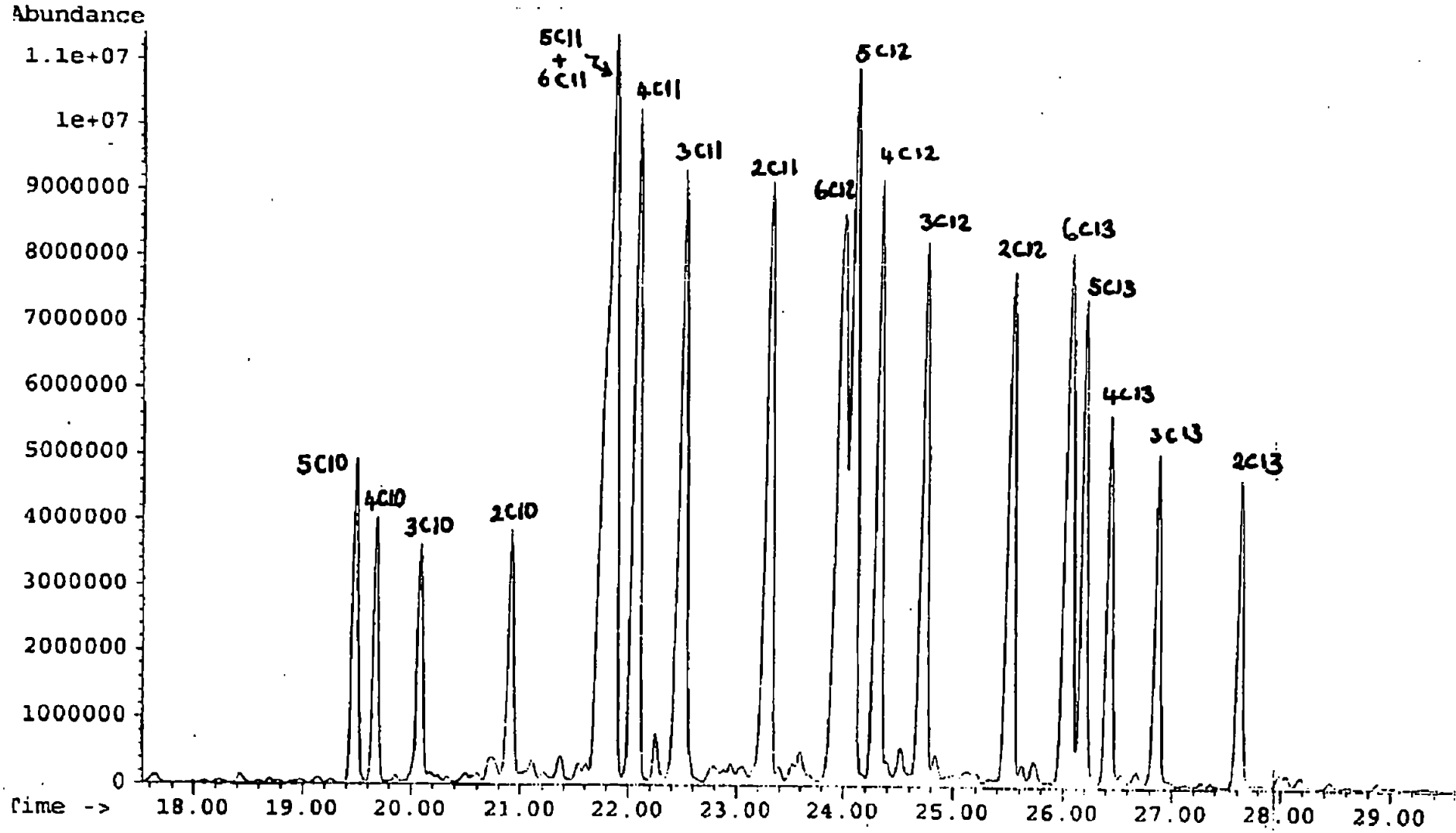

Figure 1.4 GC-MS of Cable Oil

1.5 Darcian Flow

The conductivity of a porous medium for single phase fluids can be expressed by the specific permeability k of the medium defined by Darcy's law, (Equation 1.1).

$$V = -(k/\mu)\nabla \wp = -(k/\mu)(\nabla P - \rho g)$$

Equation 1.1

Where $\wp$ is defined by the following equation:

$$= P + \rho g z$$

Equation 1.2

Z is the distance measured vertically upward from an arbitrarily chosen datum level, P the hydrostatic pressure, ρ the fluid density, and g the acceleration due to gravity. $\wp$ is measured by a pipe, called the piezometer and is indicated as the 'piezometric head' ϕ (dimension of length):

$$\phi = \wp / \rho g = (P / \rho g) + z$$

Equation 1.3

Which is the sum of the 'elevation head' z and the 'pressure head' $P/\rho g$. For a compressible fluid the pressure head is defined by:

$$\int_{P_o}^{P} \frac{dP}{\rho(P)g}$$

Equation 1.4

Where P_o is the hydrostatic pressure at the datum level. The difference in $\wp$ is equal to the pressure change in the fluid flowing through the porous sample. When the liquid is at rest, $\wp$ is constant everywhere.

$V = (\delta Q / \delta A)\mathbf{n}$ is the 'filter' or Darcy velocity where $\mathbf{n}$ is the unit normal vector of the surface area δA through which there is a volume flow at the rate δQ. The rationale behind Equation 1.1 is as follows: The porous medium is imagined to be subdivided into a network of small blocks, and Darcy's law is applied to each block. The size of each block must be small enough to approximate V, $\wp$, k, ρ and μ with constant values within each block; but the size of each block must also be large enough for Darcy's law in its

macroscopic form to apply in the block. These conditions appear to be satisfied to an acceptable degree in most practical situations, (Dullien, 1992).

In groundwater hydrology and soil mechanics, the only fluid of interest is water and, therefore, the so-called 'hydraulic conductivity' k_H defined as:

$$k_H = k\rho g / \mu$$

Equation 1.5

Darcy's law can then be written as:

$$V = -k_H \nabla \phi$$

Equation 1.6

For the case of beds of particles or fibres a different way of expressing the resistance of the porous medium to flow is with the help of the friction factor f_P, defined by the equation:

$$f_p = \overline{D_P} \nabla \wp / \rho v^2 L$$

Equation 1.7

as a function of the 'superficial' or 'particle' Reynolds number Re_p:

$$\mathrm{Re}_p = \overline{D_p} v\rho / \mu$$

Equation 1.8

Where $\overline{D_p}$ is some effective average particle or fibre diameter, ρ is the fluid density, and L is the length of the bed in the macroscopic flow direction.

Many different modelling approaches for the treatment of single-phase flow have been tried, which may be categorised in a number of different ways. In the first approach the flow inside conduits is analysed, in the other, the flow around solid objects immersed in the fluid is considered. For low and intermediate porosities the conduit flow approach is more appropriate, whereas for very high porosities only the second approach is suitable.

Phenomenological models have proved to be particularly useful in the case of packs of fairly uniform and isometric particles or fibres. They relate the transport coefficients of the porous media to grain and packing structure.

Within the conduit flow approach it is useful to distinguish capillaric and statistical models. The simplest kind of capillaric model consists of a bundle of straight cylindrical capillaries of uniform cross-section. Empirical capillaric models have resulted in excellent correlations. Channel flow has been treated mostly in the approximation that neglects all but one velocity component, resulting in Hagen-Poiseuille type flow equations.

1.6 Oil Migration at the Pore Scale

The research undertaken in this thesis is not primarily concerned with relative permeability (i.e. how does permeability / conductivity in one fluid vary in the presence of another fluid). However, it is concerned with the movement of oil on macroscopic (metre) scale. Pore-Cor is used to gain structure and demonstrate the formation of fingers. Much work on the pore-scale has been carried out and reviewed by Dullien (1992). Some of this work is reviewed in this section.

Dullien (1992) has investigated the multiphase flow of immiscible fluids in porous media. A large proportion of this work has been concerned with the traditional three- phase movement, with all experimental results cited referring to changes in permeability with water saturation. This is shown diagrammatically in Figure 1.5. The research in this thesis is concerned with changes in the permeability of water in an oil saturated, pre-wetted sample, (as shown in Figure 1.6), rather than the changes in permeability through water saturation which is analysed by Dullien.

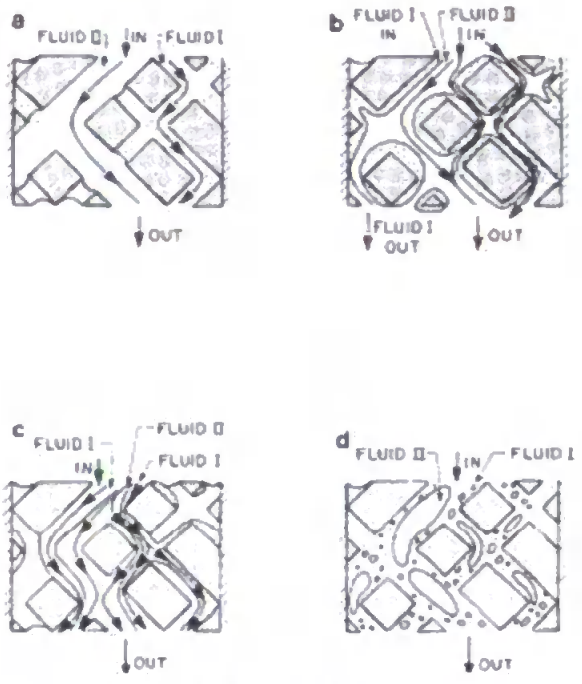

Figure 1.5 Two-dimensional representation of three-dimensional co-current steady two-phase flow in porous media, (Dullien, 1992).

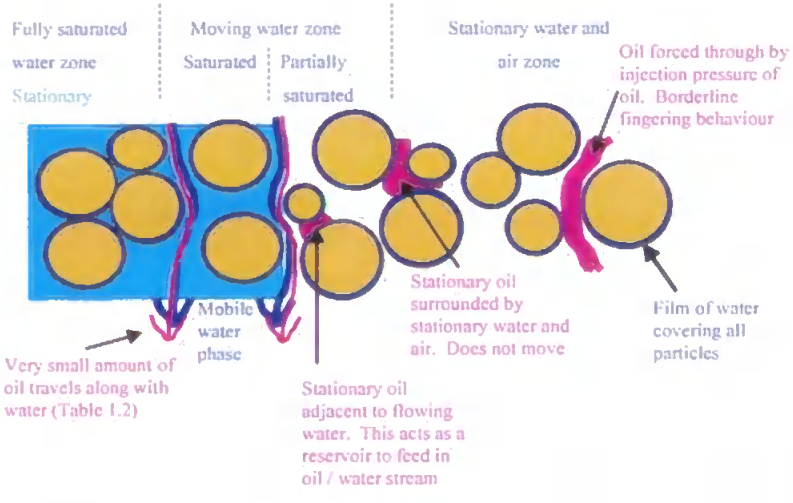

Figure 1.6 Schematic diagram showing the possible oil flow movements within sand and soil depending on the degree of water saturation. Soil shown in brown, moving oil shown in dark blue, stationary water shown in light blue, oil shown in purple and remaining colourless area represents air.

Darcy's law can also be adapted for steady and unsteady multiphase flow in porous media, (Dullien, 1998). It has been widely assumed in the literature that the effective permeabilities in a sample of the porous medium do not depend on the viscosities of the fluids. The idea behind this assumption is that the two fluids flow in separate channels, similar to the case of Figure 1.5a, and therefore the viscosities of Fluid I has no effect on the flow of Fluid II, and vice versa.

In certain instances a gas phase may also be present in immiscible displacement in porous media. One such instance involves the mobilisation of oil blobs that are surrounded by water and trapped in the pores by capillary forces. Trapping of oil blobs happens regularly in a water wet oil reservoir after water flooding and it can also happen in the soil in the course of attempted cleanup operations, (Dullien, 1998).

It was demonstrated that if the water is drained from a porous medium containing trapped residual oil, the oil blobs start spreading spontaneously immediately after they have been contacted by the air, Figure 1.7. The phenomenon of spreading oil blobs has resulted in the recovery of a very high percentage of residual oil, because films thus formed drain under the influence of gravity on the surface of the thick water films and oil is produced at the low end of this medium. This work is described in more detail in the publications by Dullien (1992 and 1998).

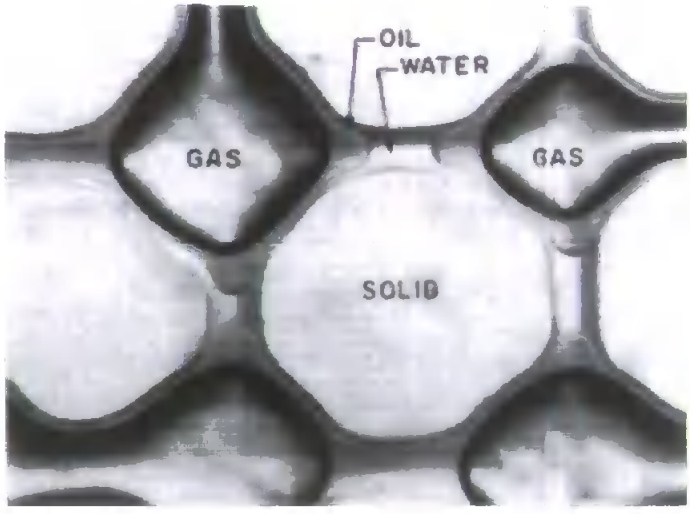

Figure 1.7 Spontaneous spreading of oil blobs on the surface on connate water in a capillary micromodel after being contacted by air, from Dullien (1998).

Lenormand et al. (1988) determined that immiscible displacements in porous media with both capillary and viscous effects could be characterised by two dimensionless numbers, the viscosity ratio $M = \mu_2/\mu_1$ and the capillary number C:

$$C = \frac{q\mu_2}{A\gamma \cos\theta}$$

Equation 1.9

where q is the flow rate, μ_1 is the viscosity of the wetting fluid i.e. water, μ_2 is the viscosity of the non-wetting fluid, A is the cross-sectional area of the sample, γ is the interfacial tension and θ is the contact angle. They describe how for certain values of C and M, either viscous or capillary forces dominate and displacement takes one of the basic forms: (a) viscous fingering, (b) capillary fingering, or (c) stable displacement.

By applying the equations above, it is possible to determine values for log C and log M. The log M value uses the bulk viscosities of cable oil and water, from Table 1.2, 6.97×10^{-3} Pa S^{-1} and 1.007×10^{-3} Pa S^{-1} respectively, (shown in Table 1.2 as mm^2s^{-1}). This results in a log M value of 0.84. In order to calculate the of capillary number, a number of assumptions have been made. The first is the value of q, the flow rate of oil. This is assumed to be 20 litres in 15 minutes or 0.0222×10^{-3} m^3s^{-1}, based on field observation in Chapter 7. A cross section of $1m^2$ has been assumed for A. The interfacial tension is assumed to be approximately $0.1Nm^{-1}$ and θ is believed to be 140° (assumed to be equivalent to mercury against air in sandstone). Using these assumptions a log C value of –5.1 is calculated for cable oil against water. If however, the contact angle is closer to 90° then the log C will be higher than –5.1.

By doing similar calculations for cable oil against air, a log M value of 2.58 can be obtained.

Using the diagram in Figure 1.8 it is possible to determine the region in which cable oil infiltrating from a typically unsaturated soil would fall. Based on the value of the viscosity ratio M, three zones can be distinguished. Zone I, at very low M, where viscous forces injected in the non-wetting fluid are negligible in comparison with viscous forces in the

wetting fluid. Zone II is the transition zone, where the viscous pressure drops in both fluids and plays a significant role. Zone III at very large M, where the viscous pressure drop in the wetting fluid is negligible.

The flow in this study is in the transition zone of Figure 1.8, and the flow intermediately between flow controlled by viscous and capillary forces. Although there seems to be a stable front separating the liquids, the region behind the front is not saturated with the more viscous fluid. Instead, it comprises a complex network of preferential flow routes. In addition, there is the possibility that the front will extend by viscous or capillary fingering at some positions. The behaviour of the oil against both water and oil in the two-phase system, is on the borderline between fingering and stable front saturation, and can be termed 'partial fingering'.

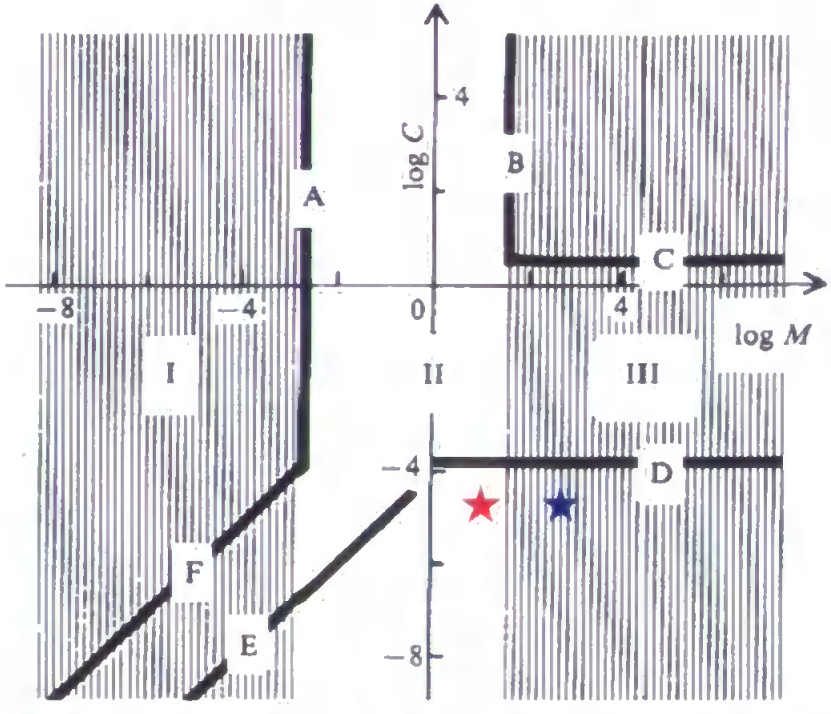

Figure 1.8 Schematic representation of the three zones where the different viscous forces are acting, (adapted from Lenormand et al. (1988)). Where the red star represents oil displacing water and the blue star represents oil displacing air.

Lenormand et al. (1988) studied the flow using simulations on two-dimensional networks, of dimensions 25 x 25 nodes and 100 x 100 nodes. Arbitrary void size distributions and connectivities were used. They simulated the two-phase flow of various combinations of liquids. These are shown in Figure 1.9, which also shows the respective values of log C and log M. The red highlighted cell most closely relates to the calculated C and M values for oil against water in this study and the blue cell represents oil against air.

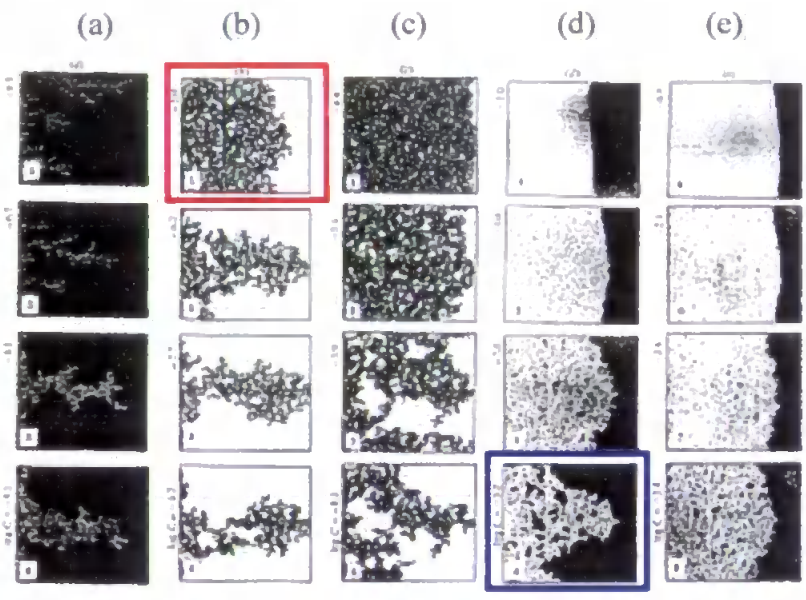

Figure 1.9 (a) Air (white) displacing a very viscous oil at various C at log M = -4.7: from viscous fingering (1) to capillary fingering (4). (b) Mercury (black) displacing hexane at log M = 0.7. (c) Mercury (black) displacing air at log M = 1.9. (d) Glucose solutions (white) displacing oil at log M = 2.0 and various C: from stable displacement towards capillary fingering. (e) Glucose solution (white) displacing oil at log M = 2.9 and various C: from stable displacement towards capillary fingering, from Lenormand et al. (1988).

Despite many years of research and the fact that the microscopic laws of fluid dynamics are well known, the predictability of macroscopic multiphase flow in porous media has not met with success, (Hilfer, 1998). Microscopic and macroscopic descriptions of multiphase fluid flow in porous media differ considerably from each other and both have their characteristic problems, (Dullien, 1992). Hilfer (1998) states that 'a microscopic description fails because it is generally impossible and not interesting to known the detailed microstructure and flow patterns on the pore scale'.

1.7 Preferential Flow

Preferential flow is used to describe situations where large portions of a flow-conducting solid matrix, often including regions of immobile water, are bypassed by the mobile water fraction. The phenomenon is a matter of concern because it can facilitate the rapid transport of nutrients and chemicals away from the surface to groundwaters, resulting in less productive soils and pollution of drinking water.

Three main types of preferential flow have been identified (Miyazaki, 1993). The first is *bypass* flow, which may develop in a heterogeneous substrate, such as cracked or stony soil, if highly permeable macropores extend to the soil surface or the water pressure within them is positive, (Beven and Germann, 1982). Flury et al., (1994) pointed out that structured soils represented a greater risk to groundwater than homogeneous soils in transporting soluble pollutants, because of the bypassing of the majority of the soil matrix, and they concluded that preferential flow should be considered the rule rather than the exception.

The second type of preferential flow is *fingering* flow, which is the progress of unstable wetting fronts through a porous substrate. Fingering has been shown to develop in sandy soils in less hydrophobic areas, and is possibly correlated to particle size (Dekker and Ritsema, 1994) and (Ritsema and Dekker, 1994). Raats (1973) showed how fingering may develop if the velocity of a wetting front increases with depth, and demonstrated with the use of a Green and Ampt model, several scenarios in which this might take place. Subsequently Henrickx et al., (1993) used these criteria to demonstrate how fingering developing from a water repellent surface layer may result in six to thirteen times as much solute being transported to groundwater compared with transport from a wettable surface. Baker and Hillel (1990) showed that fingering might arise at the interface between two layers of homogeneous sand when the bottom layer is coarser than the top layer. Kung

(1990b; 1990a), identified a third form of preferential flow, *funnel* flow, which takes place along inclined textural discontinuities.

Three phase flow in a porous medium is very difficult to predict. It is assumed that in all experiments, the solid phase was pre-wetted with water. There are no measurements of the contact angle of oil on wetted solid, but it can be reasonably assumed to be closer to 90° than, say, mercury on sandstone. If the angle is assumed to be 120° (between mercury on sandstone and 90°), this makes little difference to the value of log *C*. It changes from –5.1 to –5.5 (see Section 1.6 for the calculation of the equation) and therefore the general predicted behaviour is virtually the same.

It is also worthwhile to calculate the dimensionless Reynolds number *R*, the ratio between inertial and viscous forces in a channel by using Equation 1.10,

$$R = \frac{\rho V d}{\mu}$$

Equation 1.10

where *V* is the calculation of the flow velocity and *d* is the diameter of the channel (or capillary). For this study, *R* was calculated to be of the order of 10^{-8}, which represents creeping flow. These two calculations are assumed to represent the flow movement, and this will be tested during the investigation. However, it must be noted that the scale of the experiments conducted throughout this study are at least three orders of magnitude greater than pore scale, which these calculations represent. There are also major differences between the simulated flows in two dimensions, and the actual flow in the complex three-dimensional networks of natural samples.

It has also been demonstrated that preferential flow may occur even when there is no discernible structural cause for such behaviour. In a dye tracing experiment on field plots Ghodrati & Jury (1990), encountered considerable preferential flow, but were unable to

identify the source other than to suggest that areas conducting greater flow were more likely to have higher permeabilities than surrounding, dryer areas.

Some form of preferential flow may develop in samples, which are even more homogeneous than those used in this study - i.e. samples with particles or features of only a single primary size. Even in this type of sample, heterogeneities can be introduced to the void phase by the packing process. It has been suggested that water in such samples flows in rivulets or small streams (Porter, 1968a). These rivulets may randomly meet and coalesce to form larger rivulets, or alternatively large rivulets may divide. Experiments conducted on random packing of uniform spheres, Raschig rings, Intalox saddles and Pall rings appear to support this theory (Porter, 1968a). Porter et al. (1968b), demonstrates a possible method for predicting the number of rivulets at a given depth. This has also been interpreted to imply that increasing sample depth may be accompanied by a decrease in the total number of rivulets, and an increase in the volume of water being transmitted by individual rivulets (Dexter, 1995).

1.8 Non-Aqueous Phase Liquid Flow in Natural Systems

The principles of multiphase flow in natural systems have long been known to petroleum engineers, and involve the flow of water and other immiscible liquids. Schwille (1967) demonstrated that non-aqueous phase liquids (NAPL) such as organic solvents and other petroleum-based products, could be divided into two categories depending on their density relative to water. Immiscible liquids, both those less dense than water (LNAPL), including cable oil, and more dense than water (DNAPL) are heavier than water and infiltrate into the ground at a rate dependent on the type of soil and the NAPL characteristics.

Whether the NAPL reaches the water table or not depends upon the spilled volume and the retention capacity of the soil. If the retention capacity is exceeded in the unsaturated zone, the fate of the NAPL becomes largely dependent on its density. A light immiscible liquid

will tend to form a thin pool (len) on the surface of the water table. Figure 1.10 shows a schematic representation of LNAPL infiltration. Upon reaching a layer which it cannot penetrate, lateral spreading will occur, following not necessarily the direction of groundwater flow but the local topography of the layer, (Thomson et al., 1992). As the water table fluctuates in response to local pumping or seasonal recharge and discharge, the len of LNAPL can become smeared over a larger region, (Templeton, 1954).

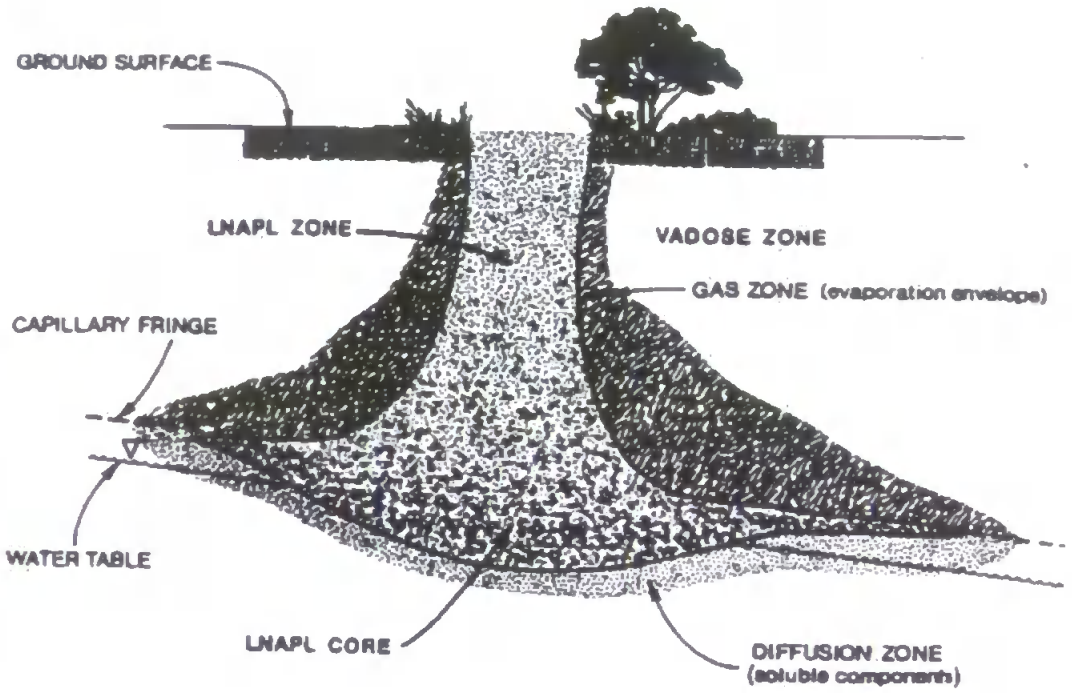

Figure 1.10 Schematic LNAPL infiltration (modified from (Pinder and Abriola, 1986)).

Six main constituents affect NAPL migration in the subsurface; (i) the volume of NAPL released, (ii) the area of infiltration, (iii) the time duration of release, (iv) the properties of the NAPL, (v) the properties of the media, and (vi) the subsurface flow conditions, (Mercer and Cohen, 1990).

When introduced into the subsurface, gravity causes the NAPL to migrate downwards through the vadose zone as a distinct liquid. This vertical migration is also accompanied to some extent by lateral spreading due to the effect of capillary forces, and to the spatial variability of the medium, (layering). As NAPL progresses downwards through the vadose

zone, it leaves residuals trapped in the pore spaces. This entrapment is due to surface tension effects. In addition to migration of NAPL, some of the immiscible fluid may volatise and form vapour extending beyond the NAPL, (Mercer and Cohen, 1990).

One of the reasons that only a limited number of comprehensive models have been developed is the complex physical and chemical nature of hydrocarbon contamination. The spreading of contaminants depends on many factors, such as volume of leakage, type of hydrocarbon product, hydrogeological conditions, hydraulic properties, and geological heterogeneity. A complex interaction between gravity and viscous and capillary forces determine the movement of the individual phases. The flow processes are further complicated by chemical and biological reactions within the two phases, (Host-Madsen and Hogh Jensen, 1992).

1.8.1 Multiphase Flow in Soil

Leverett (1941) was one of the first researchers to explain the importance of capillarity in the field of petroleum reservoir mechanics. Brooks and Corey (1964) and van Genuchten (1980) built on this work to develop models for the relationship between water saturation and the capillary pressure at the air-water interface.

Some numerical model studies of NAPL flow within soils do exist. Three dimensional, three-phase flow models have been developed by Faust et al. (1989) and by Letniowski (1989). Both of these models assume a passive air phase, implying that the air phase is infinitely mobile. Faust et al. (1989) applied their model to DNAPL from chemical landfills near New York. A number of two dimensional, three phase flow models have also been developed (Faust, 1985).

One of the first series of experiments was carried out at the Swiss Federal Institute of Technology in Zurich in the late 1970's and early 1980's. In these two dimensional, three

phase flow experiments, fluid pressures and saturations were measured simultaneously using embedded ceramic probes connected to pressure transducers and gamma-ray attention, respectively, (Schiegg, 1990). More recently, Parker et al. (1987) performed saturation-capillary pressure experiments for air-water, air-oil and oil-water two phase systems in a sandy porous medium to validate the use of scaled multiphase versions of the Brooks-Corey and van Genuchten retention functions.

Osborne and Sykes (1986) have been one of the few who attempted to model a field contamination scenario. However the model under-predicted the NAPL migration, a failure which was attributed to the uncertainties in the input data. Nevertheless, their efforts illustrate the utility of mathematical models in focussing future site investigations and evaluating the effectiveness of various remediation proposals.

Field observations by Poulsen and Keuper (1992), indicate that the migration and distribution of hydrocarbon contaminants are dominated by capillary forces and governed by the bedded structure of the sands. Detailed excavation and sampling revealed an extremely heterogeneous distribution of residual contaminant at the millimetre scale. They also discovered that a slow release of contaminant penetrated further than a ponded release.

Dawe et al. (1992), in an experimental study found that heterogeneities and the rate dependence of capillary forces have a significant effect on oil recovery. These studies show that the presence of heterogeneities can radically alter the pattern of migration and even the type of flow that develops. These results suggest that heterogeneity effects should not be ignored.

Butts and Jensen (1996) obtained experimental results from different textured sand, packed in a flume. They discovered that the initial distribution of oil in the fine sand appears to

follow a diffusion type flow. There appears to be significant horizontal spreading as the oil front reaches the slightly wetter soil above the boundary and the vertical oil permeability decreases. The low oil permeability in the fine sand close to the interface, caused by the increased water saturation, will reduce the vertical oil flux. Secondly, a capillary barrier effect may occur, causing the oil to form fingers at the point of breakthrough. Once formed, these fingers migrate downwards, the meandering pathway apparently caused by small-scale heterogeneities within the coarse layer, Figure 1.11.

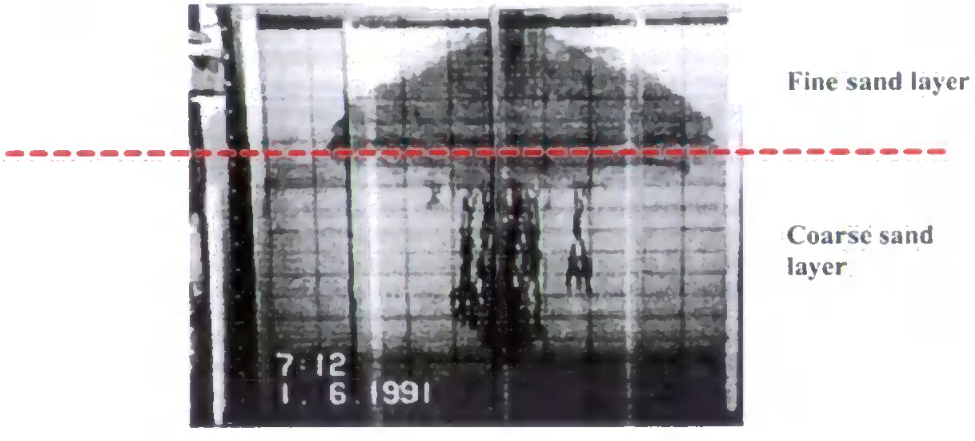

Figure 1.11 Oil distribution in a layered sand, showing fingering in the coarse layer, modified from (Butts and Jensen, 1996).

1.8.2 One - Dimensional Experiments

Joseph et al. (1994) conducted laboratory experiments to obtain data on oil migration in soil. This data was subsequently used for the development of a model, known as the Vadose Zone Interactive Processes model. The experiments used 58mm diameter glass columns, 480mm in length, filled with one of two different soils. Joseph et al. (1994) determined that the oil was more mobile in the soil with the greatest sand content. They also established that the amount of oil applied to the surface was by far the greatest determinant of the distance that the oil migrated. They then went on to model the mobility of other insoluble pollutants, such as benzene and toluene.

Many recent studies have concentrated on the effects of surfactants and other remediation technologies on NAPL transport. Surfactants enhance aquifer remediation by increasing the aqueous solubility and/or decreasing the interfacial tension of the NAPL, increasing the mobility, (Harwell, 1991).

Renshaw et al., (1997) investigated the effect of surfactants on permeability, by performing a series of column experiments filled with quartz sand and an increasing proportion of montmorillonite clay. Various concentrations of surfactant were used to determine the effect of concentration on the time taken to flush out the surfactant. Renshaw et al., (1997) established that the greater the clay content the longer it took for the surfactant to be flushed through the column and the greater the reduction in permeability. Abdul and Gibson, (1991) studied the effect of surfactant on the mobility of polychlorinated biphenyl (PCB). The addition of a surfactant enhanced the mobility of the PCB, making it possible to remove all of the PCB from a sandy material. Ang and Abdul (1991) studied the surfactant washing of transmission fluid and also performed similar investigations to Abdul and Gibson, (1991). However, neither study investigated the mobility of the NAPL used in the experiments.

Other studies include Priddle and MacQuarrie (1994) who investigated the residual dissolution of creosote in sand columns, but did not make any attempt to study the migration of the non-aqueous phase. Hatfield et al. (1993) studied the dissolved components of NAPL, and generated breakthrough curves for benzene and toluene on sand columns. Zalidis et al. (1991) carried out experiments to provide information on the long-term leaching effect of residually held gasoline in unsaturated soil columns. However, no attempt was made to investigate non-volatile compounds.

Thomson et al. (1992) carried out five separate trials using three different immiscible liquids (hydraulic oil, kerosene, and hexane) in water saturated soil columns. Irregular immiscible liquid infiltration fronts were observed in four of the five experiments. It was suggested that small-scale heterogeneities control the infiltration of immiscible liquids into soil. Other studies have looked at mineral oil and Soltrol 220 infiltration to soil columns, (Cary et al., 1989).

Studies have also been concerned with the infiltration time of immiscible chemicals such as hexane and tetrachloroethylene, (Guigard et al., 1996). This study showed that for three soils the infiltration time of 135ml of these chemicals varied when applied to the top of a column of soil, but where dependent on the soil type, chemical type and soil water content. They concluded that the movement of the wetting front was enhanced by the presence of water in the soil and rapid movement of infiltrating chemicals could be explained by the lower retention capacity of the soil for these chemicals as the water content increased. Other authors have also reported these trends, (Aurelius and Brown, 1987), (Acher et al., 1989).

1.8.3 Two Dimensional Laboratory Studies of NAPL

In 2-D experimental models, flow is constrained in only one direction. Typically, an experimental cell is used, with one dimension much smaller than the other two. For a 2-D study an experimental cell is used orientated vertically, it is assumed that fluid flow is parallel to the walls of the apparatus and fluid saturations are uniform throughout the cross section horizontally.

Numerous 2-D studies have been conducted in recent years. One of the first researchers to investigate NAPL migration in the subsurface was Schwille, (1988). Numerous laboratory tank studies were performed for homogeneous, heterogeneous, and fractured media using

chlorinated hydrocarbons. One study concentrated on the flow in layered sand, where lateral groundwater flow had little effect on the pollutant plume. Another experiment observed that a DNAPL migrated downwards in a broad group of small flow paths and that the presence of a water table had little effect, when studied using a fractured media. This work was later extended by Kueper et al. (1989) who studied the effect on migration using various bands of sand.

Illangasekare (1995b) noted that initial water saturation had a major impact on the flow of NAPL. In the unsaturated region, the fine sand layer trapped the NAPL, whereas in the saturated region the fine sand acted as a barrier to NAPL flow. In both cases, significant lateral flow of the DNAPL was observed.

Parker et al. (1991) established a LNAPL lens and introduced pulses of water at the sand surface under gravitational forces. The water table was then raised to induce LNAPL trapping in the saturated region. It was found that the proposed model overestimated the degree of oil drainage, vertical penetration, and lateral spreading that was observed.

Host-Madsen and Hogh Jensen (1992) undertook a similar study, which derived pressure-saturation and relative permeability relationships were predicted using parametric models. These were then compared to experimental data. Sand was packed into a pelxiglass tank and filled with water to establish a horizontal water table. LNAPL was added near the surface via a pump, simulating a point source at depth. They discovered that the flow of oil is characterised by a rapid spreading down through the unsaturated zone and a slower horizontal spreading within the capillary fringe. They also noted that the oil displaced the water phase at high concentrations.

A study by Pantazidou and Sitar (1993) looked at the migration of kerosene in a variable saturated sand tank. The tank was fitted with porous disk pressure ports to provide aqueous and non-aqueous phase pressure data. It was found that LNAPL migration ceased after encountering the capillary fringe, the majority of LNAPL was located in a pancake-shaped lens pooled on the tension-saturation region. Water table fluctuations were found to spread the NAPL over a larger area with some LNAPL being trapped below the water surface.

Van Geel and Sykes (1994) investigated liquid pressure and saturation distribution during LNAPL migration through homogeneous, variably saturated sand. They found an increase in water pressure prior to the arrival of the advancing LNAPL front, which did not correspond with an increase in water saturation.

Another study investigated the oil infiltration from 15mm in diameter point source, into a box (25cm x 25cm x 24cm) filled with sand or glass beads, (Simmons et al., 1992). They discovered that transmission fluid and mineral oil infiltrated differently, the transmission oil infiltrated uniformly into the glass beads, whereas mineral oil displayed channelling behaviour. Similar results were found for the sand although the channelling was more horizontally pronounced with a dendritic pattern. Additionally, they noted that the oils displaced substantial amounts of water from the plume.

Other studies have also been conducted on sand filled tanks. Many of these studies have concentrated on solvent flushing (van Geel and Sykes, 1994), although some researchers have investigated lens geometry (Schroth et al., 1995), and further studies have looked at remediation strategies (Illangasekare et al., 1995a), (van Geel and Sykes, 1997). A general review of other two-dimensional NAPL experiments can be found in Chevalier and Peterson (1999).

1.9 Soil

Soil contains matter in all three states: solid, liquid and gaseous. The solid portion is partly organic and inorganic. The inorganic, or mineral, part of the soil is made up of particles derived from the parent material, the rocks that weather to form the soil. The organic portion consists of living and decayed plant and animal materials. Soil water, its dissolved elements, and suspended particles make up the soil solution, the liquid part of the soil. The soil solution, together with the soil air, fills up the spaces or pores among the mineral and organic components of the soil.

The relation between the soil water content and the water suction is a fundamental part of the characterisation of the hydraulic properties of a soil, commonly known as water retention. This water retention function is primarily dependent upon the texture or particle-size distribution of the soil and the structure or arrangement of the particles, (Klute, 1986).

1.10 Water Retention Models

All empirical water retention models use the Laplace equation to relate the capillary pressure p to the pore radius r_i of the i th pore:

$$p_i = \frac{-2\,\gamma_i\,\cos\beta_i}{\rho_w\, g\, r_i}$$

Equation 1.11

Here γ is the interfacial tension between water and air, β is the contact angle where the water meniscus touches the solid surface, ρ_W is the density of water, and g is the acceleration due to gravity.

Various approximations are implicit in the use of this equation. The contact angle and interfacial tension are assumed to have constant values (taken to be 0 degrees and 0.075 Nm^{-1} respectively), i.e. $\beta_i = \beta$ and $\gamma_i = \gamma$ for all i. It then follows that all pores must be cylindrical, since this is the only geometry for which there is a single, invariant contact

angle β. Although much work has been published on the capillary pressure in other shapes of pores (Mason and Morrow, 1994); (Tsakiroglou and Payatakes, 1993); (Archie, 1952), in a natural sample it is difficult to measure three-dimensional shape distributions (Cousin et al., 1996). The voids are therefore explicitly or implicitly represented as cylinders, and the percolation and saturated hydraulic conductivity characteristics of each simulated void represent the actual characteristics of a real void of a possibly different shape and size (Garboczi, 1990).

The cylindrical void radius distribution f(r) is defined as :

$$f(r) = \frac{d\theta}{dr}$$

Equation 1.12

where θ is the volumetric water content. Use of this equation implies that all pores are fully accessible and that they independently experience the external applied pressure ψ. Such behaviour would be observed in a structure that contains aligned capillary tubes, (Figure 1.12), in which all the tubes are open to the surface or surfaces at which pressure is applied. In these circumstances, $p_i = \psi$ for all i.

Figure 1.12 Model of the void structure of soil comprising aligned cylindrical tubes.

Invoking Equation 1.12 allows the pore radius distribution function f(r) to be transformed into the capillary pressure distribution function g(ψ) by the following expression :

$$g(\psi) = f(r)\frac{dr}{d\psi} \quad .$$

Equation 1.13

Instead of integrating Equation 1.13, it may be summed to each of a series of j experimentally determined water retention points. If we assume that the voids are in the form of aligned cylindrical tubes, and that there are N_j tubes of radius r_j and length $l\tau$, where l is the sample length and τ is the tortuosity, then

$$\sum_{j=1}^{k} g_j(\psi) = \sum_{j=1}^{k} f_j(r) = \sum_{j=1}^{k} N_j \pi r_j^2 l\tau \ .$$

Equation 1.14

The quantity r_j may be calculated by rearranging Equation 1.11. To calculate the full distribution of cylinder sizes, it is necessary to estimate the low-tension asymptote. Having done this, a void model based on bundles of capillary tubes, Figure 1.12, can be

constructed with properties that exactly match the water retention curve at each experimental point.

However, such a model is clearly simplistic, and several other proposals for the distribution function of pore radii f(r) have been made. Kosugi (1994) proposed a lognormal function:

$$f(r) = \frac{(\theta_s - \theta_r)\, r_{max}}{(2\pi)^{1/2}\sigma\ (r_{max} - r)} \quad \exp\left[\frac{\left\{\ln\left(\frac{r}{r_{max} - r}\right) - \mu\right\}^2}{2\sigma^2}\right]$$

Equation 1.15

where r_{max} is the maximum pore diameter, and θ_r is the water content at which the capillary pressure ψ is infinitely small and the soil's hydraulic conductivity is zero. In practice, however, θ_r is treated as an empirical fitting parameter, with arguable physical significance. The quantity θ_s is the water content at saturation, and because it is measured experimentally it is not treated as a fitting parameter. The mean μ and standard deviation σ are the first and second moments of the pore size distribution function.

The model is based on the assumption that the pore-size distribution of a soil is lognormal because many particle-size distributions in soils are approximately lognormal. The assumption is not supported by experimental evidence, but the model has been found to fit several sets of water retention data.

An expression relating effective saturation S_e to capillary pressure has been derived for this pore radius distribution function:

$$S_e = \frac{1}{2}\ \mathrm{erfc}\left[\frac{\ln\{(\psi_c - \psi)/(\psi_c - \psi_0)\} - \sigma^2}{\sqrt{2\sigma}}\right] ,$$

Equation 1.16

where ψ_0 is the pressure at the mode of the distribution $f(\psi)$, which corresponds to the point of inflection on the water retention curve. ψ_C is the 'bubbling pressure' at which air intrusion begins. The effective saturation S_e is defined as:

$$S_e = \frac{(\theta - \theta_r)}{(\theta_s - \theta_r)}$$

Equation 1.17

Functions other than the lognormal water retention fitting function have also been widely used. Van Genuchten (1980) proposed the function:

$$S_e = \left[\frac{1}{1+(-\alpha\psi)^n}\right]^m$$

Equation 1.18

where α, m, n are fitting parameters.

A model proposed by Brooks and Corey (Chu, 1994), relates the effective saturation to a power function of ψ :

$$S_e = \left(\frac{\psi_c}{\psi}\right)^\lambda$$

Equation 1.19

where ψ_c and λ are fitting parameters. The Brooks and Corey expression has been found to be equivalent to a general fractal water retention model, (Perrier et al., 1995). However, this model uses a pore-size distribution based on the first derivative of the water retention curve (Tyler and Wheatcraft, 1990), and therefore it implicitly includes the structure approximations exemplified by Figure 1.12. Common to all of the functions described above is that they have at most one point of inflexion and can therefore only apply to uni-modal pore size distributions.

1.11 Modelling

One way of tackling the many problems of predicting and modelling the flow of water and solute is to employ an explicit, precise but simplified model of the soil's void structure. The simplifications are necessary to stay within computing limitations while maintaining a

realistically large simulated representative elementary volume (REV). The model should represent other important characteristics, particularly the retention and flow of water and solute, most usefully at those length scales that are too small for a continuum approach.

Other researchers have described a range of simplified geometries within their network models. Celia et al. (1995) reviewed early work in this field. Payatakes and co-workers discuss percolation characteristics within pore systems, which include 'hold-ups' for entry into spherical and sinusoidal geometry pores and the effects of correlated (Tsakiroglou and Payatakes, 1991). However, their work has not been extended to the prediction of hydraulic conductivity, nor has it been applied to soil. Many models including those proposed by Rajaram et al. (1997) and Lowry & Miller (1995) are networks of a ball and stick type. They have many of the features of Pore-Cor, such as variable connectivity and a visualisable structure, and have been used to predict pore-level properties such as entrapment (Lowry and Miller, 1995) and relative hydraulic conductivity (Rajaram et al., 1997). Lowry & Miller (1995) argue that for a model of a complex porous medium to form a representative elementary volume, 8000 or more nodes are required, which both these models possess. Rajaram et al. (1997) found that networks comprising 12 nodes in each direction were sufficiently large to give stable network predictions. Both models assume arbitrary pore-size distributions.

Within the context of these discussions, the number of nodes in the Pore-Cor unit cell size is small, being limited by the complexities of calculating the saturated hydraulic conductivity calculation. Producing different *stochastic generations* has been used to circumvent this problem. This produces a void space network that has the same percolation characteristics as the experimental sample.

Although all network models should be able to model a wide range of pore-level properties, they are rarely used to predict saturated hydraulic conductivity. This is because the application of percolation algorithms to more complex geometries is difficult, whereas the experimental measurement of saturated hydraulic conductivity is straightforward.

The Pore-Cor model has previously been applied to a range of substances including paper coating formulations (Gane et al., 1995) and reservoir sandstone (Matthews et al., 1995). In this work, we build on a recent application of the Pore-Cor model to soil, (Peat et al., 2000).

1.12 Aims and Objectives

On the basis of the current body of knowledge in this area, and the new opportunities discussed in this chapter, the following aim and objectives were drawn up:

1.12.1 Aim

- To enhance the fundamental understanding of the local (0.1 to 100 m) flow of pollutants through soil and rock aquifers.

1.12.2 Objectives

- To obtain specific information about pollutant flow of interest to the National Grid;
- To establish a predictive capability for the migration of cable oil should a leak occur in a cable;
- To demonstrate the wider application of the Pore-Cor model in relation to soil.

1.13 Structure of the Thesis

Pore-Cor is used in Chapter 2 to model the migration of cable oil in a range of sands and soils to further understand the flow of cable oil within the soil structure. Chapter 3 discusses the development of an experimental technique for analysing the quantity of cable oil in a range of sand and soil samples. The chosen technique is then applied in subsequent

experimentation. Chapter 4 seeks to identify the migration properties of cable oil in one-dimensional (vertical migration) sand columns. Chapter 5 extends this analysis to identify the migration properties of cable oil in two dimensions, using both sand and soil samples. Chapter 6 describes the development of a field-scale investigation of the migration of cable oil in soil. This investigation is discussed in Chapter 7, which seeks to identify the migration properties of cable oil in three dimensions for a range of sand and soil types. Chapter 8 discusses the experimentation and analysis and uses this as the basis from which to draw conclusions (Chapter 9) and suggest areas for further development work.

2. Pore-Cor Modelling

2.1 Introduction

Pore-Cor uses mercury intrusion or water drainage curves to model the void space of porous media, and make predictions of saturated hydraulic conductivity and dispersion. The software is based around an infinitely repeating unit cell of one thousand interconnected cubic 'pores' and smaller connecting cylindrical 'throats'. This cell connects and repeats infinitely in each Cartesian direction. It is generated such that the percolation characteristics of the resulting network fit the experimentally derived drainage curve as closely as possible.

The void geometry of Pore-Cor consists of a three dimensional-array of cubes that are connected by cylinders. In natural porous media, many larger voids are constrained by smaller apertures. The large voids have traditionally been called pores and the smaller constraining voids have been called throats. To maintain this convention we refer to Pore-Cor cubes and cylinders as pores and throats respectively. The unit cell of the model comprises a 10 x 10 x 10 network of cubic pores connected by a total of 500c cylindrical throats, where c is the connectivity. In Figure 2.1, the first pore of the unit cell is next to the axes in the bottom right-hand corner of the diagram, which also mark the origin of the co-ordinates of the unit cell. In this case, the first pore and its adjoining throats are invisibly small on the diagram. The diagram shows fourteen rows of features in each direction from this origin, extending over a distance of 4cm. As the unit cell comprises only 10 features in each direction, it can be seen that the four rows furthest away from the origin in each direction are a repeat of the first four rows next to the origin. The diagram shows only a representative part of the whole, modelled structure, which comprises an infinite array of repeating unit cells in each direction.

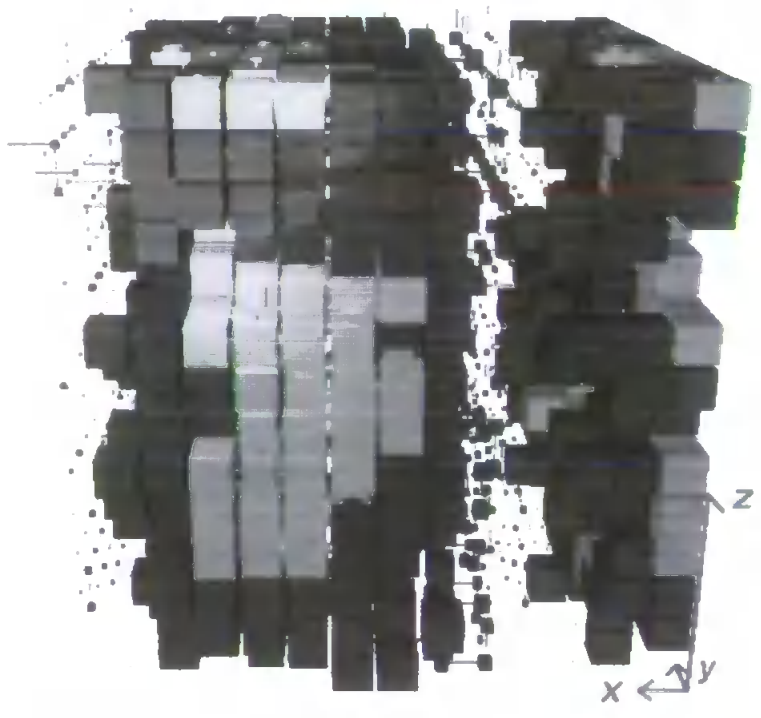

Figure 2.1 Pore-Cor void structure showing a 4cm cube of the 85cm depth Crediton series sample. Air (light grey) has displaced water (dark grey) under a tension of 3.0 kPa. Many of the features are invisibly small. Reproduced from (Peat et al., 2000).

The throats between the pores form a log-linear distribution with an average of 1% by number of each of 100 equally log-spaced sizes. The 'throat skew' of the model is defined as the percentage of throats of minimum size in the distribution, so that a throat skew of 1.2% of the smallest size generates 0.8% of the largest size, as shown in Figure 2.2. For simplicity of calculation, the positions of the pores and throats in the model are equally spaced in Cartesian planes in each direction. They therefore do not pack efficiently, and to achieve the experimental porosity it is necessary to enlarge the pores by a factor known as the 'pore skew', giving pore sizes up to, but never exceeding, the original maximum size. Figure 2.2 shows the effect of a pore skew of 12, which increases the minimum size from 0.2 μm to 2.4 μm, and increases the count of the largest size from around 1.5% to 44.7% of the total. This effect is also shown in Figure 2.2, which confirms that nearly half of the largest pores are of the same size. Such a pore size distribution arises from the

inefficiencies of the packing of the features (pores and throats) within the unit cell, rather than an experimental feature of the sample. The pore skew parameter is therefore a somewhat unsatisfactory parameter, and is kept as low as possible to be consistent with achieving the correct porosity.

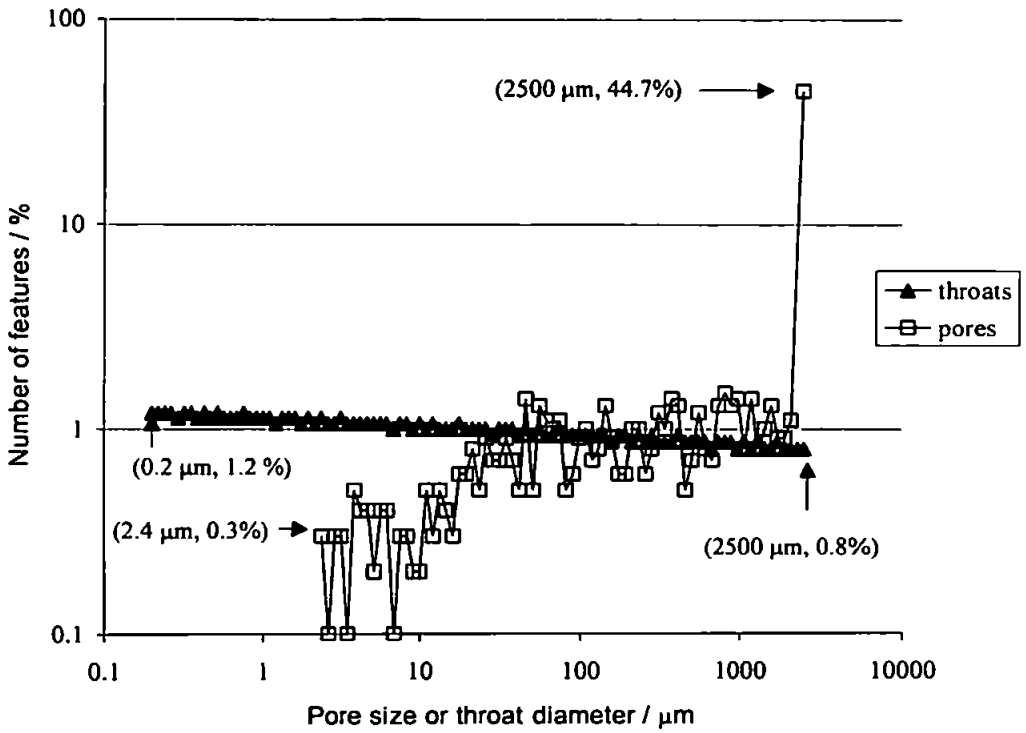

Figure 2.2 Distribution of pore and throat sizes for the optimum (best fit) structure for Figure 2.1, from (Peat et al., 2000).

The largest voids within the unit cell correspond to those required to model drainage at the smallest differential pressure. The unit cell is a little more than 10 times larger than this size — so for soil, a typical unit cell would be approximately 3cm across.

Various auto-correlations of void sizes within the unit cell are possible. The voids may be entirely randomly arranged, vertically banded, arranged so that larger voids cluster into a spherical locus in the centre of each unit cell (a 'large-centred' structure), or arranged so that smaller voids cluster centrally ('small-centred'). Degrees of structuring are possible from random (correlation 0) to fully correlated (correlation 1) in five steps of 0.2. Figure 2.1 shows a banded structure with correlation 0.6.

The Pore-Cor arrangement of pores and throats generates a void space network that has the same percolation characteristics as the experimental sample. The percolation algorithm has been described in a previous publication (Peat *et al.*, 2000). At each quasi-static pressure differential applied to the top surface of the unit cell, it will calculate the intrusion of a non-wetting fluid. The intrusion is assumed to be entirely controlled by capillarity, according to the Laplace equation. Each feature is either empty or full of non-wetting fluid, which progressively displaces the wetting fluid, or nominal air or vacuum, as it proceeds through the unit cell. The importance of the percolation algorithm is that it takes into account the 'shielding' or 'shadowing' of large pores by small throats.

Current geometric restrictions on the model and mathematical restrictions within the hydraulic conductivity algorithm make it necessary to constrain the range of pore sizes modelled. It is impossible to produce a computer model with an infinite size range, and as a result the curves are truncated to a range which nevertheless retains substantially larger voids than were represented by the original experimental data. It is therefore necessary to assume that all pores <0.2μm diameter are non conducting and pores larger than 2500μm are isolated from experimental samples, and do not contribute significantly to the modelled effects. Water retention curves, and corresponding air intrusion curves and porosities, are normalised onto a scale of 0 - 100%, representing the modelled void space between these two cut-off points.

In real soils that are unsaturated, some water is distributed over the soil matrix in films, and these films are not necessarily entirely displaced by intruding air. Pore-Cor ignores the effects of these wetting films by assuming that individual pores and throats are completely full of liquid or completely drained, a simplification which Mualem and Friedman (1991)

believe will limit the accuracy of network models. The approximation is more realistic when modelling mercury intrusion, where the non-wetting mercury can be assumed to fully displace the receding residual air in the evacuated sample. However, mercury porosimetry must be used with caution on intact soils, since it can destroy the soil structure and its use is limited to small samples. Furthermore, soil contains pores of diameter greater than 500 μm, larger than can be reliably measured by mercury intrusion (Moscou and Lub, 1981). Bartoli et al., (1999) notes that mercury porosimetry is sensitive to characteristics such as clay content.

When modelling water retention curves, air is intruded from the top face of the unit cell. The intruded structure is therefore an infinite sheet with thickness equal to the size of the unit cell, because of the repetitions of the unit cells in each direction.

The use of Pore-Cor to model water retention curves removes the necessity of assuming the approximation shown in Figure 1.11 that all voids are accessible and open to the applied pressure. Instead, the air drains only those throats and pores in the network which are exposed to the applied air pressure. Other voids, deep within the network, may be shielded or shadowed from this effect by intervening smaller voids that are still full of water. This emphasises the difference between a soil water retention experiment and a soil matrix tension experiment. In the latter, a water-filled porous tensiometer is inserted deep within the soil sample, and sets up equilibrium with all the local menisci, through the continuous water phase. The capillary pressure of all these equilibrated menisci is then measured. Haines (1927) described this effect and also pointed out the intractability of exact calculations for poly-disperse, random soil structures.

The closeness of fit between the simulated and experimental water retention curves is

measured in terms of a quality parameter σ_q :

$$\sigma_q = \frac{\sum_{i=1}^{n}\left(r_{exp(V_i)} - r_{sim(V_i)}\right)^2}{n}$$

Equation 2.1

r_{exp} and r_{sim} are the radii which are equivalent, via the Laplace equation to the experimental and simulated applied pressures which allow a volume V_i of water to remain in the sample. There are n experimental points, spaced over the entire experimental and extrapolated curve. A minimum value of σ_q corresponds to the best fit between the simulated and experimental water retention curves when they are plotted on a graph of the type shown in Figure 2.3. For some materials, sample edge effects necessitate a different type of fit (Matthews et al., 1995).

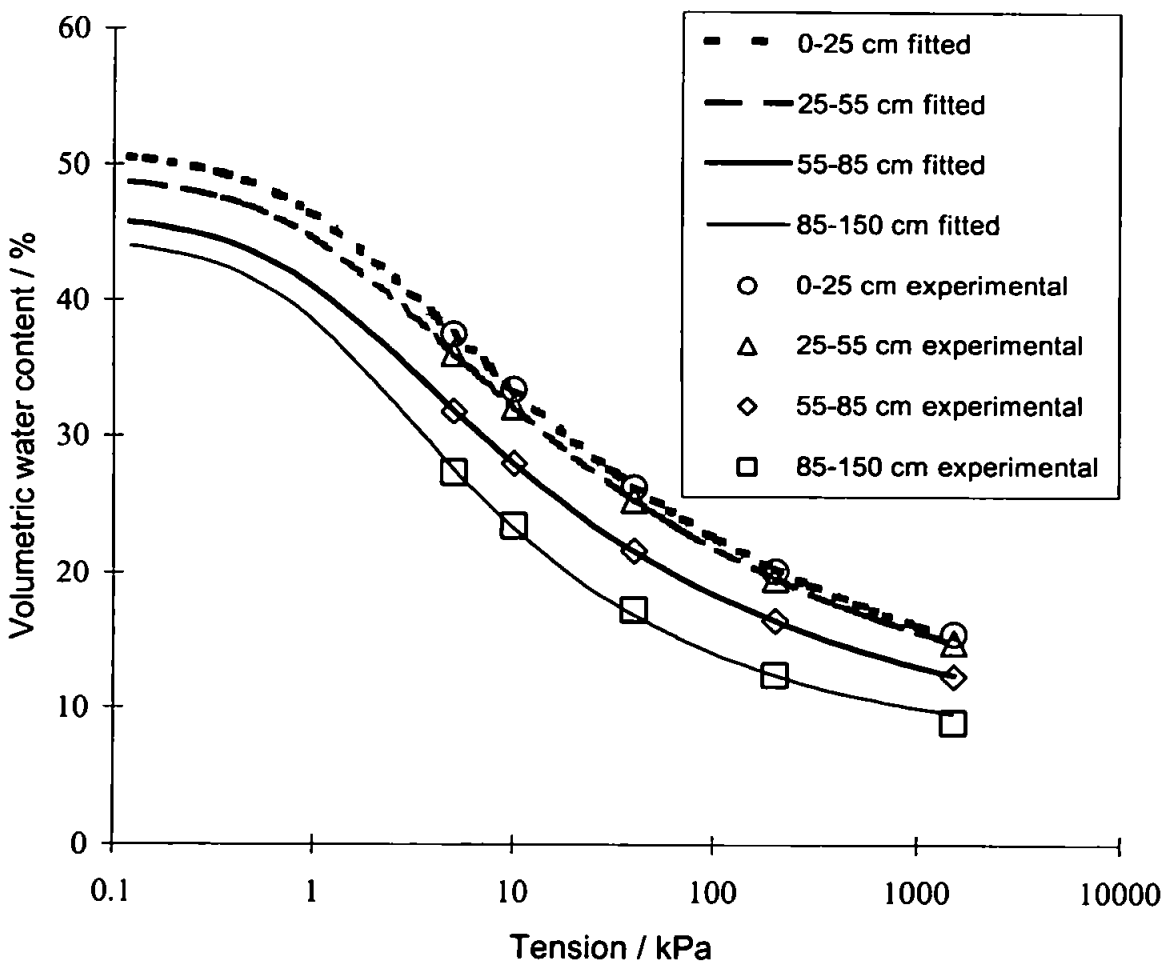

Figure 2.3 Crediton Seismic water retention data, showing depth trend and the van Genuchten extraploations, from (Peat et al., 2000).

A long-standing problem in the study of porous media has been the question of how to calculate the hydraulic conductivity of a solid from knowledge of the geometry of the void space within it. The absolute hydraulic conductivity k of a porous solid is traditionally defined in terms of Darcy's law. With reference to a cell of the solid of unit volume, this may be written:

$$\left(\frac{dV}{dt}\right)_{cell} = -\frac{kA_{cell}\delta P_{cell}}{\mu l_{cell}}$$

Equation 2.2

where μ is the viscosity of the fluid, $(dV/dt)_{cell}$ is the volumetric flow rate across the cell, $\delta P_{cell} / l_{cell}$ is the pressure gradient across the length, l_{cell}, of the cell, and A_{cell} is the cross-sectional area. Many attempts have been made to calculate k from primary parameters such as the diameters, lengths and positions of the pores and throats. Other workers have described equations based on characteristic parameters such as porosity, the total externally-accessible surface area per unit volume of the solid, the characteristic throat diameter d_c, usually defined as the ratio of the conductivity of a porous sample saturated, tortuosity, t, and the formation factor F, the diameter corresponding, via the Laplace equation, to the pressure at which there is maximum incremental change of intrusion with pressure i.e. the point of inflexion on the intrusion curve, (Matthews et al., 1993). The most successful to date has been that of Thompson, Katz and Raschke (Thompson et al., 1987):

$$k = \frac{1}{226}\frac{d_c^{\,2}}{F}$$

Equation 2.3

The equation predicts hydraulic conductivity correct to a factor of 7, for a range of sandstone and limestone samples covering several orders of magnitude of experimental hydraulic conductivity. Flow is supplied from a 'super-source' to al throats at the top of

the unit cell, and occurs in the $-z$ direction, and the $\pm x$ and $\pm y$ directions, see Figure 2.1. The absence of any arcs in the $-z$ direction is equivalent to applying a non-uniform pressure gradient which causes a pressure decrease across any arc in the $-z$ direction.

An incompressible fluid flowing through a tube takes up a parabolic velocity profile, with maximum flow rate down the centre of the tube. If the flow at the walls is assumed to be zero, integration over the velocity profile yields the Poiseuille equation:

$$\left(\frac{dV}{dt}\right)_{tube} = -\frac{\pi . r_{tube}^{\ 4} \delta P_{tube}}{8\mu . l_{tube}}$$

Equation 2.4

$(dV/dt)_{tube}$ is the volume flow rate, r_{tube} the radius of the tube and $\delta P_{tube} / l_{tube}$ is the pressure gradient along the tube. Poiseuillian flow has been shown to occur for oil displacement in capillaries down to 4-μm in diameter (Templeton, 1954).

If Poiseuillian flow is assumed to occur across the whole cell in the $-z$ direction, i.e. from the top to the bottom face of the unit cell. Then,

$$\left(\frac{dV}{dt}\right)_{cell;-z} = -\frac{\pi}{8\mu} \Omega(r_{tube;z}^{\ 4})_{cell} \frac{\delta P_{cell}}{l_{cell}}$$

Equation 2.5

Ω is an averaging operator over the whole unit cell operating on the fourth power of the individual radii $r_{tube;z}$ of all tubes lying parallel to the z axis. It is calculated by means of the 'Dinic' network analysis algorithm (Ahuja et al., 1997). Ω is defined such that Equation 2.2 is satisfied, and generates a term which is related to the effective Poiseuillian capacity of the cell for flow in the $-z$ direction. Since at this stage of the calculation, all the tube lengths $l_{tube;z}$ are identical and $l_{tube;z} = l_{cell} / \beta$, where β is the number of tubes in the z direction in the unit cell (in this case 10), we can include these lengths in the averaging function, so that

$$\left(\frac{dV}{dt}\right)_{cell;-z} = -\frac{\pi}{8\mu}\Omega\left(\frac{r_{tubes;z}^{\ 4}}{\beta l_{tube;z}}\right)_{cell}\delta P$$

$$= \frac{\pi}{8\mu}\Omega\left(\frac{r_{tube;z}^{\ 4}}{l_{tube;z}}\right)_{cell}\frac{\delta P}{\beta}$$

Equation 2.6

By considering tubes in the ± x and ± y directions as well, and comparing with the Darcy equation, it follows that

$$k = \frac{\pi}{8\beta}\Omega\left(\frac{r_{tube}^{\ 4}}{l_{tube}}\right)_{cell}\frac{l_{cell}}{A_{cell}}$$

Equation 2.7

Once this equation is corrected for the square cross-section of the pore hydraulic conductivity may be calculated (Schlicting, 1979).

2.2 Use of Pore-Cor

2.2.1 Extrapolation of Experimental Data

For Pore-Cor to generate a network covering the complete range of void sizes within a sample, the sample's water retention curve must be derived from the characteristics of the complete void-size range. In practice, this is not the case. Even at zero applied pressure, the largest, most conducting voids within a sample can drain by gravity. At the other end of the scale, the smallest pores retain residual water under the maximum practicable differential pressure of 1.5 MPa. Experimental water drainage curves therefore only sample the middle range of pore sizes, from around 0.2 to 120μm diameter. To overcome this problem, water retention curves are extrapolated from experimental data. For this investigation the van Genuchten (1980) extrapolation has been used. This has been shown to be the extrapolation that is best suited for Pore-Cor, (Peat et al., 2000). A review of the water retention models was given in Chapter 1.

The Soil Survey Land Research Centre (SSLRC), at Silsoe, undertook the experimental measurement of the water retention curves for the repacked soils used in the pit in this study. The *in situ* DeBathe soil water retention curve was derived by SSLRC at Shardlow. An average water retention curve for a sandy clay loam has been used as the best estimate of an *in situ* Teign series soil. These water retention curves are shown in Figure 2.4 below.

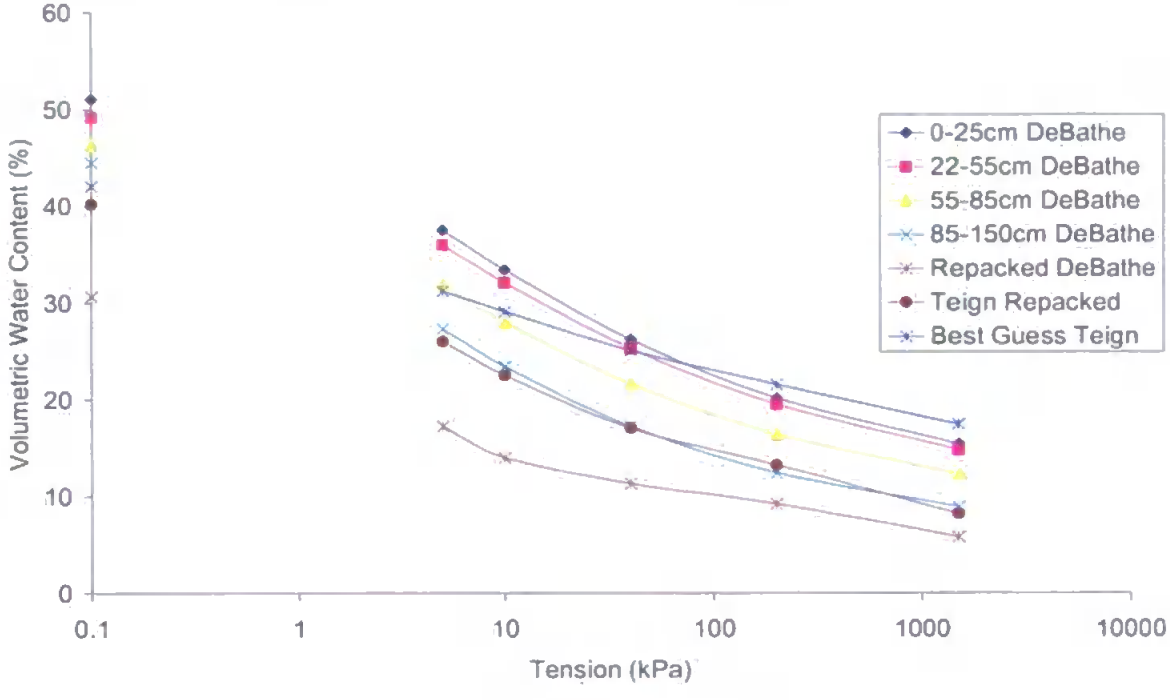

Figure 2.4 Water retention curves for the soils used in this study.

Figure 2.4 shows that the repacked soils water retention capacity is approximately one third less than the undisturbed soils. The water retention capacity is defined as the overall function of volumetric water content variation with pressure. This is also confirmed by the lower porosity of the soils. This is as a result of the repacked soils having fewer large pores than the undisturbed soils and can be demonstrated by comparing the particle size distributions that Pore-Cor produces.

The van Genuchten parameter values for the soils in this study are displayed in the table below.

Parameter	DeBathe Soil 85-150cm depth	Repacked DeBathe Soil	Repacked Teign Soil	Best Guess Teign Soil
θ_r	0.0683	0.05	0.05	0.0683
θ_s	0.445	0.307	0.402	0.4205
α / Pa	0.0009460	0.01317	0.0009463	0.002336
n	1.3648	1.45	1.45	1.188
m	0.2673	0.25798	0.2083	0.12176

Table 2.1 Fitted van Genuchten parameters for the soils in this study.

It is impossible to model the entire void size range. Consequently the data is truncated to model the void sizes between 0.2μm and 2500μm. The porosity is then reduced to take this reduction into account when using the Pore-Cor model (Peat et al., 2000).

Mercury intrusion data is used within Pore-Cor for Redhill 30 sand. This reflects the difficulties of obtaining water retention curves for Redhill 30 sand because of the speed at which the sand drains. The mercury intrusion curves were obtained using a Micromeritics Autopore III (Micromeritics, Atlanta, Georgia, U.S.). Ten runs were carried out to examine the different random packings on the apparent void size distribution and porosity. The mercury intrusion curves are shown in Figure 2.5.

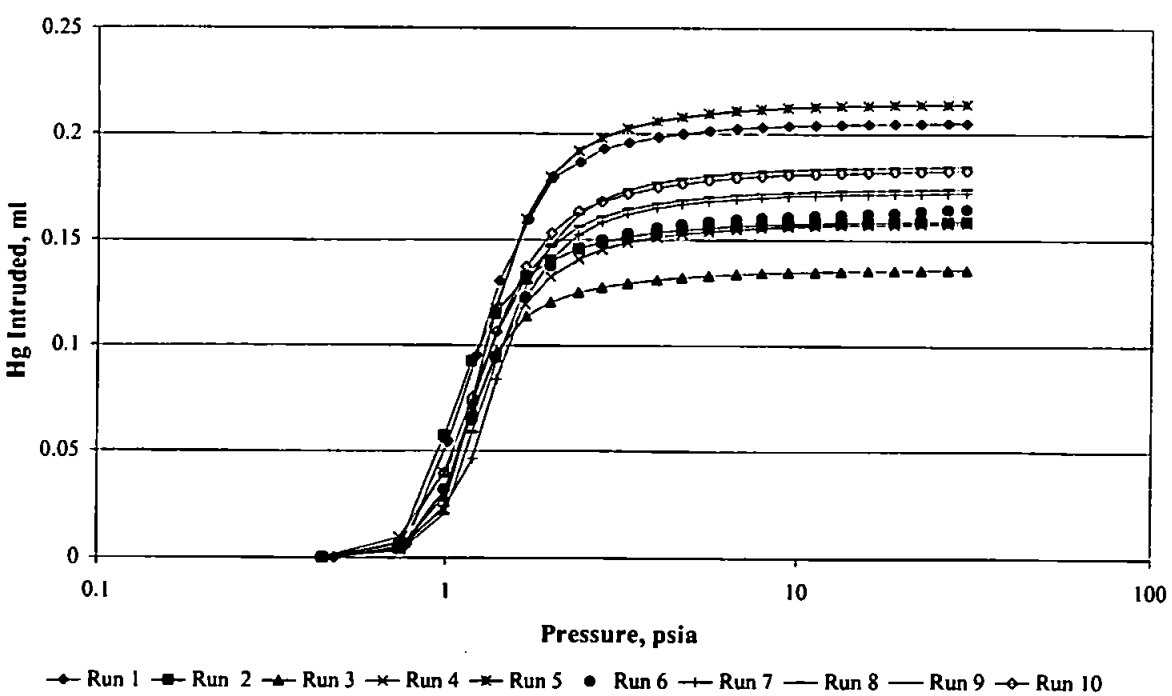

Figure 2.5 Mercury intrusion curve for Redhill 30 sand.

2.2.2 Modelling

Much of the previous work using Pore-Cor has attempted to reflect experimental variability. Pore-Cor simulations are based around the initial random positioning of throats within the 10 x 10 x 10 lattice of nodes comprising the unit cell. Different *stochastic generations*, that is different initial random arrangement of throats, of the unit cell for a given material can be thought of as equivalent to different packings of the experimental material. Each stochastic generation will have the same percolation characteristics as the experimental sample. As a result, 25 stochastic generations were created for each of the soils and sands used in this study and are presented in the following tables, (Table 2.2, Table 2.3, Table 2.4, Table 2.5, Table 2.6).

All the simulations have been carried out using a unit cell that is vertically banded with a correlation of 0.6. This has been used because it provides the best fit to the water retention data. Unit cells with both a higher and lower correlation of vertical banding or a random structure, do not produce a good fit to the experimental data. The resulting structures can be seen below in the respective tables.

Stochastic Generation	Throat Skew	Connectivity	Hydraulic conductivity, milliDarcies
1	3.0	1.01	121.15
2	3.1	1.14	1.11
3	2.9	0.91	25.22
4	3.2	1.10	184.47
5	2.8	0.93	103.66
6	2.9	1.08	5.01
7	2.9	0.98	22.98
8	2.8	0.94	40.18
9	2.9	0.98	14.71
10	3.0	1.03	52.04
11	3.0	1.07	16.40
12	2.8	0.94	9.20
13	3.0	1.18	15.21
14	2.8	1.04	9.14
15	2.7	0.92	0.955
16	2.9	0.96	34.40
17	2.9	1.10	23.15
18	3.1	1.01	78.942
19	2.9	1.24	12.62
20	3.0	1.06	5.7 0
21	3.2	1.22	3.52
22	2.7	0.98	2.60
23	3.3	1.24	10.69
24	2.7	0.81	32.00
25	3.2	1.12	14.29
		Average	**33.56**

Table 2.2 Modelling details of DeBathe repacked soil, porosity = 30.7, pore skew 12, vertical banding correlation 0.6.

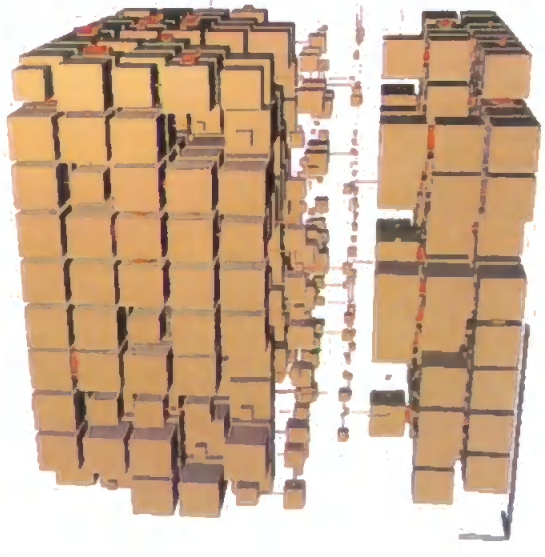

Figure 2.7 DeBathe repacked soil structure.

Stochastic Generation	Connectivity	Throat Skew	Hydraulic conductivity, milliDarcies
1	3.0	1.20	47.70
2	3.1	1.25	0.835
3	2.9	1.00	14.70
4	3.2	1.22	138.38
5	2.8	1.01	95.40
6	2.9	1.15	4.21
7	3.1	1.18	28.05
8	2.8	1.03	28.01
9	2.9	1.05	11.57
10	3.0	1.22	10.74
11	3.0	1.27	3.59
12	2.8	1.05	4.97
13	3.0	1.38	1.73
14	2.8	1.14	5.21
15	2.7	1.01	0.44
16	3.3	1.44	24.11
17	2.9	1.28	9.61
18	2.9	1.20	12.26
19	2.9	1.32	6.39
20	3.0	1.24	1.51
21	3.2	1.35	3.17
22	2.7	1.07	1.27
23	3.3	1.35	4.45
24	2.7	0.93	17.70
25	3.2	1.21	7.33
		Average	**19.33**

Table 2.3 Modelling details for DeBathe 85-150cm depth soil, porosity = 34.5%, pore skew 12, vertical banding correlation 0.6.

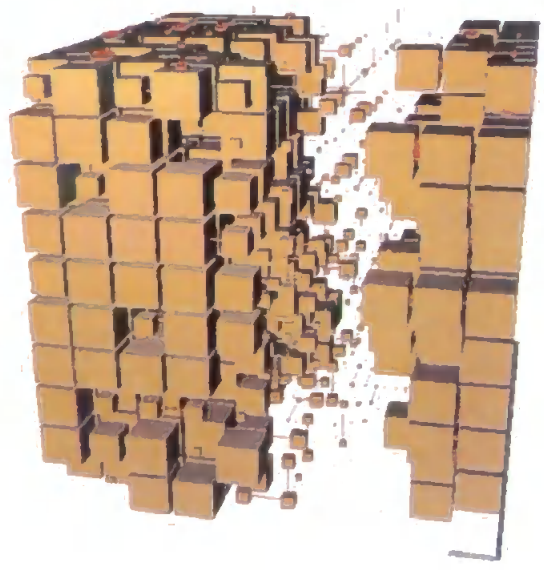

Figure 2.8 DeBathe 85-150cm depth soil structure.

Stochastic Generation	Connectivity	Throat Skew	Hydraulic conductivity, milliDarcies
1	3.0	1.25	85.68
2	2.7	1.11	21.1
3	2.9	1.05	13.23
4	2.8	1.28	0.89
5	2.8	1.06	131.52
6	2.9	1.31	5.86
7	3.3	1.30	0.45
8	2.8	1.19	11.76
9	2.9	1.10	12.53
10	3.0	1.36	4.98
11	2.7	1.03	0.0146
12	2.8	1.21	0.95
13	-	-	-
14	2.8	1.30	7.055
15	2.7	1.17	0.10
16	3.3	1.48	65.18
17	2.9	1.33	24.61
18	2.9	1.25	10.41
19	-	-	-
20	3.0	1.28	1.81
21	3.2	1.43	2.90
22	2.7	1.23	0.32
23	3.3	1.41	6.30
24	2.7	0.99	11.27
25	3.2	1.36	2.99
		Average	**18.34**

Table 2.4 Modelling details for Teign repacked soil, porosity = 40.2%, pore skew 12, vertical banding correlation 0.6.

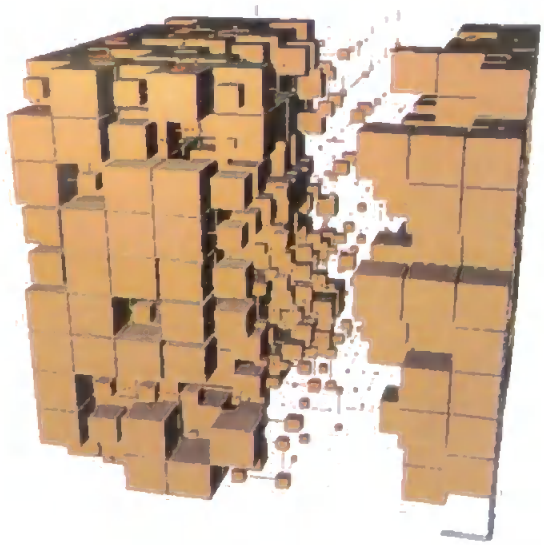

Figure 2.9 Teign repacked soil structure.

Stochastic Generation	Connectivity	Throat Skew	Hydraulic conductivity, milliDarcies
1	3.0	1.25	78.57
2	2.6	1.11	46.54
3	2.9	1.05	13.74
4	2.8	1.39	0.92
5	2.8	1.06	112.22
6	2.9	1.30	6.34
7	2.9	1.13	9.70
8	2.8	1.08	35.55
9	2.9	1.10	11.21
10	3.0	1.18	34.38
11	2.7	1.03	0.0205
12	2.8	1.11	2.91
13	3.0	1.33	11.96
14	3.0	1.10	4.39
15	2.7	1.07	0.34
16	2.9	1.08	21.15
17	2.9	1.23	25.89
18	2.9	1.25	10.11
19	2.9	1.27	15.35
20	3.0	1.18	3.94
21	3.2	1.42	6.84
22	2.9	1.03	0.56
23	3.3	1.31	10.68
24	2.7	0.99	13.82
25	3.2	1.26	6.63
		Average	**19.35**

Table 2.5Modelling details for 'Best guess Teign' soil, porosity = 42.08%, pore skew 12, vertical banding correlation 0.6.

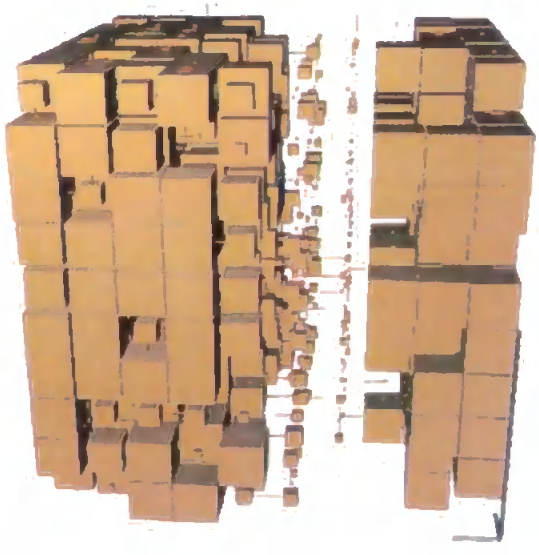

Figure 2.10 Estimate of Teign soil structure.

Stochastic Generation	Connectivity	Throat Skew	Hydraulic conductivity, milliDarcies
1	3.2	-0.1	78900
2	3.3	0.02	62494
3	3.5	0.13	58687
4	2.9	-0.12	45387
5	3.4	-0.04	102350
6	3.6	0.13	69390
7	3.1	-0.15	59698
8	3.1	-0.09	89181
9	3.1	-0.21	60196
10	3.5	0.04	89916
11	3.3	-0.06	65579
12	3.4	0	102522
13	3.4	0.07	68527
14	3.3	-0.15	62288
15	3.4	0.07	71447
16	3.4	-0.06	57054
17	3.2	-0.06	48801
18	3.5	0.03	101636
19	3.4	0.02	77006
20	3.4	0.08	96132
21	3.5	0.15	40484
22	3.5	0.07	99581
23	3.1	-0.11	50431
24	3.5	0.06	83792
25	3.3	-0.01	43171
		Average	71386

Table 2.6 Modelling details for Redhill 30 sand, porosity = 40.68%, pore skew 12, vertical banding correlation 0.6.

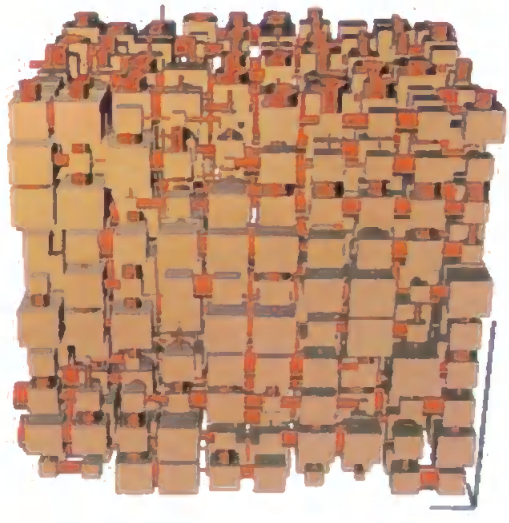

Figure 2.11 Redhill 30 sand structure

The modelled cell is then used to calculate the pore and throat size distributions. These are shown in Figure 2.12 below. These pore and throat distributions contrast markedly with the traditional Gaussian distributions centred around the characteristic throat diameter. The difference can be explained as follows (i) the inclusion of shielding / shadowing effects and (ii) the use of a full three-dimensional network, rather than the implicit parallel tube model which gives rise to the traditional Gaussian distributions.

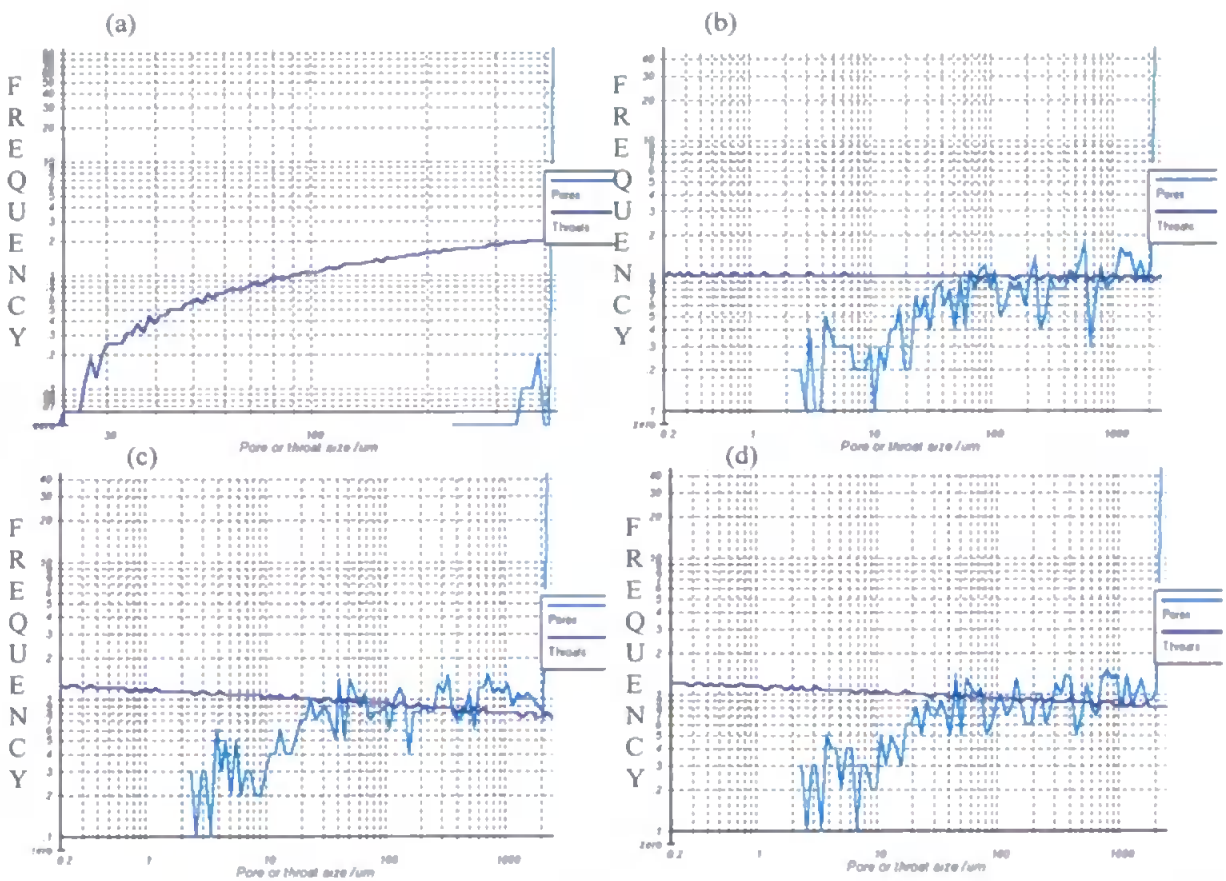

Figure 2.12 Distributions of pore and throat sizes for the optimum soil structures used in this investigation, (a) Redhill 30 sand, (b) DeBathe repacked soil, (c) Teign repacked soil, (d) DeBathe 85-150cm.

2.2.3 Hydraulic Conductivity

Table 2.2, 2.3, 2.4, 2.5 and 2.6 demonstrate that a wide range of hydraulic conductivities can be achieved from running different stochastic generations. Mathews and Matthews (1999) and Peat et al., (2000) have also noted this trend. Pore-Cor underestimates the hydraulic conductivities because it does not reproduce the complexities of the soil

structure, and the multiplicity of available flow pathways. It is possible to note the trends that occur within each stochastic generation of the hydraulic conductivity. The DeBathe 85-150cm *in situ* soil has a lower hydraulic conductivity than the repacked DeBathe soil used in the pit experiments. The converse is true for the hydraulic conductivity of the Teign repacked and best guess *in situ* Teign soil, although the difference in hydraulic conductivities is not large, 1.01 milliDarcies. This is shown in Figure 2.13. The hydraulic conductivity of Redhill 30 sand is significantly greater than that for the soils, but has been shown to be a good estimate of sand hydraulic conductivity by Mathews and Matthews (1999).

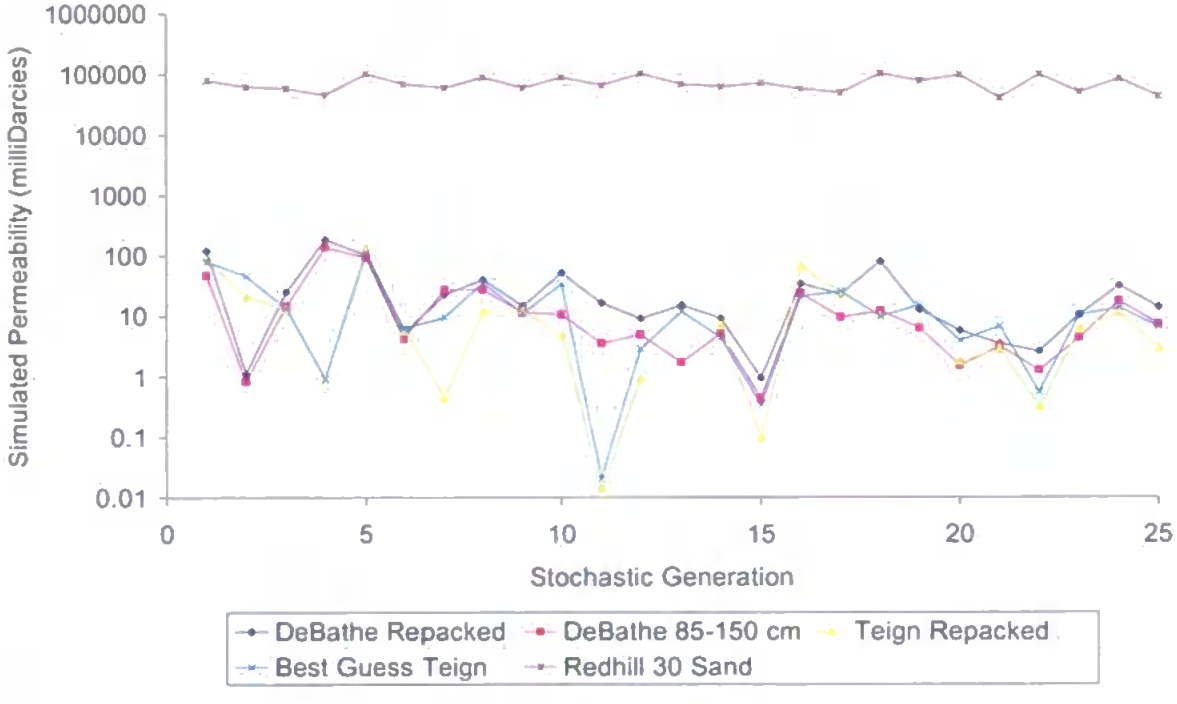

Figure 2.13 Hydraulic conductivity of the various soils, from each stochastic generation.

Peat et al. (2000) compared the hydraulic conductivity obtained from different stochastic generations of the DeBathe soil and found that the predicted hydraulic conductivities were significantly different from each other. They also noted that there was a trend with depth within all the stochastic generations, which matched the experimental trend. The repacked

DeBathe soil from this study acts similarly to that of the DeBathe soil at 85cm – 150cm depth in terms of hydraulic conductivity trends, shown in Figure 2.14 below.

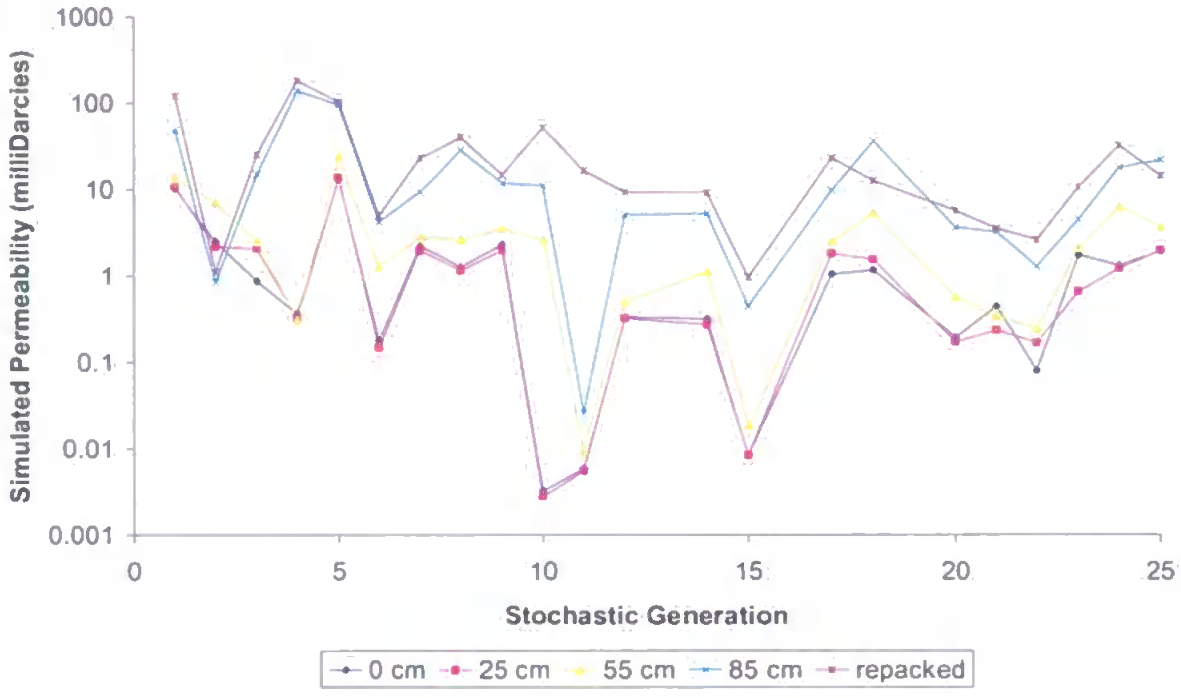

Figure 2.14 DeBathe simulated hydraulic conductivities for up to 25 stochastic generations, showing the maintenance of depth trend, despite the large variations in conductivity between the stochastic family, adapted from (Peat et al., 2000).

2.3 Oil Injection Simulation

It is possible within Pore-Cor to test the sensitivity of the overall hydraulic conductivity to oil pollution. In each case, the first stochastic generation was used to determine the size of pore that had to be blocked to affect the hydraulic conductivity of the soil, Figure 2.15. The results show that it is not possible to differentiate between the three types of sample, i.e. sand, repacked soil and undisturbed soil. This is not surprising because the water retention curves, on which the simulation is based, do not differentiate between the sands.

This is caused by the blocking of the unit cell by forcing a non-wetting substance into the structure, such as polymer, or air in the presence of water. The resulting effect is to block the larger pores and throats. The percolation algorithm is used to simulate the introduction of the non-wetting fluid into the unit cell down to a specified throat diameter. The pores

and throat that are blocked are then removed from the structure and the other Pore-Cor properties can then be recalculated. This method can also be interpreted as the invasion of the non-wetting fluid and this process can be stopped at certain stages.

This algorithm can be used in the prediction of Archies Saturation Coefficient which requires the tortuosity values at partial saturation (Archie, 1942). It can also be used for the calculation of unsaturated hydraulic conductivity in soil. However, these are both second-order effects in terms of modelling, and are limited by the relatively small size and complexity of the unit cell. Therefore the unsaturation or plugging effects are liable to impact significantly with increasing air or polymer applied pressure, and need to be studied using a series of stochastic generations.

Figure 2.15 shows that the repacked Teign soil has a very similar hydraulic conductivity when altering pore diameter as the DeBathe 85-150cm soil, reflecting the similarities between their water retention curves. However, the two repacked soils show the same trends as the undisturbed soil. The DeBathe repacked soil has a lower hydraulic conductivity barrier than the Teign repacked soil, which reflects the lower porosity of the DeBathe soil compared to Teign series soil. In the undisturbed soil this trend is expected but this has not been measured. The effect of injecting oil into the soil structure can be seen in Figure 2.16.

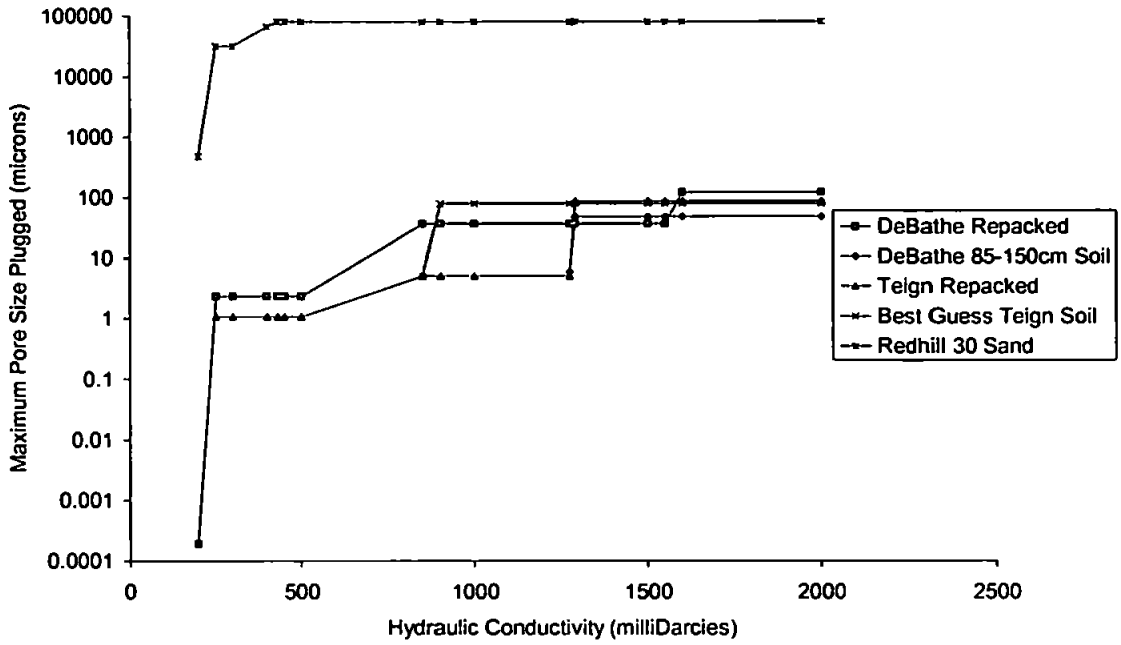

Figure 2.15 Graph showing the effects of plugging certain size pores on the hydraulic conductivity of the soils studied.

Figure 2.16a, b, c, d, e, f, g and h show that the addition of increasing amounts of oil, which prevents a few more voids from conducting water flow, can have a major impact on hydraulic conductivity without a large increase in the number of oil filled pores or voids. Figure 2.16k and j show that further additions of oil beyond a saturation point results in a substantial number of the voids being filled.

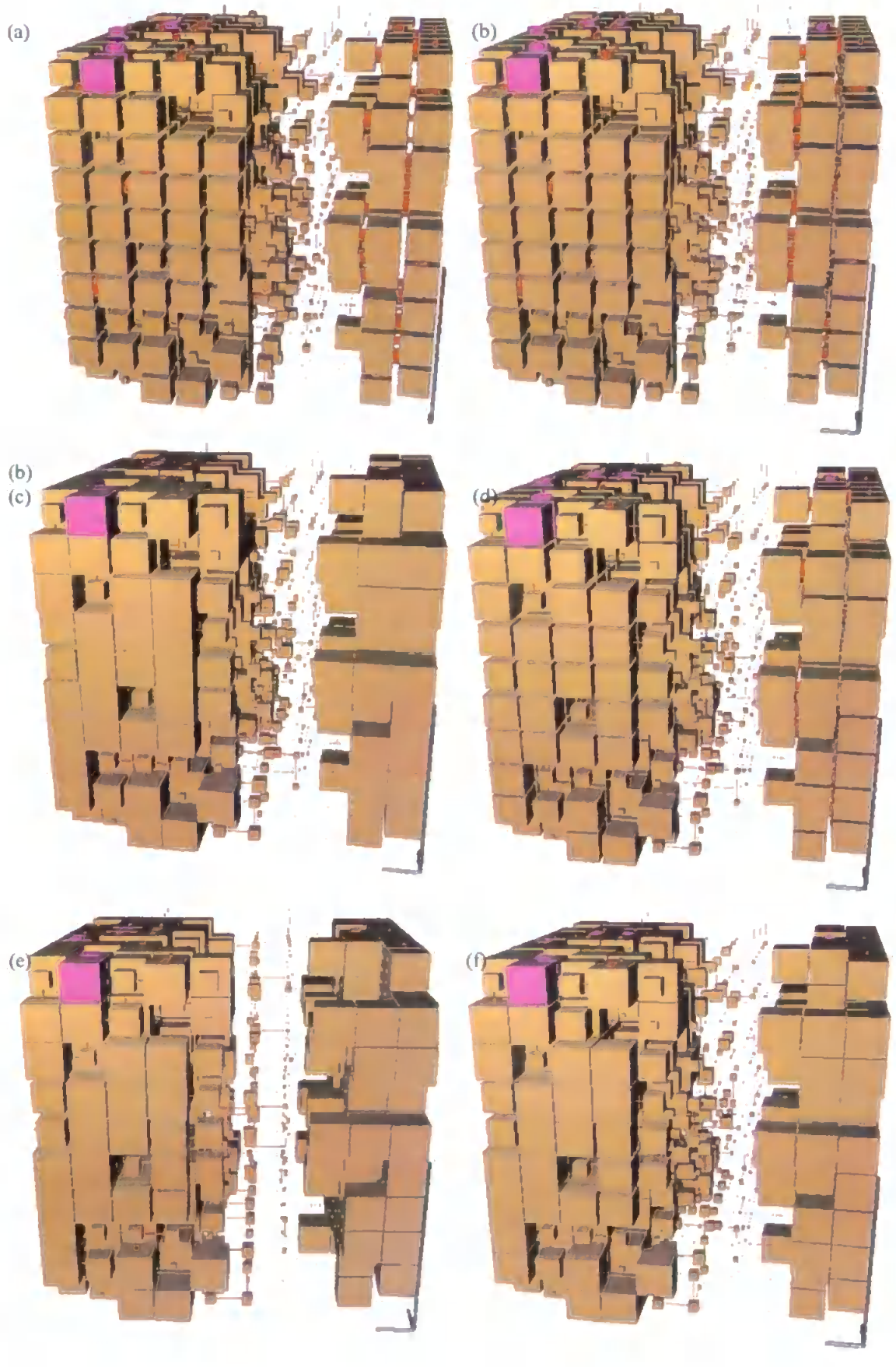

Figure 2.16 Pore-Cor soil structures for (a) DeBathe repacked soil, oil entry in pores up to 1600μm, (b) DeBathe repacked soil, oil entry in pores up to 1550μm, (c) DeBathe 85-150cm soil, oil entry in pores up to 1290μm, (d) DeBathe 85-150cm soil, oil entry in pores up to 1275μm, (e) Teign repacked soil, oil entry in pores up to 1290μm, and (f) Teign repacked soil, oil entry in pores up to 1275μm. Purple represents oil intrusion.

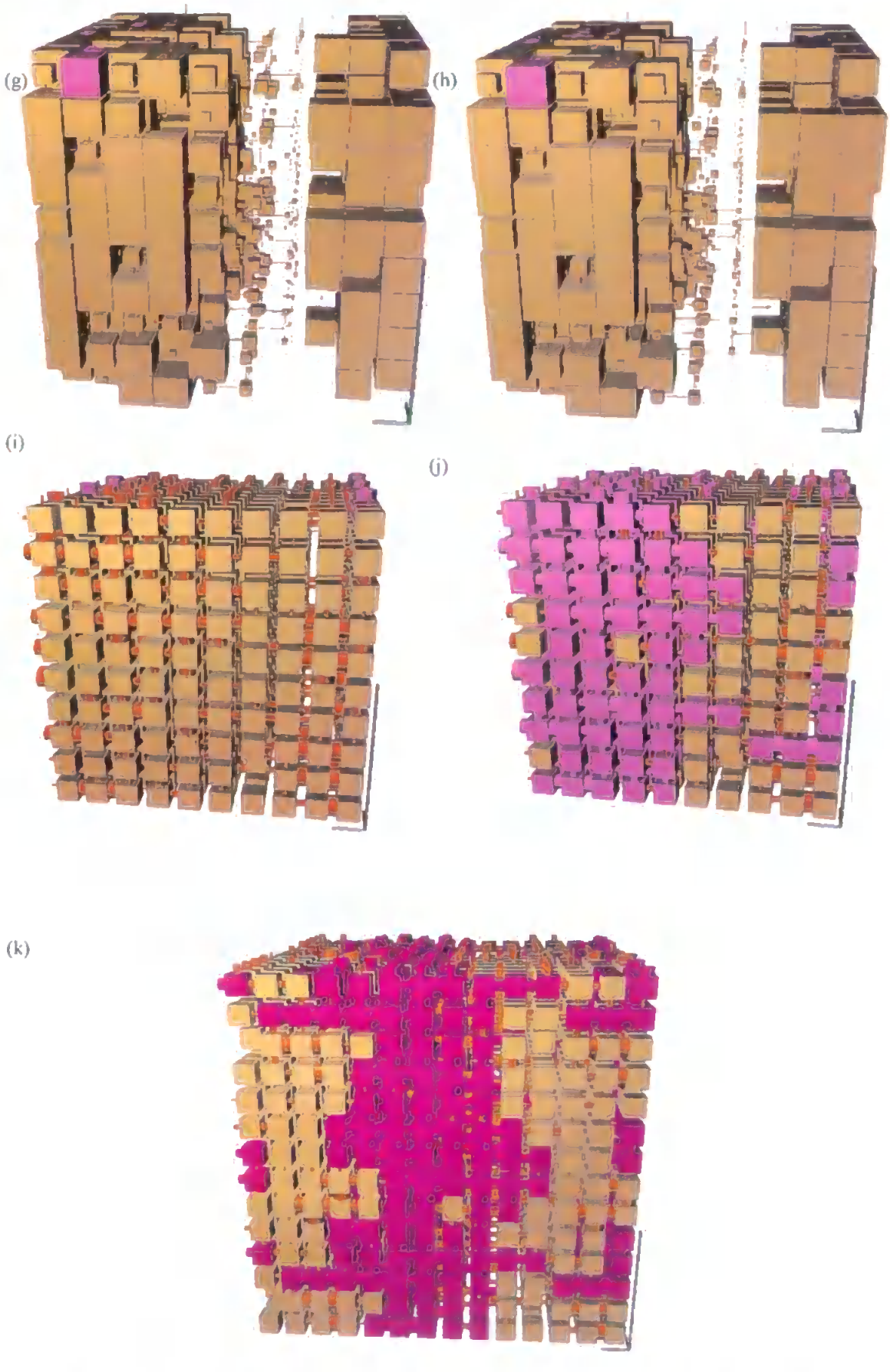

(g) Estimate of Teign soil, oil entry in pores up to 900μm, (h) Estimate of Teign soil, oil entry in pores up to 850μm, (i) Redhill 30 sand, oil entry in pores up to 400μm, (j) Redhill 30 sand oil entry in pores up to 200μm, (k) Redhill 30 sand, oil entry in pores up to 200μm with an increase in the number of voids drawn. Purple represents oil intrusion.

From Figure 2.16k it is possible to observe capillary fingering in Redhill 30 sand. The purple voids represent the oil flowing preferentially through the pore structure as demonstrated experimentally by Butts and Jensen, (1996). This demonstration of capillary fingering has been achieved by the addition of oil in the voids with sizes up to 200μm (which causes a reduction of hydraulic conductivity by two orders of magnitude) and increasing the number of voids that are shown by Pore-Cor.

2.4 Conclusions

Pore-Cor models the migration of oil through soil on three levels of increasing complexity, which we refer to as primary, secondary and tertiary.

At the primary level, Pore-Cor generates three-dimensional void structures, which have nearly the same water retention characteristics as the experimental samples. These structures are revealing in themselves, in that the closest match for all the samples is achieved by a structural array of voids – i.e. the voids are not arranged randomly, but are partially layered. Even sand Figure 2.11 has this structure, although it can be seen that the voidage covers a much narrower size range, and the structuring in the throat sizes is hidden by the many pores of similar size.

Also at this level, the Pore-Cor model gives distributions of pore and throat sizes, (Figure 2.6), that are entirely different to those based on the parallel tubes model of Figure 1.12.

Modelling at the next level of complexity is to use the generated structures to calculate simulated water hydraulic conductivity. The simulation of hydraulic conductivity gives a trend over the samples which clearly matches the experimental trend. It therefore suggests that water is flowing through the samples, much as expected – i.e. by non-turbulent

Poiseillion flow, a conclusion, which it would be impossible to make without the model.

At a higher level of complexity still, it is possible to take the simulated hydraulic conductivity and perturb it with an additional effect. Here, the results highlight the coarseness of the size scale of Pore-Cor – only 100 different sizes spread over four orders of magnitude. However, the model does reveal that within the three categories of sample (sand, undisturbed soil and repacked soil) the trends in hydraulic conductivity perturbation can be correctly predicted. That is the repacked soils are more sensitive than the undisturbed samples. However, they are not predicted from one category to another – demonstrating that surface interactions must be an important determinant of differences between types of sample. This factor can be observed by comparing the repacked Teign soil with the DeBathe 85-150cm soil, both of these have the same sensitivity to oil displacing air. This observation only applies to the perturbation of the hydraulic conductivity by oil, not the hydraulic conductivity itself.

3. Analysis of Oil in Soil

3.1 Rationale

This chapter discusses the various extraction and analytical techniques considered appropriate to establish reliable techniques for determining the quantity of cable oil in soil. The chosen techniques are then applied to the determination of cable oil in the experiments undertaken.

The analytical methods used in this study had to satisfy various criteria. In conjunction with an appropriate extraction technique, they had to quantify oil unambiguously in highly water-saturated sand, with the capability for analysis in soil. There was no requirement for a qualitative analysis, since the pollutant was known. A large number of samples were to be studied, so the method had to be relatively easy and quick. For field experiments, the method itself needed to be non-polluting. Two methods were finally chosen, namely scintillation counting of a radio-labelled analogue in the laboratory experiments, and for field experiments fluorescence spectrometry. The two methods were calibrated individually and against each other to ensure accuracy and conformity.

3.1.1 Extraction method

The reason for this choice of analytical methods partly resulted from the extraction method and solvent. Soxhlet extraction, as specified in the US Standard Methods for the Examination of Water and Wastewater (1975) and used by Joseph et al. (1994), proved to be too slow for large numbers of samples.

Accelerated Solvent Extraction (ASE) works on the same principal as Soxhlet extraction. ASE accelerates the extraction of solid matrices by using solvents at elevated temperatures and pressures. Increased temperature accelerates the extraction kinetics, while elevated

pressure keeps the solvent below its boiling point. The time taken for analysis and the level of solvent consumption are reduced compared to the Soxhlet method representing a significant advantage over the latter technique. ASE was found to be erratic, partly because of instrument parameter and operator dependence.

Sonication was initially used as the agitation method. However, parallel studies by Fu et al. (2000) showed that shaking for thirty minutes could produce equally reliable results, so later experiments used shaking only. Many of the solvents for oil, including 1,1,2-trichlorotrifluoroethane and dichloromethane, which are difficult to use for safety and environmental reasons. Therefore 1,1,2-trichlorotrifluoroethane was used initially, and for later experiments, following the findings of Fu et al. (2000), hexane was used, which was found to be give a higher fluorescence peak than dichloromethane. The use of hexane precluded any form of infra-red analysis (Cheston, 1997). Quantitative considerations regarding the chosen techniques are described in section 3.2.4, and the various techniques are described in more detail in sections below.

3.1.2 Other Techniques

A wide variety of other techniques have been used by researchers to quantify the migration of immiscible pollutants in both sand and soil with varying degrees of success. Perhaps the most commonly applied technique has been dual-gamma attenuation, (Reible et al., 1990) and (Host-Madsen and Hogh Jensen, 1992), for example to measure the saturation in a three-phase oil-air-water system (Schiegg, 1979) and (Ferrand et al., 1986). However, safety considerations prevented use of this technique in this study.

Other workers have used gas chromatography (GC) to determine the quantity of oil in soil. Zalidis et al. (1991) analysed the soluble gasoline components in leachate water, using headspace GC with a flame ionisation detector. Alternatively the sediment and fluid

sample has been washed with *iso*-propanol, and GC used on the resulting mixture, (Zhou and Blunt, 1997). GC was also rejected for the qualitative analyses in the present study, because it is a relatively slow method most suited for quantitative work over a narrow concentration range.

Other approaches have included visual inspection of the position of dyed oil, and the use of thermoprobes, which utilise the difference in thermal conductivity and heat capacity exhibited between organic liquids and water (Thomson et al., 1992). However, both techniques are unsuitable for soil studies and use in the field.

Cable oil is an organic substance and therefore the amount of cable oil in a particular sample can be determined by combustion. This is achieved by placing a small amount of pre-weighed sample inside a total organic carbon analyser and combusting it to ensure complete oxidation of the sample. The sample is then re-weighed to determine the quantity of cable oil present. Total Organic Carbon analysis is unsuitable for the quantification of oil in soil because each soil sample is unique and has a variable organic content. It is therefore not used for the sand experiments either.

A more detailed study was made of the feasibility of using FTIR, as described in section 3.4 below.

3.2 *Liquid Scintillation*

3.2.1 Principles of Scintillation Counting

A scintillator is a substance, which emits a weak light flash or scintillation, of a short duration, when struck by an ionising particle. The intensity of the scintillation depends on the energy of the particle dissipated in the scintillator. A photomultiplier tube - a device that is sensitive to weak light signals and converts them into amplified electrical pulses - is used to detect the scintillations. Figure 3.1 shows a schematic diagram of a scintillation counter.

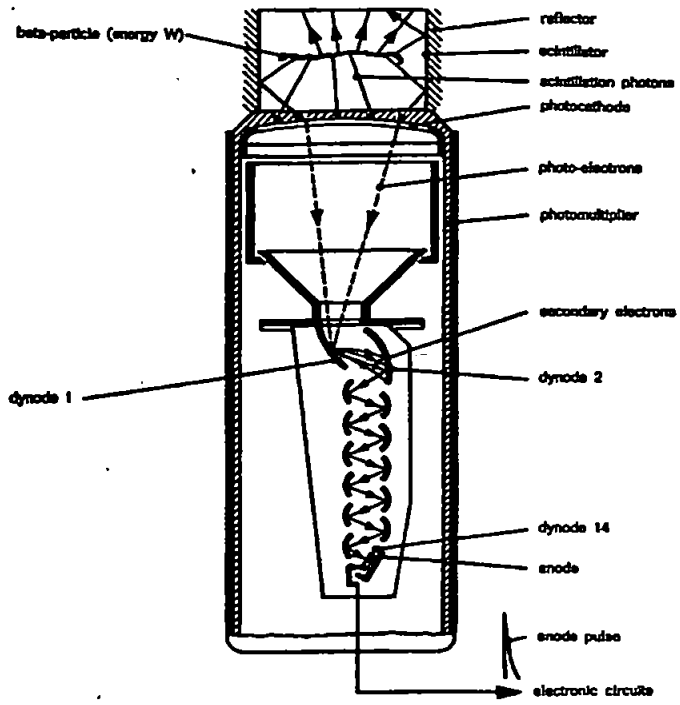

Figure 3.1 Schematic diagram of a scintillation counter showing the stages of conversion of beta-particle energy into scintillation photons, photo-electrons, secondary electrons and anode pulse, (adapted from (Birks, 1974)).

The scintillation shines on the photocathode of the tube and causes the emission of photoelectrons. These electrons are accelerated by the potential applied between the electrodes of the photomultiplier. The accelerated beam of electrons impinges on a sequence of electrodes, or dynodes, at each of which secondary electron multiplication occurs, producing successive amplification of the electron current. The overall

multiplication factor or gain M of the photomultiplier depends on the number of dynode stages and on the applied potential. The electrical pulses from the anode of the photomultiplier are fed to electronic circuits for amplification, pulse-amplitude measurement, data analysis and recording.

Where radioactive samples are used, scintillation cocktail is added to the radioactive sample to convert the energy of the radioactive decay particle into visible light. This can then be detected by the scintillation counter. The light is emitted from the liquid scintillation vial in all directions and is 'directed' into two photo-multiplier tubes that convert the light into a measurable electrical pulse.

The pulses from the photo-multiplier tube are analysed, converted into digital form and stored. The data accumulated in the multi-channel analyser over the counting time of the sample is then used to determine the Counts Per Minute (CPM), of radioactive decay in the sample. CPM is the total number of pulses in the channels of the multi-channel analyser divided by the total time in minutes for obtaining the counts. The number per minute or counting rate of the pulses is the same as that of the original scintillations detected, and this is determined by the number of Disintegrations Per Minute (DPM), or activity of the source of ionising radiation. This can then be converted into concentration by way of a calibration curve.

3.2.2 Scintillation Counter and equipment

The scintillation counter used in this study was the Beckman LS 6500 Scintillation System. This instrument is designed to provide highly accurate, automated counting of the level of radioactivity in a sample. It can hold up to 648 miniature vials at any one time. The vials used throughout this study are 6ml in volume and made of plastic with a polyethylene cap. The scintillation cocktail used for this study is Sigma-Fluor LSC Cocktail for non-aqueous

samples, (Sigma-Aldrich Company, Dorest, UK).

3.2.3 The Use of a Radio-Labelled Version of Cable Oil

In order to apply scintillation counting to the analysis of 'cable oil' concentration it was necessary to produce a radio-labelled version of cable oil. This ensured that the analysis would be compound specific.

3.2.3.1 Synthesis of Oil

A Friedel-Crafts alkylation was used to produce the radio-labelled oil.

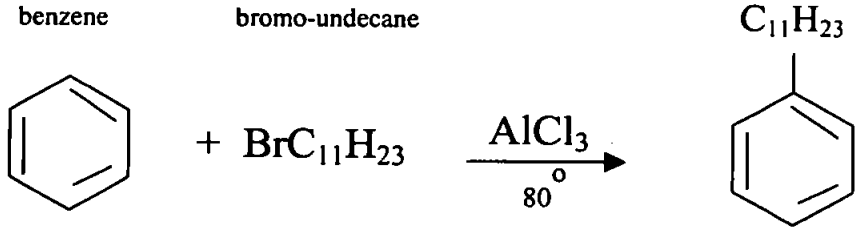

Figure 3.2 Alkylation process.

This method of synthesis utilises an alkyl halide as the alkylating agent together with a metal halide catalyst, aluminium chloride, Figure 3.2, above.

The metal-halide catalyst functions much as it does in halogenation reactions; that is, it provides a source of a positive substituting agent, which in this case is the carbonium ion. There are several factors that limit the use of the alkylation reaction. A large excess of benzene is used to limit the reaction to monosubstitution because of the introduction of one alkyl substitution that activates the ring towards another substitution. The second limitation of the reaction is the penchant for the alkylating reagent to give rearrangement products. This is actually an advantage in this study as cable oil has a range of products. The last complication of the alkylation process is that the products often isomerise. Obtaining a GC-MS of the chemical produced a check for this reaction.

3.2.3.2 Procedure for the Synthesis of Oil

A two litre three-necked flask with a seperatory funnel, a mechanical stirrer and a reflux condenser were fixed together. Attached to the top of the condenser, a tube led to an inverted funnel that dipped below the surface of 320ml of benzene (including 100μCi of ^{14}C-labelled benzene), and 8g of anhydrous aluminium chloride were placed in a flask and stirred. A mixture of 136ml of benzene and 114ml of bromo-undecane was then incorporated drop-wise into the flask. The flask was warmed to 80°C on a water bath. When this mixture had increased in weight, it was poured onto ice. Washing the mixture successively with dilute sodium hydroxide solution and water, and then drying with anhydrous magnesium sulphate, removed the upper layer of hydrocarbon. The remaining compound was distilled through a well-lagged fractioning column. The excess benzene passed over first, followed by the DDB.

3.2.3.3 Radio-labelled Cable Oil

The radio-labelled version of cable oil was analysed by GC-MS to verify that the substance produced conformed to the chemical characterisation of cable oil, (Figure 3.3). A study of the resulting compound determined that the synthesised cable oil is a close enough match to the original cable oil to be used in the analysis. The main difference between the compound shown in Figure 3.3 and the analysis of actual cable oil (Figure 1.4), is that the radio-labelled version does not have the same spread of chain lengths. The synthesised version only had C_{11} chain lengths, whilst the original, as stated in section 1.5, contained a mixture of chain lengths between C_{10} and C_{14}. However, the synthesised compound contained a mixture of both branched and linear alkyl chains, like the original.

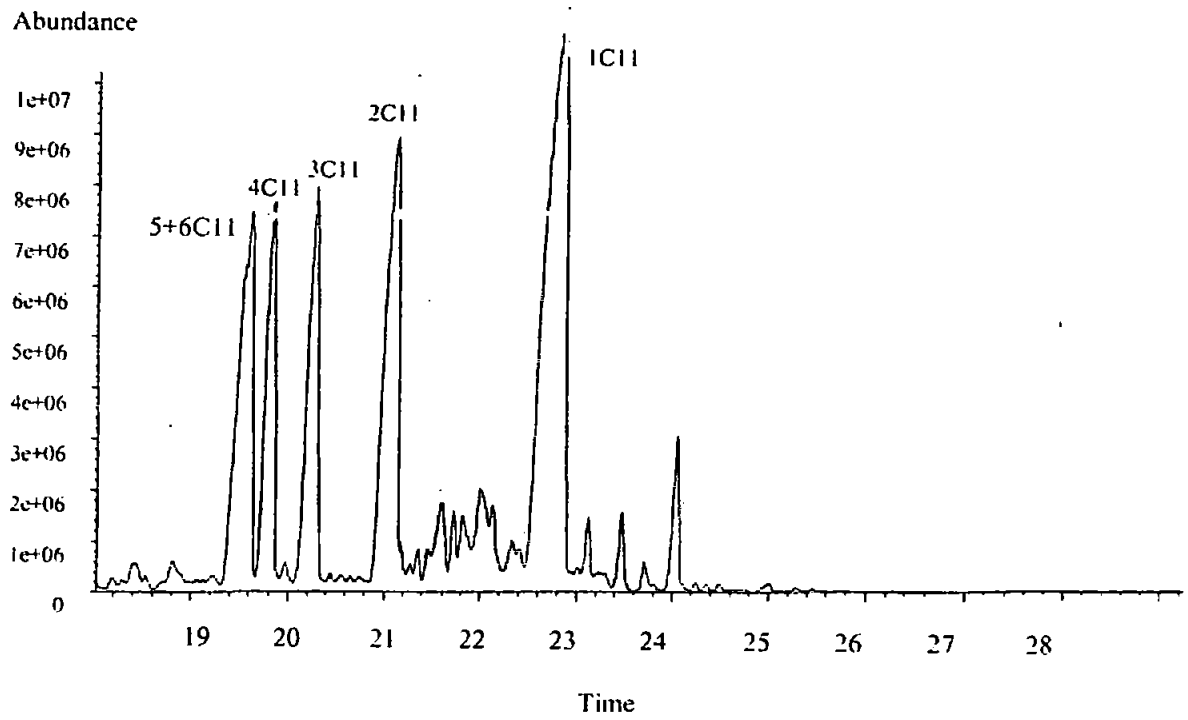

Figure 3.3 GC-MS of radio-labelled Cable Oil.

3.2.4 Solvents and Extraction Techniques

As mentioned previously, the most efficient extraction method, Soxhlet, proved too time consuming for large numbers of samples.

The second method, shaking, gave an average extraction efficiency of 49.18% and was achieved with a standard deviation of 24.83%. Although this standard deviation is high, it is nevertheless acceptable because changes were being measured in many different repeat samples, with concentrations spanning several orders of magnitude.

For sonification with hexane, the average extraction efficiency was 30.46%, with a standard deviation of 9.22%. This technique produces more reliable results than shaking, but the extraction efficiency is unacceptably low. A different solvent was used to try and overcome this difficulty. Following discussions with the NGC the solvent 1,1,2 trichlorotrifluoroethane was tested. The addition of 1ml of 1,1,2 trichlorotrifluoroethane

improved the extraction results. An average of 78.15% was extracted from the sand samples, with a standard deviation of 4.45%. This fulfilled the twin objectives of high extraction efficiency and consistency (low standard deviation). This solvent was therefore used for all the experiments in Chapter 4. However, it became increasingly difficult to obtain, due to environmental legislation, and hexane had to be used for the half-metre scale and pit experiments, (see Chapters 5, 6 and 7).

3.2.5 Calibration and Quenching

The use of the liquid scintillation counter does not specifically require calibration because the samples are compared to each other, and are measured in relation to each other in terms of DPM. Nevertheless, putting a known concentration of cable oil into the scintillation counter can be used to derive a calibration curve. Figure 3.4 shows a typical calibration curve for the scintillation counter.

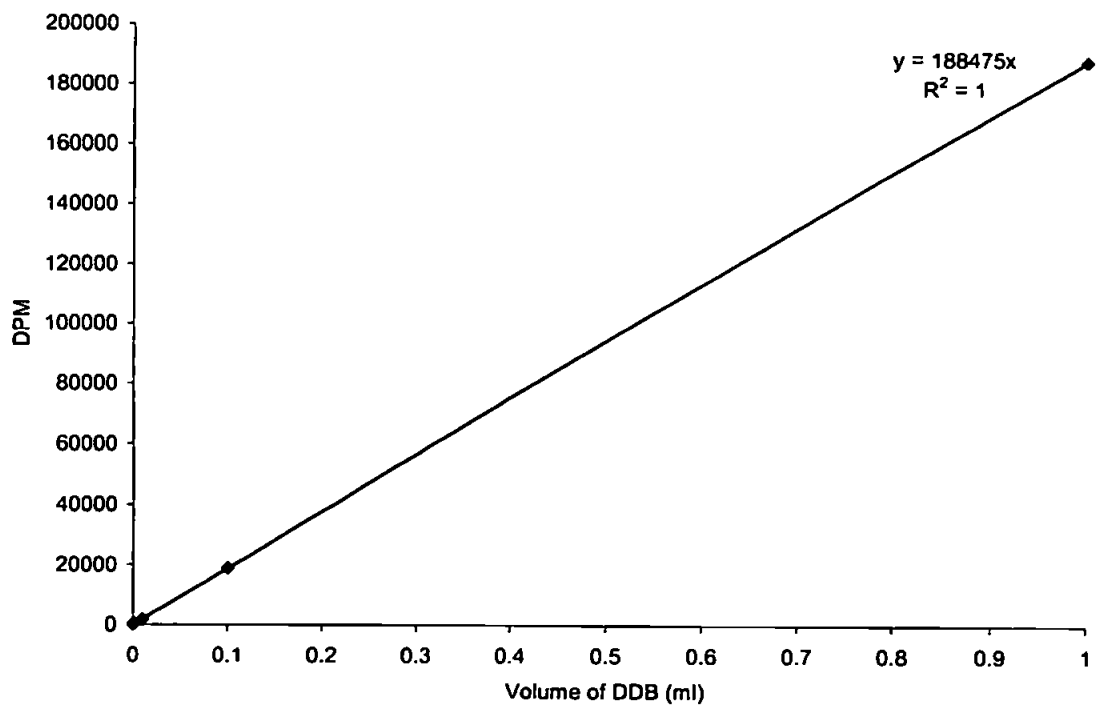

Figure 3.4 A typical calibration curve for the scintillation counter using ^{14}C cable oil.

Quenching is the reduction of the pulse voltage by material present in the sample or scintillation mixture. The scintillation counter used for this study has the ability to automatically correct for quenching. However, while using 1,1,2 trichlorotrifluoroethane the automatic quench adjustment was not sufficient to prevent a reduction in counting efficiency. In order to remedy this, a new quench curve was produced which was then used in the scintillation counter. Determination of a new quench curve involved making up a batch of standards with an equal amount of radio-labelled cable oil in each sample. The samples were run through the counter and a selection of samples whose DPM were closest together are accepted. Various amounts of quenching agent (in this case 1,1,2 trichlorotrifluoroethane) were added to the accepted samples. The samples are then run through the machine to produce a new quench curve, which relates to the 1,1,2 trichlorotrifluoroethane that is used in this study. The scintillation counter automatically produces a new quench curve that is automatically used when quench correction is required.

3.2.6 Reproducibility of Results

After testing the extraction efficiency it was necessary to test the reproducibility of results obtained from the scintillation counter. With the scintillation counter used in this study it is possible to make the same rack of samples run continuously. By doing this it is possible to determine the reproducibility. Averages of 12 samples were taken which produced a standard deviation of 1.55%.

3.3 Fluorimetry

3.3.1 Principles of Fluorimetry

Fluorescence is a physical property of certain atoms and molecules. It defines a molecule's ability to absorb light energy at one wavelength, and simultaneously re-emit light energy of another, usually longer, wavelength. The absorption of quantum light by a molecule results

in the elevation of an electron, from the molecule's ground electronic state, to one of several vibration levels in an electronic excited state. In solution, the excited state molecule rapidly relaxes to the lowest vibration level of the electronic state. The electron may return to the electronic ground state with the release of heat or with light emission (fluorescence).

Each compound that fluoresces has a characteristic excitation wavelength (the wavelength of light absorbed), and a characteristic emission wavelength, (the wavelength of light that it emits when the molecules relax and return to their ground state). Figure 3.5 shows a schematic diagram of a filter fluorometer.

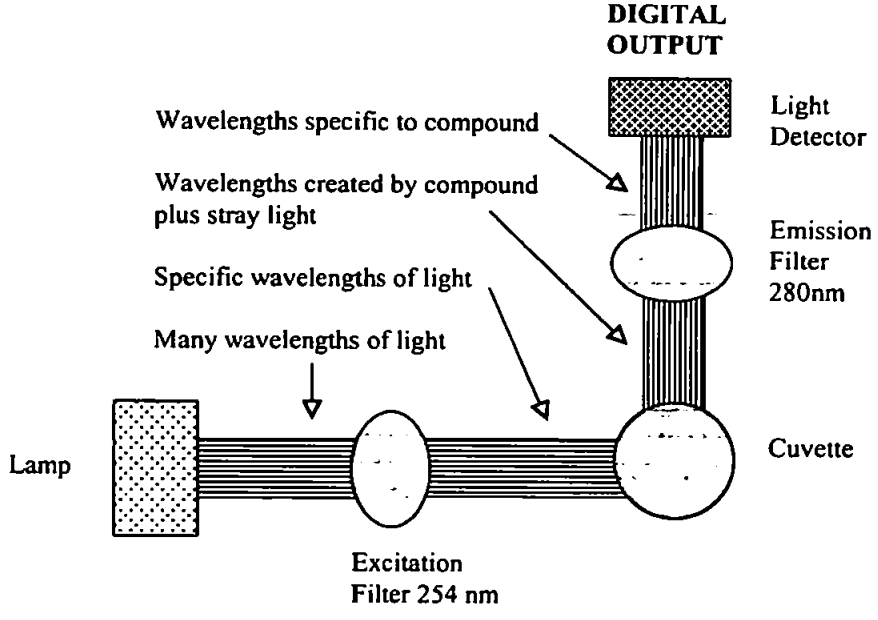

Figure 3.5 Schematic diagram of a filter fluorimetry.

The application of fluorimetry for the detection of cable oil was first demonstrated by Fu et al. (2000), who carried out a number of validation tests using spiked soil samples. Fu et al. (2000) showed that a repeatable extraction efficiency of 90% was achievable for a range of soil types using a solvent to soil ratio of 2:1 (volume : weight). They also determined that the extraction efficiency was largely independent of extraction time, although a

recommendation of 15 minutes is made.

3.3.2 Fluorometer

Fluorimetry analysis in this project was conducted using a TD-700 Fluorometer. The instrument was a compact model manufactured by Turner Designs, for the measurement of discrete samples from a wide range of fluorescent materials. When calibrated the fluorometer automatically sets the optimal sensitivity range and the range for sample measurement, giving a reading in raw fluorescence units, (fsu). The TD-700 was specifically set up to detect cable oil by changing the lamp and optical filters. An excitation filter with a wavelength of 254nm and emission filter with a 280nm wavelength were selected for cable oil analysis and a clear quartz lamp was used as a light source. The fluorometer is connected to a computer through an RS-232 serial line and the data sent in ASCII format.

3.3.3 Cuvettes

Quartz cuvettes were used to hold the extractant because of the characteristic low fluorescence background of quartz and uniformity in all four directions, through their walls. However, special care was taken to ensure that the orientation of each cuvettes remained the same when placed inside the fluorometer. After use, each cuvettes was washed at least three times in a suitable non-fluorescent purified organic solvent, in this case hexane. Where hard deposits became a problem, a solution of 50% 3N hydrochloric acid and 50% ethanol were used during cleaning. Whilst handling the cuvettes, latex gloves were worn to prevent the deposition of grease from the skin. Each cuvettes was then polished with a cleaning tissue before use.

3.3.4 Solvent

When selecting a solvent, it was necessary to identify one with high extraction efficiency and a lower fluorescence background than cable oil. Earlier research, by Fu et al. (2000)

investigated the use of both dichloromethane and hexane as potential solvents. Hexane was shown to be the preferred solvent with respect to extraction efficiency and the intensity of fluorescence.

The hexane chosen was HPLC grade due to its very low fluorescence. When excited in the range 250-750nm, it produces no fluorescence emission greater than the solvent's natural Raman signal at 350nm excitation. The maximum absorbancy of ultraviolet radiation at the wavelengths chosen as excitation and emission (254nm and 280nm) are 0.02 AU and 0.005 AU (Absorbance Units) respectively, (Fisher Chemical Catalogue, 1996). Consequently, the use of this hexane does not interfere with the measurement of fluorescence.

3.3.4.1 Solvent Extraction and Efficiency

Redhill 30 sand with known moisture content was contaminated with a known amount of cable oil. The sample was then split into smaller samples weighing approximately 10g. Hexane was added to this at a ratio of 2:1. The sample was then shaken for a period of 30 minutes, on a mechanical shaker. For the purpose of this investigation four moisture contents were studied, 0, 5, 25 and 40%. The extraction efficiencies did not vary greatly with moisture content, 89.9, 95.9, 104.1 and 82.6%. However the standard deviation varied between 24.7% and 49.0%. The variation could partly be explained by problems in the mixing and sampling from the larger sample.

Similar experiments were carried out on the two soil types (DeBathe and Teign series) used in subsequent experimentation. The DeBathe soil has an extraction efficiency of 37.21%, with a standard deviation of 3.71%. Teign series soil has an extraction efficiency of 32.98% and a standard deviation of 6.47%. The extraction efficiency levels are considerably lower for soil than for sand. However, it is not the extraction efficiency *per*

se that is of importance, but the consistency of these results, which in practice is done by using the average of three samples.

3.3.5 Calibration

The intensity of fluorescence is directly related to the concentration of material in the sample. Thus, to calibrate the fluorometer, batches of standard samples with known concentrations of cable oil were used to obtain concentration readings. By plotting these readings against the known concentration, a calibration curve was obtained. The concentration of a particular sample was then calculated by applying linear regression analysis to the calibration curve.

The direct calibration procedure on the TD-700 allowed a multi-point calibration, in which up to five standards and a blank were read. The calibration procedure automatically sets the instrument sample range (concentration range) and sensitivity was based on a chosen fluorescent standard or sample.

3.3.5.1 Standard Sample Preparation

To calibrate the fluorometer using the direct concentration calibration built into the TD-700 a number of standards were prepared using HPLC grade hexane, as previously discussed. The standards ranged from an initial blank, hexane, to a concentration (cable oil to hexane) of 10μl/ml, see Table 3.1.

Concentration (ul/ml)	Raw Fluorosence
0	0
0.013	8.705
0.07	38.25
0.1	53.95
0.3	140.2
0.5	182.3
0.8	207.6
1	261.4
1.2	271.5
1.4	274.6
1.6	279.1
1.8	251.5
2	260.6
3	219.9
4	157.7
5	125.8
6	105
7	74.02
8	51.82
9	32.64
10	34.17

Table 3.1 Calibration standard samples and raw fluorescence.

3.3.5.2 Linear Range Calibration

The linear range is the concentration range in which the readout of the fluorometer is directly proportional to the sample's concentration. The linear range for cable oil begins with the lowest detectable concentration and spans to an upper limit concentration that is dependant upon the properties of the fluorescent material, the filters used and the pathlength.

Earlier analysis by Fu et al. (2000) determined that the linear section was between 0.013µl/ml and 0.3µl/ml. The TD-700 uses this linear range to set the optimal range and sensitivity. The calibration curve for the linear range is displayed in Figure 3.6. This gives a R^2 value of 0.9995%.

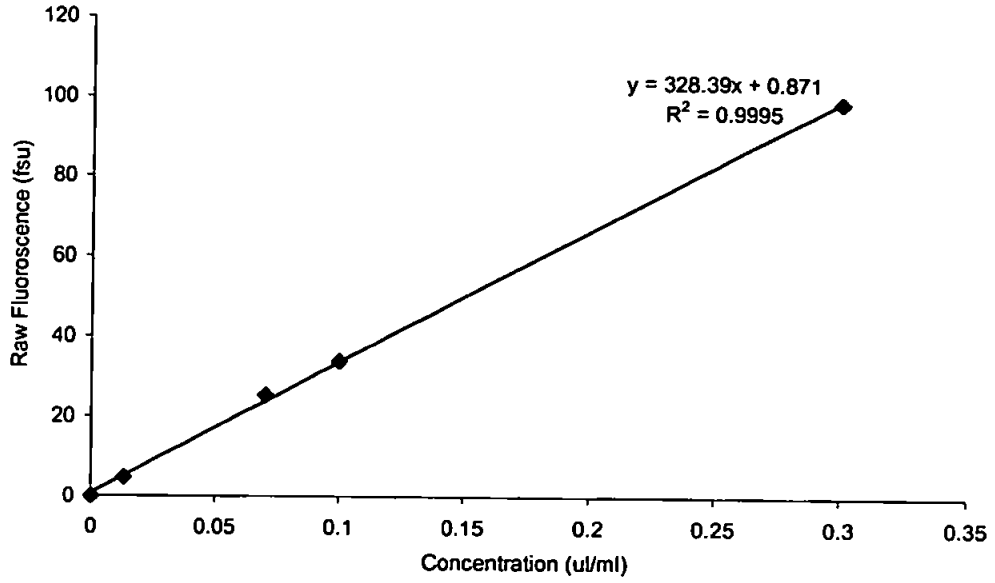

Figure 3.6 Typical linear calibration curve.

3.3.5.3 Concentration Quenching

Beyond the linear range the fluorescence reading rises at a declining rate and a calibration curve is necessary for accurate calculation. At even higher concentrations, the fluorescence begins to decrease with an increase in concentration, due to concentration quenching. The principles of fluorescence determine that the fluorescence intensity is proportional to the molecular absorptivity: the higher the absorptivity of the substance, the greater the fluorescence. However, when absorption is too high, no light can pass through the molecule to cause excitation.

At intermediate concentration ranges the light is not evenly distributed along the light path. The portion of sample nearest to the light source absorbs so much light reducing the light available for the rest of the sample solution. As a result, considerable excitation occurs at the front of the sample, but reducing the excitation, which occurs throughout the rest of the cell. The level of excitation at these intermediate concentration ranges is inversely proportional to the distance from the light source and this results in the characteristic 'n' shaped curve seen below in Figure 3.7.

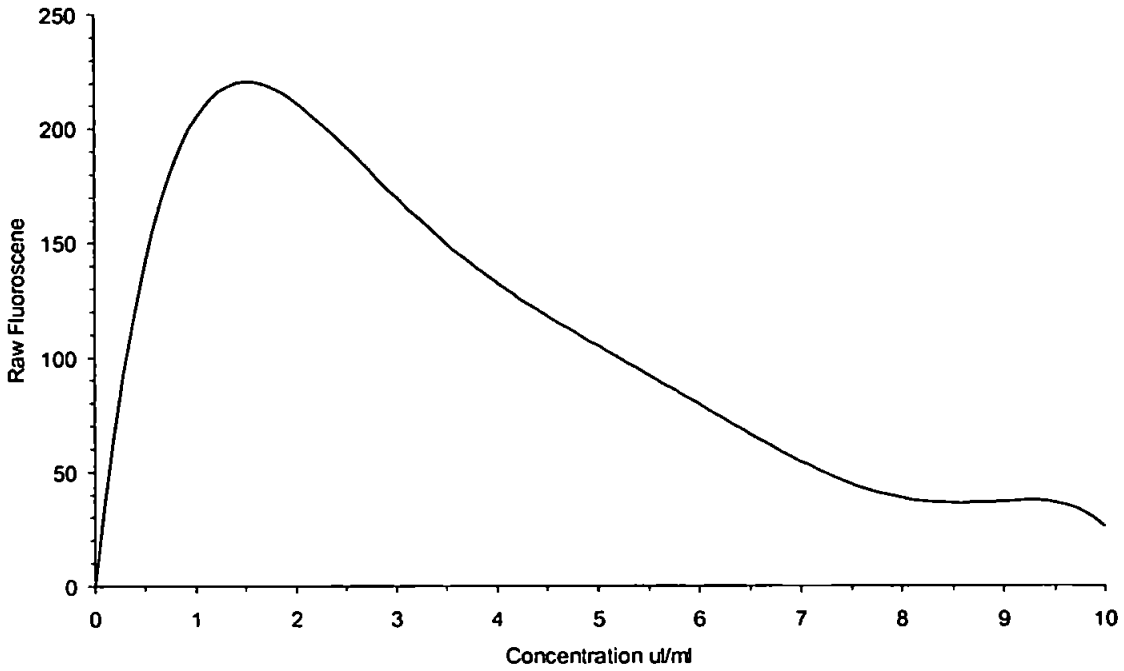

Figure 3.7 A typical calibration curve obtained for cable oil.

3.3.5.3.1 Determination of Concentration Quenching

The high likelihood of concentration quenching made it necessary to measure the fluorescence of the extractant at several different dilution ratios, 1:30, 1:300, 1:600, and 1:1500. When the fluorescence of the pure extract was found to be very low or near zero, the sample was spiked using 100µl of 1µl/ml DDB in a solution of hexane. If no significant increase in the fluorescence reading was detected, concentration quenching had occurred and further dilutions were required.

3.3.6 Calculation of Cable Oil Concentration

The concentration of cable oil in the soil samples were calculated using the equation,

$$Cs = \frac{Ce \times D \times V \times G}{M \times E}$$

Equation 3.1

where, *Cs* is the cable oil concentration in the solid sample in ppm, *Ce* is the cable oil concentration in the sample extract from the fluorometer reading in µl/ml, *D* is the applied

dilution ratio, V is the volume of solvent used in the dilution, G is the specific gravity of cable oil at 20°C, M is the mass of the sample, and E is the extraction efficiency.

3.4 Infra-Red Spectrophotometry

3.4.1 Principle

The infra-red region of the electromagnetic spectrum is subdivided into several regions. One of these regions, with wavelength in the range 2.5 – 20μm, induces vibrations involving a change in dipole movement. Thus infra-red spectra are specific to particular molecules and allow them to be identified. In Fourier Transform Infra-Red Spectroscopy (FTIR) a time-varying pulsed beam of infra-red energy with a constant frequency is passed through the sample. Fourier transform mathematics transfers the transmitted radiation intensity from the time domain into the frequency domain.

3.4.2 Previous Studies

Two preceding studies have attempted to quantify the cable oil content in soil using FTIR spectroscopy. The first study conducted by Nichols (1996) used the solvent 1,1,2 trichlorotrifluoroethane. This solvent was chosen for its ability to extract cable oil from the soil and because it does not absorb in the infra-red. However, this chemical has since been banned from use under the Montreal protocol. As a result, an alternative solvent, carbon tetrachloride was studied by Cheston (1997), which also does not absorb in the infra-red. However, the results for this solvent show large discrepancies. Cheston (1997) duplicated each sample, and discovered a wide range of results from the same sample, (Figure 3.8).

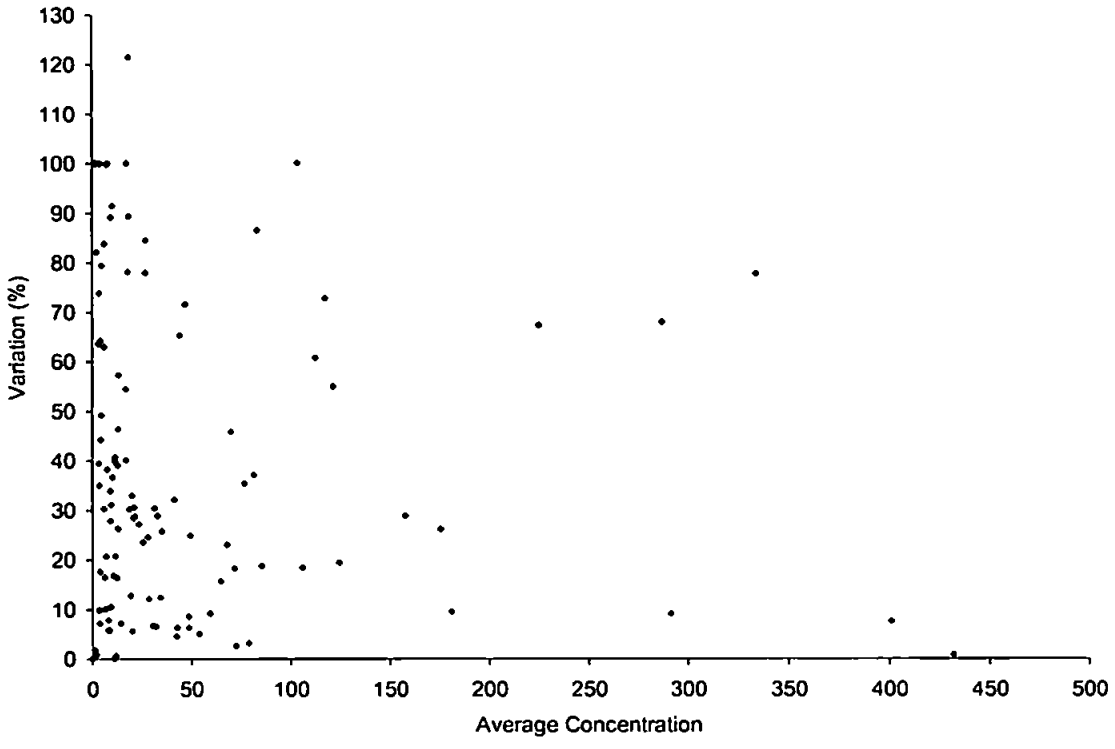

Figure 3.8 Percentage variation in results from using carbontetrachloride as an extract solvent and using FTIR as the analysis method, Cheston, (1997)

3.4.3 Fourier Transform Infra-Red Spectrometer

It was decided to test whether the results of Cheston (1997) could be improved upon. To carry out the test, a Philips PU9600 Fourier Transform Infra-Red Spectrometer (FTIR) was used for analysis. The instrument uses a Helium-Neon laser energy source of 632.8nm at a nominal 2mW. Table 3.2 lists the settings that were used during the operation of FTIR throughout this investigation.

Highest wavenumber	3200 cm^{-1}
Lowest wavenumber	2500 cm^{-1}
Resolution	1.5 cm^{-1}
Number of scans	32

Table 3.2 FTIR Settings.

3.4.4 Equipment and Operation

Standard quartz cuvettes with a 10mm pathway were used to contain the sample. Gloves were worn at all times whilst handling the cuvettes to prevent the deposition of grease from

the skin. Each cuvette was cleaned and polished before use, to decrease the possibility of contamination and interference.

The solvent used for this investigation was carbon tetrachloride because of the unsuitability of 1,1,2 trichlorotrifluoroethane used during the initial investigation. As with the other extractions, solvent was added at a 1:2 soil to solvent ratio, and shaken for 30 minutes. Quantities of solvent extract were then pipetted into the quartz cuvettes for subsequent analysis.

A calibration curve was produced at an absorbance value of 2930cm^{-1}, which represents the peak absorbance for $CH_2 - CH_3$ groups. This is based on work by Nichols (1996) which demonstrated that the gradient of this curve permitted better precision at lower concentrations and was virtually linear in the range of 0 - 0.1% (R^2 of 0.9948). The high R^2 suggests that interpolation over this range is valid. However, it became evident, from running the standards, that this method produced results which were as unreliable as those in Cheston (1997). The standards gave results with at best a variation of 16.4%.

3.5 Round-Robin

As described above, a wide variety of methods of extraction and analysis have been considered for use in the experimentation. In order to clarify which method would be most suitable to the analysis, a series of 'round-robin' tests were conducted in collaboration with NGC, University of Southampton and Cranfield University. Table 3.3 shows the results of these tests. The samples were all prepared using a known weight of dry sand, to which was added a known volume of water. A quantity of cable oil was added to provide a concentration of 1000ppm for each sample. These samples were then extracted using the various solvents and extraction methods.

Unfortunately it was not possible to compare the results from the scintillation counter at this stage because of the problems that would result in using the radio-labelled compound, at a number of different institutions.

A comparison of the results from the 'round-robin' analysis clearly demonstrates the variations in the results produced by the alternative techniques. FTIR produced the lowest extraction efficiency at 17.3%, combined with a large percentage standard deviation of 44.49%. The application of ASE instead of shaking raises the extraction efficiency to almost 100%, but with a high standard deviation of 35.9%.

The limited numbers of samples run under the TOC method does not permit a complete analysis of those results, although some, broad conclusions can be drawn. In general, TOC is a valid method of analysis. However, the samples chosen in this particular part of the study are limited to sand, whereas the technique also has to be applied to soil. Soil, by its very nature, contains varying amount of organic matter, which would also be combusted. This would impact on the reliability of the results.

The GC analysis also shows signs of inconsistencies. The use of ASE does not appear to benefit the extraction efficiency, but increases the variation in the results as demonstrated by high standard deviations.

Table 3.3 Round-robin results. (Hex = Hexane; 1,1,2 = 1,1,2 trichlorotrifluoethane).

Method	Fluor	Fluoro	FTIR	FTIR	FTIR	GC	GC	TOC	FTIR	FTIR	Fluoro	GC	Fluoro	GC
Solvent	*Hex*	*Hex*	*1,1,2*	*1,1,2*	*CCl_4*	*Hex*	*Hex*		*1,1,2*	*1,1,2*	*Hex*	*Hex*	*Hex*	*Hex*
Extact	Shake	ASE	Shake	ASE	Shake	Shake	ASE		Shake	Shake	Shake	Shake	ASE	ASE
	738.2	667	149.4	862.7	122.4	299.4	325	270.4	178	328	407	762.7	3228.5	650.0
	7389	674	179.3	854.7	141.9	451.8	611	271.1	208	300	452	508.8	2179	604.3
	796.8	662	0	1810.1	130.1	543.3	352.5	285	240	300	407	674.1	1477.5	717.7
	796.8	-	117	1215	140.5	-	-	379.1	-	-	368	594.6	1105	291.5
	796.8	-	164.7	1140	148.9	-	-	-	-	-	377	576	1099	210.9
	738	-	-	1216	126.7	-	-	-	-	-	391	752.6	1149	155.6
	738	-	-	810	130.4	-	-	-	-	-	397	596.3	1619	239.8
	-	-	-	560	184.9	-	-	-	-	-	415.5	127.1	-	159.3
Mean	**763.2**	**667.67**	**122.08**	**1058.5**	**140.73**	**431.5**	**429.5**	**301.4**	**208.67**	**309.33**	**401.81**	**574.02**	**1693.0**	**378.6**
% S.D.	**4.11**	**0.90**	**59.02**	**35.90**	**14.14**	**28.55**	**36.74**	**17.33**	**14.86**	**5.22**	**6.42**	**34.99**	**45.97**	**62.53**

The results from the fluorometer show a low standard deviation of 4%. However, further analysis of these results shows some divergence in the extraction efficiencies in this trial. This was not experienced in other extraction efficiency determination, as demonstrated in section 3.3.4.1. For the fluorimetry analysis the use of ASE as the extraction method does not increase the extraction efficiency, but in some cases benefits the variability by reducing the standard deviation. It is the low variation between samples from the different batches that make the fluorometer a preferred method for analysis by comparison to the other techniques considered in this study.

3.6 Comparison of Techniques

The techniques have various advantages from an analytical perspective. However, a low standard deviation between samples is a key criterion to ensure reliability in the results produced. Table 3.4 compares the advantages and disadvantages of the various analytical techniques. Table 3.5 compares the advantages and disadvantages of the various extraction methods.

Technique	Advantages	Disadvantages
Liquid Scintillation Counting	Specific to DDB, Quick, Small standard deviation in results	Uses ^{14}C.
Fluorimetry	Quick, Small standard deviation in results	Uses a large volume of solvent
FTIR	Low Extraction	Large deviation in results
GC	Highly accurate, Qualitative analysis	No direct method on quantification
TOC	Requires no solvent extraction	Does not work on soils

Table 3.4 Advantages and Disadvantages of the different techniques used for the analysis of oil in soil.

Technique	Advantages	Disadvantages
Soxhlet	General high extraction efficiency	Takes a long time
ASE	High extraction efficiency	Costly, High standard deviation
Shaking	Quick	Reasonable extraction efficiency (lower than ASE and Soxhlet)
Sonification	Fairy quick	Reasonable extraction efficiency (lower than ASE and Soxhlet)

Table 3.5 Advantages and disadvantages of the variation of the various extraction methods.

From the above analysis, fluorimetry and use of the scintillation counter were chosen as the methods to be used for the analysis of cable oil content in sand and soil throughout this study. The two techniques were found to be comparable in terms of the determination of cable oil in sand and soil, while having low variations in the results and therefore achieving the desired consistency of results.

Figure 3.9 plots the comparison of the derived concentration using both the fluorometer and the scintillation counter. The graph indicates that both methods are probably valid and can be interpolated over a wide range of samples. The techniques demonstrate both reasonable extraction efficiencies, (when hexane shaking is applied) combined with a low standard deviation.

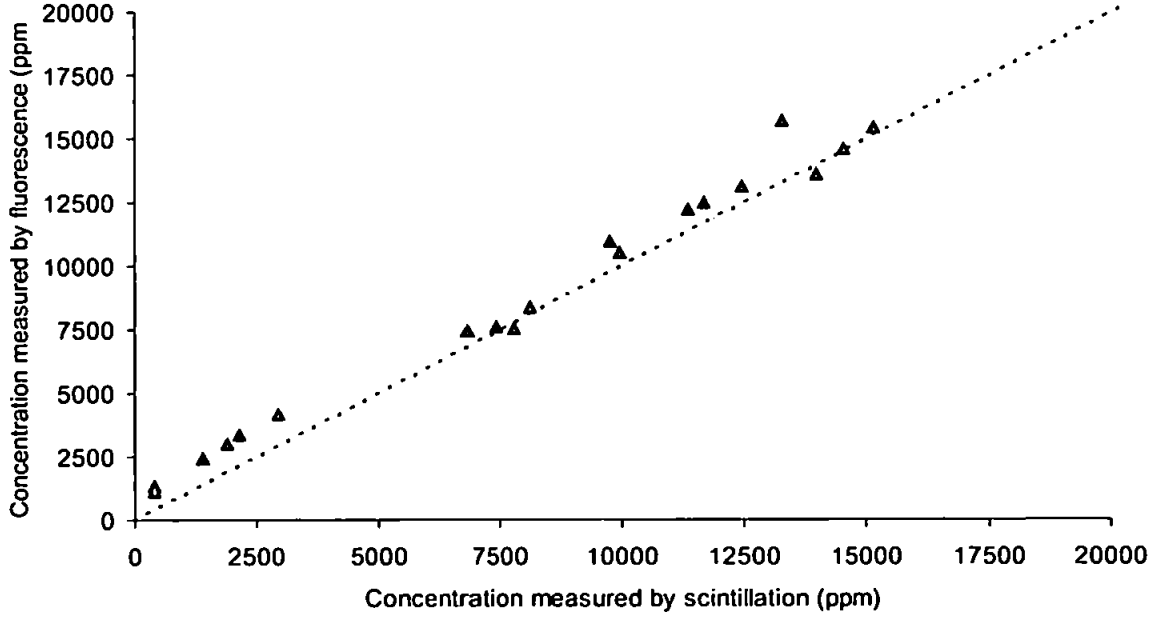

Figure 3.9 Comparison of the concentration in ppm from hexane extracts, by the techniques of scintillation counting and fluorimetry.

4. One - Dimensional Core Study

4.1 Introduction

This chapter aims to enhance the understanding of the migration of cable oil in columns of soil. The migration is measured as a function of depth down the vertical column. No lateral spread is measured, and the migration is therefore considered to be one-dimensional. This investigation provides further empirical support for the work of Joseph et al. (1994) by applying their work on oil loading in soils to the analysis of sand columns. Furthermore, the experiments examine the impact of altering the permeability of the sand on the migration of oil.

4.2 Concept and design of the oil flow experiments

The column flow experiments were designed to test and extend what is already known about the flow of oil in porous media, and to provide the foundation for experiments on a larger scale. Firstly, one must bear in mind the prediction, described in Section 1.8, that the flow will lie between the regions of viscous fingering, capillary fingering and stable front displacement (Lenormand et al., 1988). In practice, this would result in a mixed flow pattern, differing according to local variations of the structure of the solid phase and its degree of saturation. This situation is unpredictable, and liable to lead to concentrations removed from the main input concentration, which have appeared through local fingering followed by a zone of stable displacement. We have given a new name to this secondary concentration of oil, namely a *glomus*. (Glomus is from the Latin for a ball, and is the root of the word agglomerate - strictly speaking its plural should be glomeres.)

The glomus defines a zone of oil concentration within which the partial fingering behaviour occurs. The fingering can occur in all directions, even back towards the source, as seen by Lenormand et al. (1988) in their simulations. Therefore, this random behaviour

will distribute itself in a way analogous to diffusion. Diffusion can be described mathematically by error functions, and leads to Gaussian distributions. Consequently the boundary of the glomus is defined as Gaussian. In three dimensions, the glomus is therefore defined as an envelope of oil concentration approximated as Gaussian at whatever scale one is observing it, from the pore-level scale upwards to metres or even kilometres. It is recognised that a glomus at a large scale is likely to be an envelope of smaller glomuses acting in concert - i.e. there will be fractal-like structure to the glomus. In practice, the distribution of oil will be much less predictable than the distributions obtained in diffusion experiments, and the actual distribution will not be Gaussian. However, the Gaussian glomus provides a useful and simple representation of a stable displacement envelope from which further fingers may extend.

We also assume that the high concentration of oil at the injection point is in the form of a *source glomus*, although in practice the oil may pool and not act in the expected way. In one-dimension, as studied here, the glomus becomes a Gaussian function of the distance x from the point of application:

$$\text{oil concentration} = a.\exp\left(-0.5\left[\frac{x-b}{c}\right]^2\right)$$

Equation 4.1

where a is the amplitude (or maximum concentration) of the source glomus, b is the position of centre of the glomus with respect to depth (in this case at the point of injection, so that $b = 0$) and c is the standard deviation or width of the data in terms of sampling distance.

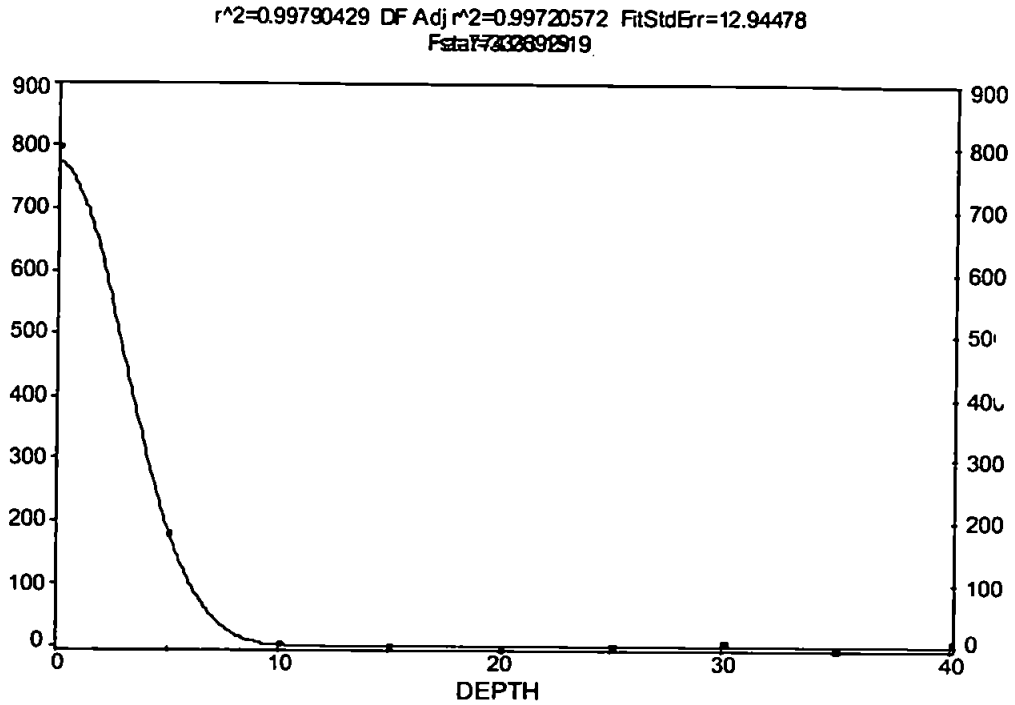

Figure 4.1 Source glomus equation fitting on column q

If a secondary glomus is formed away from the source glomus, a second Gaussian feature will be formed in one dimension. We now postulate the possibility of the formation of a secondary glomus. This might be caused by one of the fingering flow channels (e.g. as shown in Figure 1.11), encountering a barrier of reduced permeability. The permeability reduction might be caused by soil heterogeneity, such as an area of denser packing, increased clay content, or a zone of increased water saturation. The equation describing both the primary and secondary glomus now becomes:

$$\text{oil concentration} = a\exp\left(-0.5\left[\frac{x-b}{c}\right]^2\right)+d\exp\left(-0.5\left[\frac{x-e}{f}\right]^2\right)$$

Equation 4.2

where d is amplitude (or maximum concentration) of the secondary glomus, e is the position of the centre of the secondary glomus with respect to depth and f is width of the data in terms of sampling position.

The migration of immiscible oil is not diffusive, and there is therefore no *a priori* reason to suppose that the envelope of the main oil distribution zones will be Gaussian. The

mathematical definition of a glomus provides a framework for modelling the movement of the oil ganglia, and the actual movement can be interpreted in terms of agreement or disagreement to the glomus hypothesis. The glomus is not a continuous blob of liquid oil, but has a fine structure composed of numerous ganglia or capillary or viscous fingers, as described by other researchers, see Section 1.6 and 1.8.

In practice, the incomplete saturation of the sand sample, and adsorption or absorption of the oil and water onto or into the sand particles, will cause effects other than those of glomuses. The lack of saturation may lead to sand particles that are not fully coated with water, whereupon the oil can adsorb or absorb into the particles. This would lead to a stationary fraction of the oil. Flowing water moving past the particles could only move the oil by transporting the small partition of the oil that is in the aqueous phase. This effect would be most evident at high levels of oil loading.

With these effects in mind, two sets of experiments were performed. The first was at low loading, to determine whether the oil was essentially stationary under these conditions, and whether oil could be moved by flowing water. The second set was conducted at high loading, to test and characterise the idea of a glomus.

4.3 Materials and Method

4.3.1 Aims

The experiments were designed to test the analytical methods, rather than observing changes of flow as a function of saturation. This was accomplished to get a broad idea of the effect of oil loading under partially saturated conditions.

4.3.2 Overall Layout and Apparatus

The apparatus consisted of a 68mm internal diameter plastic pipe, of varying length, Table 4.2. The diameter of the column had to be small enough to ensure that fluid flow was uniform and predominantly parallel to the longitudinal axis of the column. A nylon mesh was attached to the bottom of the pipe to prevent the sample from falling out of the base of the pipe. The pipe was raised off the surface of the bench by means of a clamp stand, allowing the sample to drain freely from the base. Figure 4.2 shows the experimental set-up for the one-dimensional experiments. This arrangement allows the tube to gravity drain at the bottom, although it should be noted that this results in a saturation profile, which is not constant.

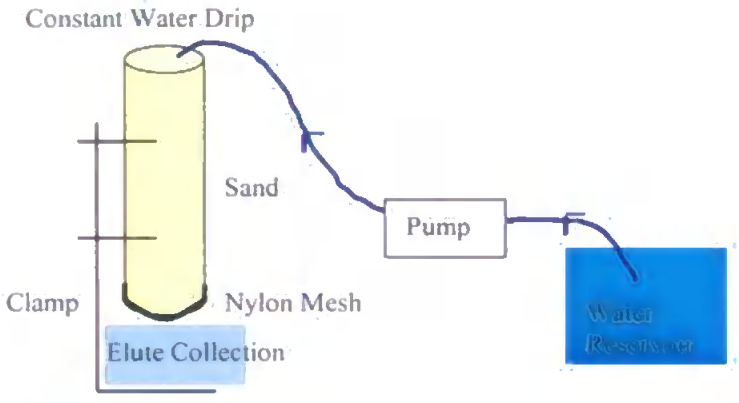

Figure 4.2 Set-up for sand column experiments.

4.3.3 Sand Characteristics

The choice of sample was important, to ensure that the sample had maximum homogeneity, without being unrealistically ordered. These criteria led to the choice of unconsolidated sand, which represents a state between the disordered, highly heterogeneous structure of a more natural medium such as soil and the artificial homogeneity of a medium such as an array of glass beads.

Three sands were used throughout this investigation, Redhill HH, Redhill 30 and Redhill 65 (Hepworth Minerals and Chemicals, Sandbach, Cheshire, U.K.). All three sands are

Lower Green Sand, a deltaic deposit of the Cretaceous period, with sub-rounded grain shape. They comprise >98.3% SiO_2, the major impurity being Al_2O_3, and up to 0.1% loss on ignition. The solid particle density of all three sands was 2650 kgm^{-3}, and the loose bulk densities were 1560 kgm^{-3} for Redhill 30, 1430 kgm^{-3} for Redhill 65 and 1350 kgm^{-3} for Redhill HH, as measured by the supplier. The particle size distribution is given in Table 4.1.

Minimum of diameter range, μm	Redhill 30	Redhill 65	Redhill HH
0	0	0.1	51.3
63	0	0.4	29.1
90	0.1	3	13.4
125	0.4	17.1	5.0
180	2.1	37.7	0.7
250	19.3	33.8	0.3
355	47.5	7.5	0.2
500	27.5	0.3	0
710	3.0	0.1	0
1000	0.1	0	0
1410	0	0	0
2000	0	0	0

Table 4.1 Particle size distributions as supplied.

Mercury porosimetry was used to calculate the porosities of the samples. Averages of the results for 10 samples gave the porosity of Redhill 30 sand as 40.68%, with a standard deviation (SD) of 1.05%. For Redhill 65, the porosity was 44.46%, with a SD of 1.78%. For Redhill HH, the porosity was 47.02%, with a SD of 1.50%. The saturated hydraulic conductivities of the Redhill 30, Redhill 65 and Redhill HH, measured using a standard constant head permeameter, were 7.99 Darcies, 3.78 Darcies and 1.07 Darcies respectively.

4.3.4 Packing and Saturation

Great care was taken in the packing of the sample into the plastic container. The sand was loaded into the pipe using a small container. The pipe was tapped at the bottom to induce settling and more complete packing when it was almost full.

Saturation of the sand in the pipe was undertaken from the base upwards. The plastic pipe was placed in a bucket of water and left for 24 hours, until water appeared to be pooling on the surface of the sample. The sample was left to drain freely for an hour before contaminating with oil by raising the sample column with a clamp.

Partial saturation was achieved in three ways (i) slow wetting of the column before the experiment began, (ii) draining the column for an hour prior to the start of the experiment, and (iii) water input into the top of the column was maximised to a level which did not cause ponding. Partial de-saturation due to gravity drainage was assumed. A hydrodynamic equilibrium was established within the sand column, resulting in the same amount of water going in as come out of the bottom. It was assumed that there was negligible air entry. Therefore, it was independent of the extent of surface coverage by oil, at the time of injection.

4.3.5 Oil application and sampling

The cable oil sample was then applied to the surface of the sample. The chosen amount of oil, as listed in Table 4.2 was applied all at once. Water was added drop wise, by means of a pump, to simulate rainfall at the same time as the oil was added. The rate of simulated rainfall was maintained at a constant rate for each individual experiment, and varied between 6ml/hour and 285ml/hour, see Table 4.2. These rates can be compared with a torrential natural rainfall rate of 1 inch or 25ml per hour. Wastewater was collected and analysed to determine whether any of the oil had been washed out.

After the experiment had run for the desired length of time, the water flow was terminated, see Table 4.2 for details of experimental run times. The column was then cut into 1cm slices at 5cm intervals, a sampling interval that provided a balance between resolution and analysis time. (Each column experiment would take between one and two weeks from the

initial saturation period to getting the results). The sand from each slice was thoroughly mixed, before weighing out three one-gram samples. To this 1ml of 1,1,2-trichlorotrifluoroethane was then added to each sample before sonicating. The 1ml of solution was then pipetted off the sand layer into the instrument vial, and 5ml of liquid scintillation cocktail was added to the vial.

Column	Column Length	Amount of DDB	Rate of Water Addition	Total Flow Time
a	40cm	1ml	6ml hour^{-1}	0.5 hours
b	70cm	1ml	None	1 hour
c	100cm	1ml	10 ml hour^{-1}	1 hour
d	100cm	1ml	10ml hour^{-1}	2.25 hours
e	100cm	1ml	20ml hour^{-1}	1.75 hours
f	100cm	1ml	10 ml hour^{-1}	1 hour
g	50cm	1ml	1ml hour^{-1}	20 hours
h	50cm	1ml	1ml hour^{-1}	20 hours
i	50cm	1ml	None	1.5 hours
j	50cm	1ml	25ml hour^{-1}	24 hours
k	50cm	1ml	22ml hour^{-1}	27 hours
l	30cm	0	Control experiment	0 hours
m	50cm	1ml	3.5ml hour^{-1}	120 hours
n	50cm	1ml	2 ml hour^{-1}	120 hours
o	50cm	1ml	8ml hour^{-1}	96 hours
p	50cm	1ml	175ml hour^{-1}	2 hours
q	50cm	1ml	285ml hour^{-1}	2 hours
r	20cm	1ml	None	2 hours
s	20cm	2ml	285ml hour^{-1}	2 hours
t	50cm	50ml	180ml hour^{-1}	19.5 hours
u	50cm	50ml	180ml hour^{-1}	23.5 hours
v	50cm	25ml	180ml hour^{-1}	25 hours
w	50cm	75ml	180ml hour^{-1}	25 hours
x	45cm	47ml	60ml hour^{-1}	78 hours
y	45cm	25ml	54ml hour^{-1}	72 hours
z	45cm	75ml	180ml hour^{-1}	25 hours
aa	45cm	75ml	180ml hour^{-1}	Column Broken
ab	45cm	75ml	None	168 hours

Table 4.2 Column studies conducted in relation to length, oil application, water flow rate and duration of the experiment.

The scintillation counter proved very stable over time. The mixture of hexane and scintillation cocktail was measured on its own, to provide a background reading of 22.6 disintegrations per minute (DPM). This compared to neat oil, which gave a count of 190,000 DPM. Samples well away from the injection point, clearly containing no oil, occasionally gave negative readings after background correction. However, assuming a scatter in the point of 190 DPM, i.e. 0.1% of the neat oil, removed these negative values. The background reading for a particular column was reduced by values up to this amount to remove negative values when they appeared.

4.4 Oil Migration Results

4.4.1 Low Loading Study

The low loading experiments were conducted using two of the three sand types previously discussed in section 4.3.3, (Redhill HH and Redhill 30). The low loading experiments initially concentrated on the Redhill HH sand and consisted of applying 1ml of cable oil to the top of a sand column. A wide variety of water flow rates and duration of experiments were tested to determine the effect of these variables on oil mobility. The experiments showed that there was very little oil movement. These results can be seen in Figure 4.3. As can be seen from the graph, there was very limited migration of the oil in the Redhill HH sand with only a small proportion of oil penetrating beyond 5cm in depth.

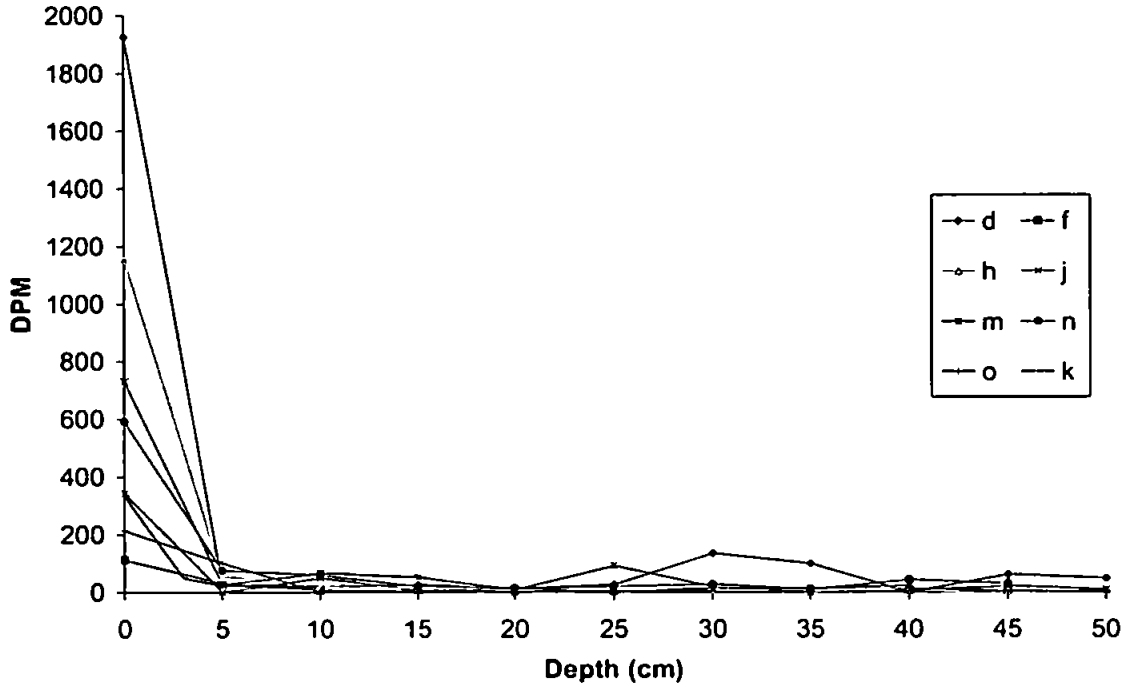

Figure 4.3 Rehill HH low loading experimental results, (background corrected).

Experiments were then conducted on the more porous sand (Redhill 30) to test whether this phenomenon would vary with the type of sand. However, the change had little effect on the mobility of the oil. Figure 4.4 shows that the oil remained in the upper region of the sample with little penetration beyond 10cm in depth.

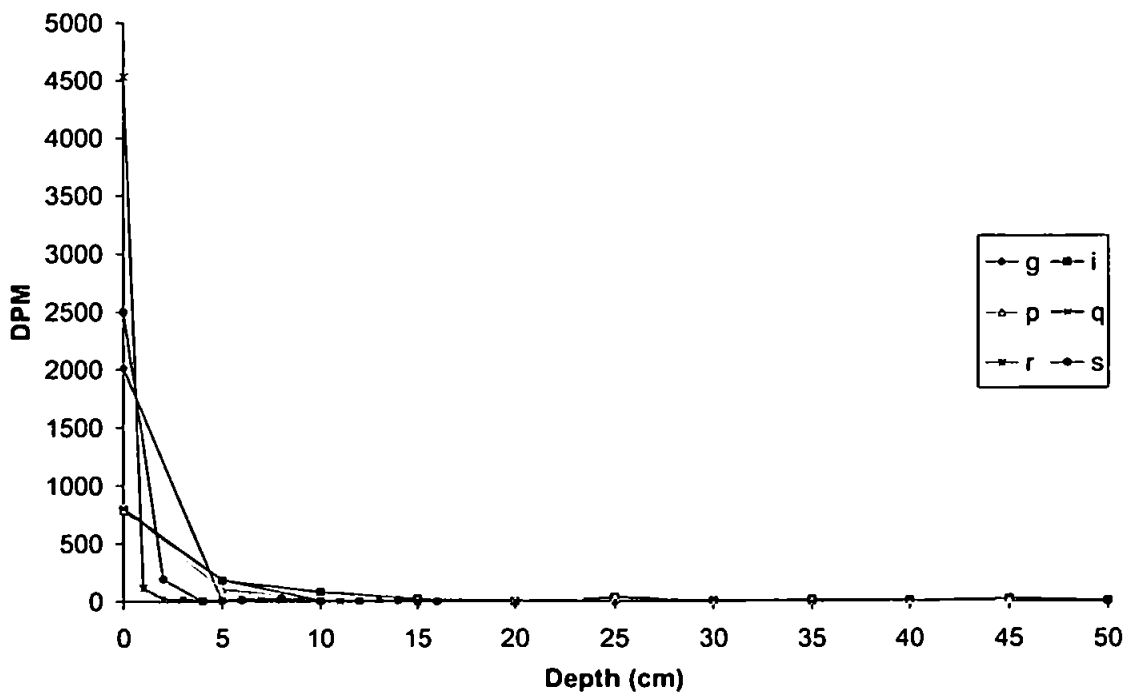

Figure 4.4 Redhill 30 low loading experimental results, (background corrected).

Equation 4.1 was fitted to all of the low loading experimental results, producing R^2 values, corrected for the number of degrees of freedom of the fit, within the range 0.62% to 0.99%, Table 3.3. The two low R^2 values (columns d and g) relate to the columns that had a high oil concentration at the surface, and for which the change in concentration with depth was steeper than Gaussian. Columns m and d for Redhill HH showed a possible secondary maximum further down the sand column. However, both of these maximums were within the estimated scatter of 190 DPM, and were therefore ignored since their significance could not be proven statistically.

Equation 4.1 was also used to interpolate a depth at which the oil concentration was 10% of the surface value. Analysis of the 10% oil concentration depth values shows that there is no correlation between the duration of the experiment and depth, Figure 4.5 (maximum R^2 for linear correlation = 0.13). In addition to this, Figure 4.6 shows there to be no correlation between the volume of infiltrating water added to the column, and the depth the oil migrated (maximum R^2 for linear correlation = 0.04). This conclusion holds for both sand types.

Column	Sand	Water added (ml)	Duration (hours)	Adjusted R^2	10% oil concentration depth (cm)
d	HH	30	2.25	0.6594	0.00
f	HH	10	1	0.9878	8.35
g	30	20	20	0.6239	1.96
h	HH	20	20	0.9987	3.60
i	30	0	1.5	0.9761	7.72
j	HH	590	24	0.8514	0.24
k	HH	590	27	0.9715	0.31
m	HH	420	120	0.8271	0.31
n	HH	240	120	0.9210	4.99
o	HH	740	96	0.9749	10.72
p	30	350	2	0.8958	5.47
q	30	570	2	0.9972	7.38
r	30	0	2	0.8561	0.61
s	30	570	2	0.8141	1.76

Table 4.3 Modelled R^2 values for low loading columns, and 10% oil concentration in relation to depth.

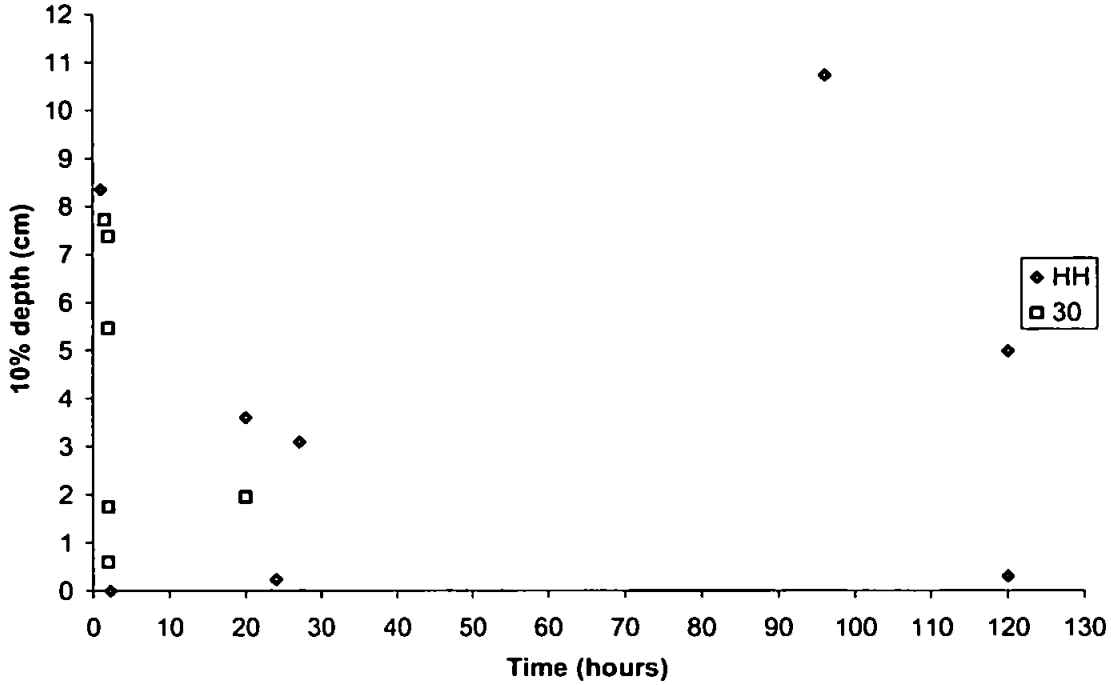

Figure 4.5 10% oil concentration depth against the duration of the experiment.

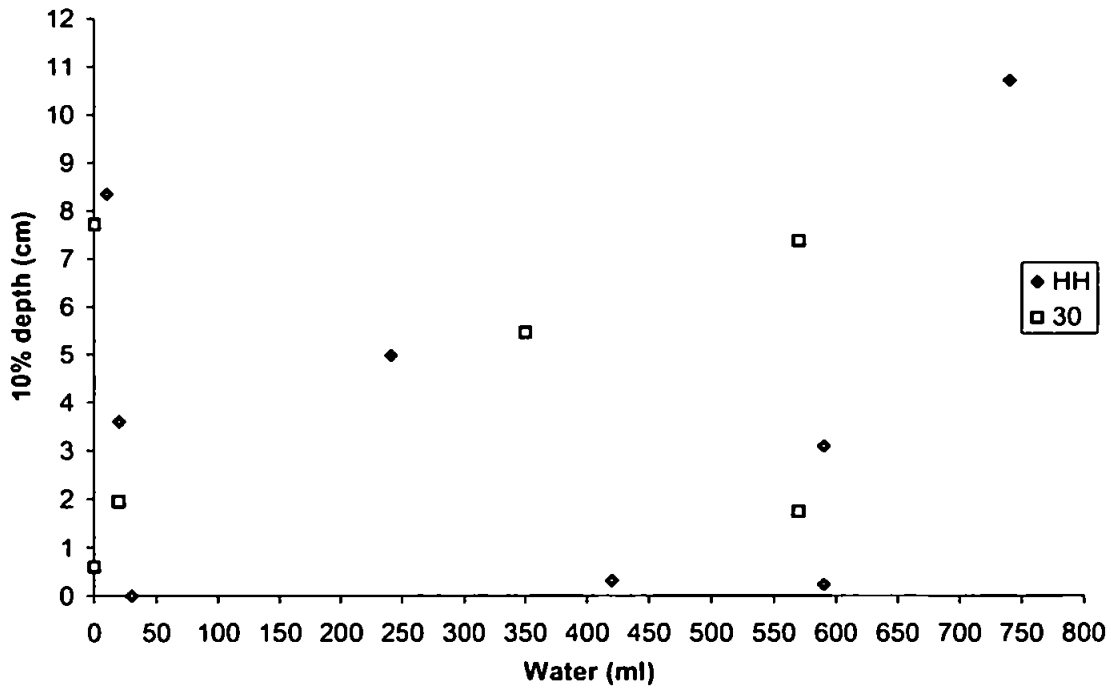

Figure 4.6 Total water flux - 10% oil concentration depth against the volume of simulated rainfall (total).

4.4.2 High Loading Study

Initial experiments at high loading concentrated on the mobility of cable oil in the most porous of the three sands studied - Redhill 30. Various quantities of cable oil were applied

to the top of the column, ranging between 25ml to 75ml, Table 4.2. The results of these experiments can be seen in Figure 4.7. It is evident that in general, the greater the loading of cable oil, the greater the extent of the migration of cable oil through the sand column.

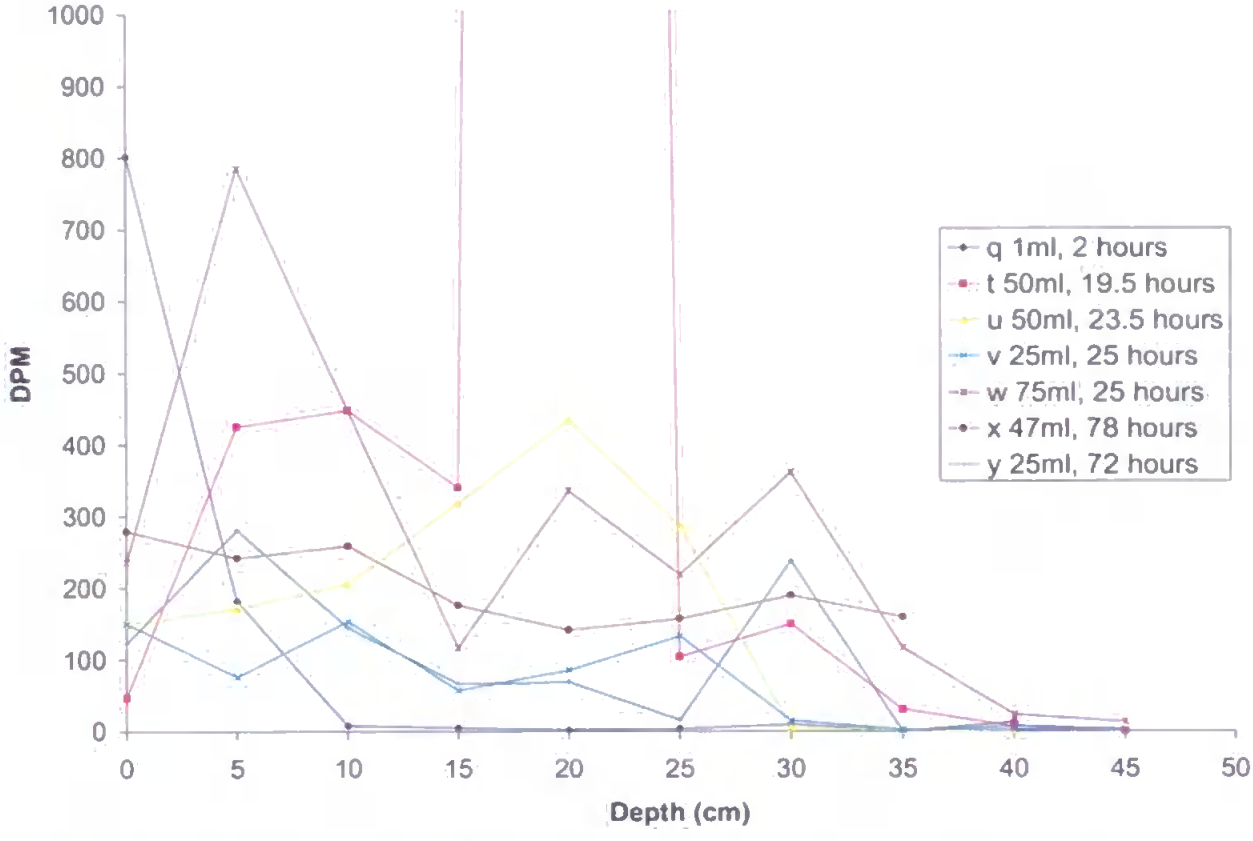

Figure 4.7 Results of the high loading experiments carried out on Redhill 30 sand. N.B. Column T peaks at a concentration of 12000 DPM.

The experimental results demonstrate that increased loading of cable oil makes the cable oil travel further. This is demonstrated by comparing columns v and w. This result is confirmed by comparing each of the other columns where varying quantities of oil were added. The results demonstrate further that the observed cable oil migration is also partially dependent on the duration of the experiment. In general, it can be shown that the greater the duration of the experiment, the further the cable oil migrates.

Experiments comparable to those conducted on Redhill 30 were undertaken on the other two sands, (Redhill HH and Redhill 65). The experiment consisted of applying 75ml of

cable oil to a pre-saturated and partially drained 50cm column of sand. Water was allowed to infiltrate the sample at a rate of 3ml per minute. However, an exception was made to the Redhill HH sand because the 75ml oil did not infiltrate completely from the top of the sand column, which resulted in water pooling at the surface faster than the water or oil could be infiltrated. The results confirm that for identical experiments on columns containing three different sand types the cable oil moves furthest in the most porous sample, (Redhill 30), and least in Redhill HH, the least porous sample. These results are presented in Figure 4.8 and are consistent with prior expectations.

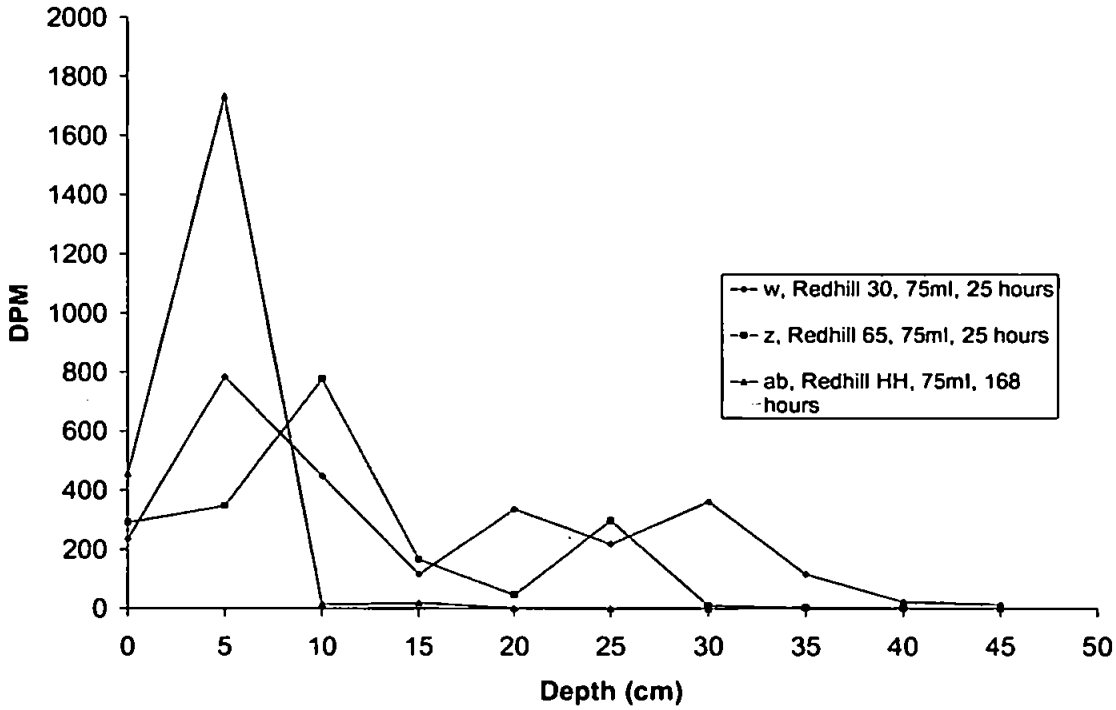

Figure 4.8 Comparison of cable oil migration at high loading, in three different sand types.

In general, Equation 4.2 models the experimental results well in terms of the R^2 value. Identifying the position of both the source and secondary glomus. However, due to the high number of parameters relative to the number of data points, there are few statistical degrees of freedom, so that the adjusted R^2 values are less than previously, Table 4.4.

Column	Coefficients						Adjusted R^2	R^2
	a	b	c	d	e	f		
t*	9703.04	19.84	3.00	-	-	-	0.8164	0.8776
u*	463.81	19.3	4.99	-	-	-	0.4251	0.6406
v	797.26	5.74	3.64	327.25	25.43	7.51	0.8164	0.9388
w	129.64	6.1838	6.99	139.69	23.35	3.54	0.2244	0.7415
x	272.74	1.49	15.15	154.60	32.03	5.67	0.4882	0.9269
y	252.74	5.63	5.18	280.80	28.99	1.648	0.7824	0.9275
z	762.36	9.06	3.708	310.93	24.37	2.11	0.6029	0.8672
ab*	1332.11	4.27	3.00	-	-	-	0.9090	0.9090

Table 4.4 Modelled one-dimensional results for high loading study, using two Gaussian equations as shown in Equation 4.2. * Represents the columns that were modelled using the first Gaussian equation.

4.4.3 Comparisons of High and Low Oil Loading Migration

In order for the high and low loading results to be compared it was necessary to re-optimise the column results. To achieve this, three factors were taken into account. Firstly, it was necessary to apply a dilution factor to the columns in the high loading study, (because the amount of radio-labelled oil had to be diluted with actual cable oil to produce a sufficient amount of oil). It was then necessary to select only the columns with consistent extraction efficiency. This was achieved by measuring the total area under the smoothed curve and comparing this to the amount of oil added to the top of the column. Lastly, it was necessary to re-optimise all the remaining curves to a single equation,

$$\text{oil concentration} = a\exp\left(-0.5\left[\frac{x-b}{c}\right]^2\right) + d\exp\left(-0.5\left[\frac{x-e}{f}\right]^2\right)$$

Equation 4.3

where a is the maximum concentration of the source glomus, b is the centre point of the source glomus, and c is its standard deviation or width. d is the maximum concentration of the secondary glomus, e is its centre and f its width. The results of the re-optimisation can be seen in Table 4.5.

Column	Sand Type	Oil loading (ml)	Rate of Water Addition (ml hr-1)	Water added (ml)	Duration (hours)	Water Flux Parameter	Glomus smoothing coefficients						Source glomus penetration	Secondary glomus penetration	rms df dvn (DPM)
							a	b	c	d	e	f			
H	HH	1	1	20	20	20	1150		2.02				3.22		9.81
D	HH	1	10	22.5	2.25	22.5	1924		1.71				2.72		49.84
N	HH	1	2	240	120	240	591		2.48				3.94		22.92
M	HH	1	3.5	420	120	420	730		1.95				3.10		35.86
R	30	1	0	0	2	0	4531		0.37				0.59		6.70
G	30	1	1	20	20	20	2014		1.50				2.38		2.26
P	30	1	175	350	2	350	805		2.49				3.96		9.54
S	30	2	285	570	2	570	2498		0.88				1.40		10.10
Y	30	25	54	3888	72	3888	3960	5.63	5.18	4400	28.99	1.65	8.24	63.86	265.86
V	30	25	180	4500	25	4500	2031	6.18	6.99	2188	23.35	3.54	11.11	53.65	309.99
X	30	47	60	4680	78	4680	4273	1.49	15.15	2422	32.03	5.67	24.09	74.41	259.82
U	30	50	180	4230	23.5	4230	2808	4.00	8.00	6738	20.00	5.50	12.72	48.42	302.00
W	30	75	180	4500	25	4500	12493	5.74	3.64	5000	25.43	7.51	5.79	62.08	566.14
Z	65	75	180	4500	25	4500	11946	9.06	3.71	4872	24.37	2.11	5.90	54.41	884.74

Table 4.5 Summary of the column experiments used to compare the low and high loading study.

The observed behaviour can be split into three types, as exemplified in Figure 4.9. At low oil loading, there is virtually no migration, even with extremely high water flow (column s). At high loading, a secondary glomus forms. The maximum concentration of the source glomus can either be less that the secondary glomus (column u) or greater (column w). The formation of only one secondary glomus is an approximation, as evidenced by the poor fit of the smoothing curve to column 13 at depths of around 25 cm, and characterised by the corresponding high rms deviation (adjusted for degrees of freedom of the fit) shown in Table 4.5. The poor fit of column z, Table 4.5, is due to a highly skewed source glomus.

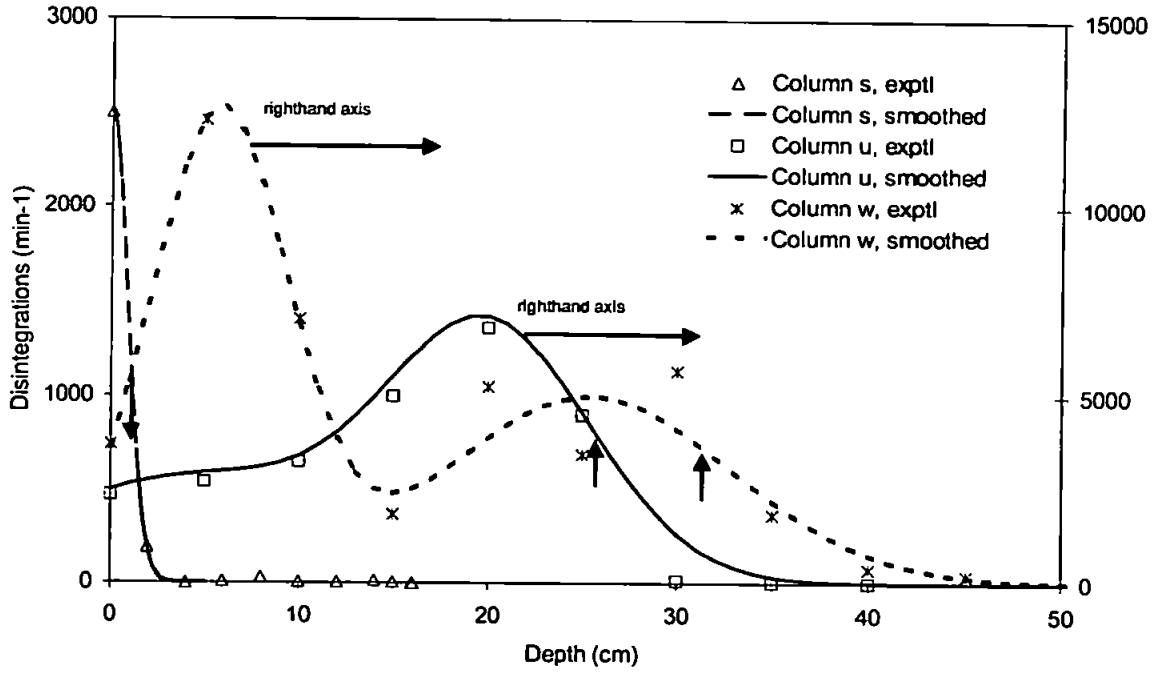

Figure 4.9 Examples of three types of flow behaviour of oil in sand columns. Vertical arrows show depth penetration of 90% of source glomus of 90% of total.

Overall, the movement of the oil glomuses is dependent on four independent factors: (i) the sand type and permeability, (ii) the loading of oil, (iii) the rate of water flow, and (iv) the total amount of water added. (The duration of the experiment is equal to (iv) / (iii).) The extent of movement of the oil can be conveniently measured as the distance down the column above which there is 90% by concentration of the total amount of oil. For precision this is estimated from the smoothing curves rather than from the experimental data. The smoothing curve parameters and 90% depths are shown in Table 4.5, and shown

in Figure 4.9. To reduce the number of water flow parameters, (ii) and (iv) were combined as a lumped water flux parameter $(iii)^{p}.(iv)^{(p-1)}$. The exponent p (=1/3) was chosen to give the most monotonic trend of the water flux parameter against 90% penetration depth.

If the penetration extent of the source glomus in Redhill 30 sand is plotted against loading and water flux, Figure 4.10 results. It can be seen that the penetration of the source glomus goes through a maximum with respect to loading and the water flux parameter. It decreases at high loading or water flux because a secondary glomus is formed. When a secondary glomus forms, the overall 90% point is plotted in Figure 4.11. It can be seen that the overall penetration rises with both water flux and loading. The relationship reaches a maximum at high water flux and loading, but there is insufficient data to be able to extrapolate beyond the experimental conditions.

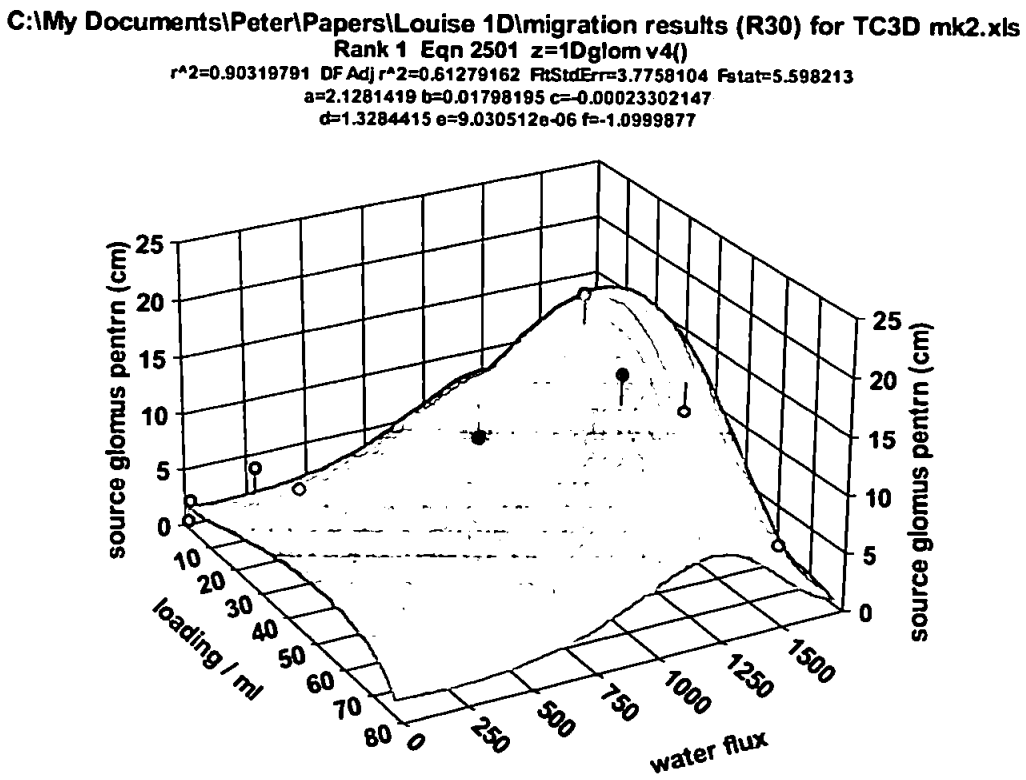

Figure 4.10 Penetration of 90% of the source glomus with oil loading and water flux.

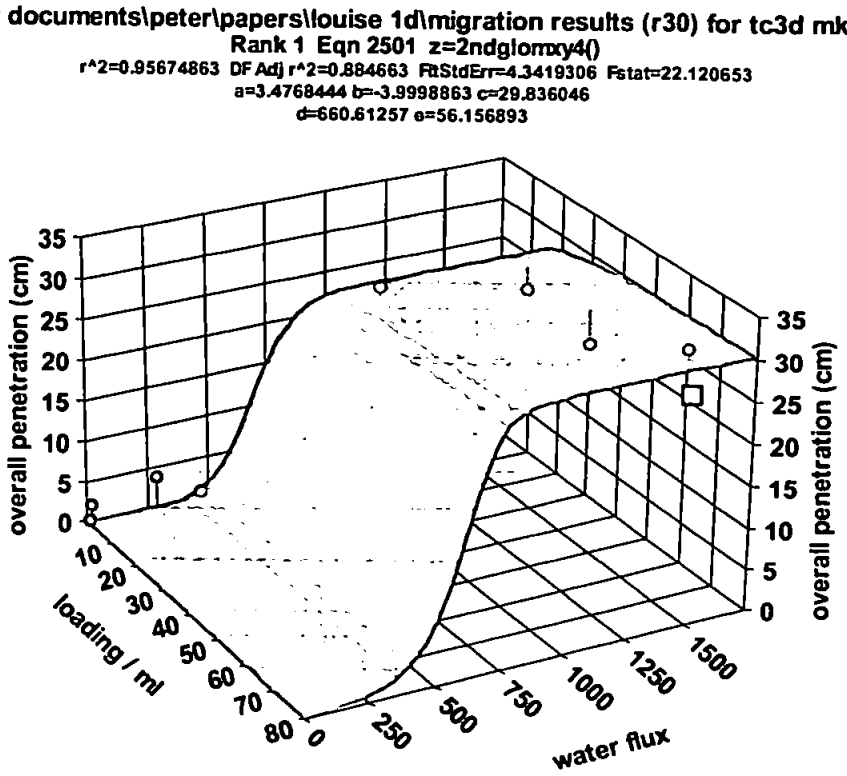

Figure 4.11 Penetration of 90% of the total oil concentration glomus with oil loading and water flux.

At low loading, both Redhill HH and 30 can be fitted to the same trend. As shown in Figure 4.11, Redhill 65 (•) produces less penetration than Redhill 30 at high loading and water flux, in accord with its lower saturated hydraulic conductivity, but further experiments would be required to establish a definite trend.

4.5 Discussion and Conclusions

The migration patterns shown in these results can be explained in terms of glomuses, (described in Section 4.2). Low loading results in a source glomus at the sand surface, with no secondary glomus forming. With increased loading the glomus can be seen to spread down the column vertically. If the oil loading is large enough, a secondary glomus forms. Comparing, for example, columns v and y, it can be seen, (see Table 4.5), that the secondary glomus is further removed from the source glomus under conditions of longer time and greater water flux. These finding are in line with those of Joseph et al (1994), as described in Chapter 1.

As migration of the cable oil takes place, capillary and adsorption forces begin to immobilise the oil. For low oil saturations, the capillary and adsorption forces give rise to disconnections of the oil phase. The secondary glomuses can form a secondary source of pollution, in line with the findings of Schwille, (1988) and Pennell et al. (1996), described in Chapter 1.

The concept of a glomus is of limited benefit on one-dimensional studies, because the one-dimensional component of a glomus is simply a Gaussian curve. The use of column studies in analysing the migration process of a NAPL in the subsurface tends to be limited by the flow boundaries imposed by the column. In an attempt to gain further insight, researchers often turn to two- or three-dimensional laboratory studies or numerical simulation. In such investigations, a NAPL spill can be simulated under the same capillary, viscous and buoyant forces that are found in the field, although still on a smaller scale. The glomus also becomes a more useful concept when studied in more than one dimension. Chapter 5 develops this framework by conducting half metre scale laboratory studies on sand and soil samples.

5. Half-Metre Scale Laboratory Studies – Grid Lysimeter with Rainfall Simulator

5.1 Introduction

The aim of this section of work is to conduct half-metre scale laboratory experiments to study the migration of cable oil in two dimensions, namely lateral and vertical movements. Laboratory investigations on this scale provide realistic analysis of NAPL flow in porous media because the flows are studied under the sample forces (capillary, viscous and buoyancy forces) as full-scale systems. A review of laboratory investigations, many of which were two-dimensional, has been given in section 1.8.3. This chapter begins with a brief review of various experimental features of relevance to the laboratory lysimeter used in this work.

5.1.1 Rainfall simulators

Rainfall simulators are used to deliver water and tracer solutions to a sample surface, at flux rates comparable to typical rainfall rates integrated over the period of the experiment. The most common types comprise spray nozzles or grid needle-like drippers. Spray nozzles tend to produce a non-uniform distribution of rainfall flux that decreases with horizontal distance from the nozzle (Chow and Harbaugh, 1965). Therefore more recent work, including this, has favoured grids of needles (Romkens et al., 1975); (Bowman et al., 1994); (Phillips et al., 1995); (Hignett et al., 1995). Other recently reported delivery systems involve grids of capillary tubes (Dexter, 1995), or a single catheter traversing the entire sample surface via a motorised assembly (Andreini and Steenhuis, 1990).

5.1.2 Eluate collection

To provide information about eluate composition and flux at different horizontal positions below the sample, the sample must be positioned above an array of collectors. These can be ceramic plates (Buchter et al., 1995), open-tray metal grids (Andreini and Steenhuis, 1990), or a plastic sheet with triangular cross-section corrugations cut into it, (Porter, 1989). In this study, we used an aluminium block with an array of square funnels machined into it (Romkens et al., 1975); (Bowman et al., 1994); (Hignett et al., 1995). The advantage of this arrangement is that by precision-milling the block with sharp boundaries between each collection element, the degree of positional ambiguity of sampling can be minimised.

It is also important to prevent any resistance to flow into the sampling array, or sample saturation discontinuities at the sampling horizon (Phillips et al., 1995), (Bowman et al., 1994). In the present study, the sand sample was continued into the sample collection funnels, thus minimising such effects.

5.1.3 Moisture Content Determination

Determination of moisture content is crucial in any migration study. Soil water content is a key variable in most types of soil study including agricultural water management and hydrological modelling. Monitoring the volumetric water content in the field calls for a fast and sufficiently accurate method that allows repetitive measurements to be taken at the same location.

The standard method of measuring the volumetric water content of a soil sample is the thermogravimetric method. This consists of determining the weight loss after a specified time of oven drying at 105°C and relating it to the volume of water for a given

measurement. This method is time consuming and destructive to the sampled soil. It cannot therefore be used for repetitive measurements at exactly the same location. However, this method is invaluable for calibration of alternative, less intrusive methods.

Other techniques for in situ measurements of volumetric water content include neutron probe and gamma attenuation methods. These approaches are non-destructive, except for the initial installation of tubes. They are also comparatively fast. However, both methods involve radiation that has a consequential environmental impact and was therefore considered unsuitable for these experiments. Moreover, neutron probes require soil-specific calibration, and ordinary field gamma probes are relatively imprecise, (Roth et al., 1990).

The degree of saturation of the sample was measured in this study using time domain reflectometry (TDR). The derived volumetric water content has been shown to be almost independent of sand and soils type, by Topp et al. (1980), although there is some dependence on bulk density and temperature, (Ledieu et al., 1986). Work by Topp and Davis (1985) demonstrated consistency in the measured water content between TDR and other more traditional methods of saturation measurement. A more detailed analysis of TDR can be found in section 5.2.3.

5.2 Apparatus

5.2.1 Overall layout, sample and sample containment

The entire rig was constructed within a square cross-section, tubular steel frame approximately 2.7m high, Figure 5.1. The sample was contained 1.24 m above the floor in a waterproof open-ended cubic Perspex case of approximately half metre side (cross-sectional area 506 x 506 mm^2) which was mounted on the collector plate described below.

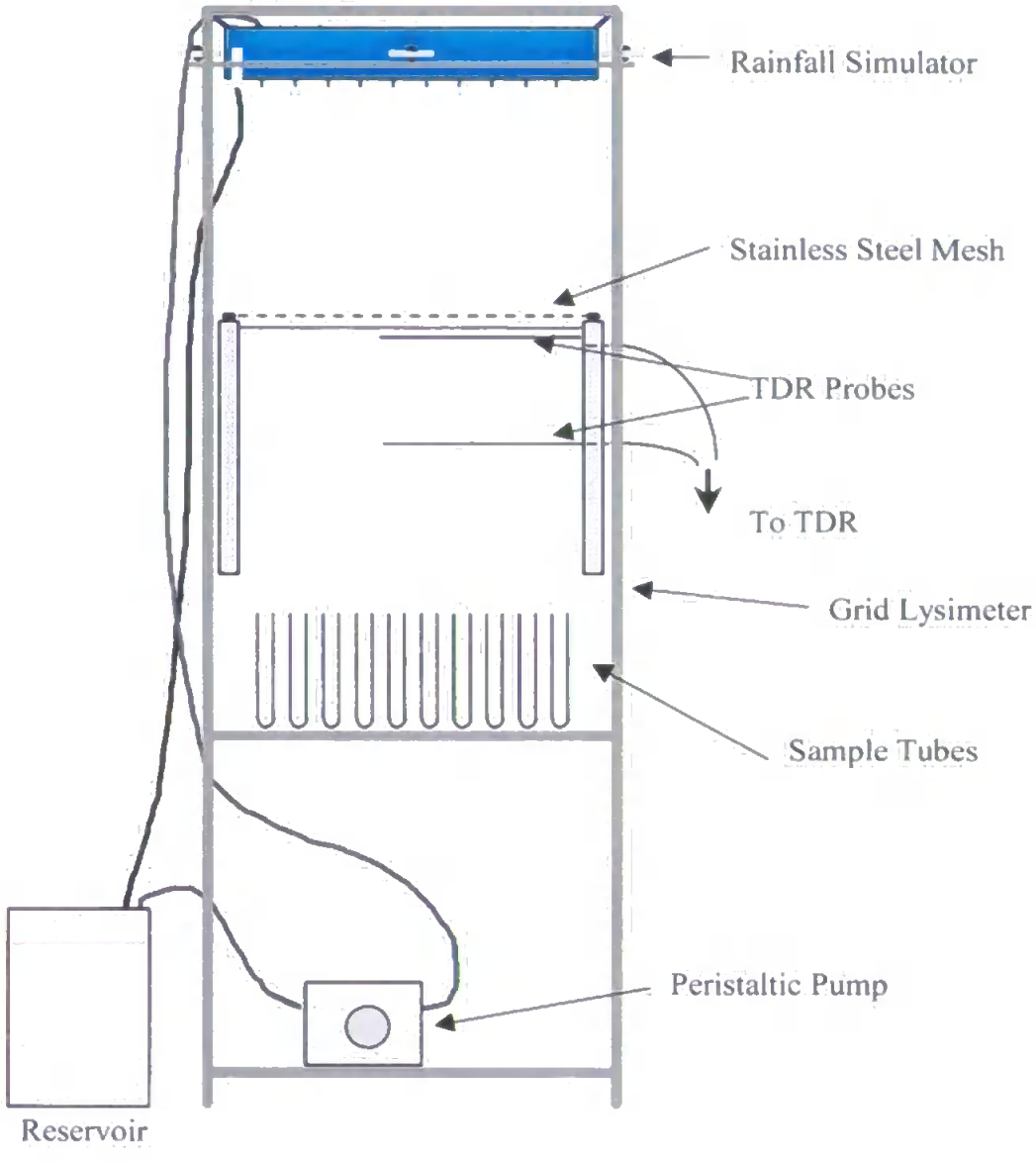

Figure 5.1 Schematic of experimental flow/transport apparatus.

5.2.2 Rainfall simulator and collector plate

The rainfall simulator comprised a square reservoir constructed from PVC with dimensions 451 x 451 x 114 mm, Figure 5.2. An adjustable constant-head device was used to supply the water in this apparatus, although other workers have regulated the supply in a closed supply system (Chow and Harbaugh, 1965); (Romkens et al., 1975). It was found that the syringe needle array had to overlap the sample, as discussed below.

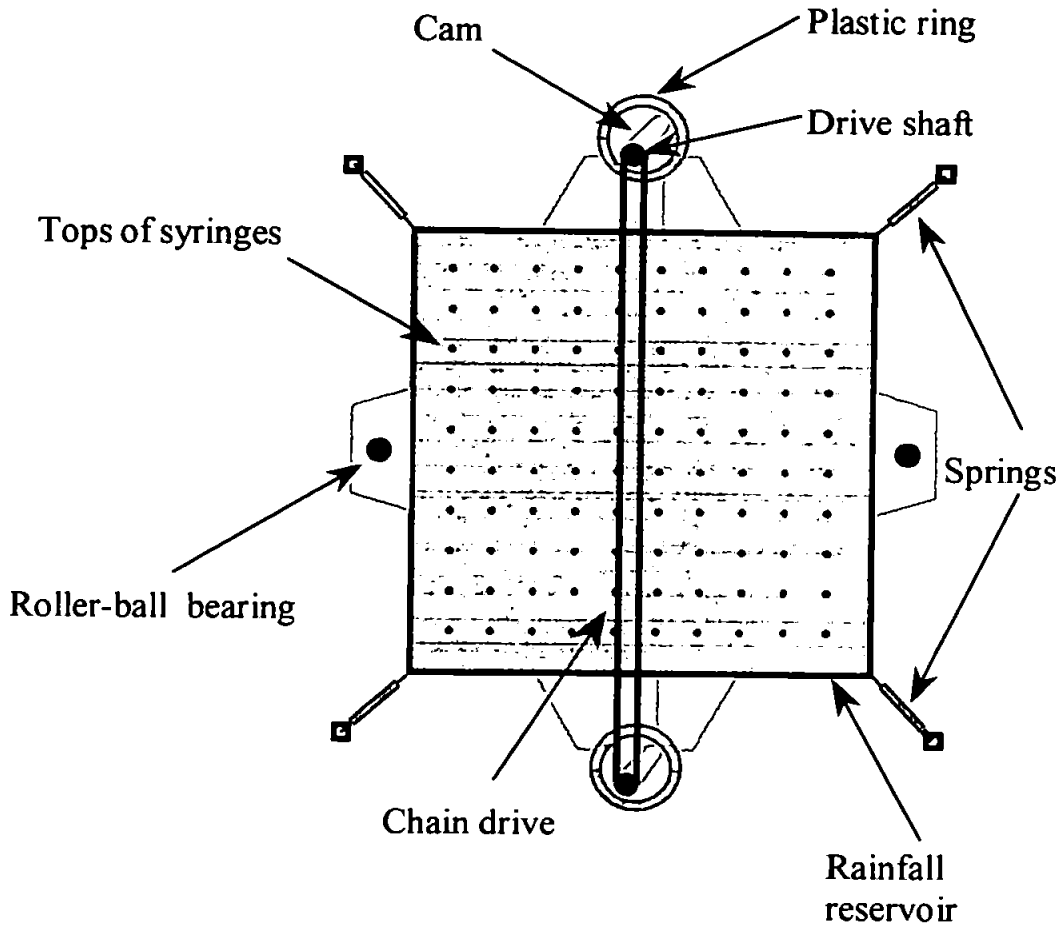

Figure 5.2 View of the rainfall simulator from above.

The mechanism for providing a degree of x-y translation to the rainfall delivery system took the form of an electric motor that turned a vertical brass rod, upon which a cam was mounted. The cam turned within a PVC ring attached to an edge of the rainfall reservoir, which was supported on roller-ball bearings running on horizontal metal plates.

This arrangement could be connected to a similar cam on the other side of the apparatus via a chain drive, Figure 5.2. Other workers have used more complicated stepper motor arrangements (Romkens et al., 1975), but these do not produce greater uniformity than the apparatus described here.

Mathews and Matthews (1999) discovered that the choice of needle gauge size was crucial with this type of rainfall simulator. They discovered that where the diameter of the needles was too small it proved impossible to keep the needles flowing. Where the needles were too large, a flow equivalent to rainfall of more than 20mm an hour was generated. The needles used were 23G needles (I.D. 0.318mm, Richards, Leicester, UK). Needles that did not flow, due to inconsistencies in the manufacturing process, were replaced with new ones, producing an application rate of 1660ml an hour. All 100 needles flowed constantly, unaided, over two days, with uniformity discussed below in section 5.2.2.2.

To guard against particles entering the water, and then blocking the needles, an inline filter unit was installed (Part Number 1119, Gelman Sciences Inc., U.S.A.) downstream from the pump, fitted with 30μm filter paper (Grade 113, Whatman International Ltd., U.K.).

A stainless steel mesh with 2mm diameter circular holes was interposed between the underside of the rainfall simulator and the surface of the sample, this further increased the homogeneity of application (Mathews and Matthews, 1999).

5.2.2.1 Collector plate and sample tubes

The collector plate was similar in design to those of Phillips et al. (1995) and Bowman et al. (1994). It was constructed of an anodised aluminium plate with a ten by ten array of square funnels of side 38 mm machined into it, Figure 5.3. Around this array larger, sloping edge channels of width 63 mm were also machined to allow the integrated collection of edge flow from the container walls. The plate was machined such that the smallest possible flat contact area (approximately 880 mm^2, or 0.6% of the total collecting area) was presented to the underside of the sample. This very small contact area at the

sampling horizon minimised both the impedance to drainage of the eluate, and the spatial ambiguity of sampling.

Stainless steel tubes cemented to the outlets from the square collector funnels conducted flow to specially constructed removable racks of sample tubes for sample collection. Entry of large particulates was prevented by glass wool.

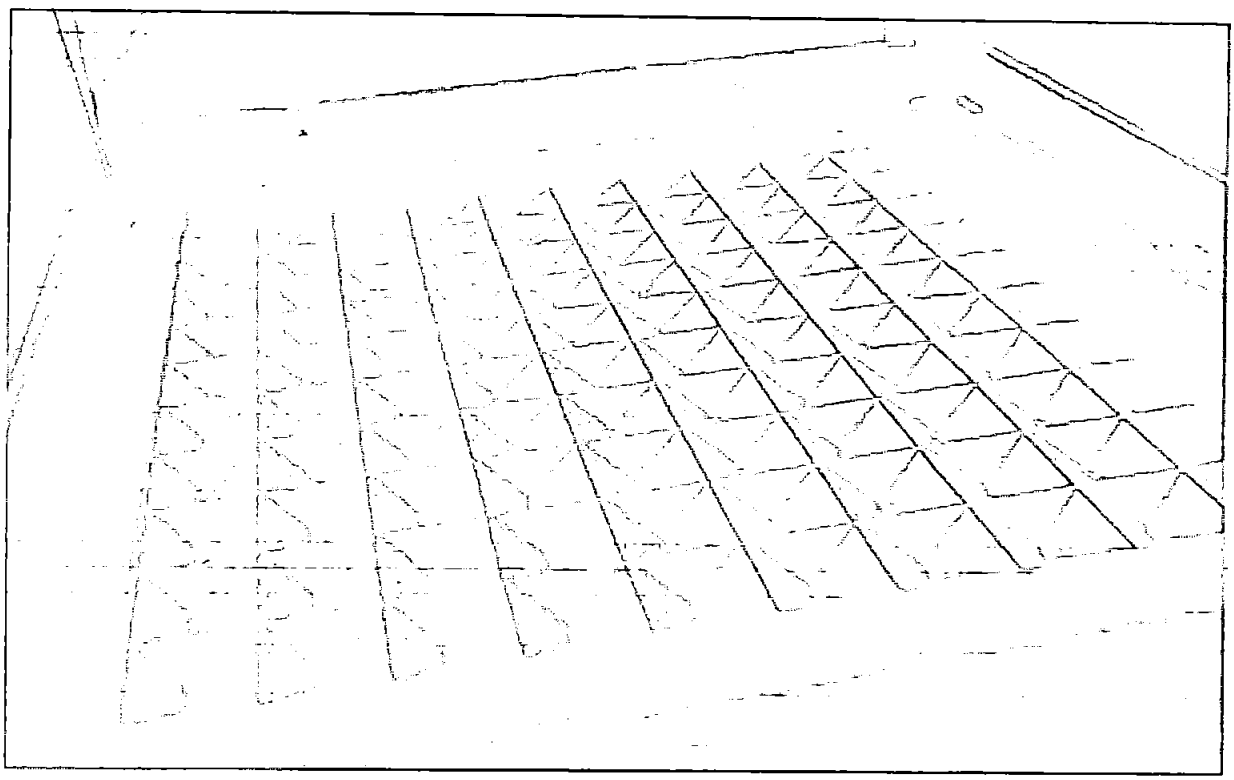

Figure 5.3 The grid lysimeter

5.2.2.2 Uniformity of Application

Mathews and Matthews (1999) study with the addition of a second cam, an increase of the needle array to 12 x 12 and the introduction of the 2mm mesh showed that the rainfall simulator had a standard deviation of 8.8%. This compares favourably with the results achieved by other researchers, Table 5.1. The introduction of a larger array of needles prevented the edge regions from drying out.

Workers	RSD %	Uniformity Coefficient, %
Mathews and Matthews (1999)	8.8	93.04
Bowman et al. (1994)	n/a	>98.00[1]
Dexter (1995)	≈19.0	-
Phillips et al. (1995)	11.6 – 22.4	-
Romkens et al. (1995)	8.5[2]	-
Andreini & Steenhuis (1990)	n/a	94.08 [3]

Table 5.1 Homogeneity of application of various rainfall simulators.
[1] No details given except that this figure is for rainfall rates in the approximate range 5-25 mm hour^{-1}.
[2] Average of five figures carried out at five different rainfall rates.
[3] Average of four figures each of which is an average of the 'before' and 'after' values for an experiment.

5.2.3 Saturation measurement

Time Domain Reflectometry (TDR) has become a popular and recognised method of measuring the water content of soil. The use of TDR for measuring soil water content was originally proposed by Davis and Chudobiak, (1975), Davis and Annan, (1977) and Topp et al. (1980).

The technique is based on measuring the velocity of a pulse, which travels along an electromagnetic transmission line as a guided wave. The pulse velocity is used to calculate the dielectric constant of soil, which is dominated by the contribution from soil water. Free water has a dielectric constant about 20 times greater than that of mineral matter, and so the effect of the mineral matter on the pulse velocity is small, (Whalley, 1993). Cable oil has a dielectric constant of 2. A comprehensive review of its development is given by Gardner et al., (1991).

The principle of TDR is that a high frequency electromagnetic pulse is fed into the soil between two metal rods. Part of the pulse is reflected back up through the soil from the bottom of the rods, and the time interval between the incident and reflected pulses is measured, (Smith and Mullins, 1991).

Topp et al. (1980) determined a third order polynomial relationship between dielectric constant, ε_c, and volumetric water content θ, for which they gave an error estimate of 0.013 for θ.

$$\theta = -5.3 \times 10^{-2} + 2.92 \times 10^{-2}\varepsilon_c - 5.5 \times 10^{-4}\varepsilon_c^2 + 4.3 \times 10^{-6}\varepsilon_c^3$$

Equation 5.1

The main advantage of this calibration equation is that it does not require the determination of any additional soil parameters. The dielectric constants were calculated from the pulse velocity assuming that the imaginary part of the dielectric constant was negligible. The calibration suggested by (Topp et al., 1980) was widely accepted and thought to be substantially independent of soil type, (Whalley, 1993).

Pairs of TDR probes, in the form of 3mm diameter stainless steel welding rods (Rightons, Plymouth, Devon, U.K.) spaced 20mm apart and connected to the Tektronix 1502C cable tester, were inserted through holes drilled in the sample container at various depths throughout the samples. At each depth two pairs of probes of two different lengths were inserted, one pair of length 100 mm the other of 300 mm. The pairs of TDR probes were located at 45, 43.5, 39, 30.5, 22.5, 10.5 and 4.5cm from the base of the sample. This arrangement allowed monitoring of the water content across the whole width of the sample and also across the region closest to the edge of the container directly over the edge flow channels of the grid lysimeter.

5.3 Materials and Methods

5.3.1 Sample characteristics

The 2-D investigation was performed on three soil types, whose particle size distributions and texture were distinct from each other. The distribution of these soils by textual class is shown in Figure 5.4.

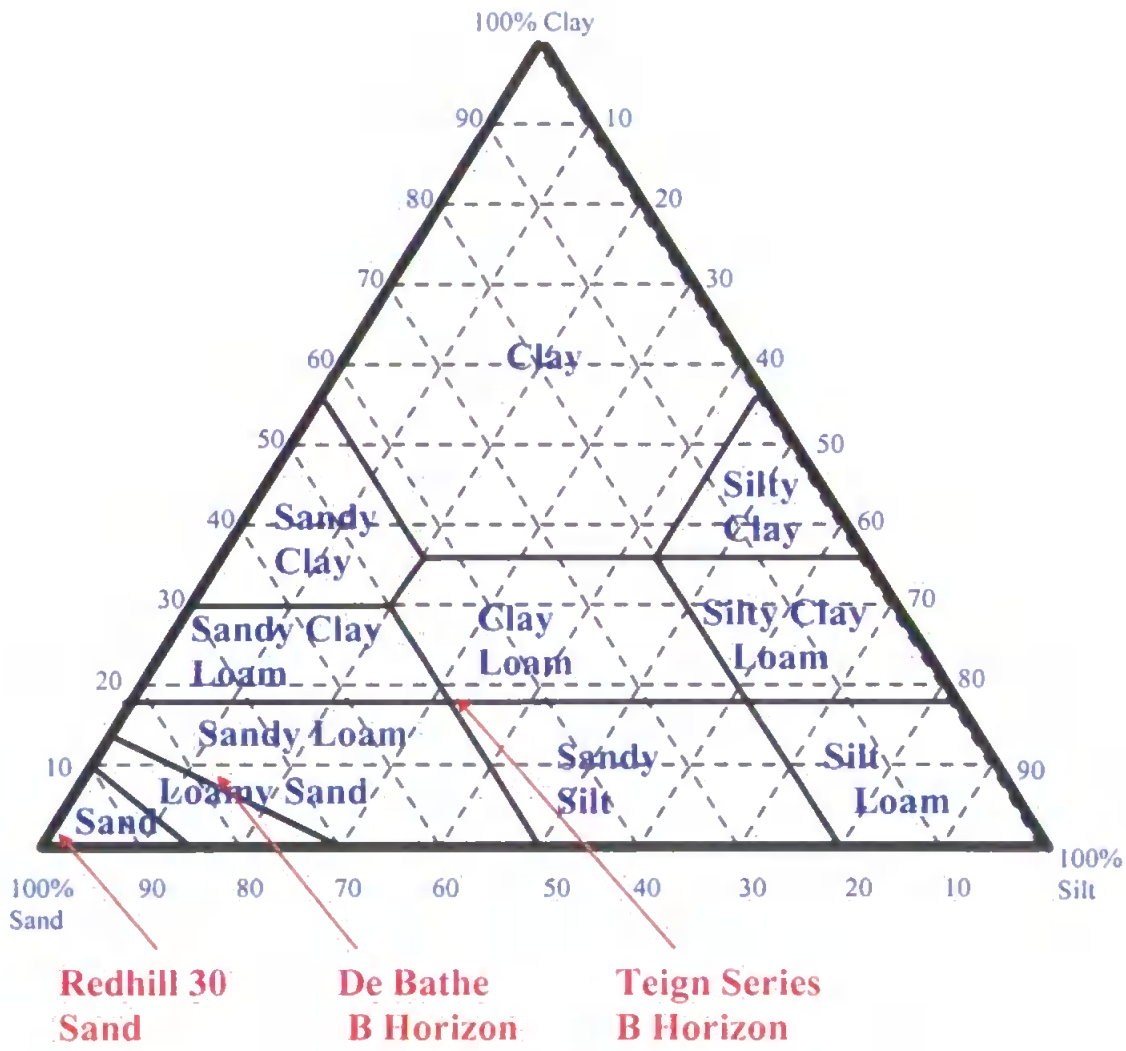

Figure 5.4 Position of the soil used for this study in relation to their location on the textural class triangulation diagram.

The first soil type used in this study was Redhill 30, as described in Chapter 4. The second soil investigated was known as DeBathe soil. The DeBathe soil is a sandy loam, which has been classified as a stony member of the Crediton series, located at Bathe Cross, near

IGER North Wyke, Devon, UK. This soil has been used in other investigations and consequently its soil characteristics are already well established, (Peat et al., 2000), and (Holden et al., 1995). Table 5.2 shows some of the soil characteristics for the DeBathe soil.

Analysis	DeBathe	Teign Series
Horizon	B	B
Depth (cm)	30-100	25-40
600μm – 2mm	16.97	25.22
212μm – 600μm	31.86	13.41
106μm - 212μm	4.27	6.39
63μm - 106μm	26.52	5.33
20μm – 63μm	5.19	15.24
2μm – 20μm	7.44	18.92
< 2μm	7.75	15.50
Organic Carbon Content (%)	0.3	0.1
pH	5.7	6.9

Table 5.2 Comparison of soil characteristics between the two soil types.

The other soil used is known as Teign Series soil, which was extracted from the natural levees of the Taw floodplain in North Wyke, Devon. The profile of the horizon 20-40cm from where the soil was taken consisted of gravel with a clay loam matrix, well rounded to sub-rounded, 1-10cm diameter, mainly black, fine grained siliceous rocks showing banding, with small amounts of grey fine micaceous sandstone, granite and metamorphic or volcanic rocks. Table 5.2 shows the soil characteristics for the Teign series soil.

5.3.2 Packing

Great care was taken in loading the sample into the Perspex container. The sand was taken from bags in a way that avoided sorting effects during travel, loaded into the container via a spinner wheel, and finally agitated during repacking. The soil was excavated using a spade, and transported to the laboratory. It was then loaded into the container dry and hand compacted in layers with a $10cm^2$ hand pommel. Each layer was no more than 7cm in

depth. The preceding layer was 'keyed' into the next by raking the surface of the compacted layer. The TDR probes were installed at appropriate depth during the packing procedure.

It was possible to bring an *in situ* soil block of the DeBathe soil in to the laboratory. The soil block was excavated using a mechanical digger to the approximate dimensions of the container. The container was then placed on the surface of the soil block (which had the A horizon removed), and the edges of the block were trimmed with a trowel so that the container would fit tightly. The bottom of the sample had a sharp metal plate hammered through the soil to prevent loss of soil during transportation from the field to the laboratory. The plate was then removed when the soil block was in place on the grid lysimeter. It was not possible to obtain an *in situ* Teign soil block because the B horizon was only 20cm deep whereas, for the half-metre study a $50cm^3$ block was required.

5.3.3 Saturation

Prior to commencement of a transport experiment a sample was first saturated and then allowed to drain to an unsaturated state. This was achieved by placing silicone bungs in all but one funnel, and this remaining funnel was connected to a peristaltic pump. The pump was then used to pump water extremely slowly, typically over a period of at least 4 days, into the sample. This was normally done until ponding was evident on the surface, and TDR readings were taken to ensure that required saturation had been achieved.

The rainfall simulator was connected towards the end of the saturation, initially with a barrier (plastic tray) to prevent water being applied to the sample. The simulator was then run for three hours to check that it was functioning correctly i.e. all needles were dripping providing uniform rainfall. The tray was then removed allowing water to fall on the ponded sample surface. The bungs were removed, simultaneously (made possible by

threading cotton through all the bungs) from the grid lysimeter allowing the sample to freely drain. The rainfall simulator was then run continuously throughout each experiment, with a rate of 1660 ml per hour for each funnel and standard deviation of 8.8%.

5.3.4 Tensiometers

Soil suction is the difference between the ambient atmospheric pressure and the measured pore water pressure. It is a measure of the energy needed to remove water from the soil, (Ridley and Brady, 1997). Tensiometers are used to estimate the energy status of the soil solution, and the use of tensiometers has become a standard method to monitor the soil water potential, (Cassel and Klute, 1986).

A typical tensiometer consists of a water-saturated cup constructed of porous material, usually ceramic, which is in close contact with the soil. The cup can be connected to either a vacuum gauge, water or mercury manometer, or an electronic pressure transducer by a water filled tube, (Stannard, 1992).

As the water content of the soil surrounding the tensiometer cup decreases, the energy level of the soil decreases relative to that of the water in the tensiometer cup. This causes the water to move out of the cup and into the soil, reducing the pressure of the water in the tensiometer cup. As the water content of the surrounding soil increases, the energy level of the soil increases relative to that of the water in the tensiometer cup. This increases the soil water pressure, and soil water flows through the walls of the porous cup into the tensiometer, increasing the pressure of the water in the tensiometer cup, (Cassel and Klute, 1986).

The tensiometers used in the study have been hand-made to a design by Dowd and Williams (1989). Each tensiometer consists of a ceramic cup 7cm long (Soil Moisture

Equipment, Santa Barbara, USA, No. 0640X05-B01M1), which is connected to a pressure transducer (RS No. 286-692) by three Teflon pipes with 1mm internal diameter. Two of these pipes allow de-aired water to be injected into the cup and the remaining pipe is connected to the transducer. The transducer is powered by a 12V power supply and is connected to a Campbell CR23X datalogger (Campbell Scientific, Logan, USA) via a series of relay multiplexers (also from Campbell Scientific; Campbell AM416). The datalogger was programmed to collect data from all the tensiometers every fifteen minutes for the duration of the experiment.

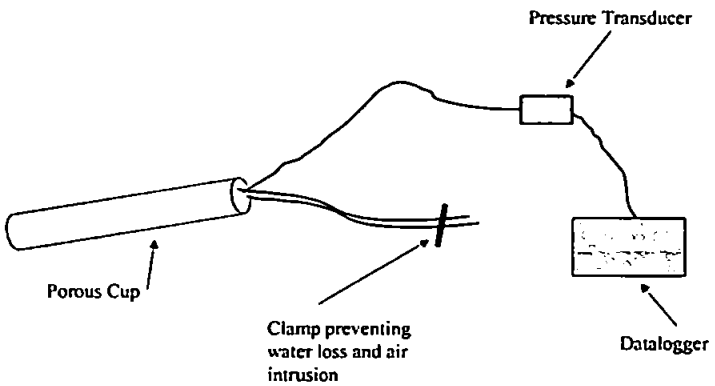

Figure 5.5 Tensiometer design

Prior to installation the tensiometers were tested to ensure that they were working correctly. They were soaked in de-aired water overnight to ensure that water would pass into the tensiometer cup and accumulate in the barrel. Pressure was applied using a syringe into one of the Telfon pipes to test for potential leaks from the top or bottom of the ceramic cup. Each pressure transducer had to be individually calibrated. This was achieved using a hanging column as described by Dowd and Williams (1989). The tensiometers were installed horizontally 10cm from the edge of the sample, at the same time as the soil was packed into the Perspex box. Three tensiometers were installed at 4.5cm, 22.5cm and

39cm respectively.

5.3.5 Oil Injection

The oil injection took place on the surface of the soil by means of a 68mm diameter plastic pipe inserted into the middle of the container. The pipe was pushed 5cm down into the sample, to prevent oil moving laterally on the sample surface. Oil was then poured into the tube. For each of the experiments, 75ml of oil was used. Oil application took place after full equilibrium had been achieved, on days 6.5, 9.5, 8.5 and 13.5 for the Redhill 30 sand, Teign repacked soil, DeBathe soil and DeBathe repacked soil respectively.

5.3.6 Sampling

Sampling was undertaken using a 2cm internal diameter steel gouge auger (Van Walt Limited, Haslemere, Surrey, U.K). The auger was twisted into the sample removing a 2cm core from the sample block. The sample was removed in sections, weighed into 5g samples and stored in glass vials (with a volume of 28.25ml) until analysis was performed, as described in Chapter 3.

5.4 Results

5.4.1 Saturation

The TDR saturation data showed the degree of saturation to remain fairly constant throughout the duration of each experiment, see Figure 5.6. The solid lines in Figure 5.6 represent the 30cm long TDR probes and the dotted lines represent the 10cm long probes. At the start of each experiment the degree of saturation was characterised by a rapid decline, which corresponds to the removal of the bungs and the initiation of rainfall. After this initial decline in saturation, the saturation remained roughly constant for all TDR probes, with a maximum standard deviation of 6.57% from the volumetric water content for any one set. It can also be noted that in general the 10cm long probes show lower water

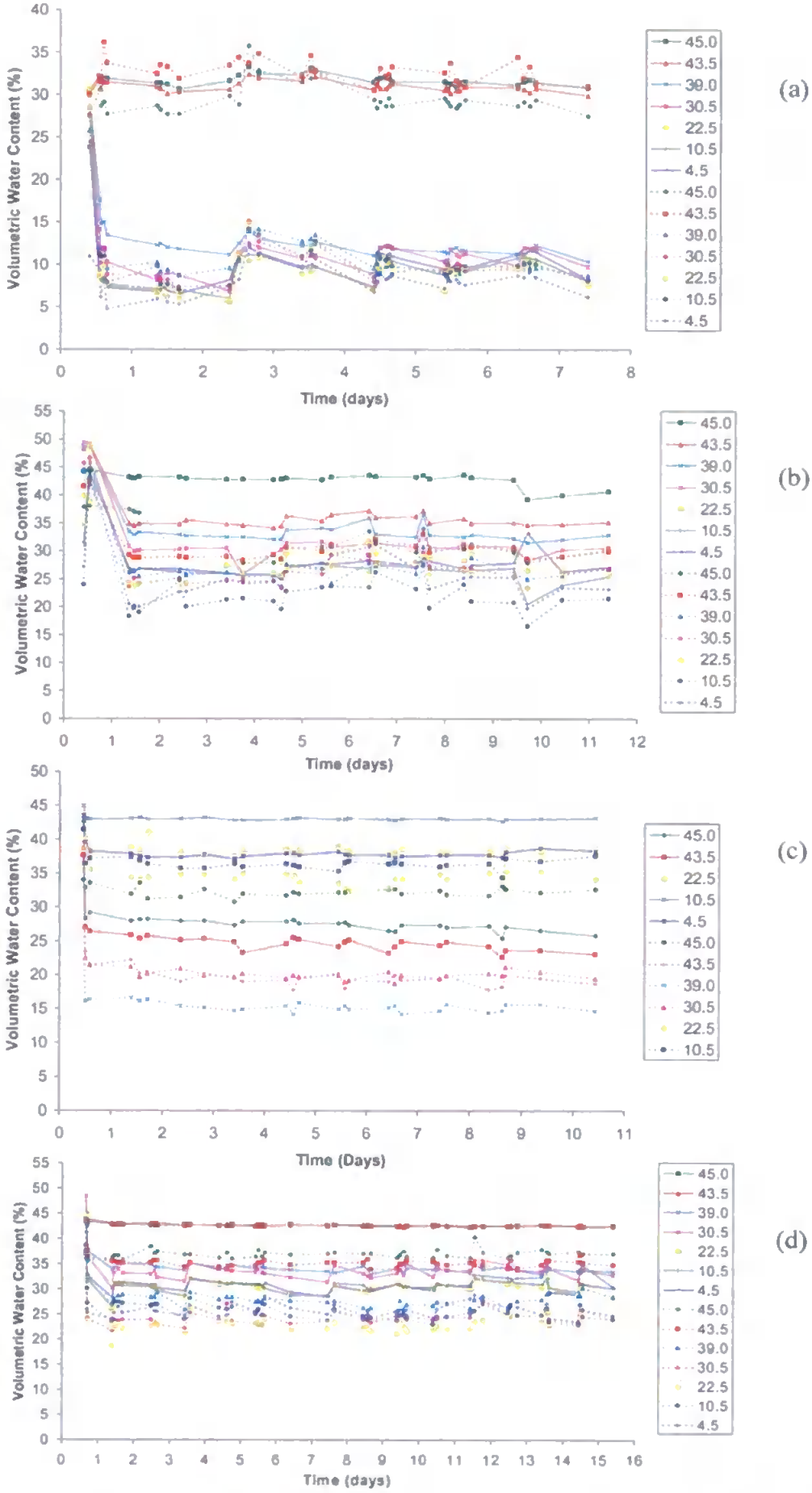

Figure 5.6 TDR measurements from the commencement of draining to end of experiment, (a) sand, (b) Teign repacked, (c) DeBathe, (d) DeBathe repacked.

contents, which suggests that the edge of the sample was drier than the main bulk of the sample.

From the diagrams in Figure 5.6 b, c and d it is possible to note when the oil injection took place, on days 9.5, 8.5, and 13.5 for the Teign repacked soil, DeBathe soil and DeBathe repacked soil, respectively. This occurred because the rainfall was suspended for between 2 and 8 hours depending on the experiment. Suspension of the rainfall was necessary because the oil would not infiltrate into the soil, but remained in the tube. This observation suggests that the saturation of the sample was too great to allow the oil to infiltrate, and the small decrease in the saturation level was sufficient to allow the infiltration to take place. This observation was also noted by Illangasekare et al. (1995) who suggested that the initial water saturation had a major impact on the flow of a NAPL.

All the graphs in Figure 5.7 show that the top of the sample was the wettest, with the exception of the DeBathe *in situ* soil. These graphs demonstrate that where the soil is wettest the degree of saturation is close to the porosity of the sand or soil. For the sand and repacked soil this is the top (or surface) whereas for the DeBathe *in situ* soil it is the bottom of the sample. This again demonstrates the effects that repacking has on the soils water retention capacity.

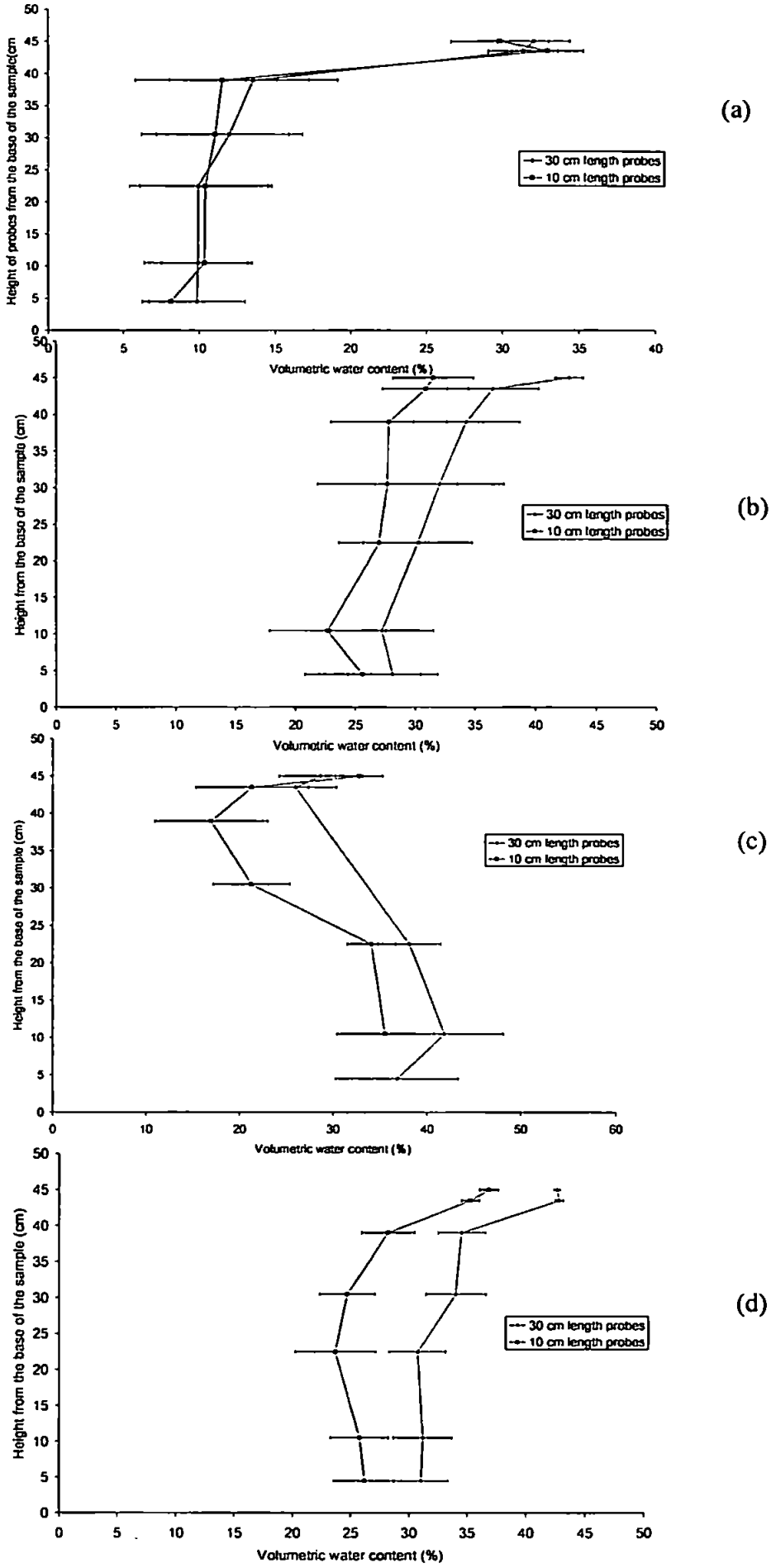

Figure 5.7 Average TDR saturation profiles with depth of sample, (a) sand, (b) Teign repacked, (c) DeBathe, (d) DeBathe repacked soils.

5.4.2 Tensiometer Results

The results from the tensiometers suggest that the soil suction within the small volume (of soil) is small and negative, and that it varies by at most ±1cm during the duration of the experiment. One may conclude that the experiment was running under stable soil tension conditions, and that the continuous rainfall did not cause transient loss of soil suction or hydrostatic heads. The tensiometer data itself shows diurnal variations, the initial sample drainage and the effects of de-airing. The tensiometer data is displayed in Figure 5.8 and Figure 5.9. The tensiometer located at the top of the DeBathe soil does not appear to work as shown in Figure 5.8.

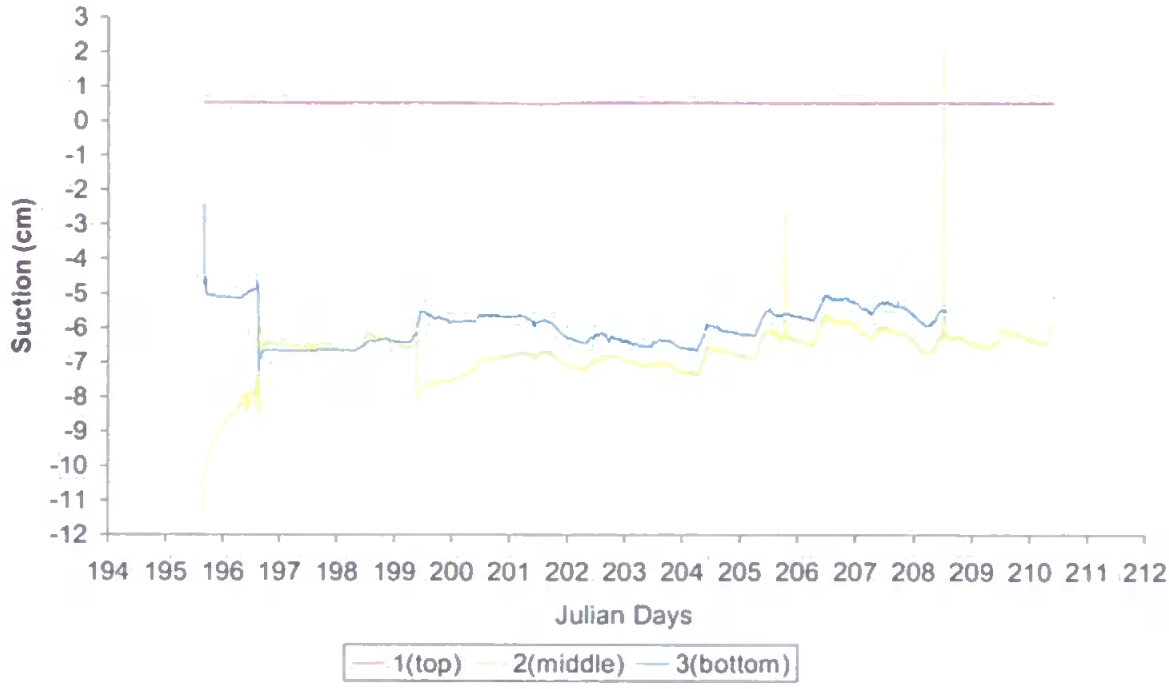

Figure 5.8 DeBathe repacked soil tensiometer data.

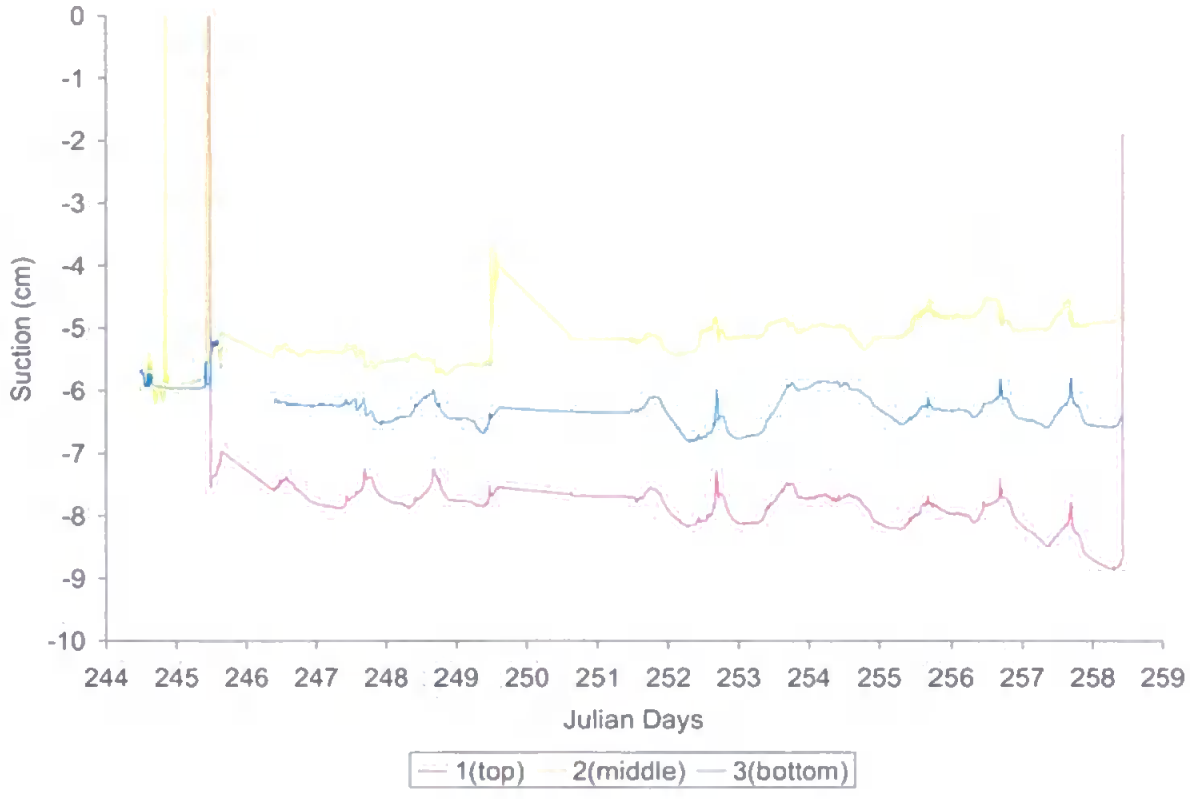

Figure 5.9 Teign repacked soil tensiometer data.

5.4.3 Water Flow Velocities

One of the simplest studies possible was the measurement of lateral variations in the flow of water through a sample. This was carried out by regularly collecting the individual funnel outputs and monitoring the flow rate through each funnel. This method was used to note the existence of paths of preferential flow allowing potential correlations with lateral flow of the cable oil to be investigated. It was possible to use the Darcy velocity to compare the flow rates, with Darcy velocity (V_d) defined as:

$$V_d = \frac{Q}{A}$$

Equation 5.2

Where Q is the volumetric flow rate (the average flow of all the funnels) and A is the sample cross-sectional area. Using the average of all the flow rates throughout the duration of the experiment it is possible to visually compare the flow rates before and after the oil injection into the sample, Figure 5.10. Visual inspection of the flow rates shows that

adding oil to the centre of the sample has little effect on the flow velocity patterns, (Figure 5.10).

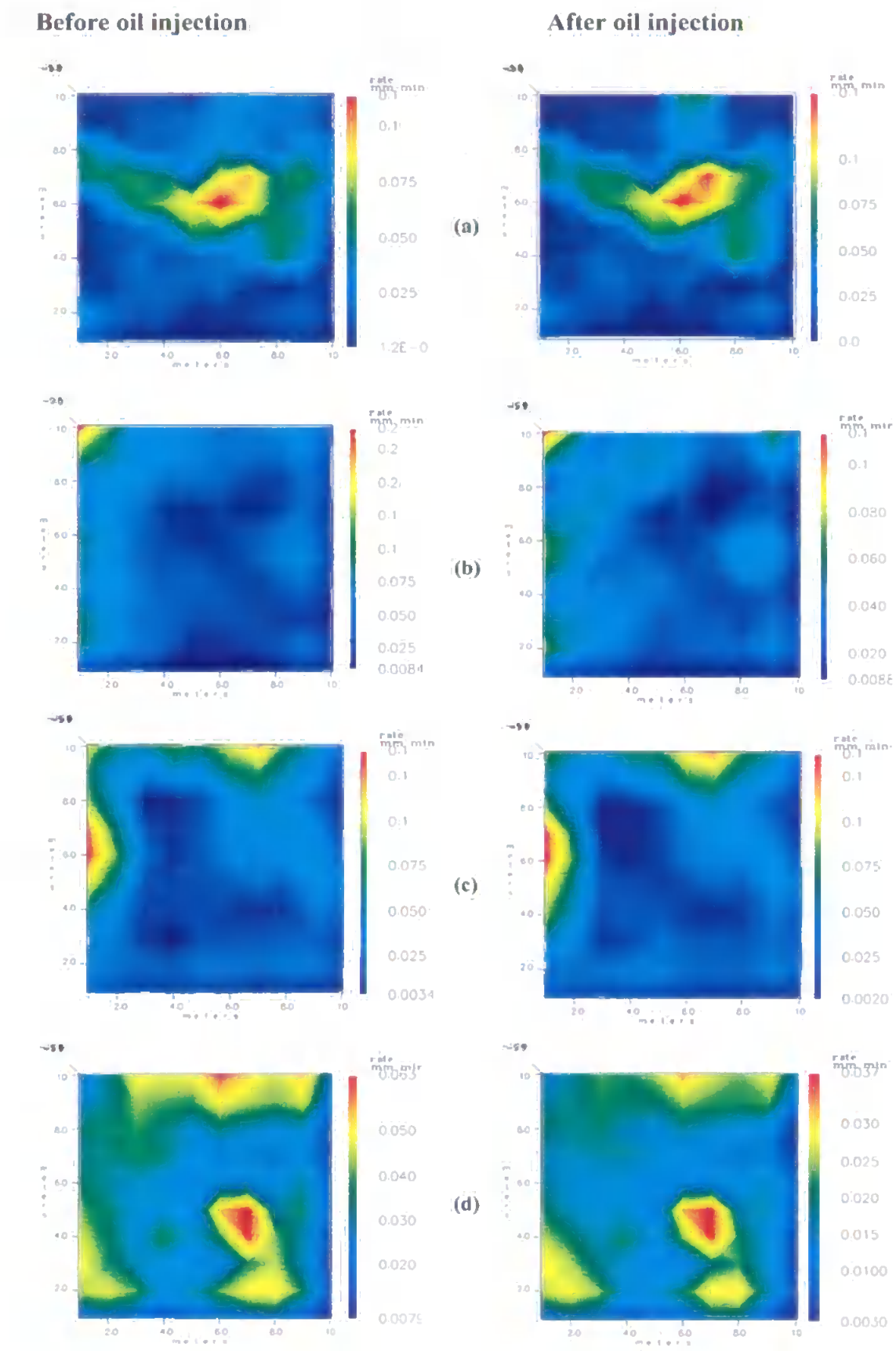

Figure 5.10 Average water flow velocities at the base of the sample before and after oil injection in (a) Redhill 30 sand, (b) DeBathe repacked, (c) DeBathe, and (d) Teign soil.

For each experiment that was conducted various measurements were made pertaining to variations in the lateral distribution of the flow of water through the sample and the average numbers of funnels conducting no flow over the course of an experiment. These are summarised in Table 5.3.

Sample	Porosity (%)	Permeability (Darcies)	Bulk Density	Average Number of Non-Flowing Funnels
Redhill 30 Sand	38.00	7.99	n/a	(a) 0 (b) 16
DeBathe Soil	44.5	2.59×10^{-5} m/sec	n/a	(a) 1 (b) 11
DeBathe Repacked Soil	30.7	5.85×10^{-5} m/sec	1.27 kgm^{-3}	(a) 0 (b) 0
Teign Repacked Soil	40.2	5.65×10^{-5} m/sec	1.16 kgm^{-3}	(a) 0 (b) 0

Table 5.3 Summary of spatial variations in flow for all soil types, where (a) is the average flow before oil injection and (b) is the average flow after oil injection.

The most notable point is that there were very few non-flowing funnels in the experiments conducted, with both the repacked soil samples showing zero non-flowing funnels. One possible explanation of this is that repacking causes the sample to become more homogeneous, resulting in a more even pattern of flow. It is also possible to note from Table 5.3 that the Redhill 30 sand and the *in situ* DeBathe soil are acting similarly, and the two repacked soils are acting likewise.

Visual inspection of the velocity flow patterns through the sample, Figure 5.11 from Mathews and Matthews (1999) shows similar results to those found in this study. The diagrams a and b show a similar pattern to that observed in this study whereas c does not appear in this study, where initial sample saturation had not been achieved.

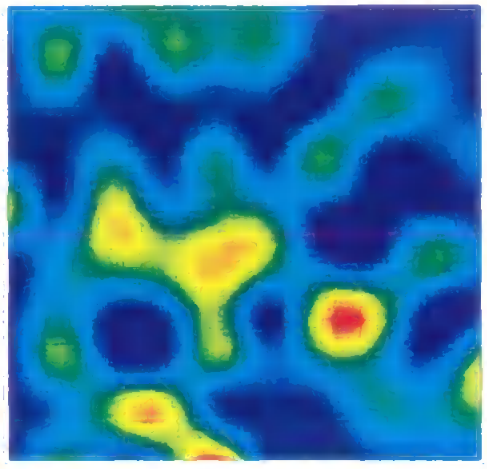

a)

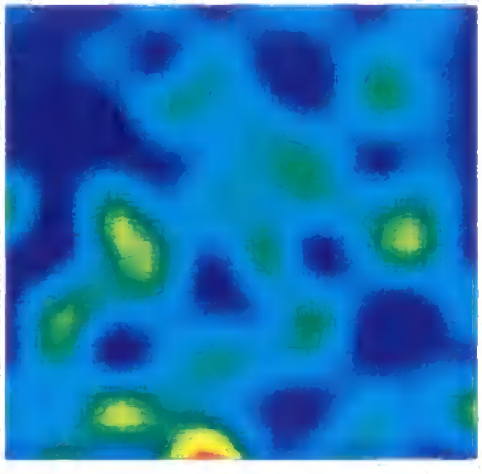

b)

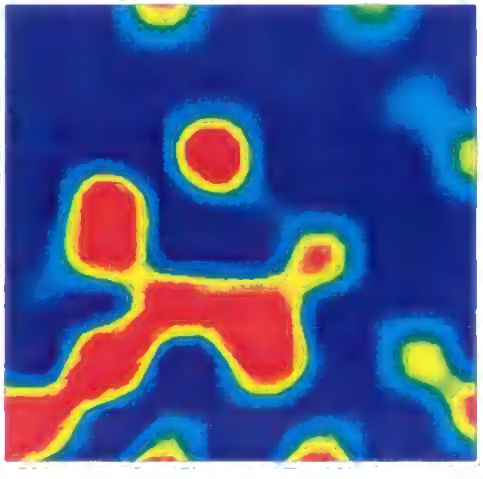

c)

Figure 5.11 Velocity flow patterns through a sand sample from Mathews and Matthews (1999)

Figure 5.12 is a comparison of the number of funnels conducting the majority of the flow before and after oil injection, in all four cases there is a decrease the number of funnels conducting flow after oil has been injected. However, the flow patterns are not radically altered. This could be explained by the respective parts of the oil glomus gathering in low flow and stagnant channels causing an increase in the flow in preferential flow channels. This effect was predicted and discussed in Chapter 1.

By comparing the cumulative number of funnels conducting flow in this investigation to those of Mathews and Matthews (1999), Figure 5.13, it is possible to determine that these results from this study are very similar to those of Mathews and Matthews (1999). These results also show that none of the samples are like the outlayer, which indicated that the sample had not been fully saturated initially.

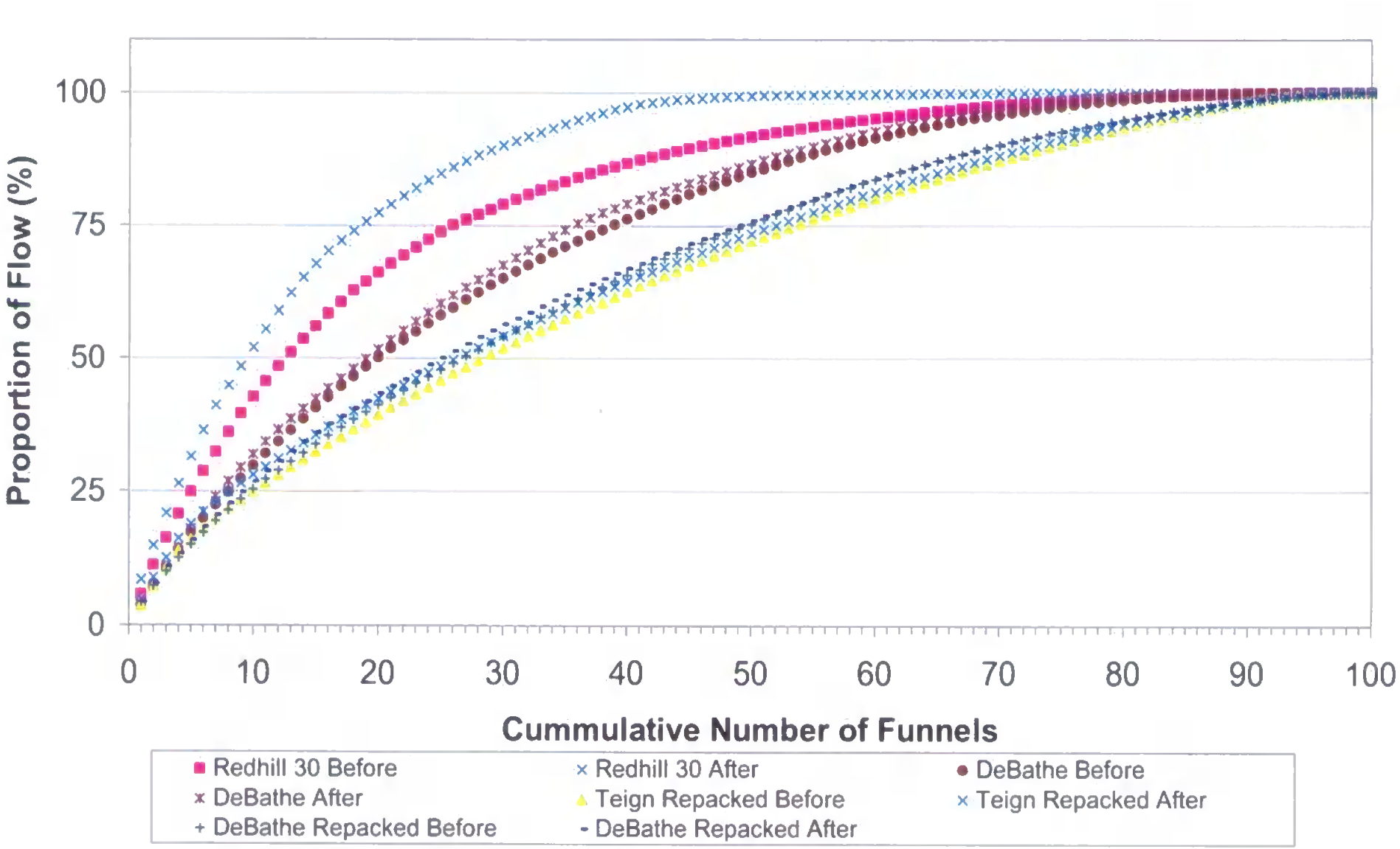

Figure 5.12 Cumulative number of funnels conducting the majority of the flow in this study.

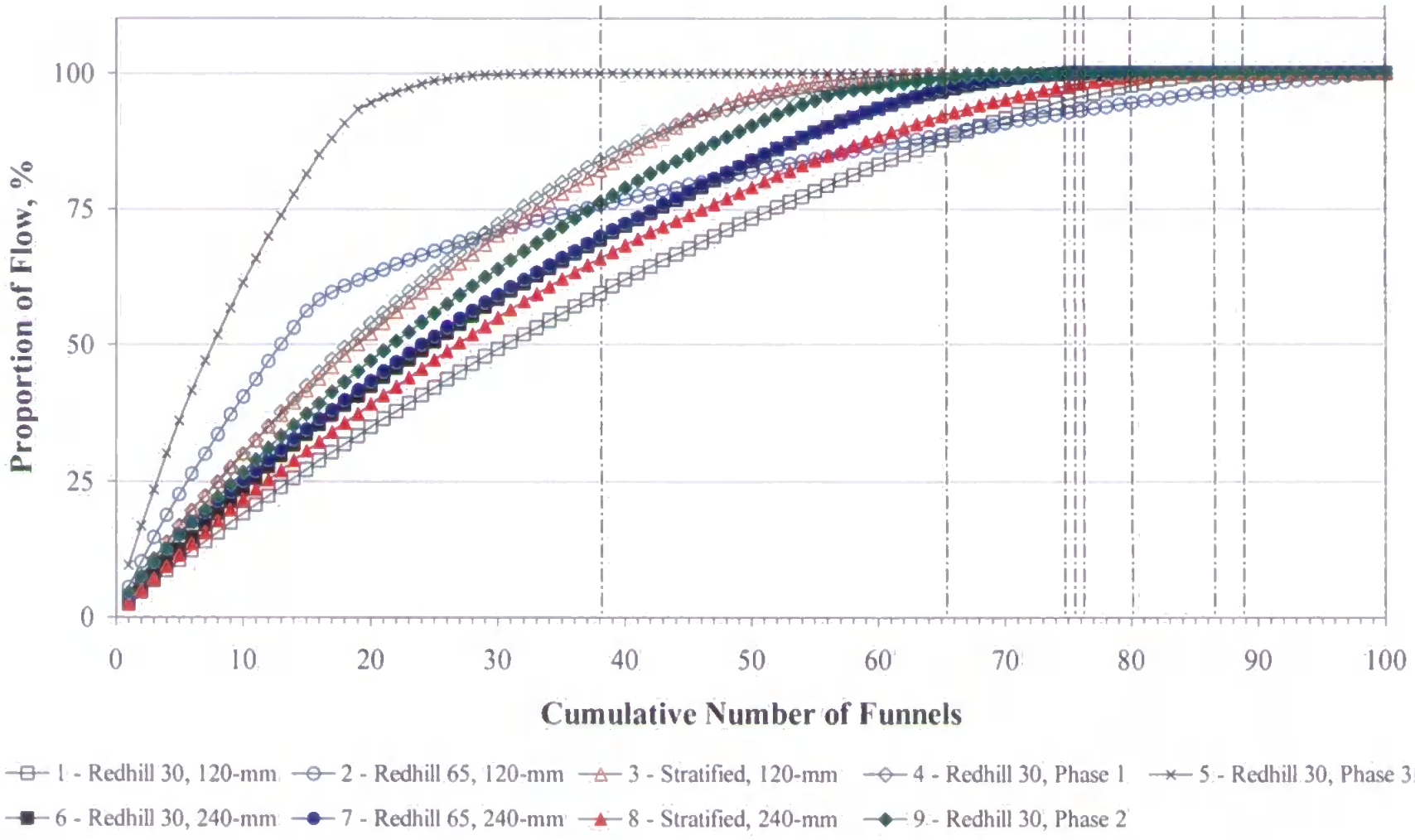

Figure 5.13 Cumulative number of funnels conducting the majority of the flow in Mathews and Matthews (1999)

A comparison of the frequency of flow velocities, allows additional conclusions to be drawn. In general, all the flow velocities show a large number of funnels conducting low flow. However, the number of low flow velocity funnels is greater after oil injection. A phenomenon which was also observed by Mathews and Matthews (1999).

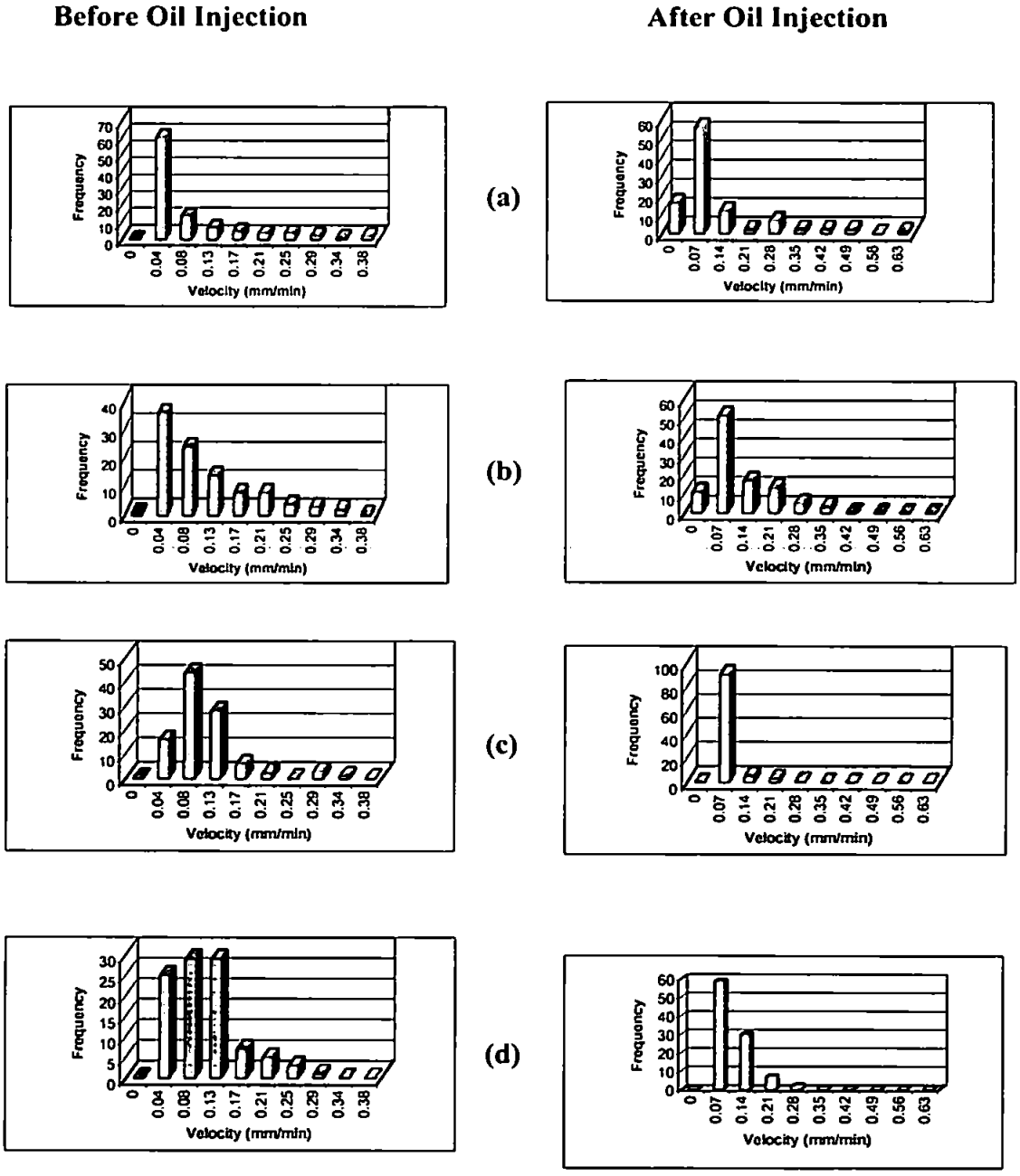

Figure 5.14 Velocity of flow histograms for (a) Redhill 30 sand, (b) DeBathe soil, (c) Teign Repacked soil, and (d) DeBathe Repacked soil.

Results of χ^2 tests on the distributions, before and after oil injection, are shown in Table 5.4. This form of statistical test compares one distribution with another – for there to be a similarity, the confidence level is usually required to be greater than 95%. To provide a valid statistical test, categories containing fewer than six observation were combined. It can be seen that velocity flow distributions for both of the repacked soils do not show any similarity before and after oil injection, whereas there is a high similarity for the sand and a high similarity for the *in situ* soil suggesting that packing causes changes to water flow after oil contamination.

Sample	χ^2 Statistic	Degrees of Freedom	Confidence (%)
Redhill 30 Sand	0.807	3	80
DeBathe	5.06	4	30
DeBathe Repacked	11.30	4	<0.25
Teign Repacked	108.31	2	<0.001

Table 5.4 χ^2 tests of the water velocity flow distributions before and after oil injection.

5.4.4 Oil Migration Study

The oil migration results show little similarity between the water flow patterns and the location of the cable oil. In general it can be seen that the cable oil remains in the centre of the sample. In the Redhill 30 sample, Figure 5.15, the oil migration remains almost totally in the centre of the sample with the oil migrating vertically downwards from the point of injection, (designated the –y direction). However there does appear to be a slight tendency to migrate laterally in the same direction as the increased flow velocity results. Compare, for example, Figure 5.10(a) and Figure 5.15(a), which have the same orientation. However, as can be seen, this is only observed in the top 15-20cm of the sample.

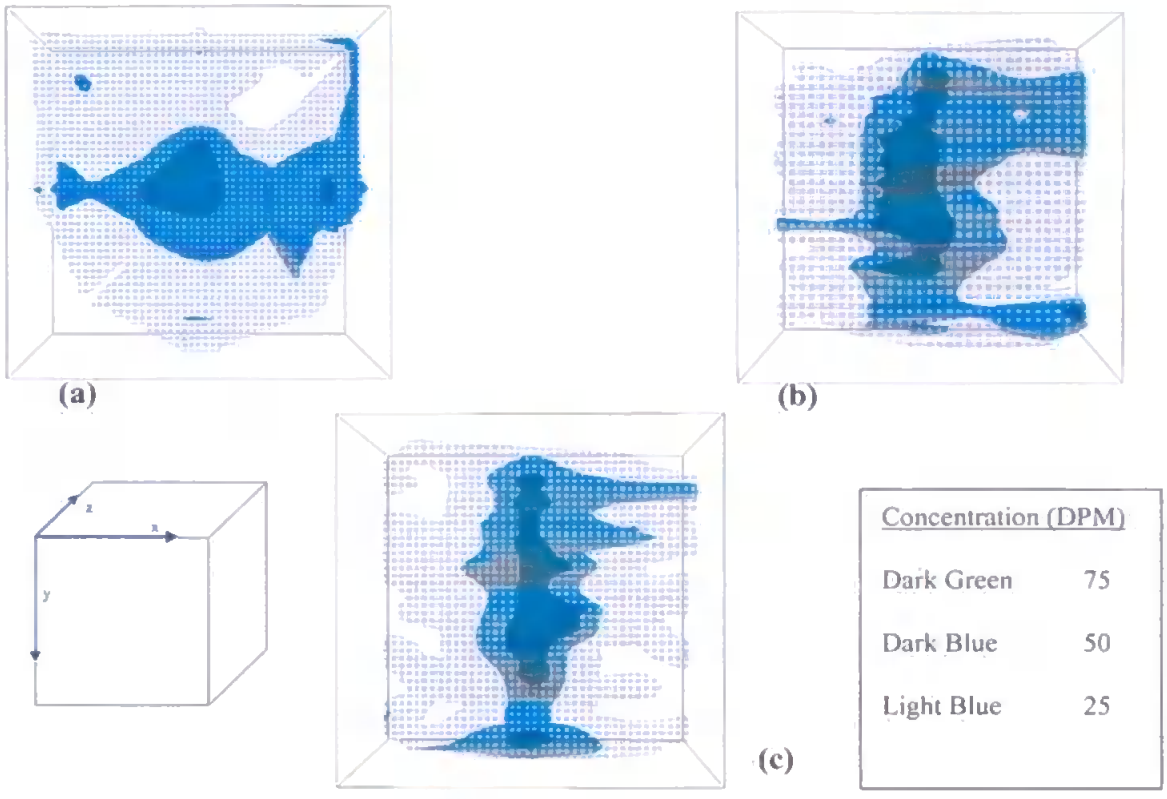

Figure 5.15 Oil migration results for Redhill 30 sand, (a) looking through the surface (xz plane), (b) looking through the xy plane, and (c) looking through the yz plane. The darker colours represent increasing oil concentration in DPM.

NB: All of the visualisations show x, y and z coordinates. These have no relation to either Pore-Cor co-ordinates or the x, y and z values in the glomus equations.

The oil migration results for the Teign series soil, Figure 5.16, display very similar patterns to the Redhill 30 sand, with the greatest proportion of the flow in the centre of the sample, although the oil does not migrate to the bottom of the sample. The water flow velocity suggests that it is unlikely that the spread of oil has been caused by the increase in water flowing through the sample at that point. The pattern that is represented suggests only vertical spreading of the oil through the soil.

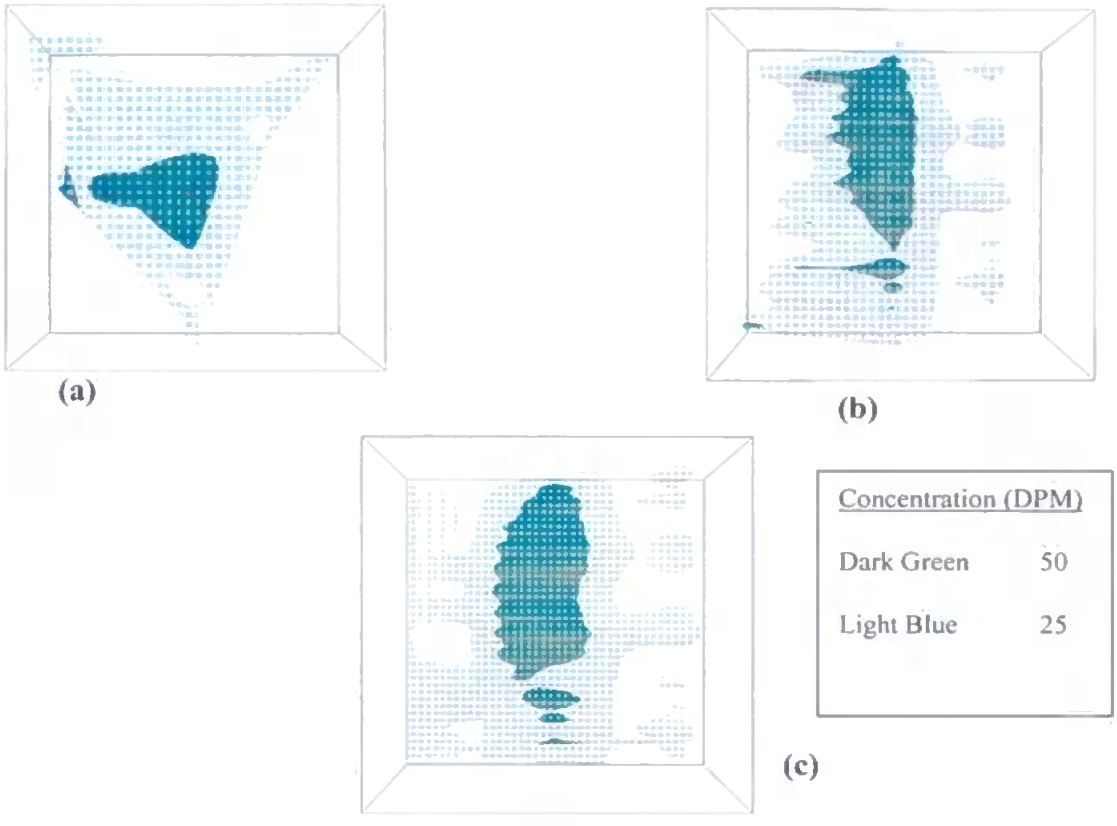

Figure 5.16 Oil migration results for Teign series soil, (a) looking from the surface (xz plane), (b) looking through the xy plane, and (c) looking through the yz plane. The darker colours represent increasing oil concentration in DPM.

The DeBathe *in situ* soil, shown in Figure 5.17, demonstrates that the migration of the infiltrating oil remains very close to the injection site with little lateral migration apparent. The water flow velocities do not exhibit any obvious preferential flow patterns.

For each of the three soils described so far, the oil migration patterns have been very similar, with very little lateral flow and primary migration occurring vertically. This may be partly explained by the saturation of each of these samples, with a general decline in saturation from the surface of the sample to the bottom, at the collector plate. This movement could be explained in terms of a glomus moving vertically through the sample towards the bottom.

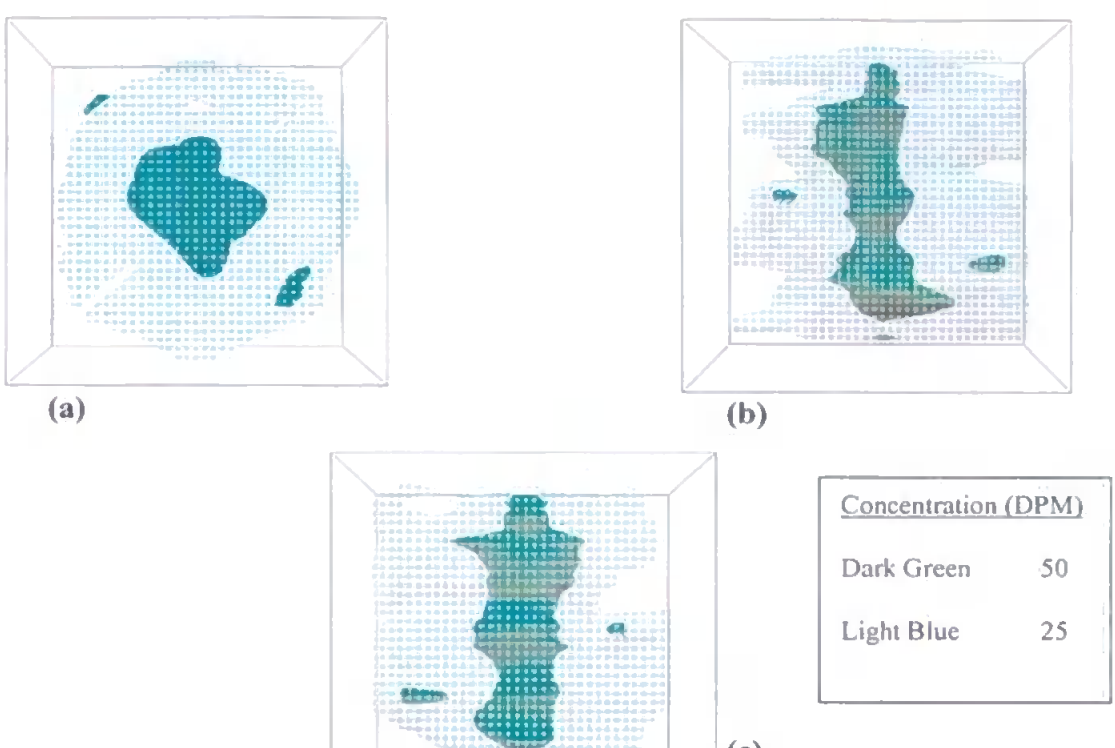

Figure 5.17 Oil migration results for DeBathe soil, (a) looking from the surface (xz plane), (b) looking through the xy plane, and (c) looking through the yz plane. The darker colours represent increasing oil concentration in DPM.

However, the oil mobility study for the DeBathe repacked sample presents a totally different extent of the oil migration, Figure 5.18. The extent of the oil shows that instead of just spreading vertically through the sample, as the other three studies have shown, there appears to be a relatively large amount of horizontal (lateral) movement of the oil. Initially the oil appears to move laterally instead of vertically from the point of injection. The glomus then to separates to form multiple secondary glomuses. Even after the formation of secondary glomuses little vertical movement occurs. The main bulk of the oil seems to dissipate over the soil block. This pattern of movement can be seen more clearly in Figure 5.19. It shows horizontal and vertical slices through the soil block. This movement may also be evidence that the packing of the sample had created impermeable barriers in which the cable oil could not penetrate.

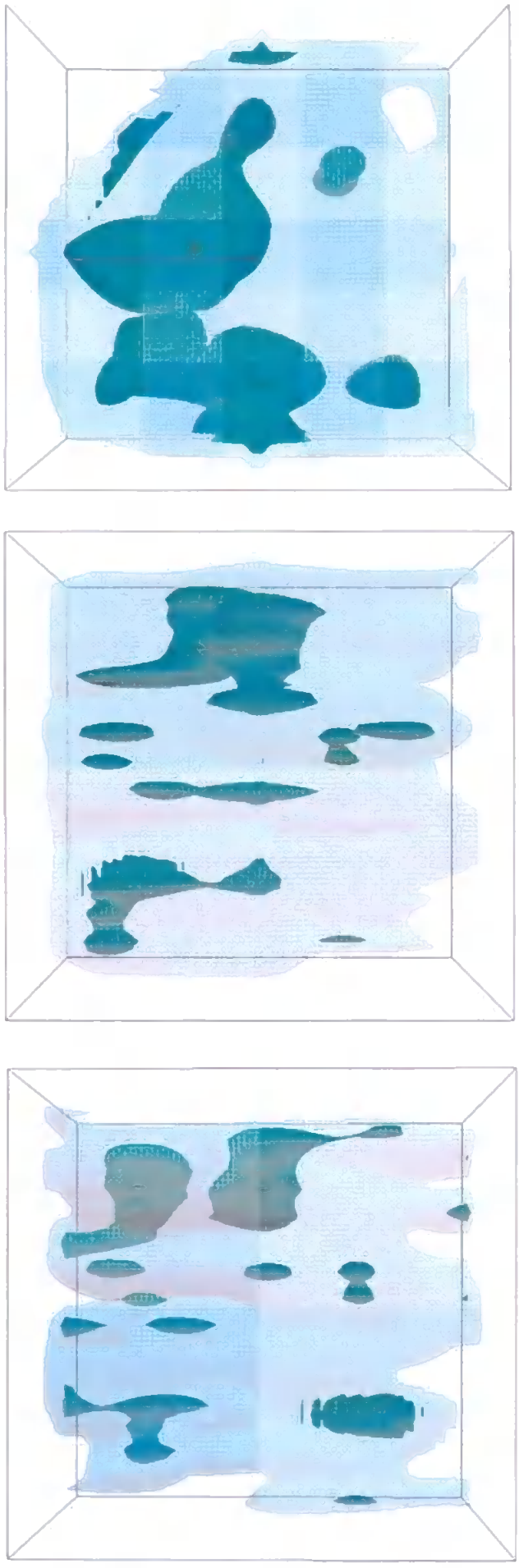

Figure 5.18 Oil migration results for DeBathe Repacked soil, (a) looking from the surface (xz plane), (b) looking through the xy plane, and (c) looking through the yz plane. The darker colours represent increasing oil concentration in DPM.

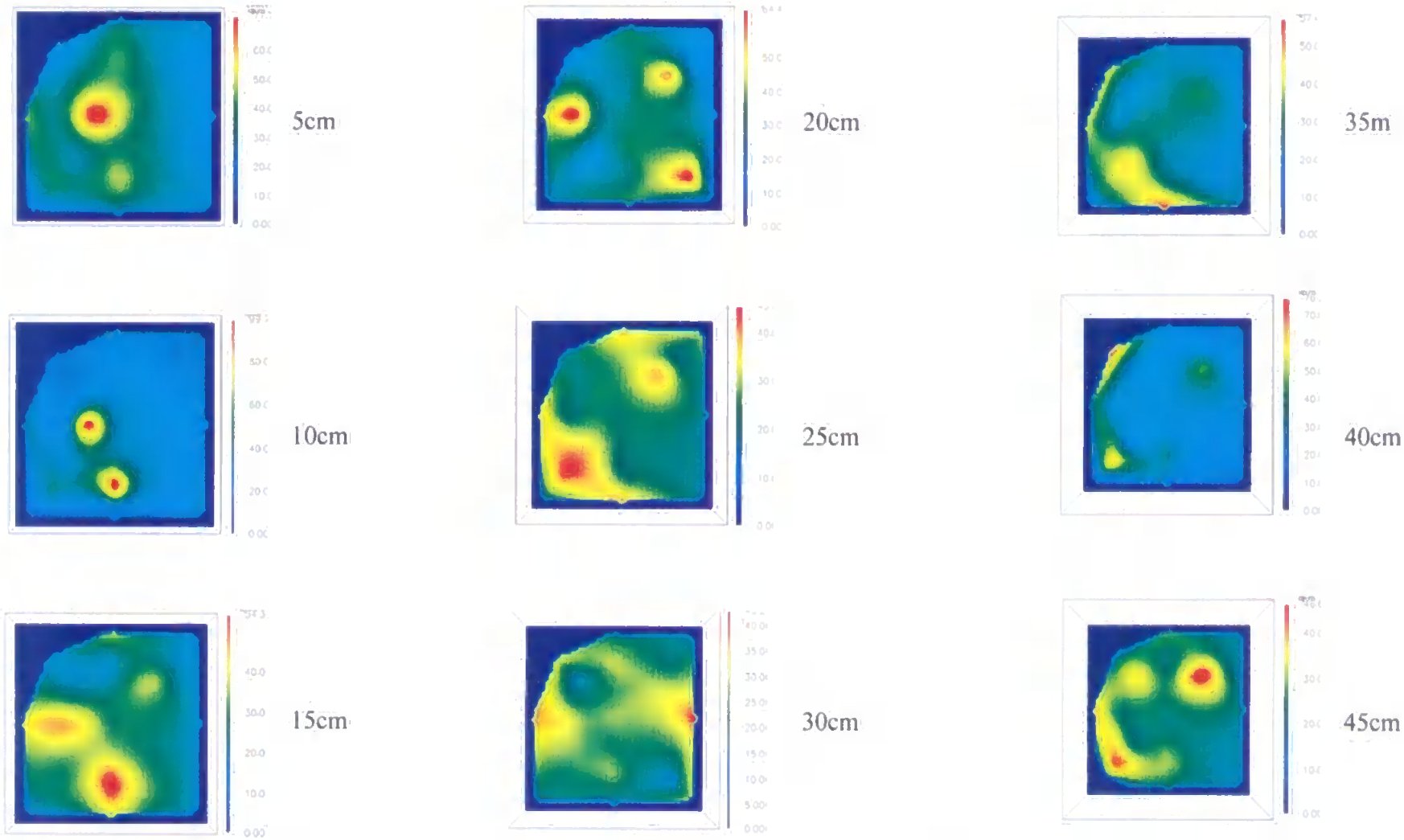

Figure 5.19 DeBathe repacked oil migration results, horizontal slices every 5cm (xz plane) at the end of the experiment.

5.5 Conclusion

In this study, significant preferential flow has been observed from the water flow velocities, with flow bypassing a large proportion of the sample volume. This shows there to be significant lateral variations in the flow regimes, in apparently homogeneous samples. The flow was more uniformly distributed in the repacked soil samples which could suggest that repacking affects the structure of the soil thus causing it to flow less preferentially. Small variations exist after the addition of an immiscible pollutant, causing a decrease in the number of funnels conducting the majority of water flow.

In the oil mobility study, significant vertical migration occurred in all but the repacked DeBathe soil. This lateral migration in the DeBathe repacked sample could suggest that packing caused the creation of less permeable areas (to oil, but not to water), which prevented vertical migration, as Butts and Jensen (1996), discovered. They noted that fingering occurred in coarse sand layers and when the migration reached a fine sand lateral, diffusive flow occurred.

It was also noted in the course of these experiments that the saturation level under the constant rainfall conditions was too great (initially) to permit the oil to infiltrate into the soil. Hence the rainfall had to be stopped to allow penetration. This effect did not occur for the more permeable Redhill 30 sand. Guigard et al., (1996) noted that oil migration was largely independent of water content. The results from these experiments appear to support this conclusion, although when the soil is close to or at full saturation, the ability of oil to migrate into the soil is significantly reduced.

6. Design of the Cranfield Pit Experiments

6.1 Introduction

The Cranfield pit experiments were designed to investigate the migration of the cable oil on a much larger scale than is possible within the confines of the laboratory. The scale of the experiment made it imperative that the experiment worked first time. As a result, several hypotheses were constructed with respect to the distribution of oil in each pit, to make the best use of the experiment. The hypotheses are as follows:

- That a plane of symmetry exists from the point of injection for oil migration,
- That the plinth does not affect the migration of cable oil;
- That the extent of flow is dependent on the quantity of oil added;
- That the extent of oil migration (vertical and lateral) does not alter during water table movement;
- That the two soil types are identical in respect of soil structure, suction, water table and rainfall.

It was not expected that these hypotheses would necessarily be true, but that the testing of them would provide a structure for the design of the experiments.

Due to the size and nature of the experiment the climate conditions were left to those which naturally occurred during the duration of the experiment. As a result the ambient rainfall and evaporation occurred. The rainfall over the period was typical for the season of winter period and evaporation would not have been significant during this time. However, the evaporation would have been slightly higher than the B soil horizon would normally experience due to the lack of an A horizon and vegetation.

6.2 Construction of the Pits

The pits were constructed within one of a pair of existing submerged concrete lined flood tanks, located at Cranfield University's sewage treatment works. The tank used was 10m

long, 4m wide and 1.5m deep. The existing reinforced concrete shell was extended above ground level by 0.5m to increase the depth of the pit to 2m, Figure 6.1. A schematic diagram of the pits is given in Figure 6.2.

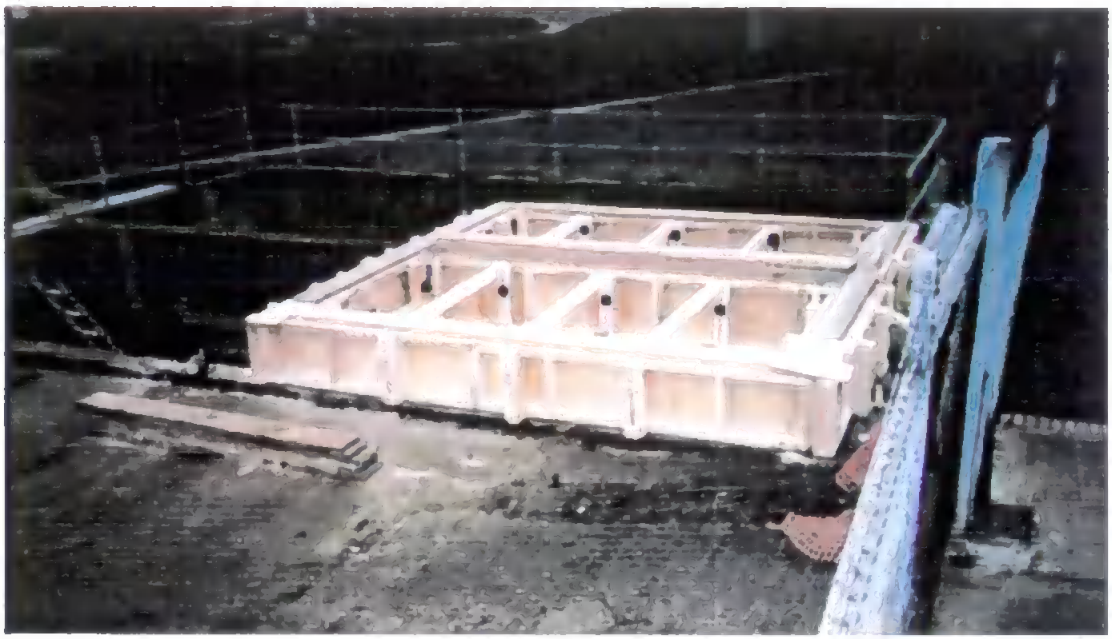

. (a)

(b)

Figure 6.1 The construction of the pits at Cranfield University.

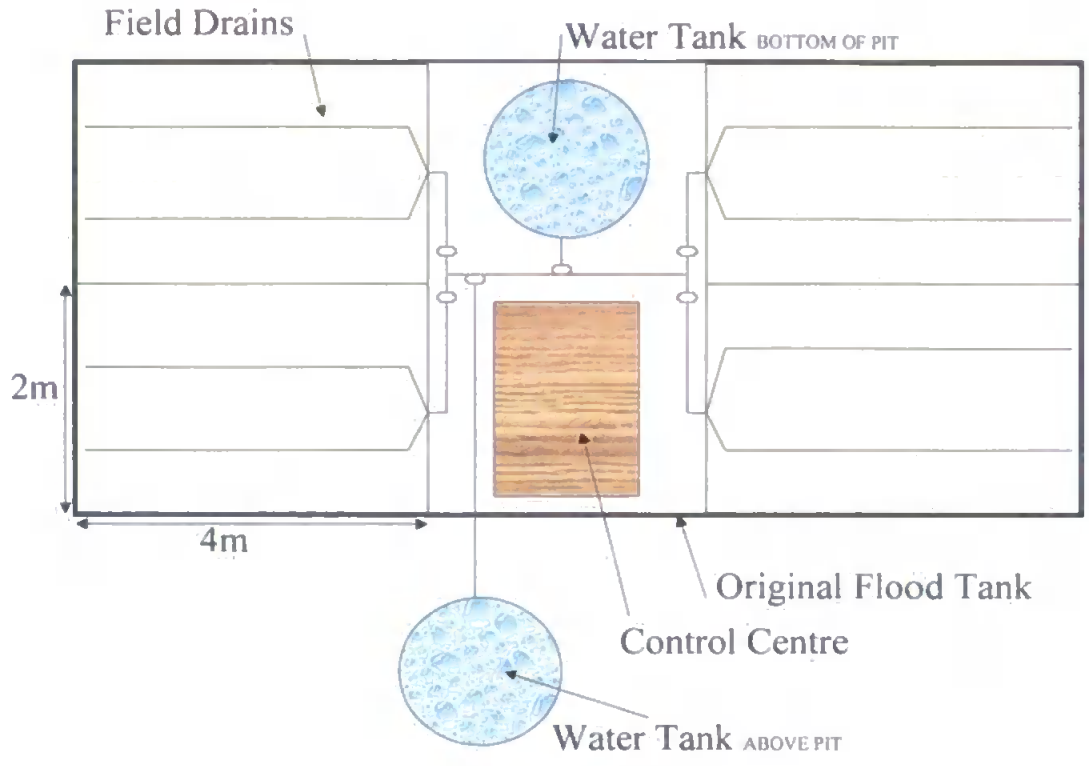

Figure 6.2 Shows a schematic layout and cross-section of the pits.

Modifications to the internal structure of the tank provided two pairs of symmetrical pits, each approximately $16m^3$ in volume and separated by reinforced concrete walls. The pits were used to represent the cable joints constructed by the NGC in true scale. Each pit had a concrete plinth, 1.15m by 1.3m in size, located adjoining the internal wall at the bottom of the pit dividing the two pits. The plinth, Figure 6.3, simulates the concrete slab that the NGC use to support cable joints, in joint bays in the field. Each pair of pits were to be filled with the same soil, one to be used to study the migration of cable oil and the other to study bioremediation techniques, as part of another NGC funded project. This underpinned the assumption throughout the experiments that the pits within each pair would produce identical results.

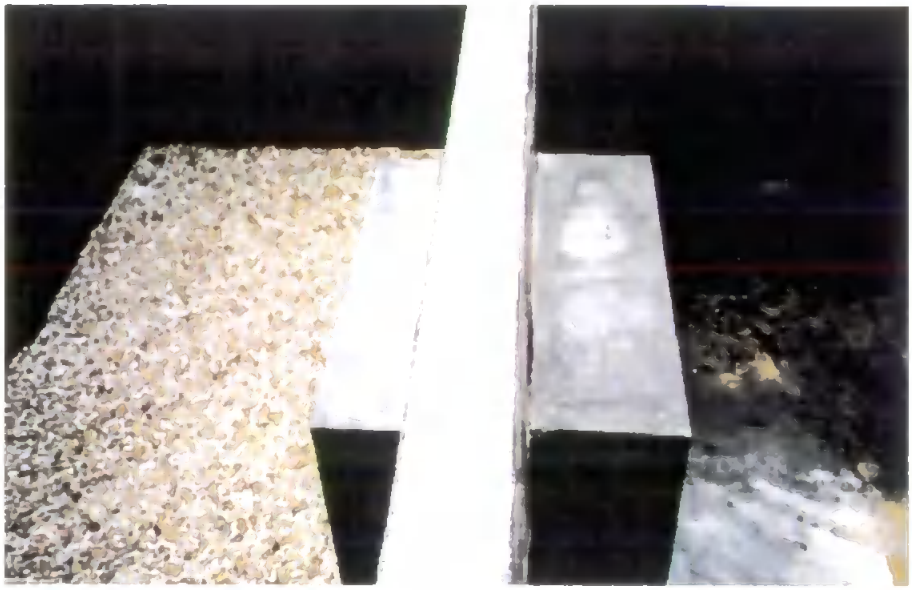

Figure 6.3 View of the pair of plinths. The left hand pit has the gravel layer in place.

The potential environmental impact of the oil and the location of the pits meant that no oil or effluent could be lost from the system. A key component of this was to ensure that no leakage of contaminants was possible through any existing cracks in the concrete walls. To achieve this, each bay was lined using a geomembrane resistant to hydrocarbon degradation. A Kaliko polyester fleece separation layer was laid on all four sides and the base of each pit. All angles were covered using pre-formed Kaliko PVC coated steel trims which were mechanically fixed over the fleece onto the concrete surface. A Kaliko 'SF 1.5 BVBR' reinforced PVC membrane, was lapped a minimum of 50cm on the joints and heat welded using a bead of Kaliko liquid PVC sealant which was applied along each welded seam.

Two 10cm diameter perforated field drains were placed at the bottom of each bay to act as collection conduits. These were covered with a 25cm deep layer of washed gravel to prevent the conduits becoming clogged, Figure 6.3.

6.3 *Materials and Methods*

6.3.1 Sample Characteristics

With 650km of underground cables located throughout England and Wales, the NGC encounters a wide range of soil types. It is not possible within the scope of the experiments to examine all possible soil types and so the soils selected have been identified by the NGC as those most representative of the wide variety of soils encountered. The soils used are those previously identified in Chapter 5, namely the DeBathe soil and the Teign series soil. Due to the scale of the experiments it was not possible to run a repeat experiment if things went wrong. To fully test the methodology, and analysis prior to conducting the experiments on the soil, a simulation was conducted using Redhill 30 sand.

6.3.2 Soil Extraction

Excavating soil to be used in mobility studies is a complex process. The soil needs to remain as intact as possible to maintain the structure of the soil. The main concern about the soils used in this study was that the edges of the soil would smear during digging, resulting in a destruction of the soil characteristics. In particular, the smearing risked the formation of an impermeable barrier because of the alignment in clay particles artificially preventing migration of water and oil. As a result, it was considered imperative to extract the soil only when it is dry, i.e. when there has been a period of dry weather, to prevent the occurrence of smearing.

This criterion caused substantial problems with extraction of the two soils because of the unseasonal amount of rain that fell during the summer of 1998. Delays resulted which meant that the DeBathe soil could not be extracted until August 1998 and the Teign Series soil was not extracted until December 1998. Continuing rainfall meant that the Teign soil had to be covered prior to extraction to keep the soil sufficiently dry enough to prevent smearing.

The soil was extracted using a mechanical digger from its *in situ* state, after removal of the topsoil, (the top 25cm of soil and vegetation), Figure 6.4. The soil was transferred into lorries and transported to Cranfield University where it was placed onto a hard standing adjacent to the pits and covered with plastic sheeting, overnight, until it was packed into the pits.

Figure 6.4 Extraction of the DeBathe soil, August 1998.

6.3.3 Soil Packing

6.3.3.1 Sand

The Redhill 30 sand was delivered to the site, kiln dry, allowing for easier packing because it could be poured directly into the pit. TDR probes were laid at specified depths, Table 6.1, to allow the volumetric water content to be determined across the pit as a whole. The table shows depths at two types of location as described below in Figure 6.8. Above the plinth a 1.5m length of 75mm diameter plastic pipe was inserted to provide a point source for the oil contamination.

Depth (cm) Redhill 30 Sand		Depth (cm) DeBathe Soil		Depth (cm) Teign Soil	
10	10	10	10	10	10
55	25	55	40	55	40
100	40	100	55	100	55
150	55	120	70	120	70
	70	135	85	135	85
	85	150	100	150	100
	100		120		120
	150		135		135
			150		150

Table 6.1 Depths of TDR probes for the pit experiments.

6.3.3.2 Soil

The method used for packing the soils was identical in all four pits. Placement of the soil was carried out when the soil was dry to ensure good compaction and prevent smearing. The soil was inserted into the pits using a front loader, spread using a spade and compacted in layers no greater than 15cm in depth. The compaction was undertaken using a 4cm plank of wood and $10cm^2$ hand pommel over the whole area of the pit. The compaction resulted in bulk densities of 1.81 kgm^{-3} for the DeBathe repacked soil and 1.58 kgm^{-3} for the Teign repacked soil.

The surface between layers was then raked to provide a 'key' for the next layer. This key helped prevent smearing and the creation of preferential flow pathways. TDR probes, Table 6.1, and the plastic injection pipe were installed at various depths in an identical way to the sand experiments. The soil was left for a minimum of three weeks (including pre-saturation) to ensure maximum compaction and settling of the soil prior to the oil being added to the pits. Figure 6.1 shows a pair of pits after soil packing had taken place.

Figure 6.5 Photograph of a pair of pits containing DeBathe soil after soil packing. The black vertical tubes are the oil injection pipes. The black wires are connected to the TDR probes contained within the pits. The brown pipe in the left hand pit was used for subsequent testing of bioremediation techniques.

To simulate the sand:cement backfill of joint bays in this study, the area surrounding the point of injection was filled with Redhill 30 sand. This sand area was 1.3m x 20cm x 20cm, as shown in Figure 6.6.

Figure 6.6 Injection point surrounded with sand (to simulate sand:cement backfill used by the NGC), the wooden shuttering was removed as the soil level got higher.

6.3.4 Water Level Control

6.3.4.1 Hydraulics

The moisture content of the pit was carefully controlled during all experimental stages of the investigation. Within each pit the water level was controlled allowing water to drain using gravity, from a 2.6m^3 water tank located at the surface, through 25mm flexible pipe, into perforated conduits. The water level was further controlled with a U-tube arrangement located on the front wall of the pit, Figure 6.7. This could be adjusted to any height within the 2m depth of the pit. The U-tube was prevented from acting as a siphon by a 1m-vent pipe located at the top of the tube. Excess water within the system above the groundwater level set by the U-tube was collected in another water tank located in the centre of the existing flood tank.

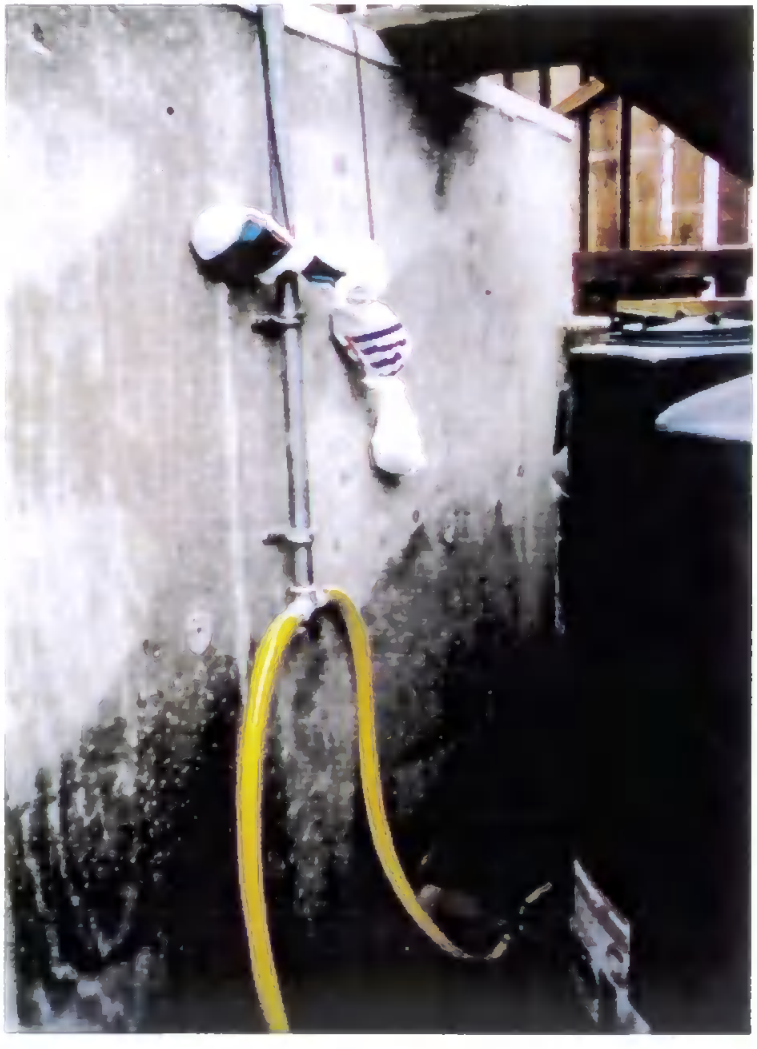

Figure 6.7 The U-tube arrangement to control water table height.

6.3.4.2 Saturation

Before contamination could commence it was necessary to fully saturate the soils to achieve further compaction and packing. The taps to the U-tubes were fixed at the soil surface and each pit was left overnight to saturate. Full saturation was determined to have occurred when ponding was visible on the soil surface. It was possible to prevent a pit from overflowing during saturation, by moving the U-tube to the height of the soil surface and operation the system of valves. Valves were opened at the bottom water storage tank during saturation to act as an overflow for surface water.

The water table was set at a pre-determined level before the oil contamination commenced. Once the pit had been fully saturated, the free water in the pit was drained, by opening the lower valves, and using the bottom water tank as a store for this water. The level of water was 100-120cm below the surface. No further water was removed once the oil injection phase of the experiment had started.

6.3.5 Moisture Content Determination

Time Domain Reflectometry (TDR) was used to measure saturation, with probes installed during the packing of the soil and sand at predetermined locations, Figure 6.8. The initial design of the TDR probes in the sand trail was the two pronged design, but this was found to be difficult to interpret. As a result, a three pronged design by Zegelin et al. (1989) was used, which can be seen in Figure 6.9. This system attached the central wire of the coaxial cable to a single rod, the outer shielding of the coaxial cable was then attached to two outer prongs. The advantage of the multi-wire transmission lines was the simplicity of the design and a resultant clear reflectance trace.

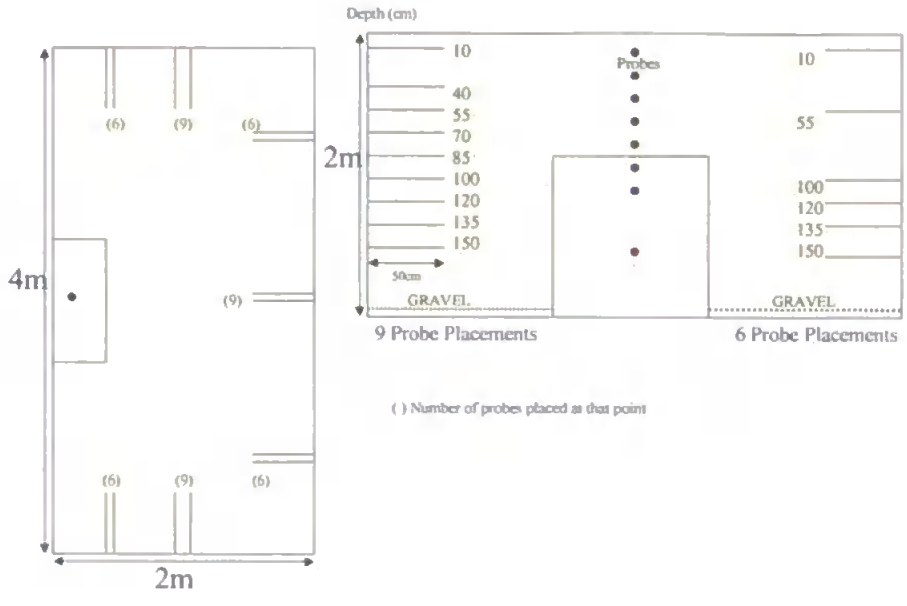

Figure 6.8 TDR location for the two soil experimental pits.

The 50cm length probes were located around the outside of the pit. This allowed water content to be determined without interfering with oil migration by causing preferential flow.

Figure 6.9 Placement of the TDR probes during repacking of the Teign series soil.

6.3.6 Tensiometers

The tensiometers were saturated in de-aired water for a twenty-four hour period prior to installation. To install the tensiometers, a hole was dug to the required depth with a 2cm auger (Van Walt Limited) in the DeBathe soil and a 7cm stony auger in the Teign series soil. The tensiometers were installed vertically between two sets of TDR probes at each end of the pit, so that the relationship between saturation and suction could be investigated. The tensiometers were located at 50cm, 100cm, 125cm and 150cm from the soil surface.

To ensure good contact between the cups and the soil, a soil / water slurry was poured into the holes following installation, (Cassel and Klute, 1986). At the surface the gap between the tubes of the vertically installed tensiometer and the soil was carefully surrounded with bentonite clay, minimising preferential flow. After installation the tensiometers were filled (to remove any air from the tubing) with de-aired water and left to stabilise for a period of five days.

6.3.7 Weather Data

Weather data throughout the experimental period was recorded daily at the site using a Cumulus Automatic Weather Station, designed and manufactured by ELE International. This allowed the accurate monitoring of any excess rainwater entering the system, together with other parameters that may affect oil mobility. The data logger provided 8 analogue and 3 digital channels, allowing measurement of the following parameters; windspeed, wind direction, solar radiation, air temperature, relative humidity, barometric pressure, rainfall and soil temperature.

Further weather data was obtained from Silsoe College, approximately 10 miles from the experimental site. This data provided daily rainfall and maximum and minimum air temperatures over the whole period.

6.4 Oil Injection

The oil was discharged into the pit down the injection pipe (which was placed in the soil during repacking), into the surrounding soil, 85cm from the soil surface. Twenty litres of oil were introduced into the injection pipe every day for a four-day period, giving a total injection of eighty litres of oil into each of the four pits. This oil leak rate was chosen as a typical leak rate that the NGC were concerned about based on actual leakage data. It was also calculated from the one-dimensional study in Chapter 4 that eighty litres of oil was sufficient to traverse the majority of the pit over the timescale of the experiments. No head of oil developed during the addition of oil through the injection pipe.

6.5 Soil Sampling

6.5.1 Sampling Method

Sampling was carried out using a 7cm hand auger (Van Walt Limited) on the DeBathe soil and a 7cm stony hand auger on the Teign series soil, because of the stony nature of the Teign series soil. Samples were taken every 15 – 30cm depending on the sampling location. Samples were taken from the middle of the auger to avoid cross contamination, and the auger was wiped clean in between samples. The samples were transferred into plastic sample bags, taken back into the laboratory and then weighed before analysis was undertaken. The holes made by sampling were backfilled with soil of an identical soil type.

6.5.2 Sampling Plan

Sampling in the pit containing sand was carried out in a radial pattern from the point of injection, increasing the distance from the injection point with time. However this made analysis of the results difficult, because each of the locations close to the point of injection were sampled at day one, and consequently, increasing concentrations of cable oil could not be determined over time. The sampling plan for the sand pit is shown in Figure 6.10.

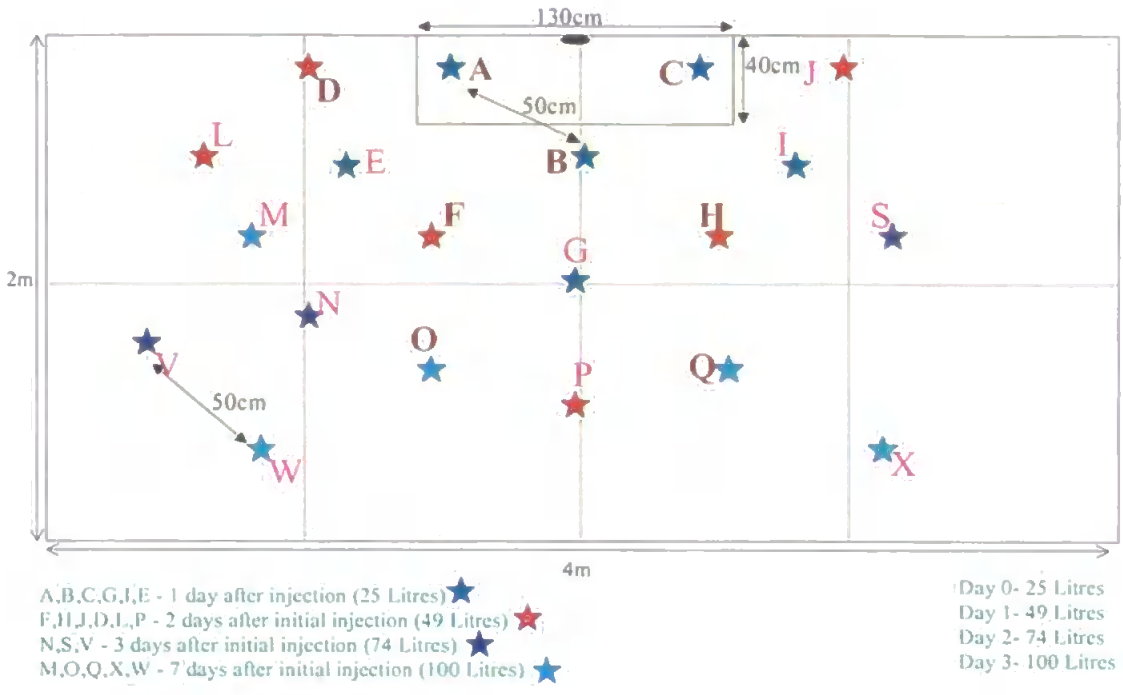

Figure 6.10 Sampling locations in the sand experimental pit.

The difficulties incurred in analysing the data from the sand experiment led to the design of a new sampling plan for the soil experiments. This plan involved taking samples along lines spreading outwards from the point of injection, over time, Figure 6.11. This scheme allowed increasing oil concentrations to be determined close to the injection point as well as the locations further away. Sampling locations were also chosen to test the other hypotheses, which included testing to see if a plane of symmetry existed in the pit (samples N, O, P, Q, R, T, U, V, β and δ).

The effect of the plinth was studied at sampling locations R, S and T. Others of these sampling locations were used to determine the effect of water table movements and to determine if the two soils were heterogeneous.

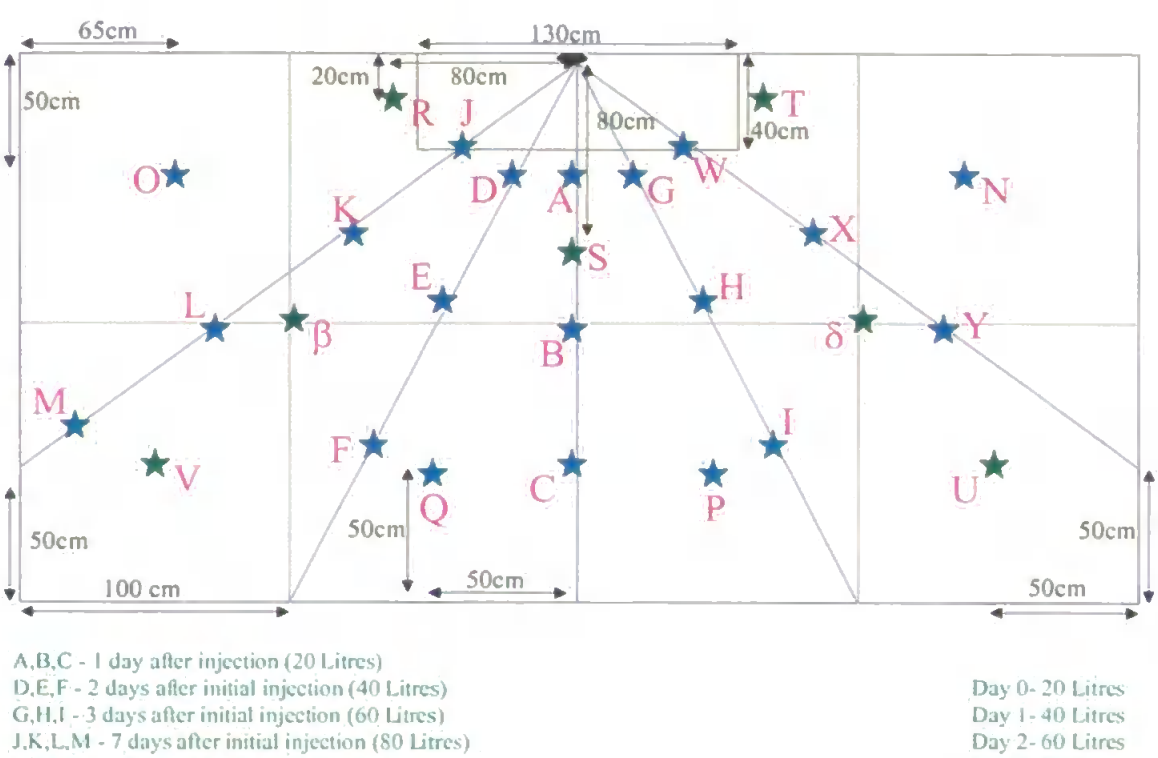

Figure 6.11 Sampling locations for the two soil experiments. The green type to the bottom left hand side refers to the sampling interval of the DeBathe soil, and the right hand side relates to the time when oil was injected into the sample.

6.6 Conclusion

The results of these experiments are discussed in detail in the following chapter.

7. Cranfield Pit Results

7.1 Introduction

The following chapter presents the results of the experimentation, the methodology of which is outlined in Chapter 6. The chapter then describes the modelling of the migration of cable oil in three dimensions.

7.2 Saturation

The volumetric water content of the two pits containing soil can be determined using the TDR data obtained from the pits. As mentioned in Chapter 6, the saturation of the two soils was such that prior to the oil injection the water table was located between 100cm and 120cm below the soil surface, as measured by the TDR readings. Once the oil had been injected the TDR probes continued to provide an accurate representation of the water saturation of the soil and any changes that occurred throughout the duration of the experiment. No drainage from the bottom of the pits occurred once the water level had been established throughout the entire experiment.

7.2.1 Sand

The TDR measurements from the initial sand trial showed that the TDR probes could be better positioned. This reflected the fact that many of the probes were located above the water table. The probes in the pit containing sand showed that the saturation within the pit containing sand decreased rapidly with decreasing depth from full saturation to almost dry sand, as shown in Figure 7.1, once the pre-saturation phase had ended. This is because the water retention of the sand is such that it can not hold or draw much water away from the point of full saturation. The water content of the sand fell in all locations from between 30-35% volumetric water content at 150cm deep to less than 10% at 100cm. However, the poor location of the probes, and the lack of probes at depth, meant that it was difficult to accurately establish the level of the water table within the pit. The saturation levels remained generally constant over the oil injection period of the experiment, after the initial

pre-saturation, although some decreases in saturation were recorded (as seen from Figure 7.1). These were quickly rectified with the addition of more water from the bottom of the pit. To rectify the problems caused by the location of the probes in the pit containing sand, the TDR probes were relocated prior to the installation and packing of the soils.

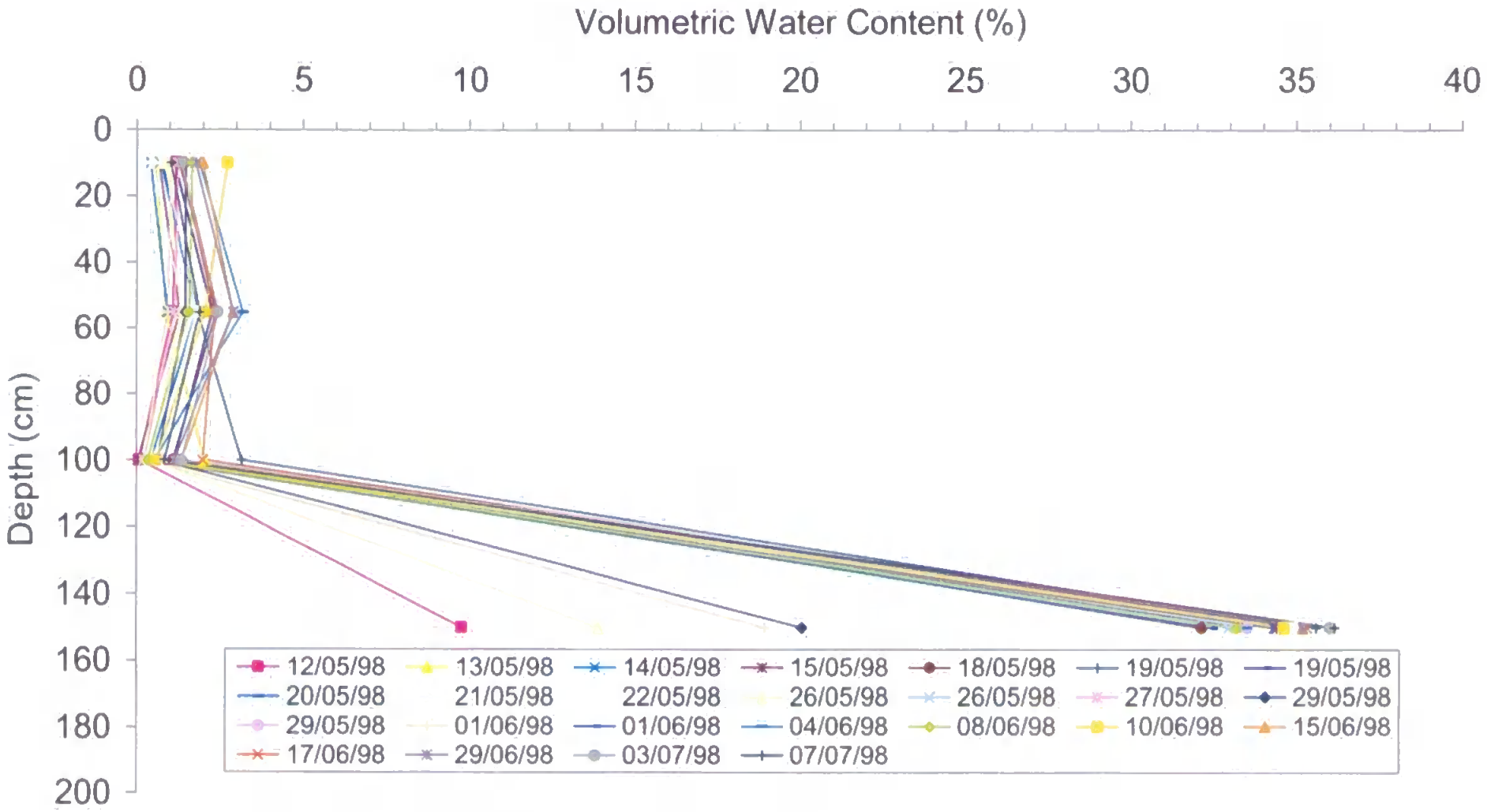

Figure 7.1 TDR measurements at location A for the sand trail experiment.

7.2.2 DeBathe Soil

The volumetric water content of the repacked DeBathe soil pit remained reasonably constant during the initial oil injection phase of the experiment. However, over the Christmas period (22/12/98 - 5/1/99) the volumetric water content increased, raising the water table to between 40cm and 55cm below the surface. The water could not be drained from the bottom of the pit because this would have resulted in both water and cable oil draining from the pit, and thereby reducing the quantity of oil within the pit. This would have reduced the reliability of the oil migration data. It would also have been difficult to quantify the amount of oil drained from the pit into the lower water tank. The volumetric water content for placement F (Figure 5.8) of the repacked DeBathe soil is shown in Figure 7.2.

In general, the saturation profiles for each location show a steady decline in water content from the bottom of the pit upwards towards the soil surface, as expected. However, some anomalies exist where the saturation profile at a point dropped between two higher measurements. This trend recurs for all the TDR measurement at that location, Figure 7.3. This has been attributed to the packing of the soil around the TDR probe and is in all probability due to poor contact between the probes and the surrounding soil.

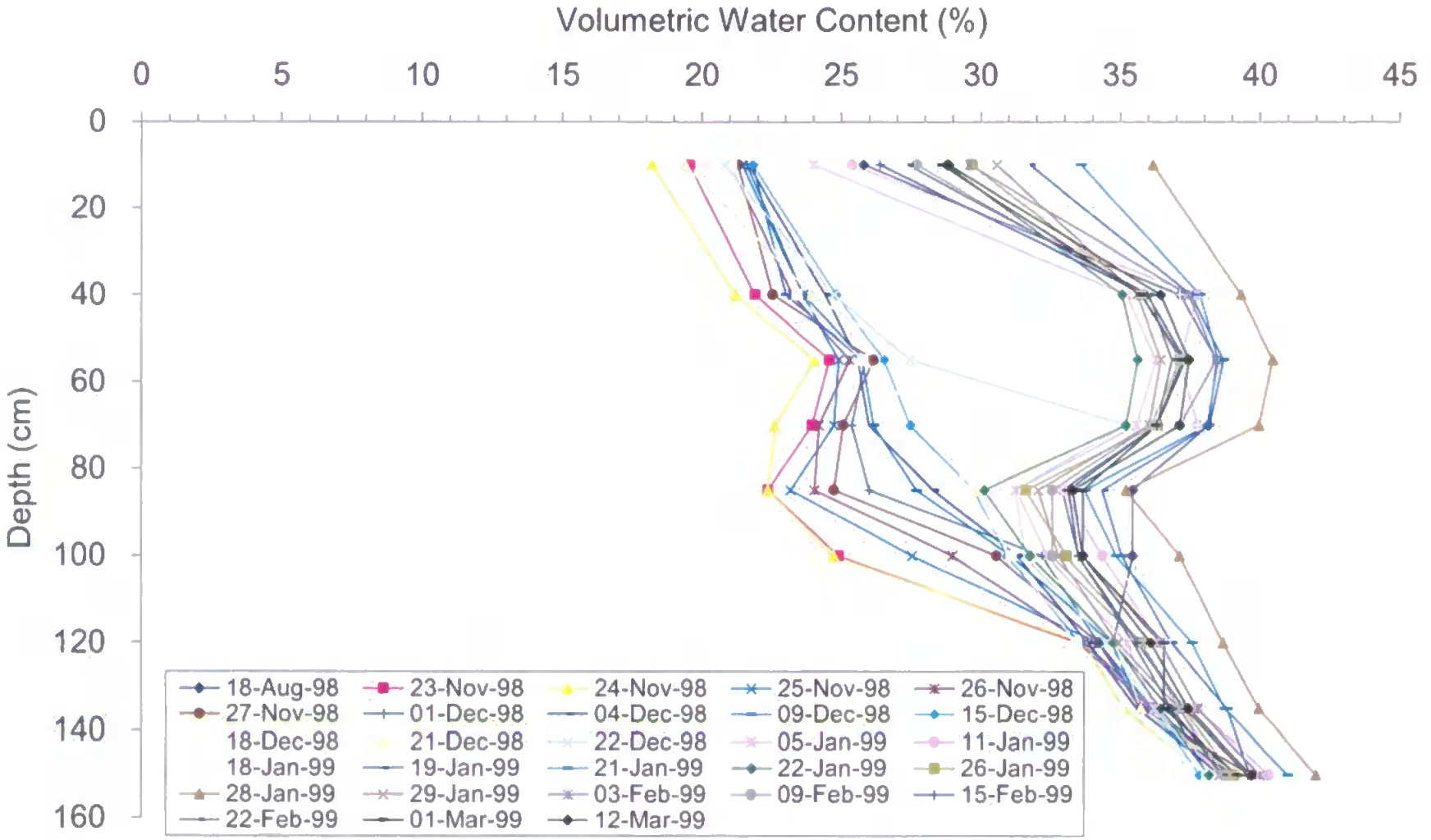

Figure 7.2 TDR measurements at location F for the DeBathe soil pit.

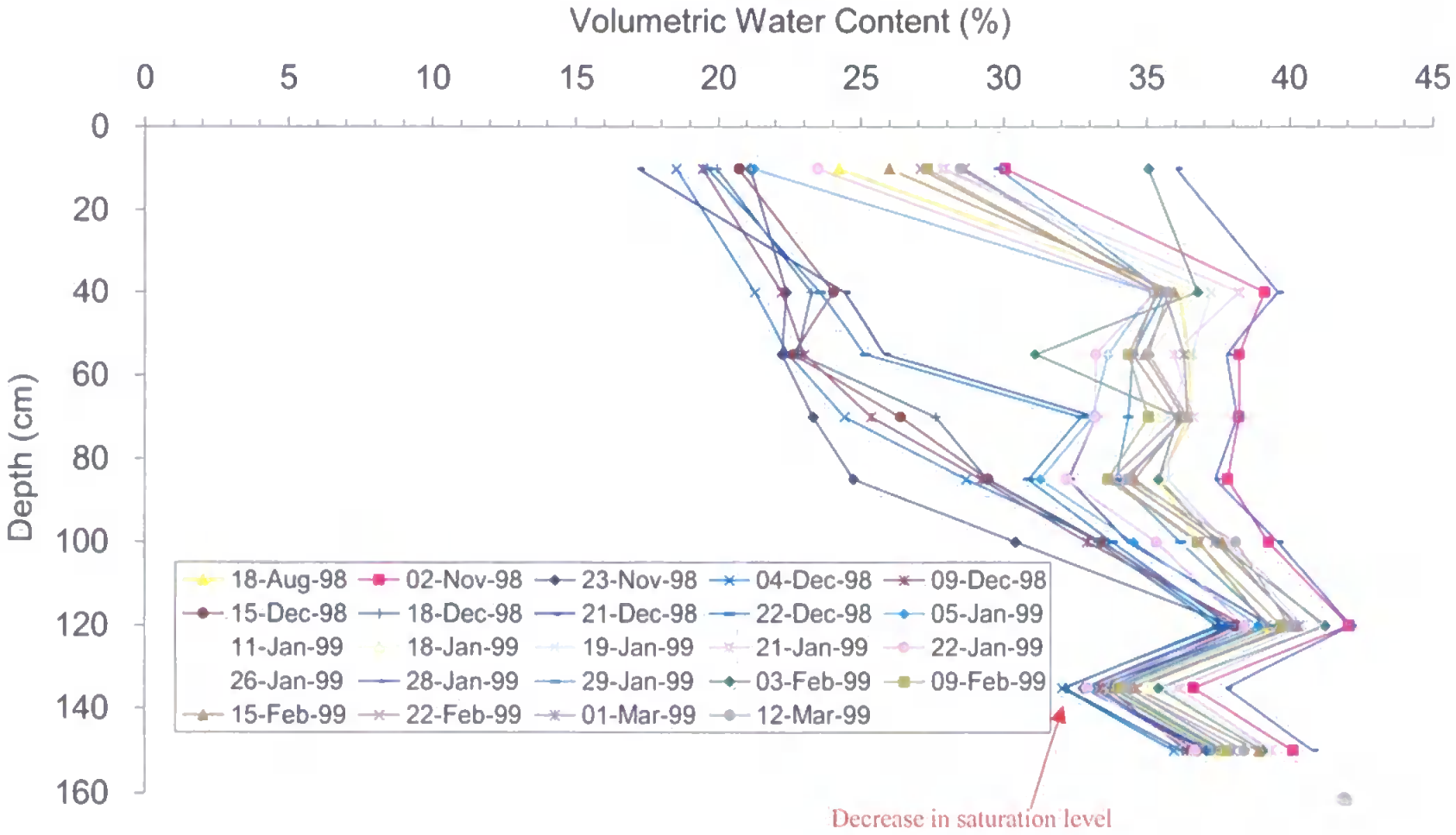

Figure 7.3 TDR profile for location D in the DeBathe soil pit, showing a rapid decrease in saturation content.

Overall, the saturation levels follow coherent trends from one location to the next. However, small variations are noticeable when comparing the water content at each of the various locations at a particular point in time. This reflects soil-packing effects on the saturation content of the soil surrounding the probe. If the soil surrounding the probe does not make good contact with the TDR probes, the soil's ability to hold water is altered, and this has a consequential impact on the measurement of soil water content around the probe. It should be noted that despite this effect some fluctuation in measurements can be expected because of the nature of the experimental method.

7.2.3 Teign

Figure 7.4 shows the TDR measurements for one set of probes in the Teign pit. The volumetric water content shows a greater variation than exhibited in the data for the other soil. During injection of oil, the water content at the bottom of the pit (120cm to 150cm) was in excess of 40%. However after contamination, the level decreased to approximately 35%. The remaining soil profile had a slightly declining water content.

One noticeable anomaly appears on the 22 February 1999. This corresponds to an attempt to raise the water table within the pit. The water table was successfully raised to 50cm below the surface but fell back to its previous level within five days. The general decrease in the saturation levels of the pit, which can be seen from the TDR measurements of 11 January 1999 onwards in Figure 7.4, can be attributed to a leak in the bottom of the pit. The leak prevented the pit from holding water beyond a certain point. It is believed that the lining, which was meant to be resistant to the cable oil, split at an unknown location.

The overall characteristics that were exhibited in the DeBathe soil pit are also present in the Teign pit. The saturation profiles for each location show a steady decline in water content from the bottom of the pit upwards towards the soil surface, as expected. However, as with the DeBathe soil, some anomalies exist where the saturation profile at one point drops between two higher measurements. These effects have been attributed to the effect of repacking the soil.

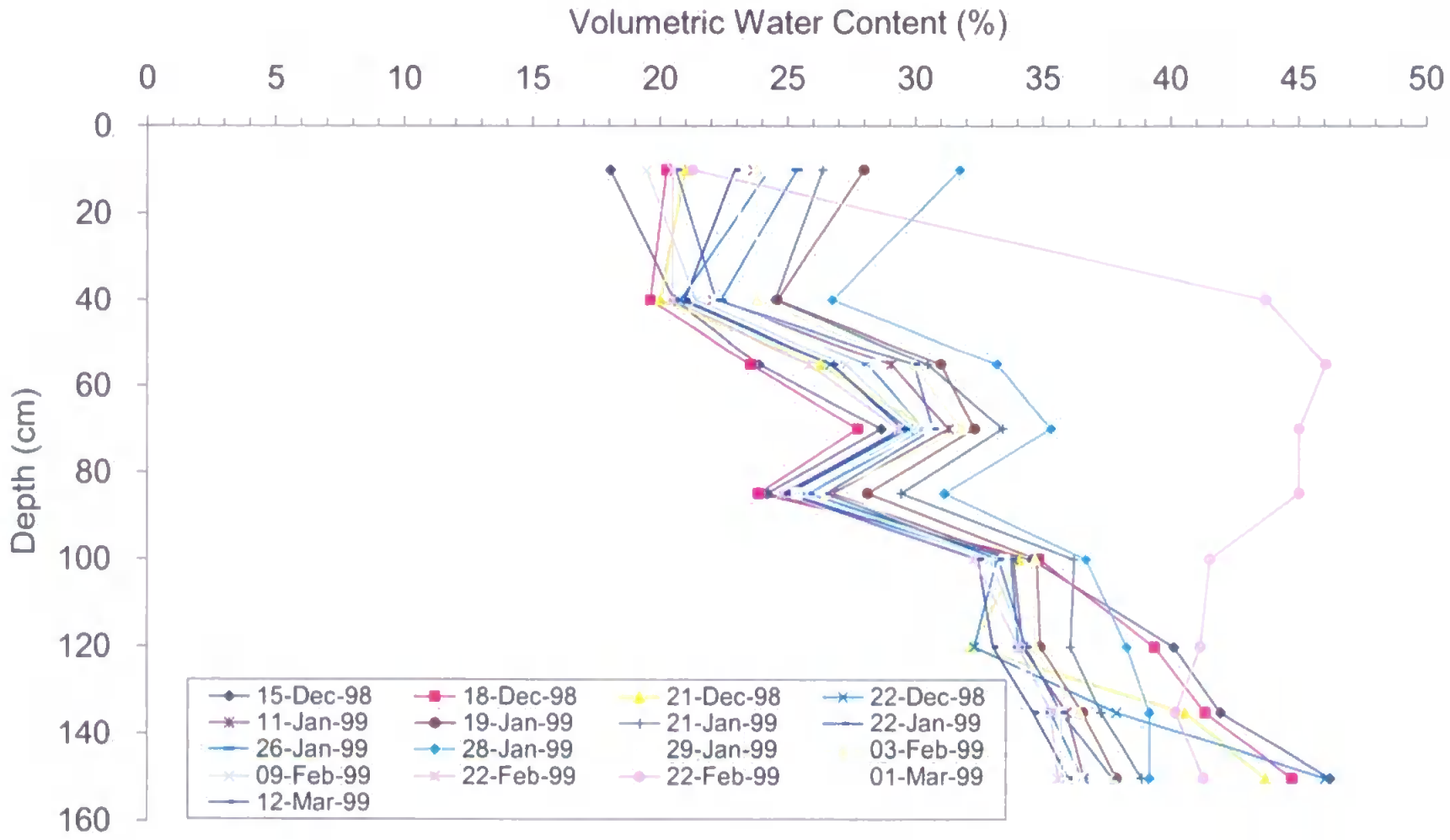

Figure 7.4 TDR profile of volumetric water content in Teign soil pit, location FF.

7.3 Tensiometers

The results from the tensiometers show that there is some soil suction. This corresponds to expectations based on observations of the TDR data. The TDR data suggests that although the degree of saturation in the soil is large it is not fully saturated and ponding, and thus has some soil suction. The tensiometer data also suggests that over the duration of the experimental period the saturation of the pits remain reasonably consistent. The results clearly show diurnal variations, gross water table movements, water filling and air removal from the tubing. The tensiometers were placed as far away from the point of oil injection as possible to minimise the risk of them being in contact with the cable oil. The results below (Figure 7.5) relate to the end of the experimental period.

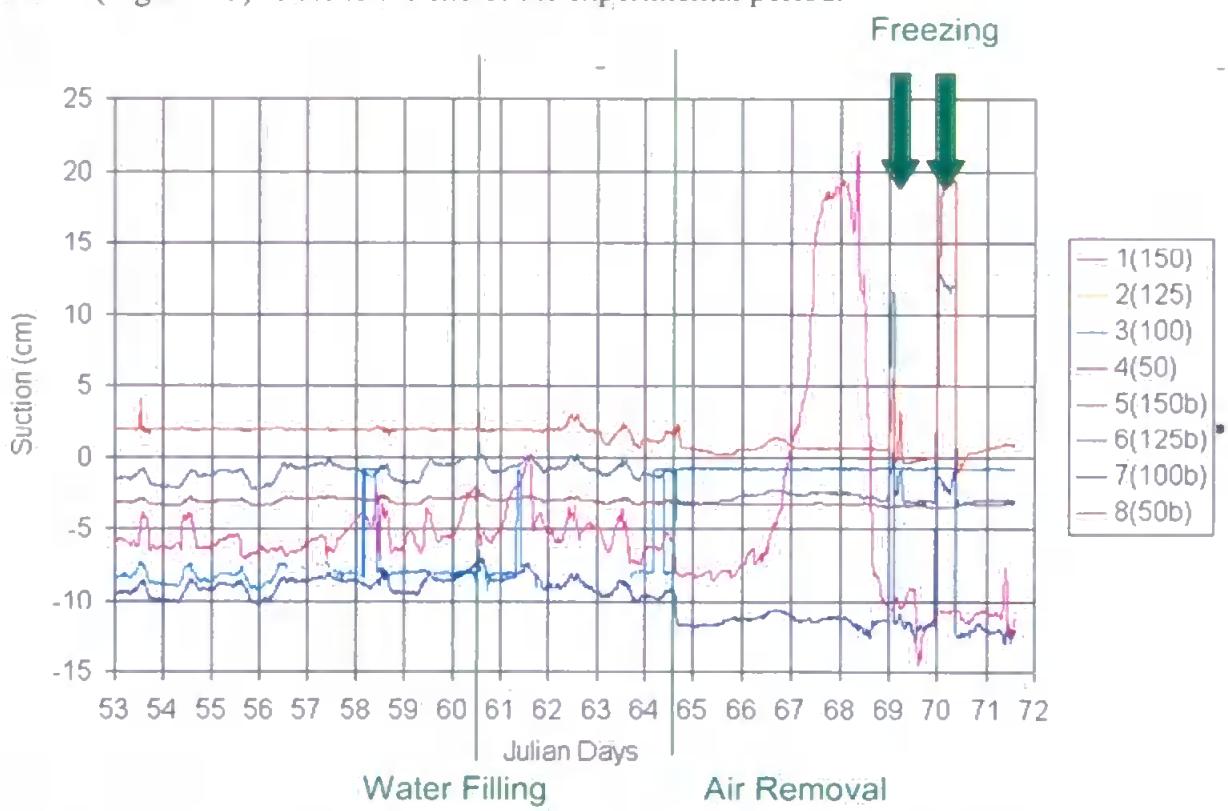

Figure 7.5 Some of the tensiometer data collected for the DeBathe repacked soil.

7.4 Weather Data

The weather data collected on site proved to be incomplete. A good comparison was found between the rainfall data collected 'on site' and the data received from Silsoe, which was sampled ten miles away from the site. No other weather data for the Cranfield site was

available. As a result of this, Silsoe supplied much of the weather data used in this study. No temperature data from the on site weather data collector recorded, and so the study has assumed that the same temperatures would have been recorded at both sites. Given the proximity of Silsoe to the test site, this is a reasonable assumption.

Rainfall over the duration of the experiment was characterised by periods of heavy downpours, particularly at the beginning of the experiment during oil injection (December 1998). In the latter half of the experimental period, about one-month after the initial oil injection (January 1999), the amount of rainfall reduced considerably. The rainfall data is shown in Figure 7.6.

The increase in the saturation level within the DeBathe pit can be explained by the period of heavy rainfall that occurred during December 1998. The pit was a closed system, which prevented water from draining out of the pit. The heavy rain resulted in more water entering the pit through the soil surface with a consequential increase in the water table.

The temperatures recorded over the duration of the experiment suggest that temperature did not have an impact upon the operation of the experiment. Recorded temperatures suggest that it was not warm enough to cause significant evaporation of water from the soil surface but it was cold enough to cause freezing of the tensiometers. No apparent freezing of the ground was observed. The minimum and maximum temperatures during the experimental period are given in Figure 7.7 on the right hand column.

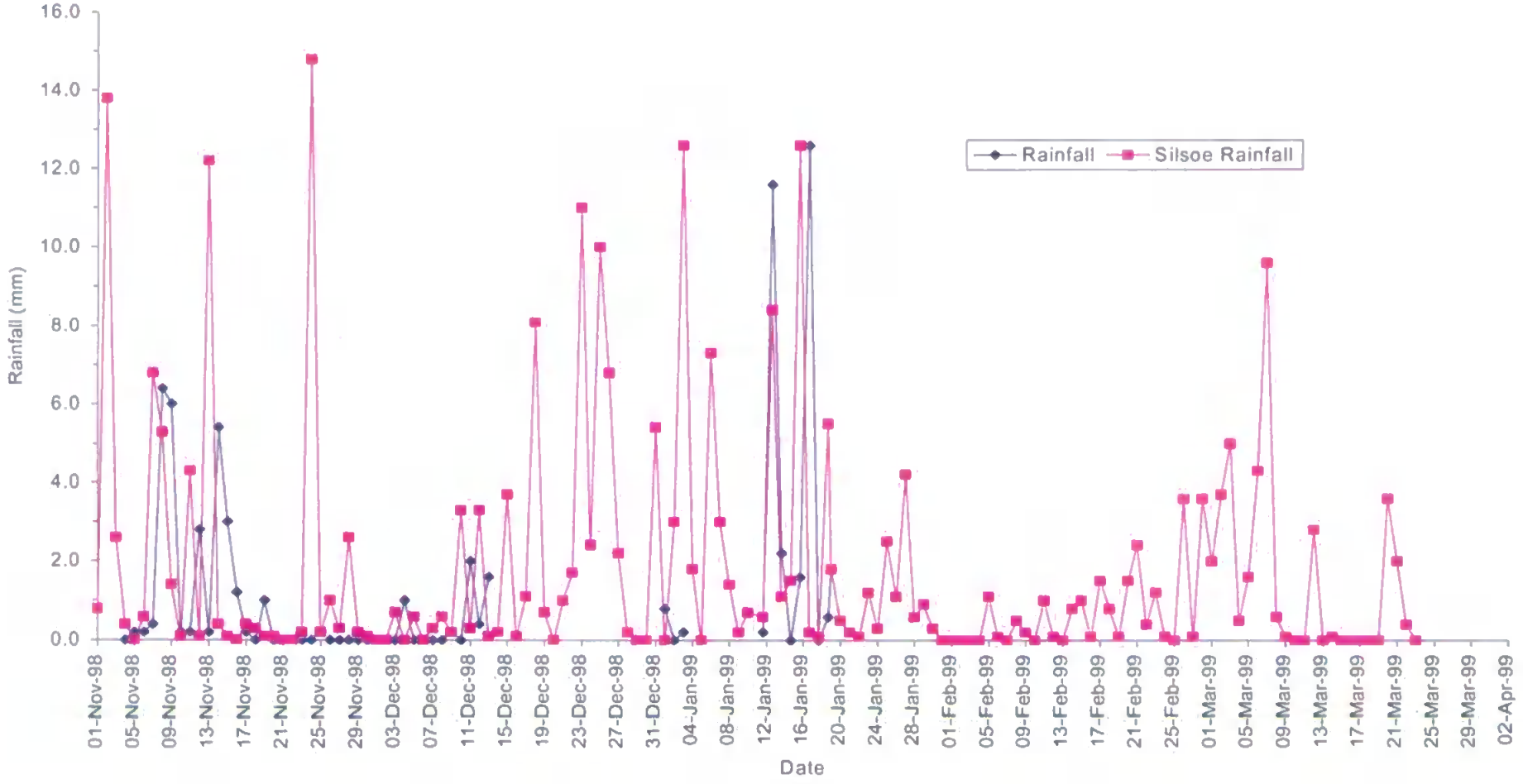

Figure 7.6 Comparison of Cranfield rainfall and Silsoe rainfall.

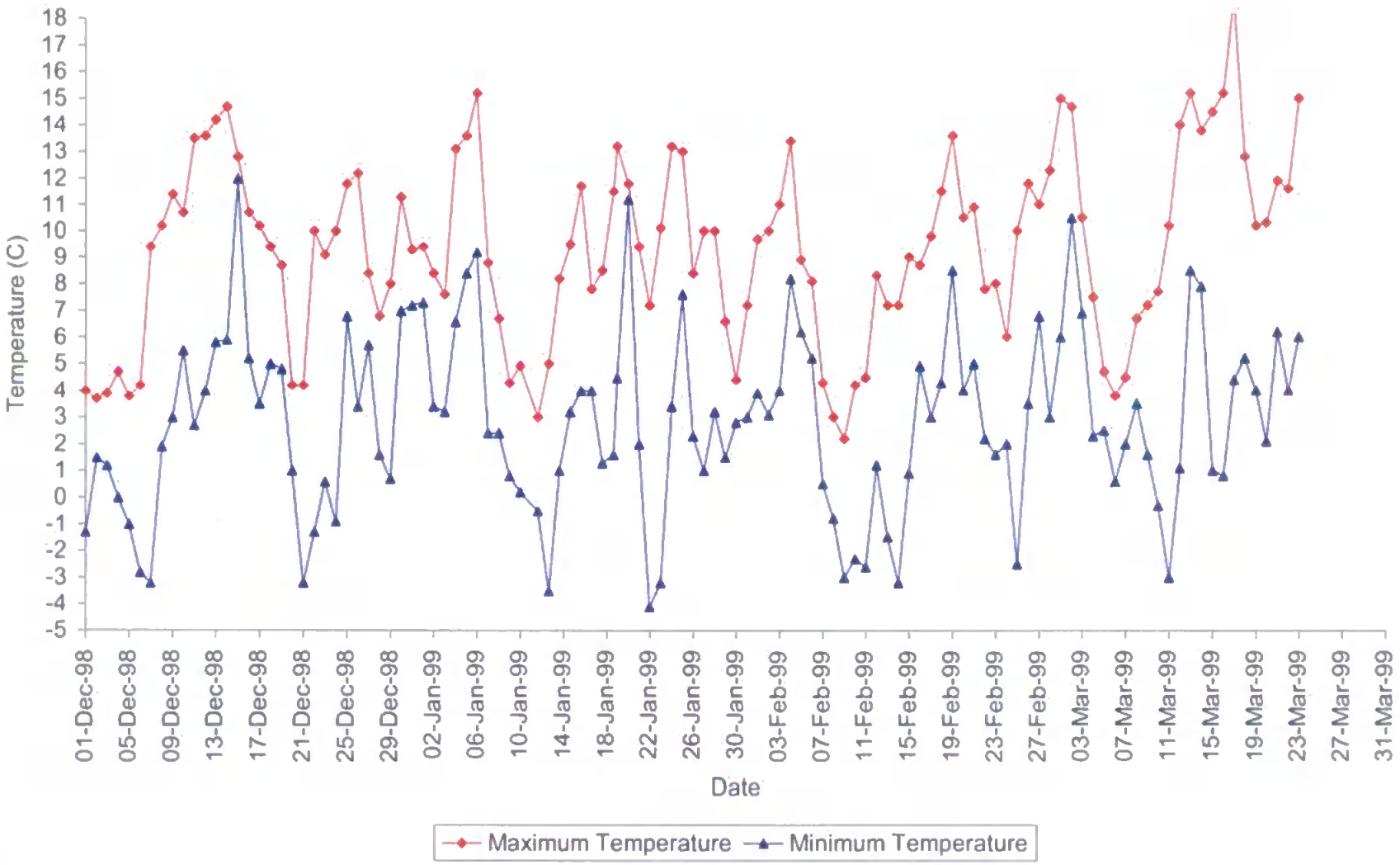

Figure 7.7 Temperature over the duration of the experiments

7.5 Oil Mobility Studies

7.5.1 Sand

The results from the trial experiment on the Redhill 30 sand show that the cable oil had migrated 50cm laterally from the point of injection after the first 25 litres of oil had been added, (Figure 7.8). The oil had migrated by 100cm after 2 days, following the injection of a total of 49 litres of cable oil. After 3 days, the progression of oil had not reached 150cm from the source, see Figure 7.8(c). Seven days after the initial injection of oil into the sand, the oil had reached 150cm from the point of injection. The results of the sand oil mobility can be seen in Figure 7.8.

Further information can be drawn from the sampling depth data. This shows that close to the source of contamination, the oil had spread vertically (both up and down) from the point of injection. The cable oil was injected at a depth of 85cm from the surface. After one day the oil had spread upward to a depth of 75cm and downward to a depth of 180cm, see Figure 7.8(b). At distances further from the point source the oil spread is more variable. At location D, the spread of oil ranges between 90cm and 165cm deep, whereas at sampling locations F, H, O and P, oil is only detected between 150cm and 160cm. At location J, oil is only found at a depth of 90cm. These are displayed graphically in Figure 7.8. The results would suggest that the oil spreads furthest, laterally along the longest edge of the pit, i.e. where the plinth is at its widest. Where the plinth is narrow the oil extends vertically outwards, possibly influenced by the water table, which is situated 150cm below the surface.

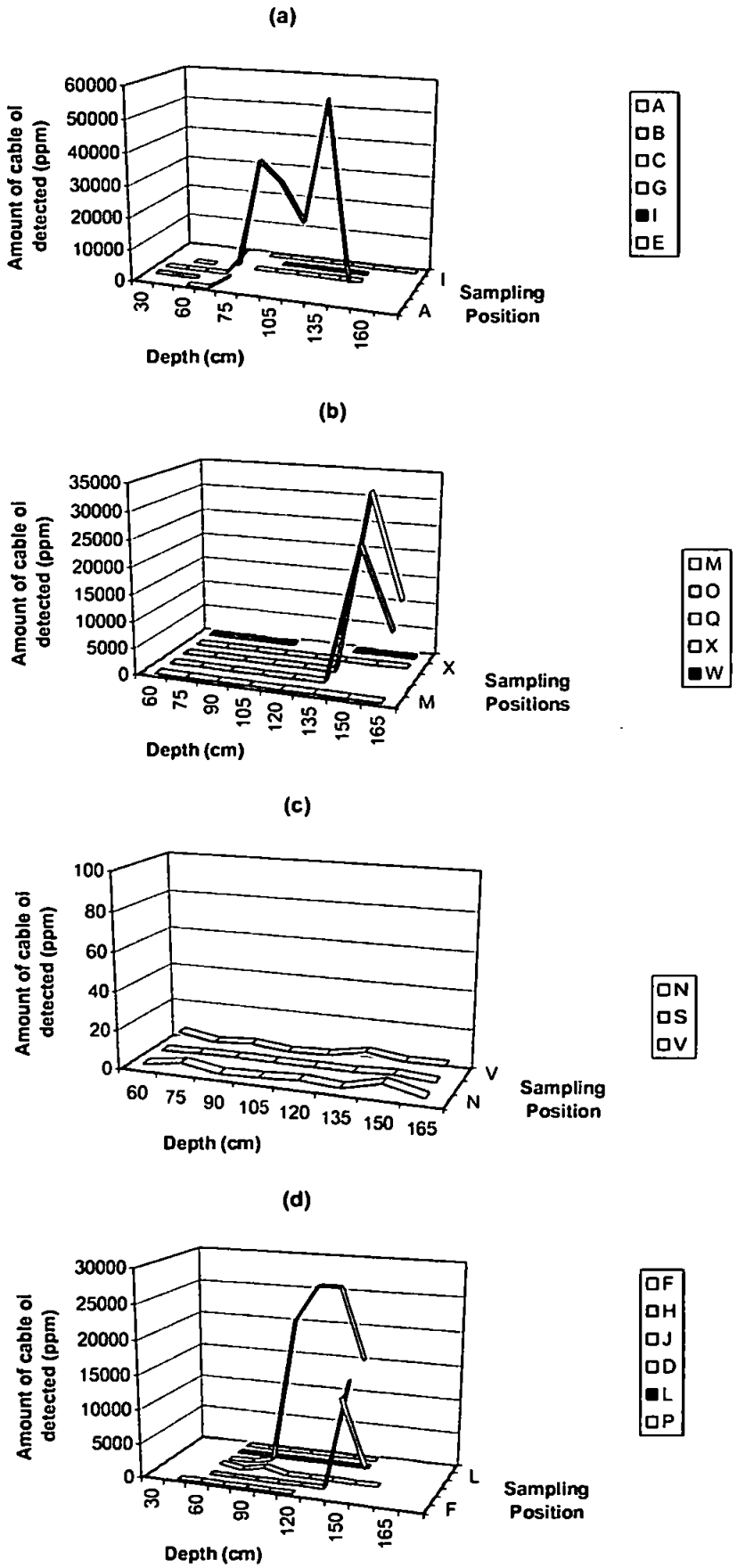

Figure 7.8 Sand sampling results at the different sampling locations, (a) 1 day after initial oil injection, (b) 2 days after oil injection, (c) 3 days after oil injection and (d) after 7 days after initial oil injection. Expressed in terms of ppm which is μg of cable oil per kg of soil.

The limited numbers of samples that contain cable oil preclude a more detailed analysis of the flow of pollutants within the sand, using only the raw data. Little meaningful analysis of the presence or otherwise of symmetry within the pit in terms of the migration of oil is possible. Sampling locations F and H suggest that there is symmetry in the flow of pollutants about the point source, whereas the data from sampling points D and J contradict this evidence.

Because of the difficulty in visualising the data from the pit containing sand, a more complex approach has been undertaken for the soil experiments that included redesigning the sampling procedure and interpolation of results.

7.5.2 DeBathe Soil

The results of the mobility studies in the pit containing the DeBathe repacked soil reveal the progression of an oil front, over time, which is associated with an increase in the volume of cable oil, see Figure 7.9. This is observed in the soil samples taken after the addition of oil into the pit. On day one, after 20 litres of oil had been injected, the oil had progressed 50cm laterally from the point of injection. Following the addition of a further 20 litres of oil on the two days following the initial oil injection, the oil had progressed laterally to 100cm. After seven days (80 litres of oil), the oil had moved 150cm laterally from the point of injection. This suggests that the total volume of oil added is critical in determining the extent of the migration of the pollutant.

It is possible to infer patterns of movement of the oil from the data itself. On the whole, the oil migration in the DeBathe pit appears to be symmetrical with distance about the point of injection. This is shown by the similarity between the results from sampling at N, O, P and Q. This similarity however, reflects not the absolute values of oil contained in the soil but in the trends of oil migration that are exhibited. The oil has migrated

symmetrically, although there is a 15cm depth offset from one side of the pit to the other in relation to the point of injection. This is further demonstrated by analysis of sampling positions β and δ, which although they do not have the same concentration levels, they do behave similarly.

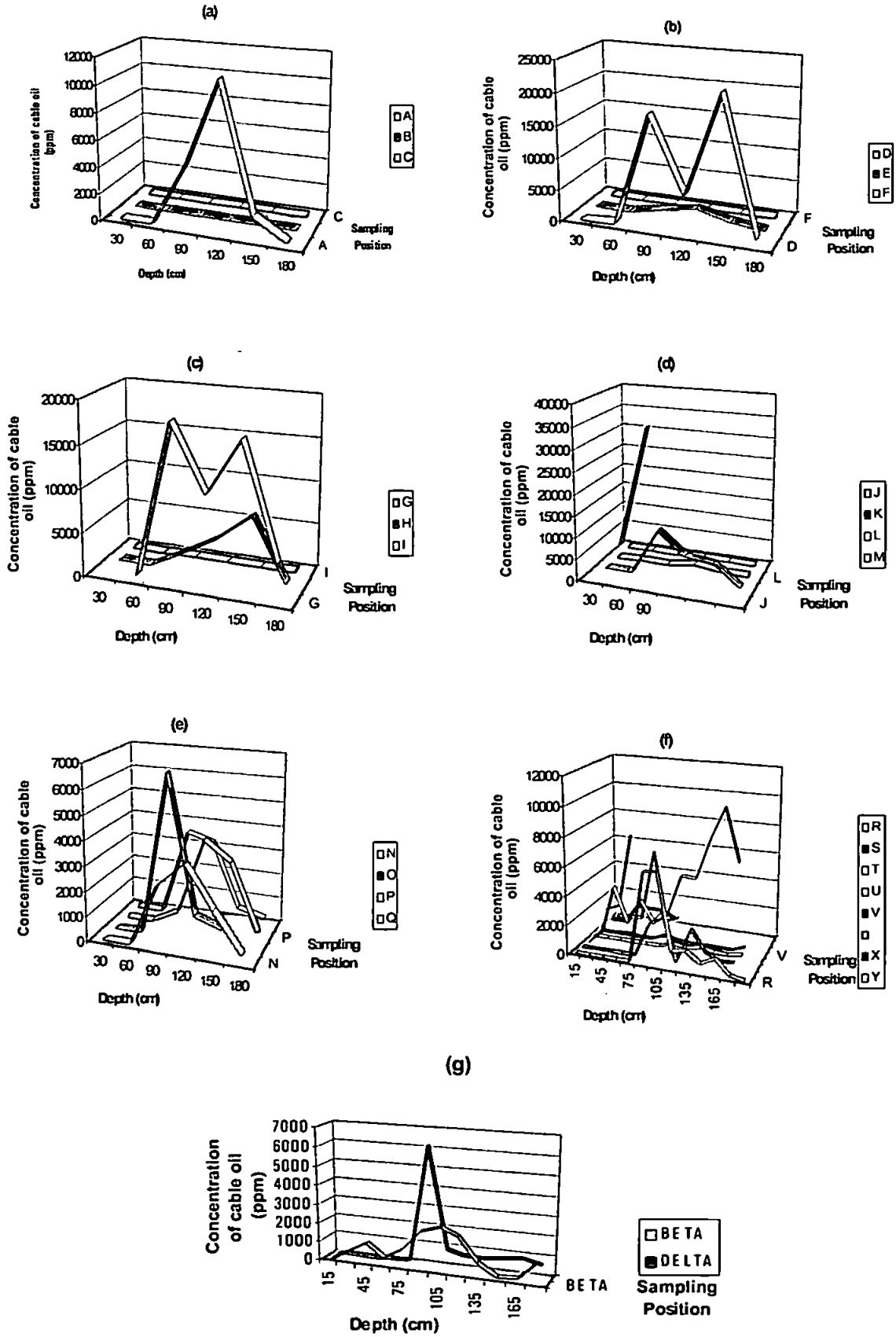

Figure 7.9 Results for the DeBathe soil samples oil migration study, (a) after 1 day, (b) after 2 days, (c) 3 days, (d) after 7 days, (e) after 10 days, (f) after 63 days, and (g) after 65 days.

It is difficult to draw any conclusions from the data on the effect of the plinth on the migration of the cable oil. The sampling locations R, S and T show varying patterns. If the plinth was affecting the migration of cable oil in the DeBathe soil, the samples extracted from location S would be expected to behave differently to samples from R and T. Samples extracted from locations R and T would be expected to behave similarly. Visual inspection of the data reveals that sampling location R and S behave similarly to each other whereas location T behaves differently from the other two. This suggests that the plinth has little or no effect on the migration of cable oil but this cannot be stated conclusively from the results obtained from locations R, S and T.

It is possible to study the effect of an increase in the water level on the distribution of cable oil in the soil by studying the sample data. Initially, when the oil is introduced into the soil, the oil remains close to or just below the water table, (120cm deep). The level of the water table was increased to 40cm from the surface over the Christmas period (22/12/98 – 5/1/99) and the samples taken from day 63 (see Figure 7.17f) are taken at this increased level. The results prove that some of the oil rises with the rising water table. However, a large proportion of the oil remains trapped below the water table.

7.5.3 Teign Soil

The results of the migration study on the repacked Teign series soil suggest that the quantity of oil added determines the distance that the oil migrates. This is observed from an analysis of the results from the first four days. The oil had spread laterally to 100cm between the second and fourth days. By day seven the oil had spread 150cm from the source of contamination, Figure 7.10. Observations of the depth that the oil had migrated, show that the cable oil remains at the water table height, with all early sampling positions displaying this trend.

The effect of the plinth on the migration pattern is also not clear, as with the DeBathe soil. Analysis of the data shows that all three sampling positions exhibited the same inclination. Sampling locations S and T are reasonably similar with the greatest deviation shown at position R, which exhibited lower concentration levels.

Symmetry in the pit can be observed from an analysis of samples N, O, P and Q. These illustrate that although the absolute concentrations of oil differ, the trends in oil migration appear to be very similar. Unlike the DeBathe pit there appears to be no offset in the depth profile.

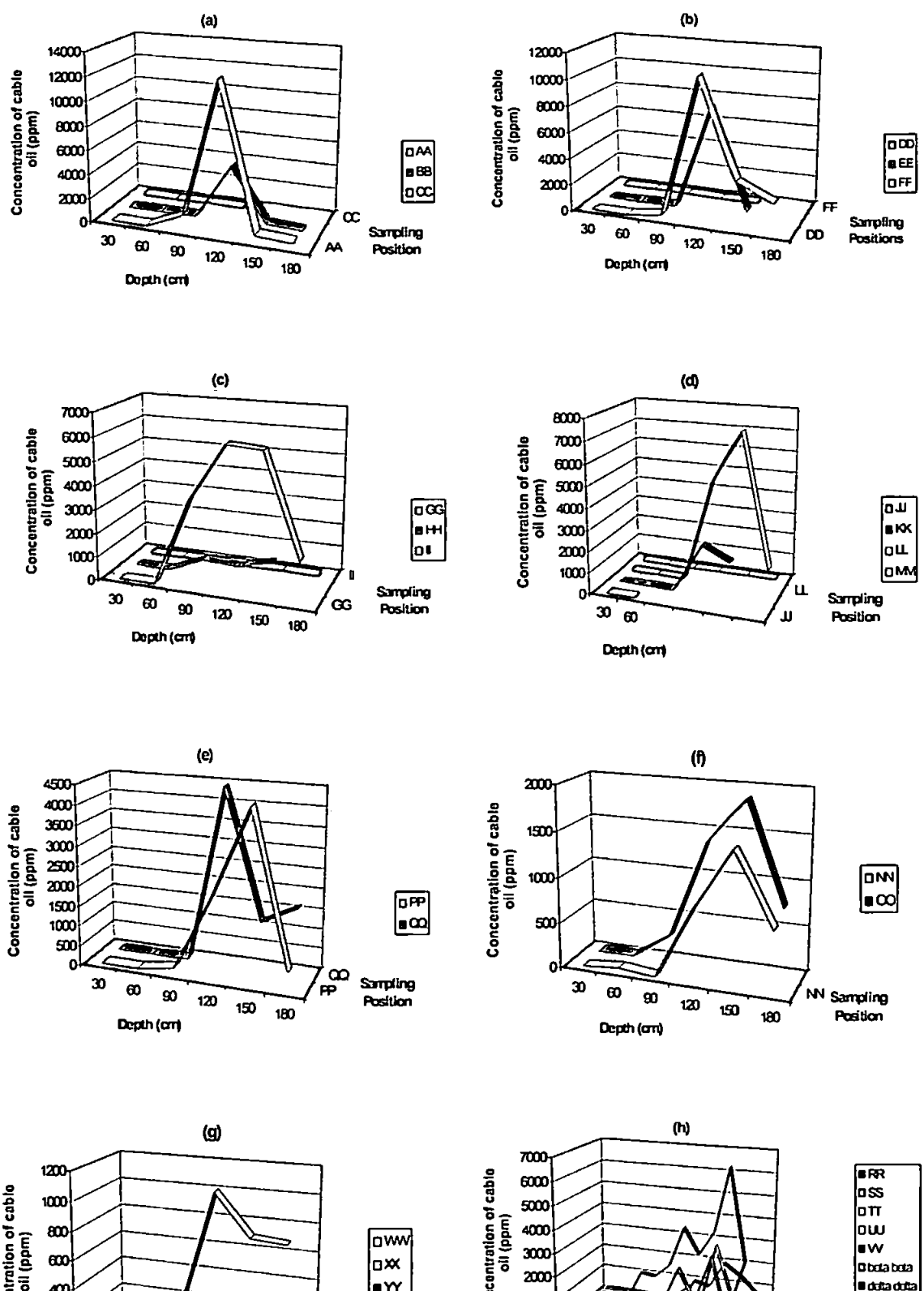

Figure 7.10 Results for the Teign soil samples oil migration study, (a) after 2 days, (b) after 3 days, (c) after 4 days, (d) after 7 days, (e) after 8 days, (f) after 45 days, (g) after 46 days, and (h) after 77 days.

The effect of a change in the level of the water table is not obvious. During the initial injection phase of the experiment the water table remained constant. After this period, the level of the water table declined. The resulting soil samples show that there was a modest decrease in the oil concentration depth profiles, falling on average by 30cm to 150cm deep, matching the decrease in volumetric water content. The attempt to induce a consistent rise in the water table appears to have had a negligible effect on the distribution of cable oil in the soil profile. This is shown in Figure 7.10(h) where only SS and ββ display any evidence that an upward movement of oil has taken place.

7.6 Data Interpolation and Modelling

In order to further the understanding of the migration of cable oil in soil, the ability to model and interpolate the data obtained from the pits was a fundamental objective. Interpolation facilitates an increased data-set which is required to 'fill-in' the sampling grid for all locations and all time periods over the experiment. It also allows visualisation of the oil through the use of software packages and enables the interpolation and comparison of actual and modelled concentration depth profiles. The modelling and interpolation carried out here is some way between curve fitting (i.e. using any function to fit the experimental data set) and modelling (i.e. truly predicting data).

The oil injection is symmetrical with respect to angle from the point of injection measured in a horizontal plane. Therefore, this symmetry is incorporated into the glomus theory, and it is assumed to be Gaussian in semi-polar coordinates, i.e. when expressed as a function of angle from the point of injection. Also, there may be some degree of symmetry around the horizontal plane through the level of injection. To allow for this, height is expressed as displacement from this plane. This can be shown diagrammatically in Figure 7.11 overleaf.

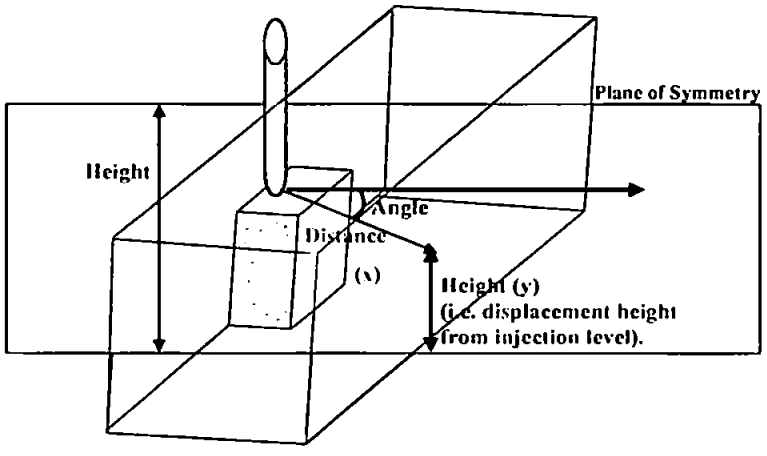

Figure 7.11 Schematic representation of the pit, in terms of interpolation parameters. Oil is injected at the bottom of the tube, above the retangular plinth.

7.6.1 DeBathe Soil

The one-dimensional modelling technique, using Gaussian equations to fit the experimental data, was applied to the three-dimensional data set. As with the one-dimensional analysis, the equations allowed for the existence of a single secondary glomus. The secondary glomus was variable with depth. The following Gaussian equation is used to model the data:

$$\text{Concentration of cable oil}\,(z) = \exp\left(-0.5\left[\frac{x}{a}\right]^2\right) \times b\exp\left(-0.5\left[\frac{y-c}{d}\right]^2\right)$$

$$+\exp\left(-0.5\left[\frac{x}{e}\right]^2\right) \times f\exp\left(-0.5\left[\frac{y-\left(\frac{[c+20]\times h}{x}\right)}{g}\right]^2\right)$$

Equation 7.1

where, x is the horizontal distance from the point of injection in metres, y is the height (vertical) displacement from the point of injection in centimetres. The other variables are defined as; a is the distance width of glomus one, b is glomus one depth amplitude (maximum concentration), c is the height of the centre of glomus one depth, d is glomus one depth width, e is the distance width of the second glomus, f is glomus two depth

amplitude or maximum concentration of the second glomus, *g* is the height of the centre of glomus two and *h* is the point in relation to distance where the two glomus convergence. A typical curve-fitting graph can be seen below in Figure 7.12.

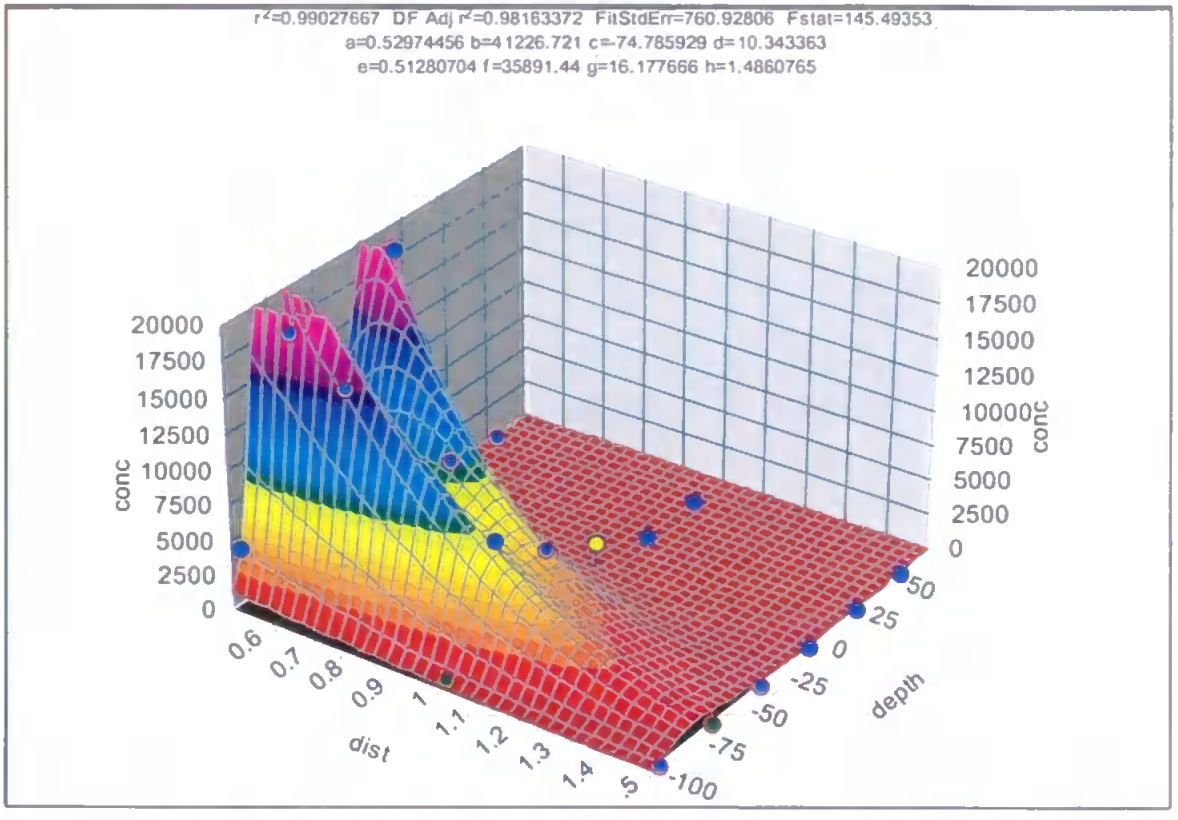

Figure 7.12 Table Curve 3D graph showing the convergence in the distance direction of two glomuses.

Using an equation-fitting program (TableCurve 3D) it was possible to determine values for the variable parameters in Equation 7.1. By applying Equation 7.1 to each daily set of data it was possible to determine equations for the variables *a* to *h*. This was achieved by plotting the values graphically, and calculating an equation which best fitted these points by drawing straight lines through them. The resulting graphs can be seen below (Figure 7.13).

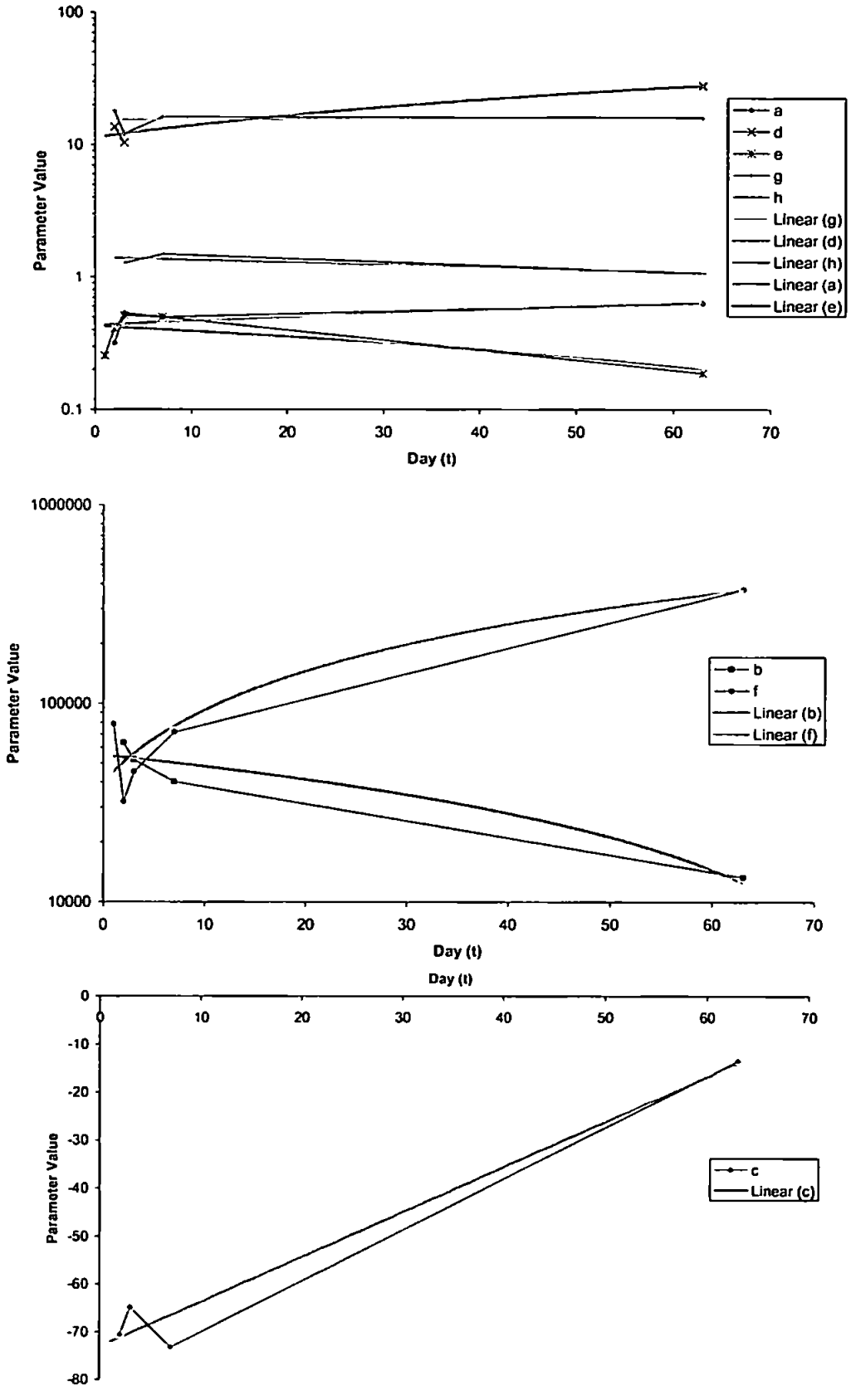

Figure 7.13 Parameter values extrapolation over *t* days.

The equations are expressed in terms of the time since the start of the experiment t. The individual equations for each parameter are listed below.

$$a = 0.0032t + 0.4344$$

Equation 7.2

$$b = -671.63t + 54800$$

Equation 7.3

$$c = 0.9399t - 73.116$$

Equation 7.4

$$d = 0.262t + 11.326$$

Equation 7.5

$$e = -0.0036t + 0.4271$$

Equation 7.6

$$f = 5293.5t + 40138$$

Equation 7.7

$$g = 0.0082t + 15.4$$

Equation 7.8

$$h = -0.0053t + 1.4052$$

Equation 7.9

One of main objective of this interpolation was to produce 3D views of the oil movement over time. Without the interpolation it was not possible to visualise the oil migration in 3D because of the scarcity of the experimental data. As a result interpolation was used to obtain the best possible fit of the experimentally derived data.

Observations of the data determined that it was conceivable to make a correction for the symmetry of data. The concentration values derived for each side of the pit showed that the symmetry was slightly skewed. The maximum concentrations were displaced by ±10cm depending on the sampling location in relation to the point of injection. This resulted in a symmetry depth correction of ±10cm. In order to apply this to the model Equation 7.4 was altered to take this into account, resulting in the new equation below.

$$c = (0.9399t - 73.116) + k$$

Equation 7.10

Where k is the depth correction (±10cm) and is dependent on the sampling location. In addition to the symmetry depth correction, an amplitude correction was also required, which was dependent on the location of the sampling point, in the relation to the point of injection. This is best explained diagrammatically (Figure 7.14).

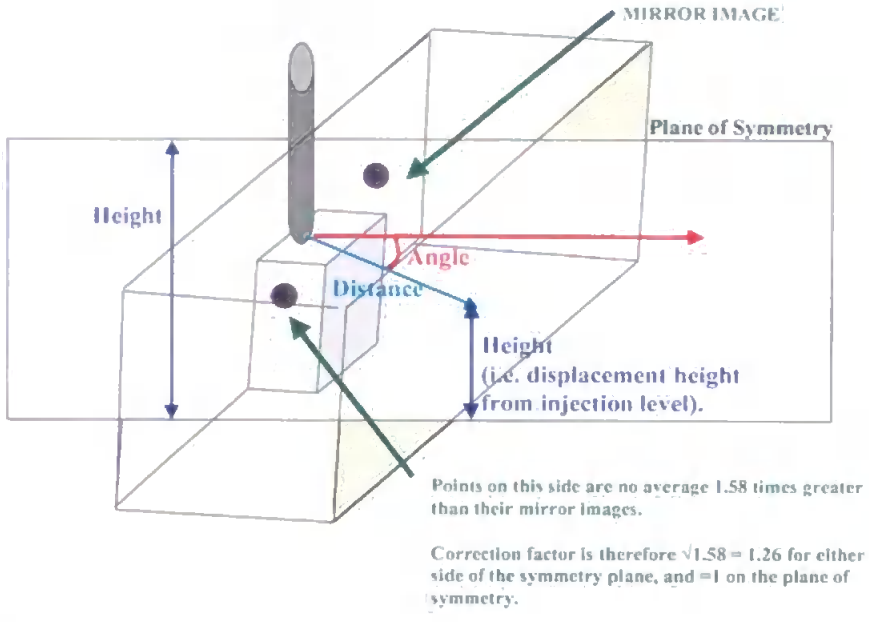

Figure 7.14 Explanation of the amplitude correction factor used in the DeBathe interpolation.

This resulted in variable b and f equations altering to:

$$b = (-671.63t + 54800) \times l$$

Equation 7.11

And

$$f = (5293.5t + 40138) \times l$$

Equation 7.12

Where l is equal to the multiplication or division of 1.26 depending on the location of the sampling point compared to the point of injection of the oil.

Applying Equation 7.1 to a matrix of all sampling points in all time periods made it possible to fill-in the data required and hence illustrate the migration of cable oil, over the duration of the experiment diagrammatically. Appendix A has the full list of the interpolated concentrations. The results of the interpolation are shown diagrammatically in Figure 7.17.

Comparison of the actual (experimentally derived concentrations) and interpolated concentrations suggests that, in general, the equation and parameters used to interpolate across the whole pit is valid. Although there is deviation between the experimentally derived concentrations and the interpolated ones, the overall interpolation fits well with the experimental data. The comparison was undertaken using Equation 7.13:

= log [(difference between the two values) X (relative difference between them)]

Equation 7.13

The interpolation has a maximum log RSD of 4.28, this is the same as being incorrect by a factor no greater than 2 (an actual value of 100 and an interpolated value of 10000). However, for most of the interpolated points the log RSD is lower, and is incorrect factor of one at most. Comparing the log of the RSD (relative standard deviation) and various parameters of the pit, i.e. depth, distance, angle and day, one can see that there is little trend between the deviation in RSD and with any of these parameters, (Figure 7.15).

(a)

(b)

(c)

(d)

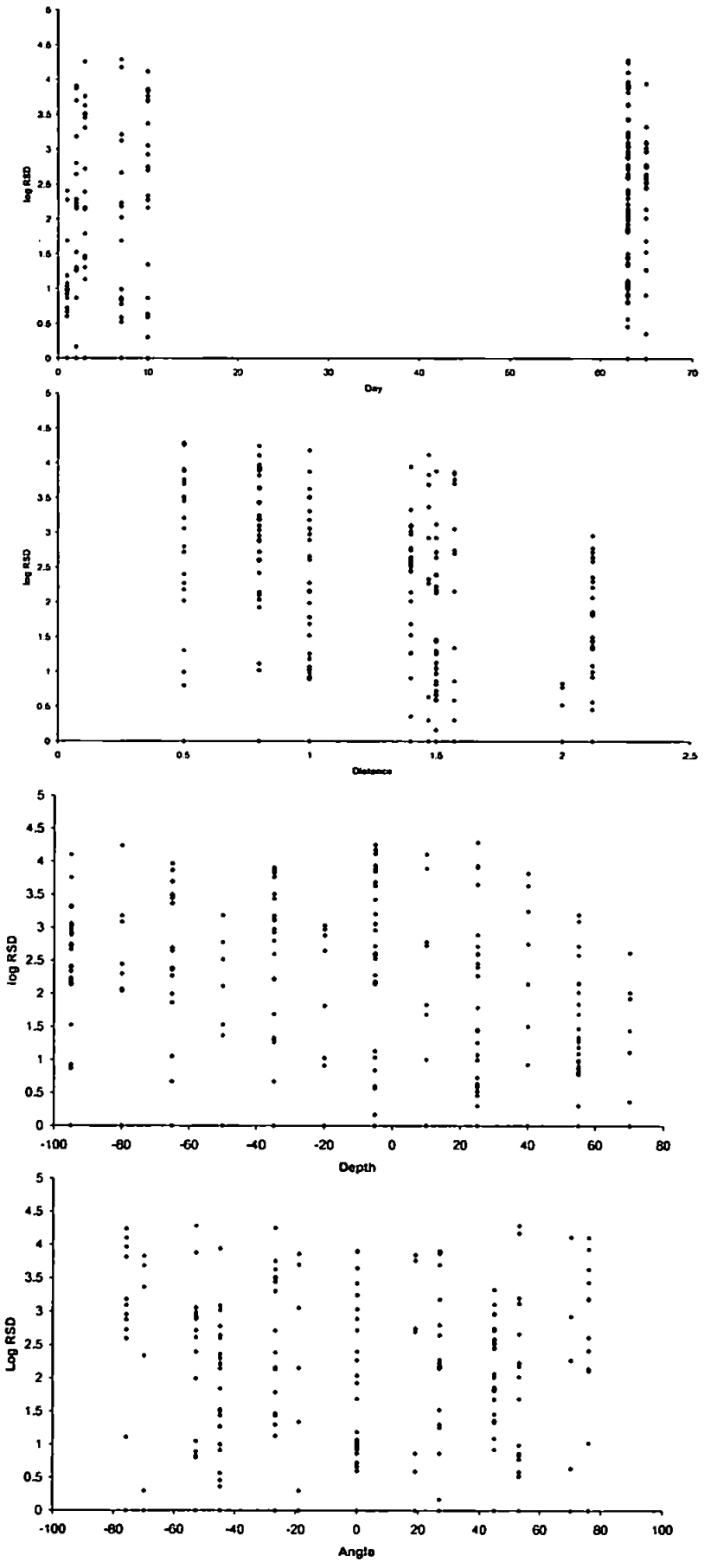

Figure 7.15 Graphs showing the log RSD in relation to (a) day, (b) distance from the point of injection, (c) depth from the point of injection and (d) the angle from the point of injection.

It is possible to attempt to model the data using a slightly different approach. Instead of suggesting that the migration of oil was Gaussian, it was possible to change this to a spherical migration pattern. Spherical migration would be a valid model for the migration of oil if the movement was symmetrical in all three planes. However, after attempting to interpolate the data, it proved to be impossible even to interpolate any one specific data-set, whereas with the Gaussian approach all the data-sets could be interpolated.

Using the Gaussian approach enables broad conclusions to be inferred about the migration of cable oil in DeBathe repacked soil. The first point to note is that as the concentration of cable oil increases over time, the extent of the plume increases as demonstrated by Figure 7.17. Secondly, the oil plume appears to split as loading increases, resulting in the formation of two distinct glomuses, by Figure 7.17c. These glomuses appear to form and move vertically, with one remaining at the height of injection and the second positioned below it. Thirdly, it can be seen that after the water table is raised the main bulk of the oil plume remains trapped below the water table, Figure 7.17g. This is probably the residual oil, which is highly immobile. However, the labile oil moves up with the associated increase in water table height.

The following figures show that the extent of the cable oil plume are 3D semi-transparent isosurfaces, i.e. a series of semi-transparent coloured balloons that join corresponding concentrations. Figure 7.16 is a diagrammatic representation of the views that the 3D visualisation has been taken from.

Actual and Modelled **Modelled**

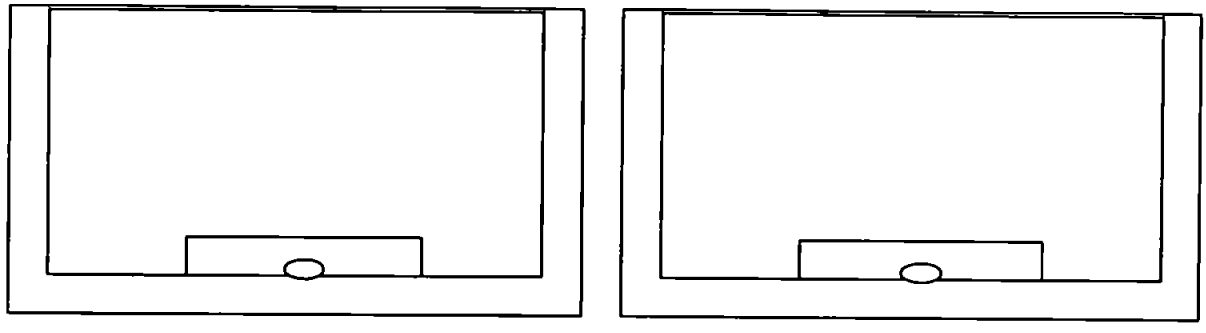

Transparent view looking through the soil surface

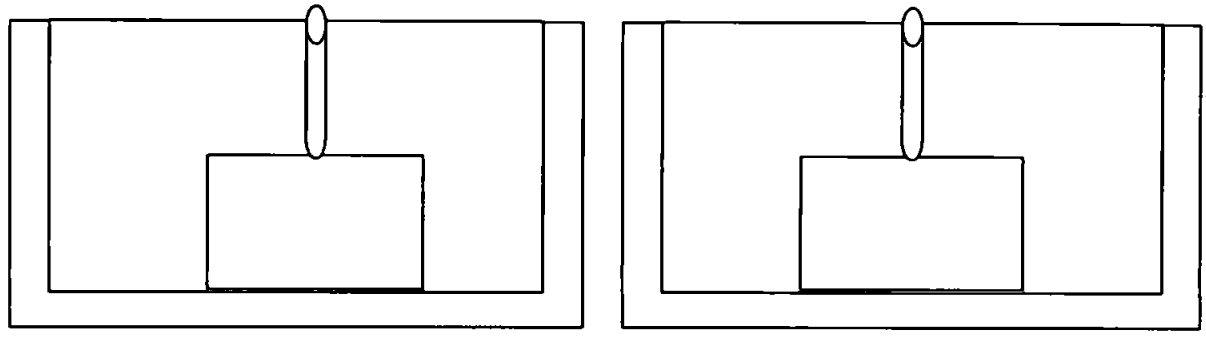

Transparent view looking through the side of the sample from the plinth wall

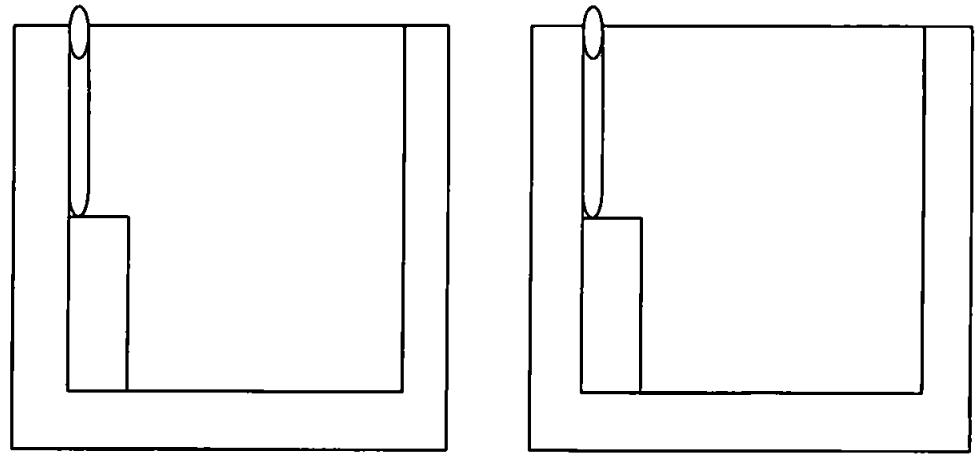

Transparent view looking through the side of the sample from the small side of the pit, (towards the plinth).

Figure 7.16 Layout of the views used for the 3D visualisation

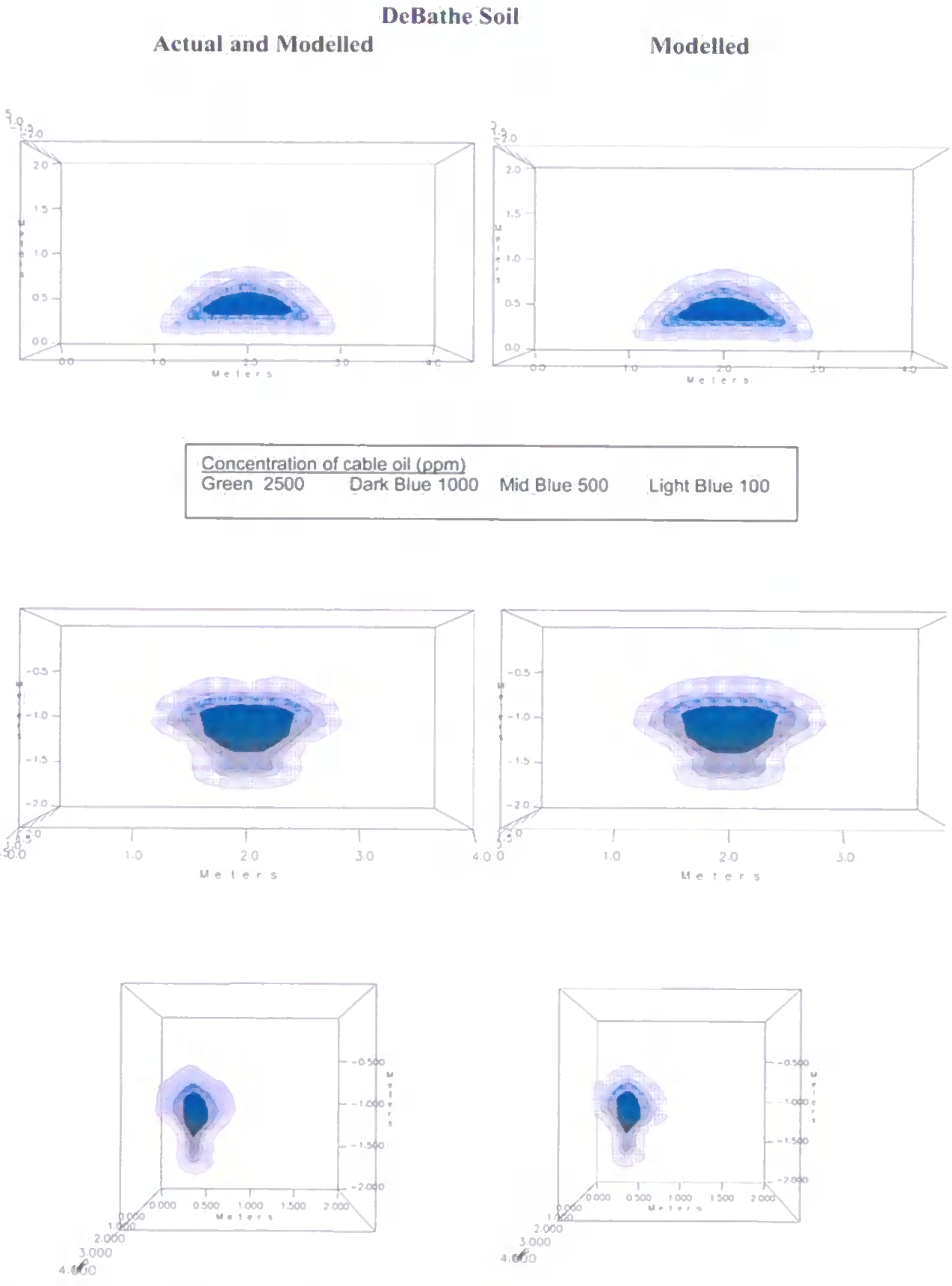

Figure 7.17(a) Day 1 Actual and modelled cable oil migration for the DeBathe soil.

DeBathe Soil

Actual and Modelled **Modelled**

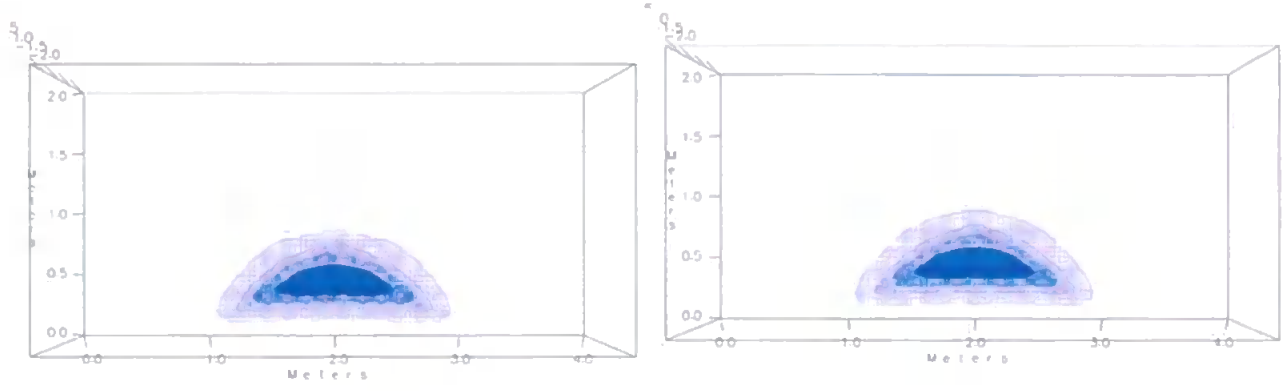

Concentration of cable oil (ppm)
Green 2500 Dark Blue 1000 Mid Blue 500 Light Blue 100

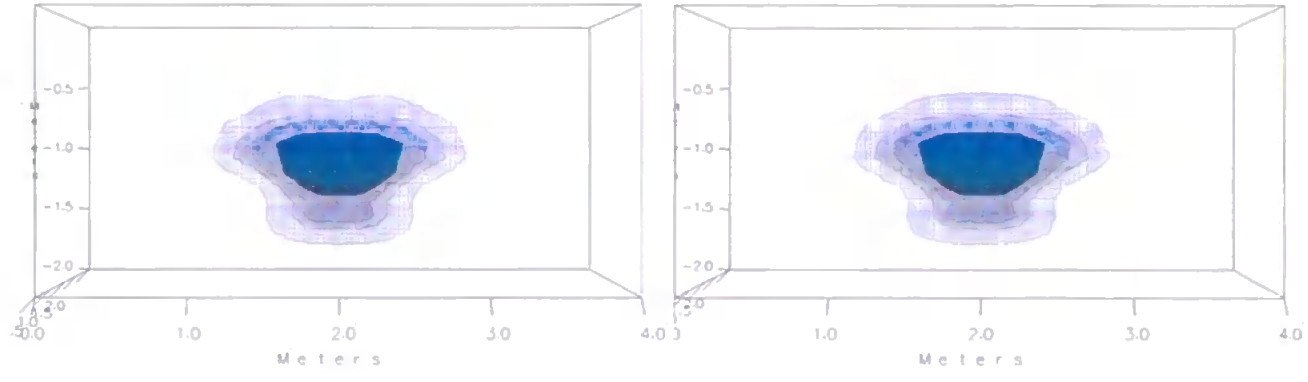

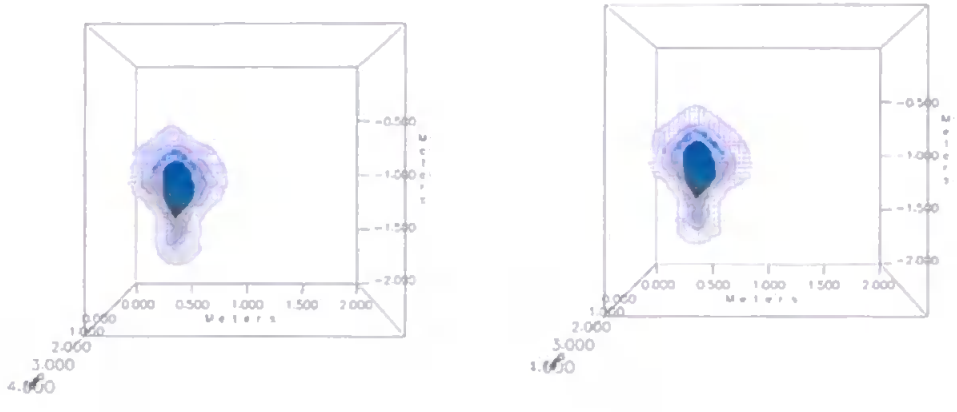

(b) Day 2, Actual and modelled oil migration for the DeBathe soil.

DeBathe Soil

Actual and Modelled **Modelled**

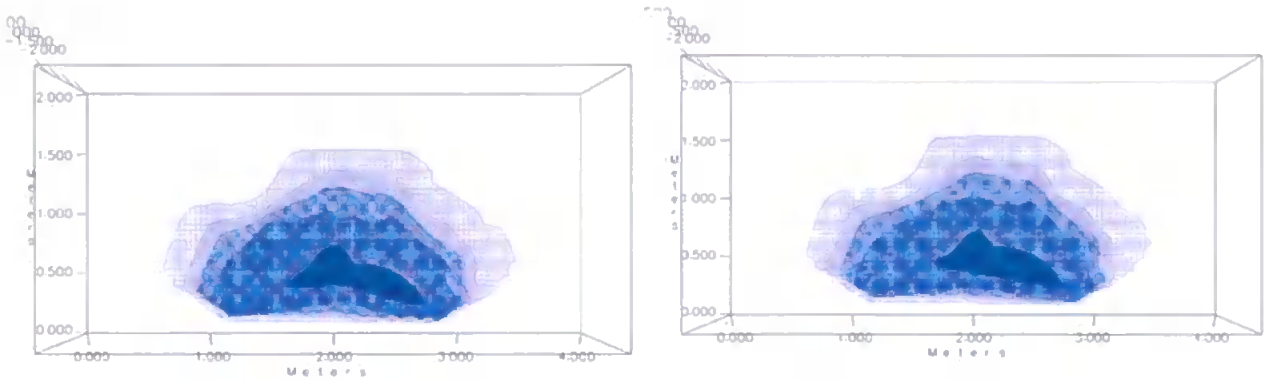

Concentration of cable oil (ppm)
Green 10000 Dark Blue 2500 Mid Blue 1000 Light Blue 500 Very light blue 100

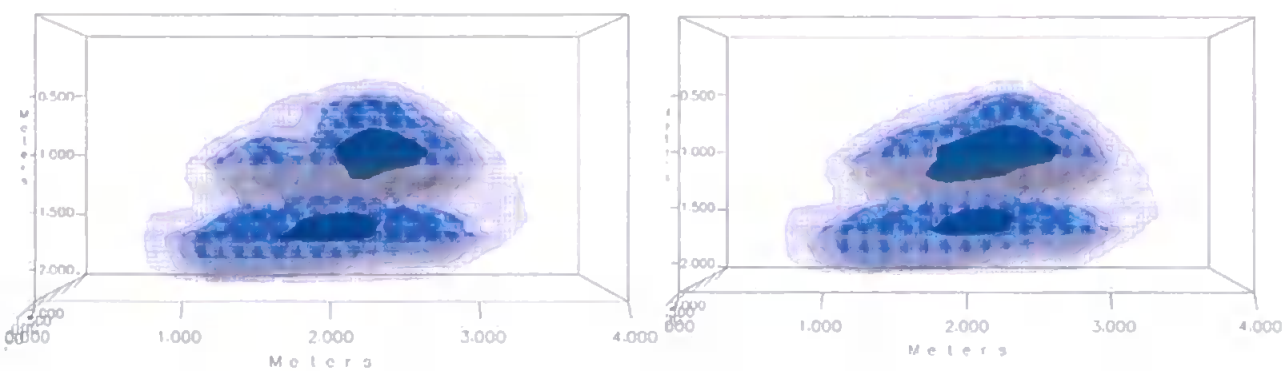

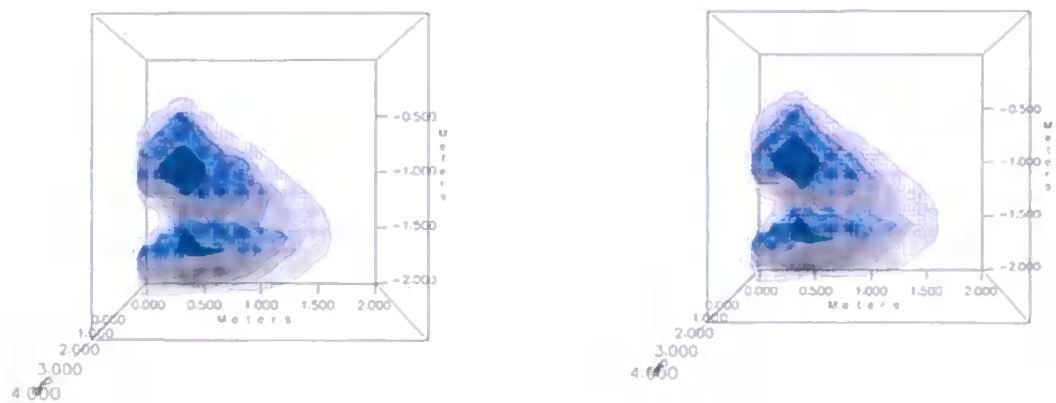

(c) Day 3, Actual and modelled oil migration for the DeBathe soil.

DeBathe Soil

Actual and Modelled **Modelled**

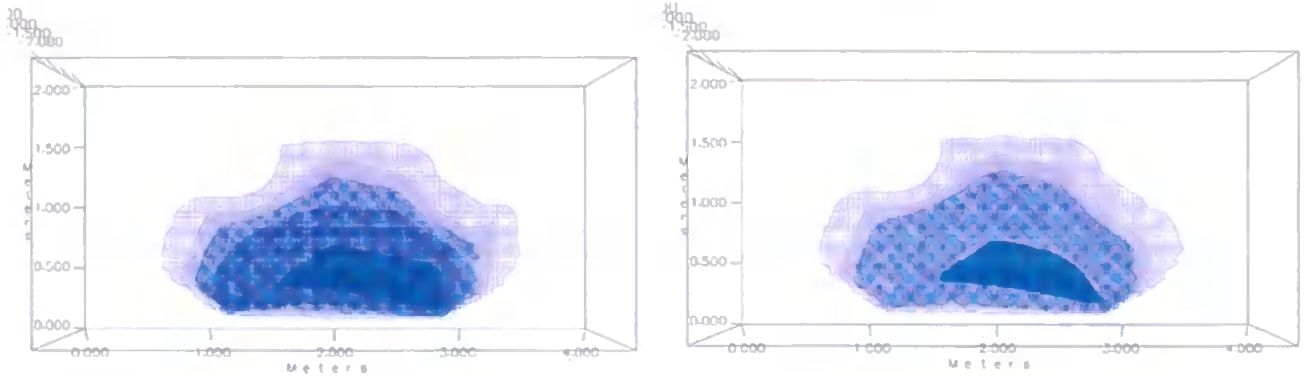

Concentration of cable oil (ppm)
Dark Green 20000 Green 10000 Dark Blue 2500 Mid Blue 1000 Light Blue 500 Very light blue 100

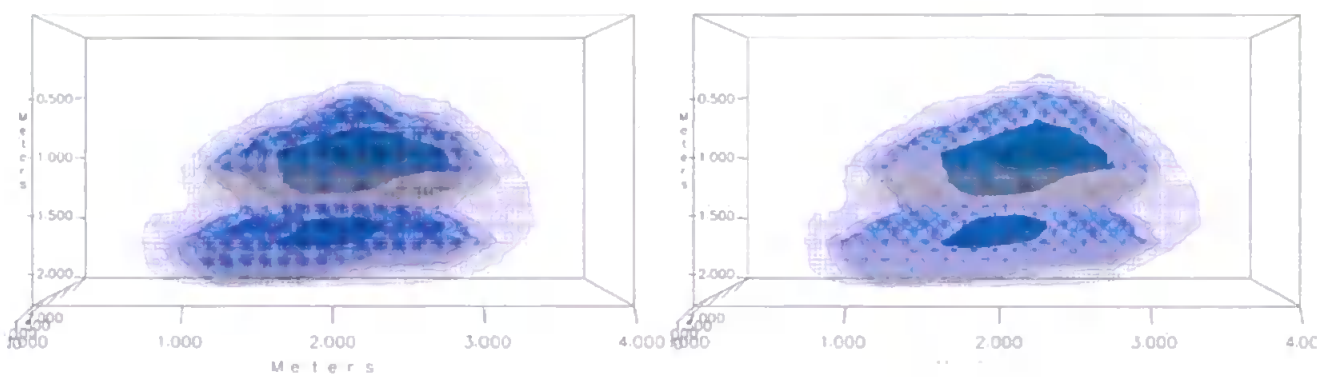

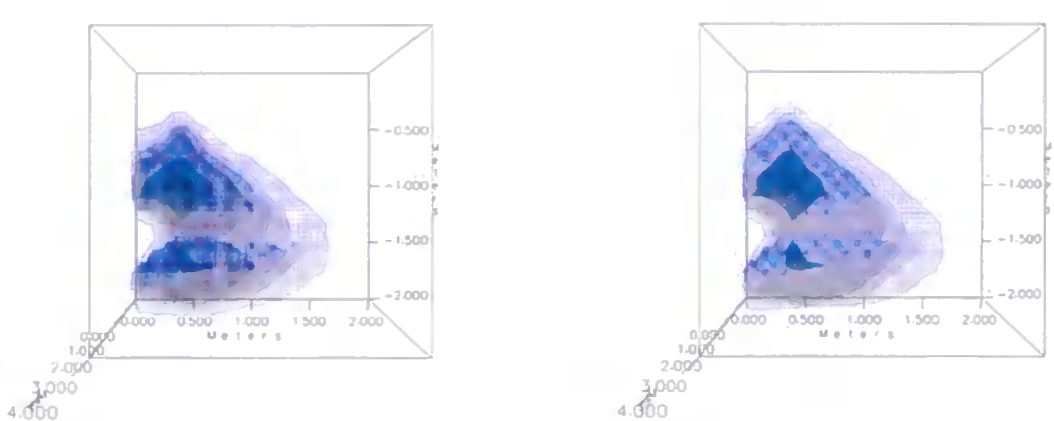

(d) Day 7, Actual and modelled oil migration for the DeBathe soil.

DeBathe Soil

Actual and Modelled **Modelled**

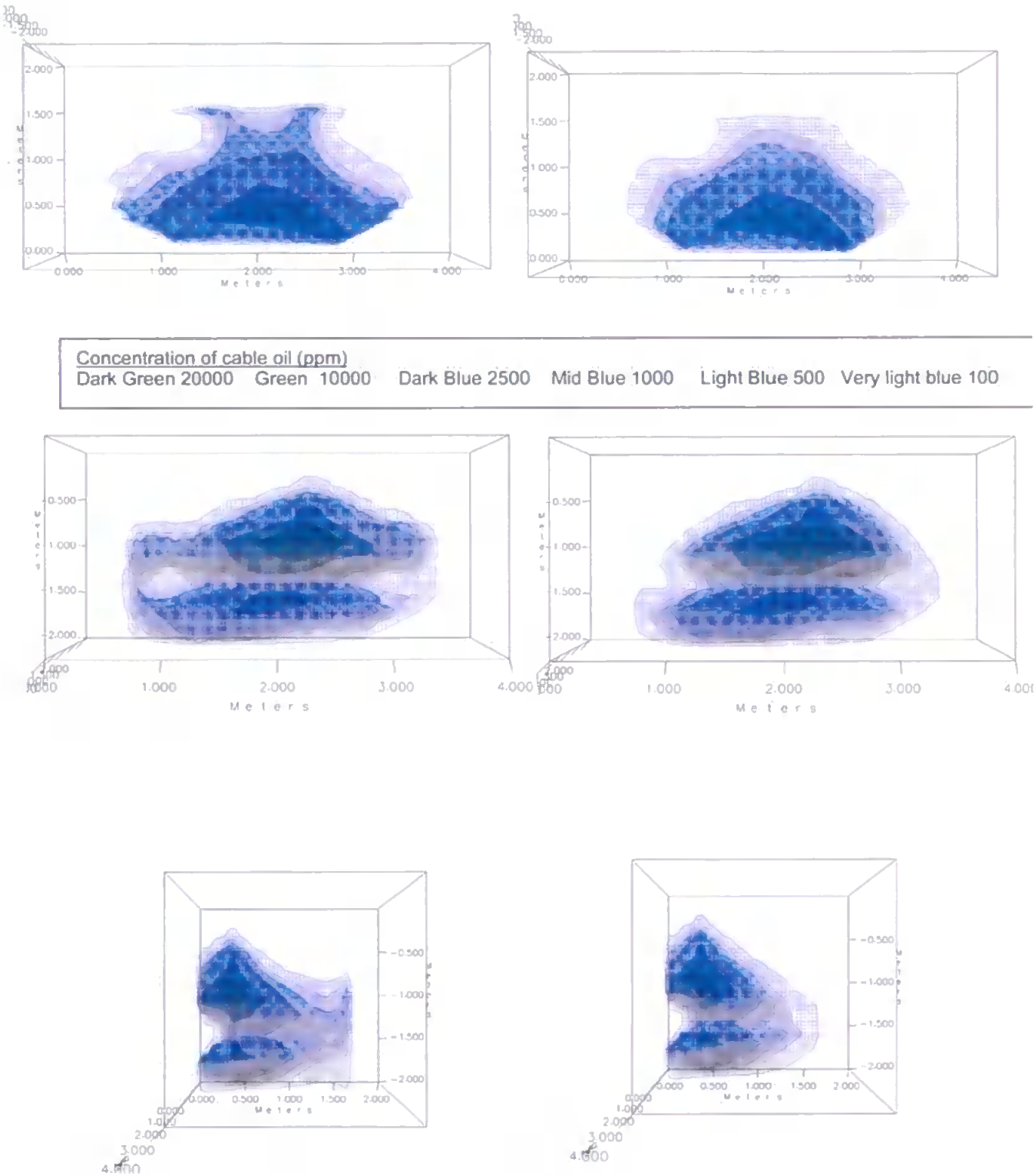

(e) Day 10, Actual and modelled oil migration for the DeBathe soil.

DeBathe Soil

Actual and Modelled **Modelled**

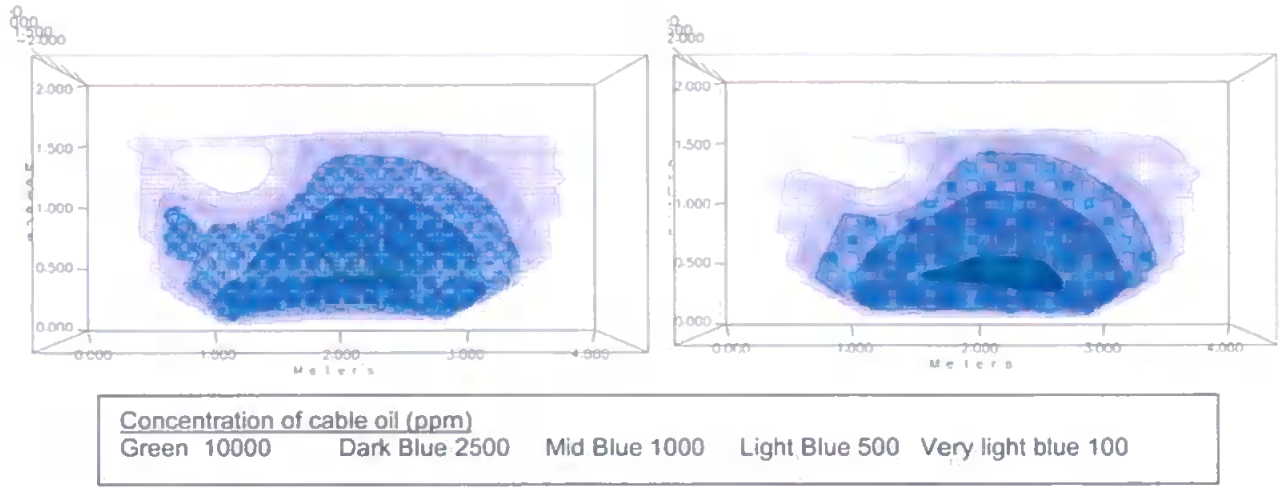

Concentration of cable oil (ppm)
Green 10000 Dark Blue 2500 Mid Blue 1000 Light Blue 500 Very light blue 100

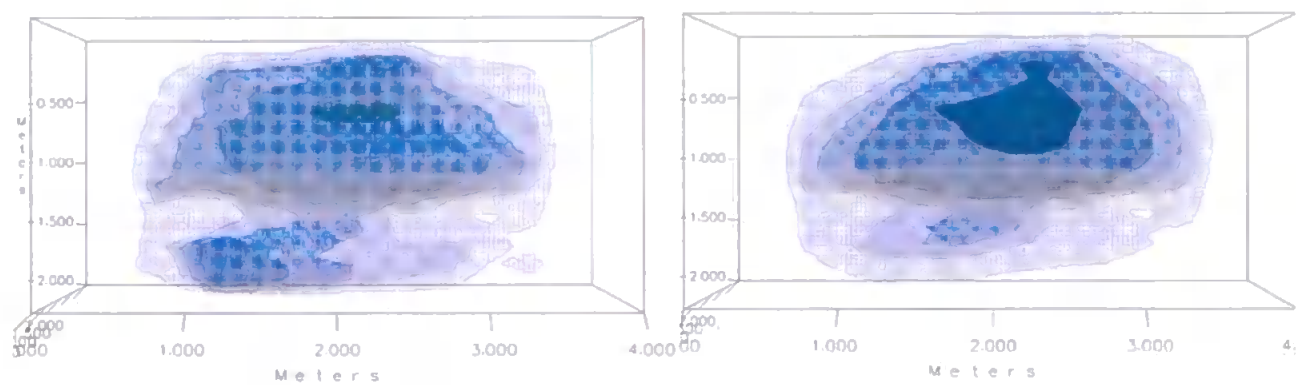

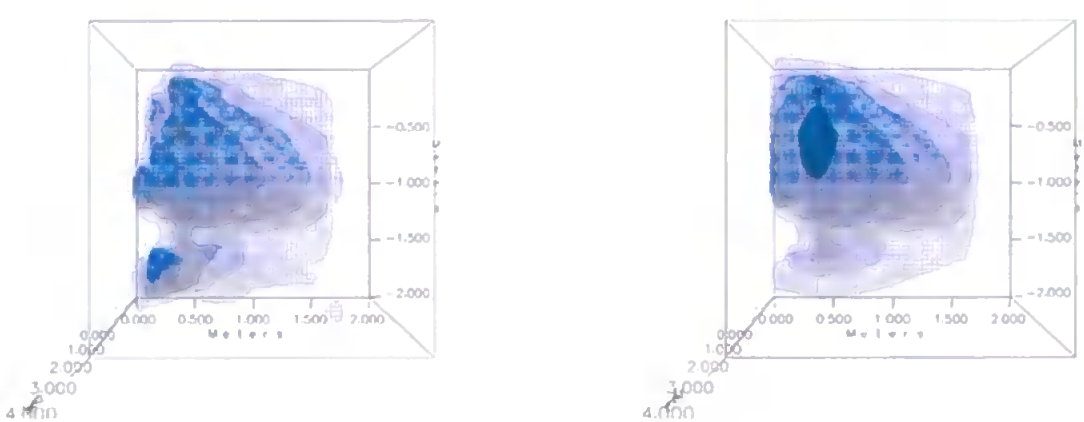

(f) Day 63, Actual and modelled oil migration for the DeBathe soil.

DeBathe Soil

Actual and Modelled **Modelled**

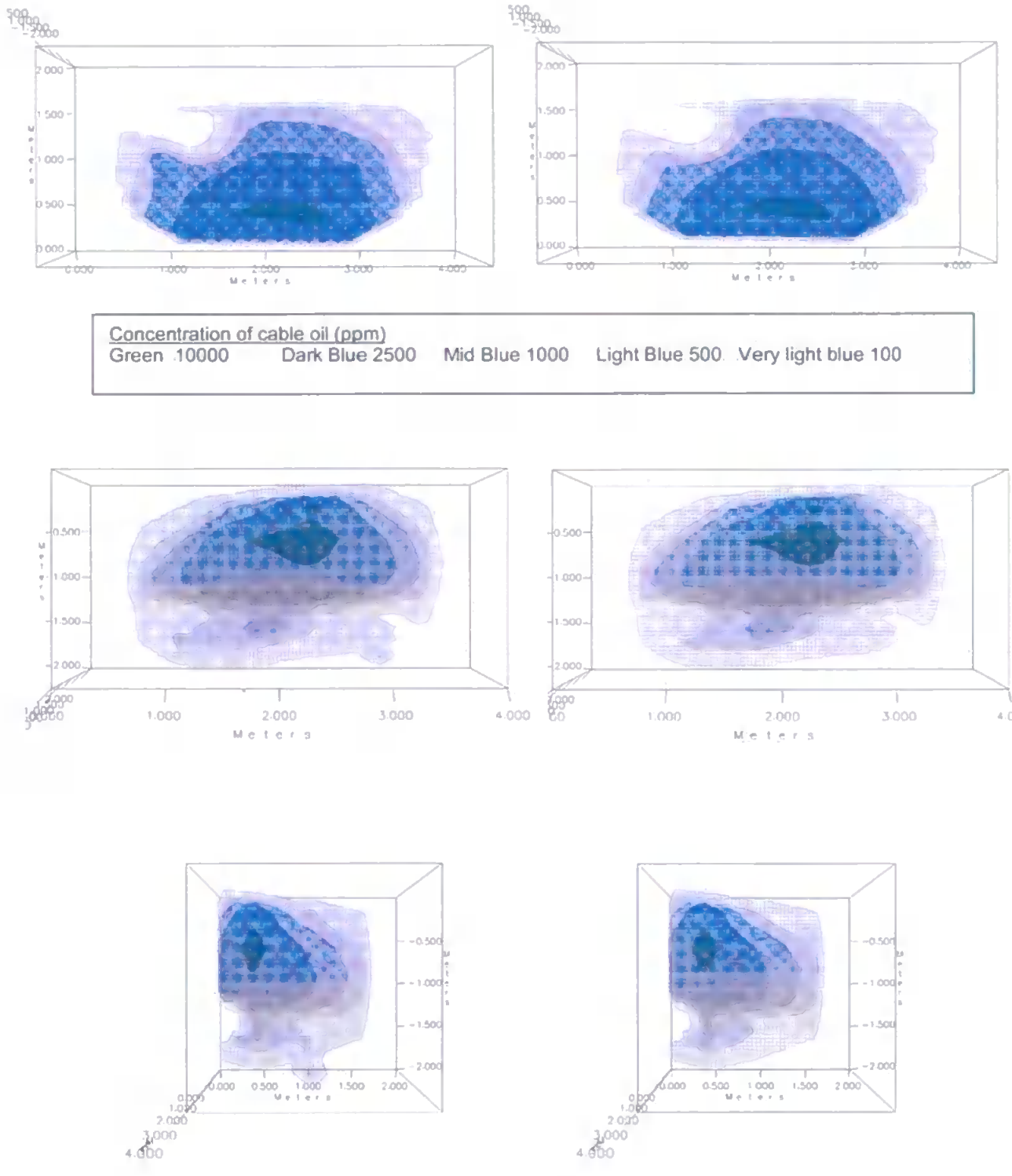

(g) Day 65, Actual and modelled oil migration for the DeBathe soil.

7.6.2 Teign Soil

A similar approach has been used to model the Teign soil ass the approach used for the DeBathe soil. However, the oil behaves in a fundementally different way in the Teign soil. This can be seen by reference to the sampling plan (Figure 6.11), positions J, K, L and M, which are referred to as JJ, KK, LL and MM for the Teign soil. Figure 7.10a shows that at day 2 there is a single source glomus, i.e. the peak occurs closest to the source at position AA. However, by day 7, Figure 7.10d, the major peak has moved away to 1.5m from the source at position KK, although there is still a reduced source glomus. Therefore we now need a double glomus equation, but with the secondary glomus displaced by distance from the source, not depth. The new equation is given below in Equation 7.14:

$$\text{Concentration of cable oil}\,(z) = \exp\left(-0.5\left[\frac{x-0}{f}\right]^2\right)\times g\exp\left(-0.5\left[\frac{y-h}{i}\right]^2\right)$$
$$+\Gamma\exp\left(-0.5\left[\frac{x-1.4}{0.21}\right]^2\right)\times 9000\exp\left(-0.5\left[\frac{y-(-55)}{19.35}\right]^2\right)$$

Equation 7.14

Where, x is the distance from the point of injection, y is the height in polar co-ordinates from the point of injection, i.e. depth. The other variables are defined as; the width f of the source glomus as a function of distance with time, where f is:

$$f = 0.39 + 0.4277\exp\left(-\left[2^{0.5}\right]\right)\times\left|\frac{t-2.287}{1.054}\right|$$

Equation 7.15

Where t is time from the moment of injection (in days). The form of the equation is chosen to be that which fitted the data, but still remains relatively simple. This was achieved using Tablecurve 2D.

Parameter g is the overall concentration amplitude and h the centre of the glomus with respect to height, both of these also change with time t. Equation 7.16 shows that the

source glomus amplitude decreases with time, as expected, and Equation 7.17 shows that the centre of the source glomus sinks at the rate of 5.2cm a day.

If greater than 7 days g = 5438 otherwise,

$$g = -2620.8t + 24114$$

Equation 7.16

If greater than 7 days h = -60 otherwise,

$$h = -5.2233t - 24.153$$

Equation 7.17

As with f, i it was not possible to express i with a linear equation, so an equation was chosen which, while still relatively simple, fitted the data as shown:

$$i = 12.677 + 29.018 \times \left[\left(1 + \frac{\begin{matrix}\left(1 - \exp\left[-4.0301 \times \left(t - 3.5381\right)\right] - 0.9894\right) \times \\ \left[4.0301 \times \exp\left(-1.3006 \times \left[t - 3.5381\right]\right)\right]\end{matrix}}{\left[-1.3006 \times \exp\left(-4.0301 \times \left[t - 3.5381\right]\right)\right]} \right) \Big/ \frac{}{1.3006 - 4.0301} \right] \Big/ 1.3006$$

Equation 7.18

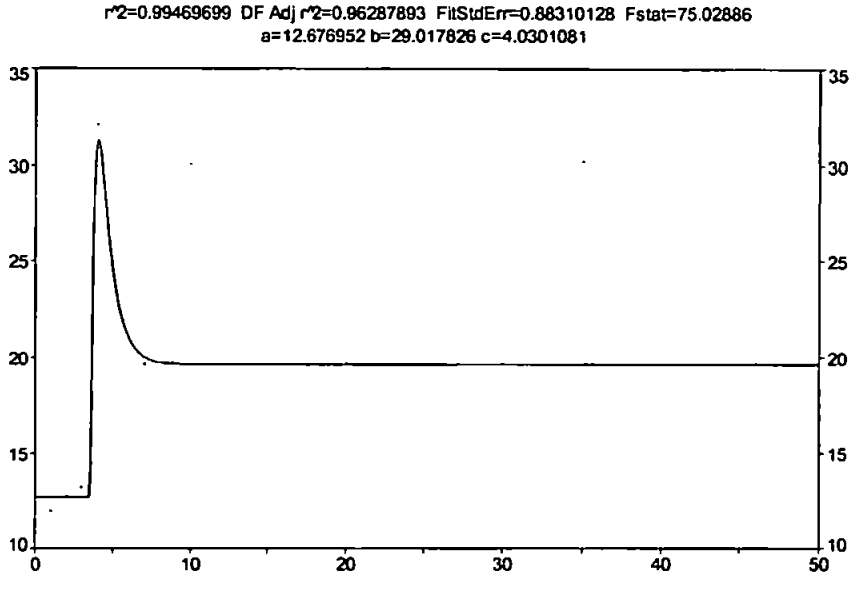

Figure 7.18 TableCurve 2D fit of parameter *i*. X-axis is time (days) and y-axis is the parameter value.

These equations combine to give the overall double glomus equation, which for day 7 is as shown in Figure 7.19. The analysis of the core samples showed no definite angle dependence. For example, Figure 7.10a at zero angle, and Figure 7.10b, at an angle of 27° from the point of injection, gives similar results. Thus the glomus equations do not incorporate any angle dependence for the Teign soil.

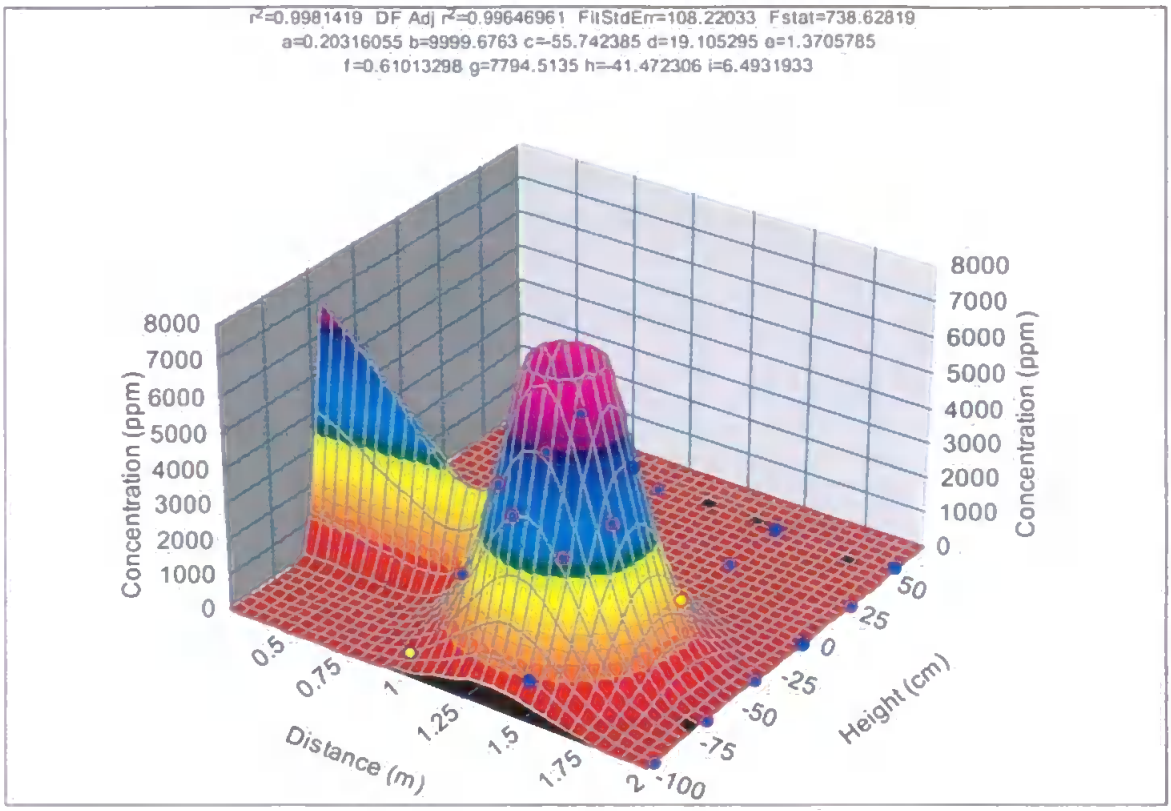

Figure 7.19 TableCurve 3D fit for day 7.

In practice, in Figure 7.20f, g, and h it can be seen that looking down on the pit from above (the top set of diagrams) there does seem to be an angle dependence, i.e. less concentration on the left of the diagram than the right. This is an artefact due to the absence of sampling at lower depths because of the presence of a large stone.

A full list of the actual and interpolated values with the pit dimensions can be seen in Appendix B.

Teign Series Soil

Actual and Modelled **Modelled**

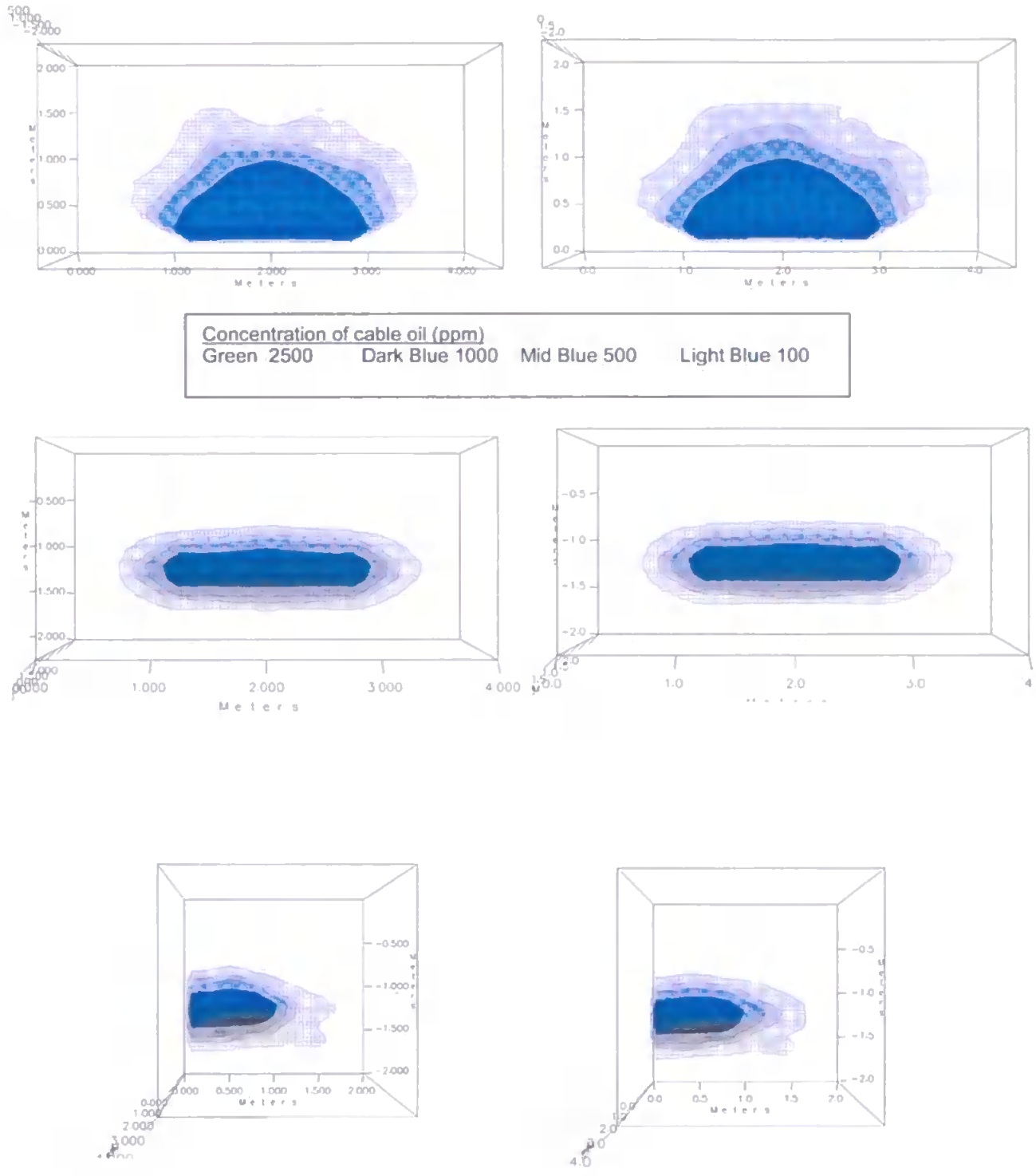

Figure 7.20 (a) Day 2, Actual and modelled cable oil migration for the Teign series soil.

Teign Series Soil

Actual and Modelled **Modelled**

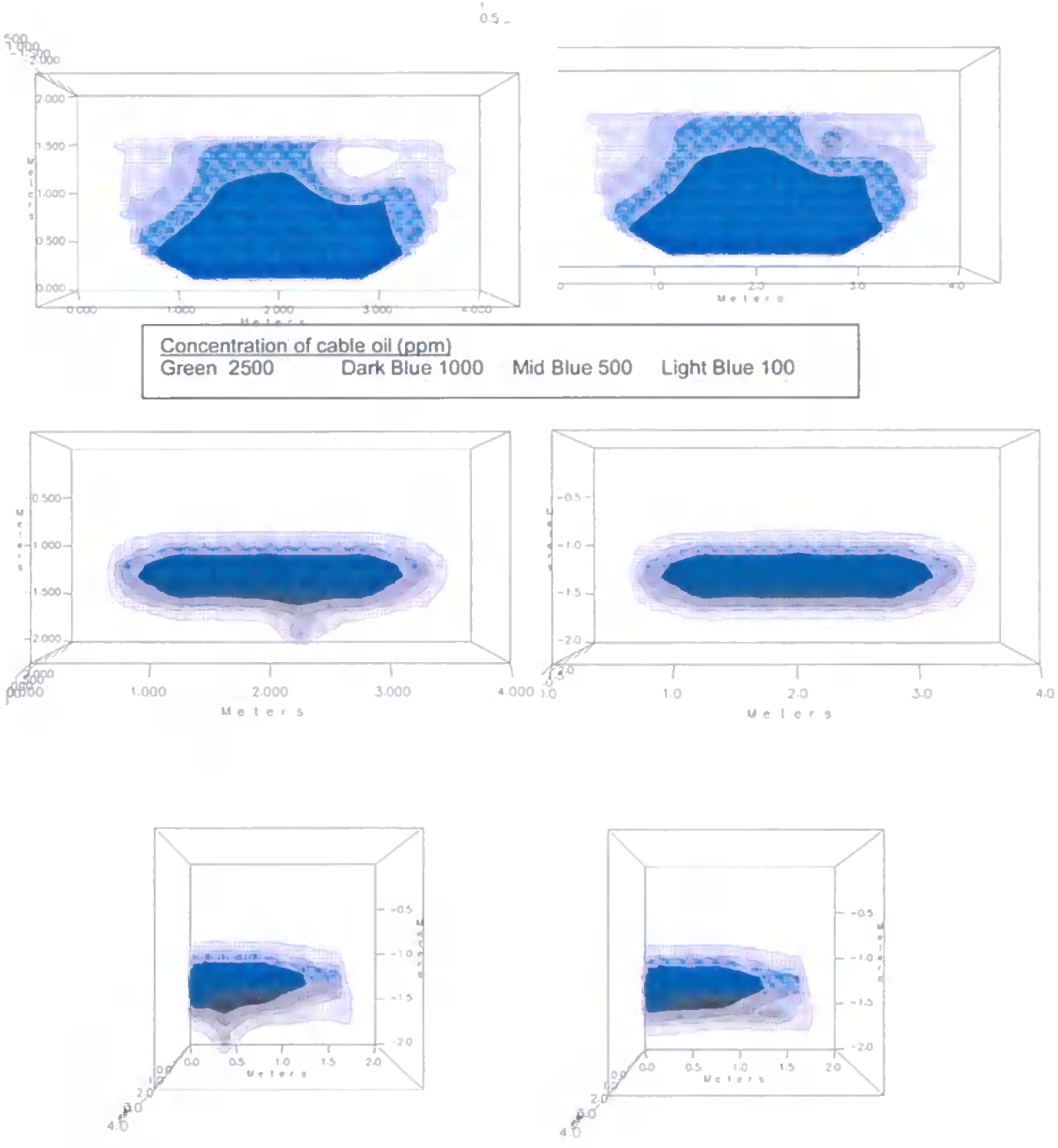

(b) Day 3, Actual and modelled oil migration for the Teign series soil.

Teign Series Soil

Actual and Modelled **Modelled**

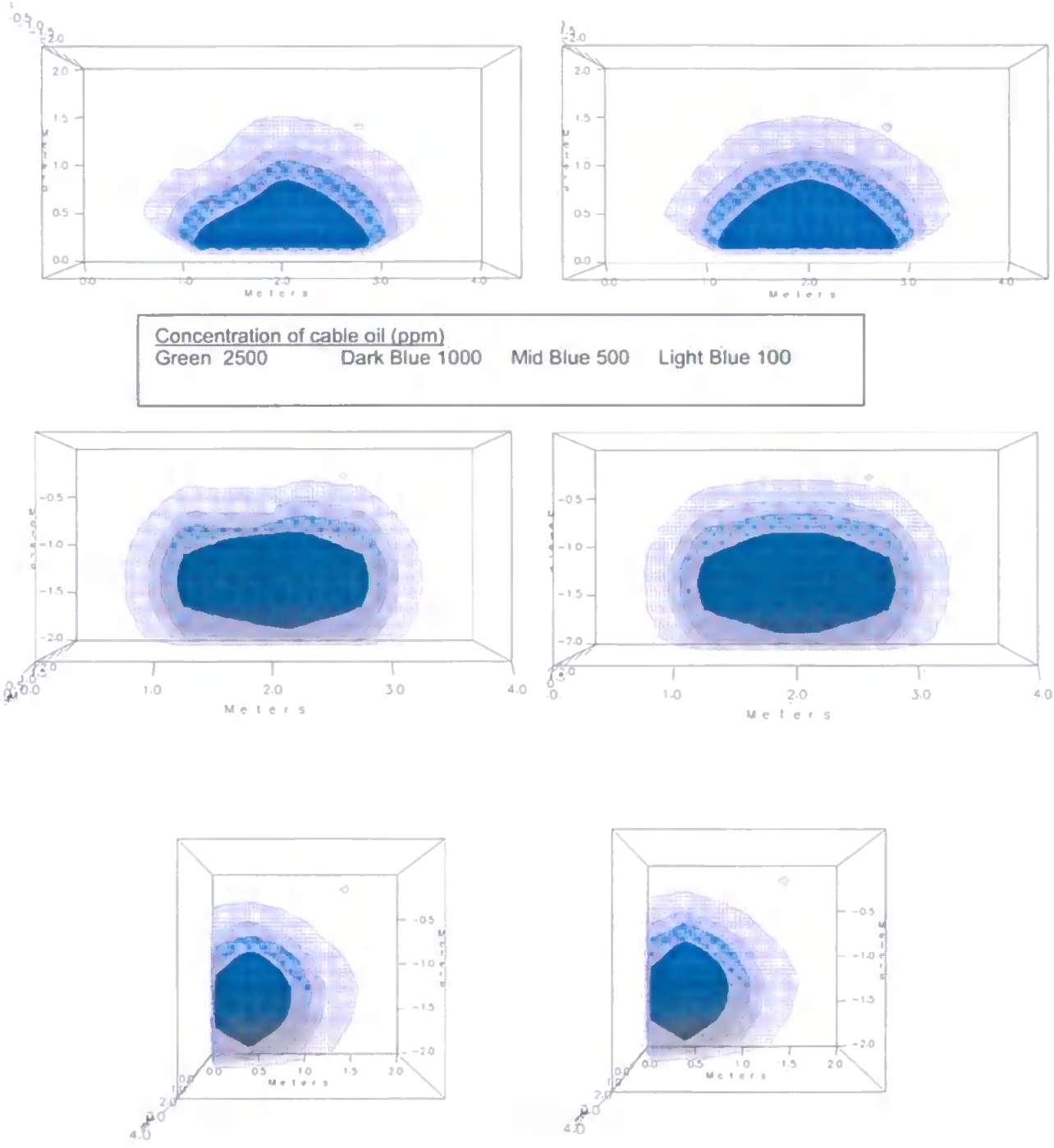

(c) Day 4, Actual and modelled oil migration for the Teign Series soil.

Teign Series Soil

Actual and Modelled **Modelled**

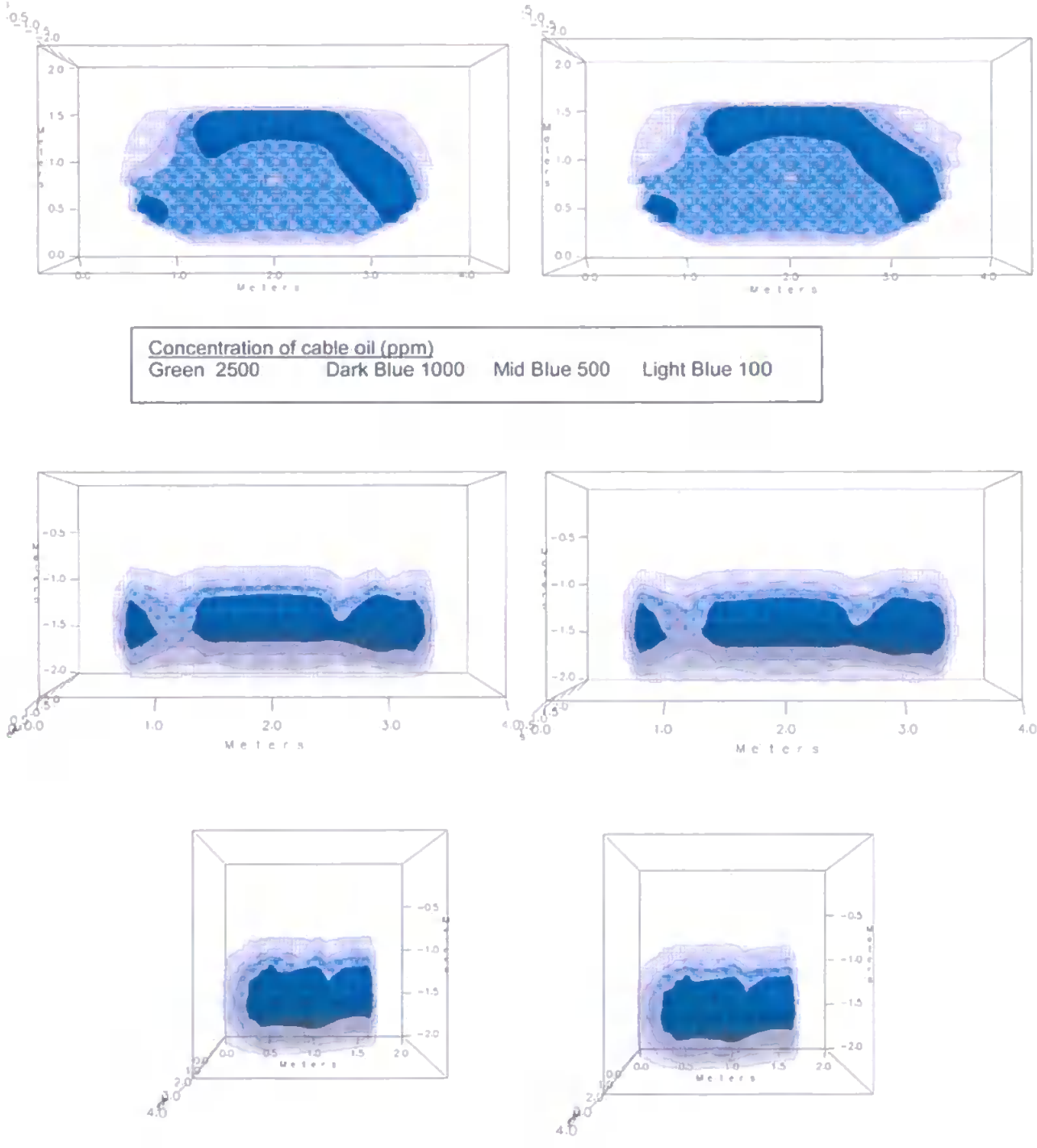

(d) Day 7, Actual and modelled oil migration for the Teign series soil.

Teign Series Soil

Actual and Modelled **Modelled**

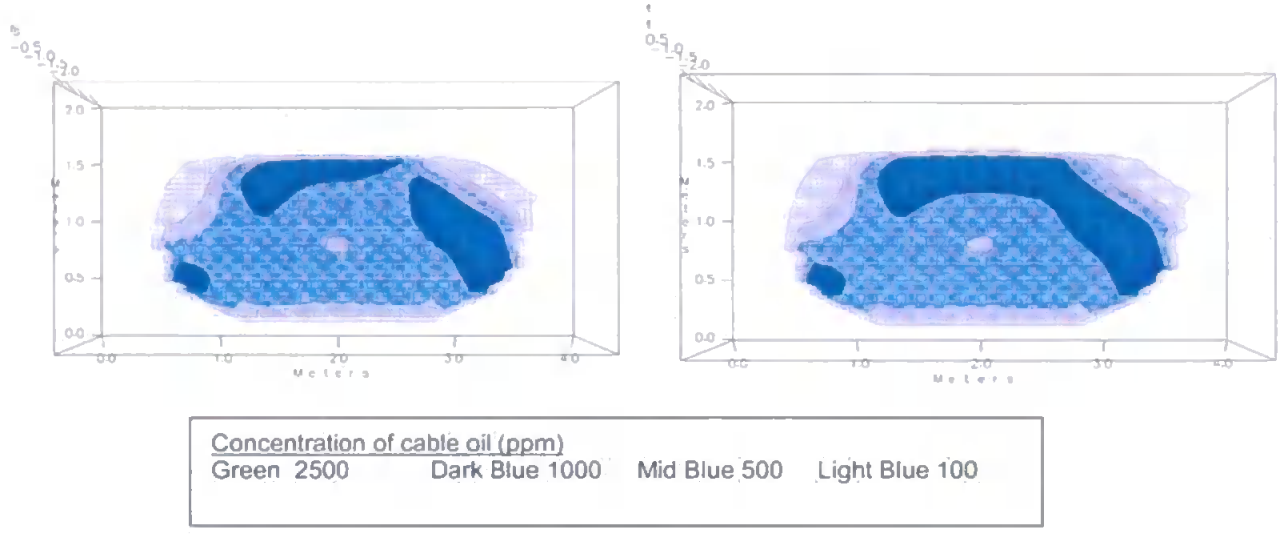

Concentration of cable oil (ppm)
Green 2500 Dark Blue 1000 Mid Blue 500 Light Blue 100

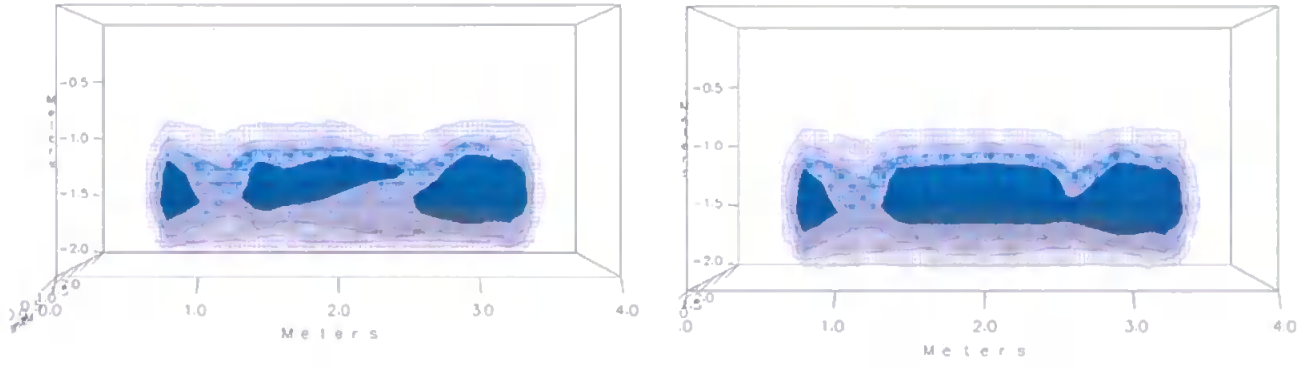

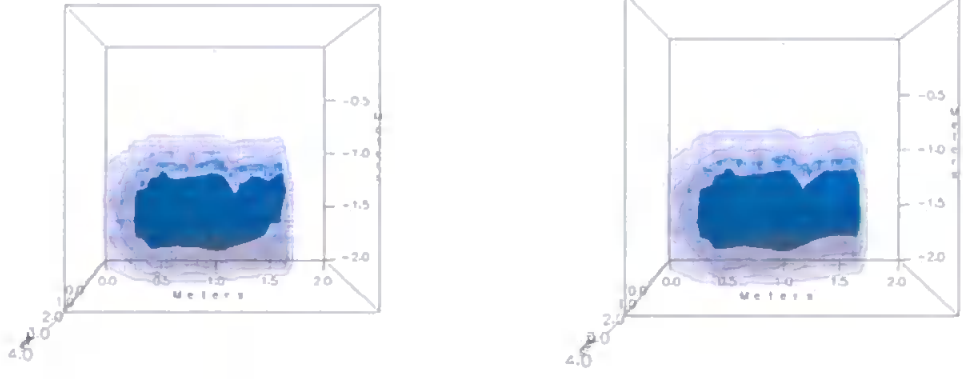

(e) Day 8, Actual and modelled oil migration for the Teign series soil.

Teign Series Soil

Actual and Modelled **Modelled**

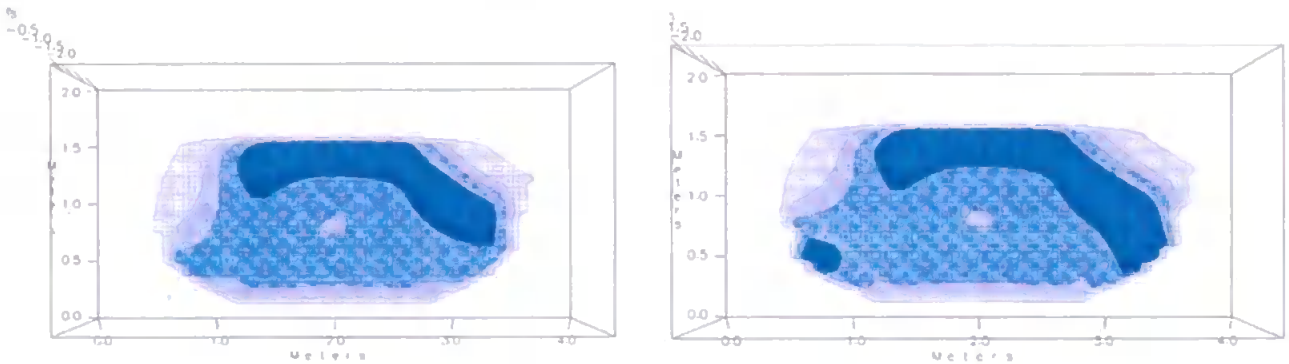

Concentration of cable oil (ppm)
Green 2500 Dark Blue 1000 Mid Blue 500 Light Blue 100

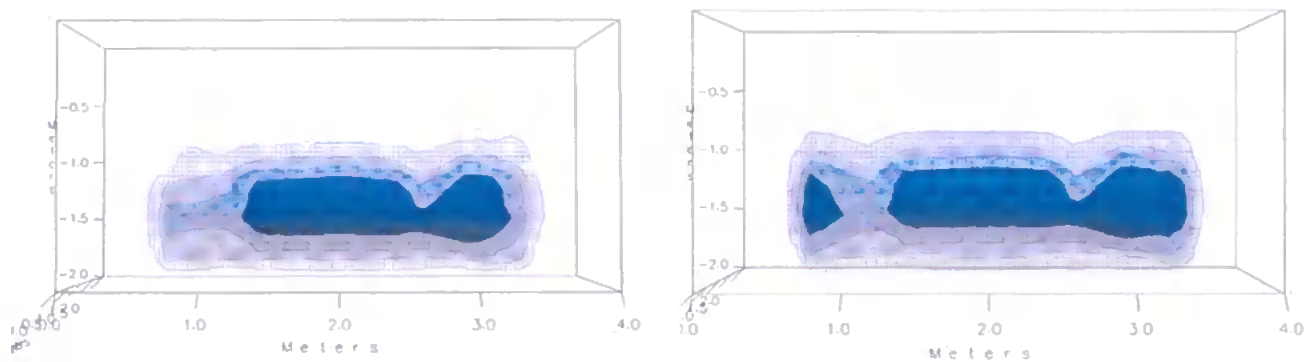

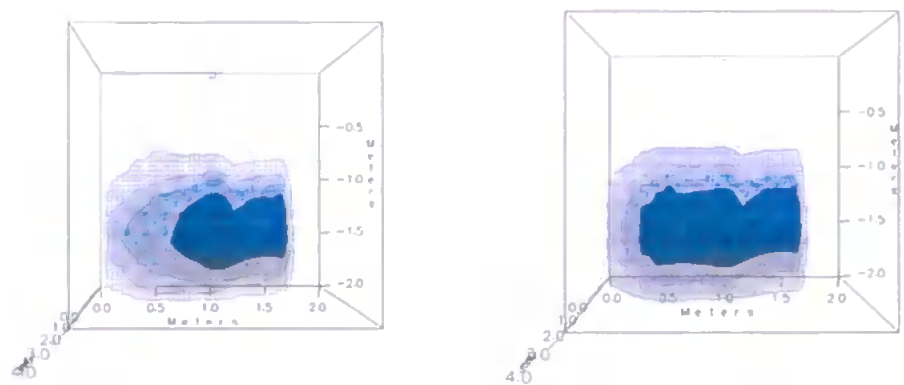

(f) Day 45, Actual and modelled oil migration for the Teign series soil.

Teign Series Soil

Actual and Modelled

Modelled

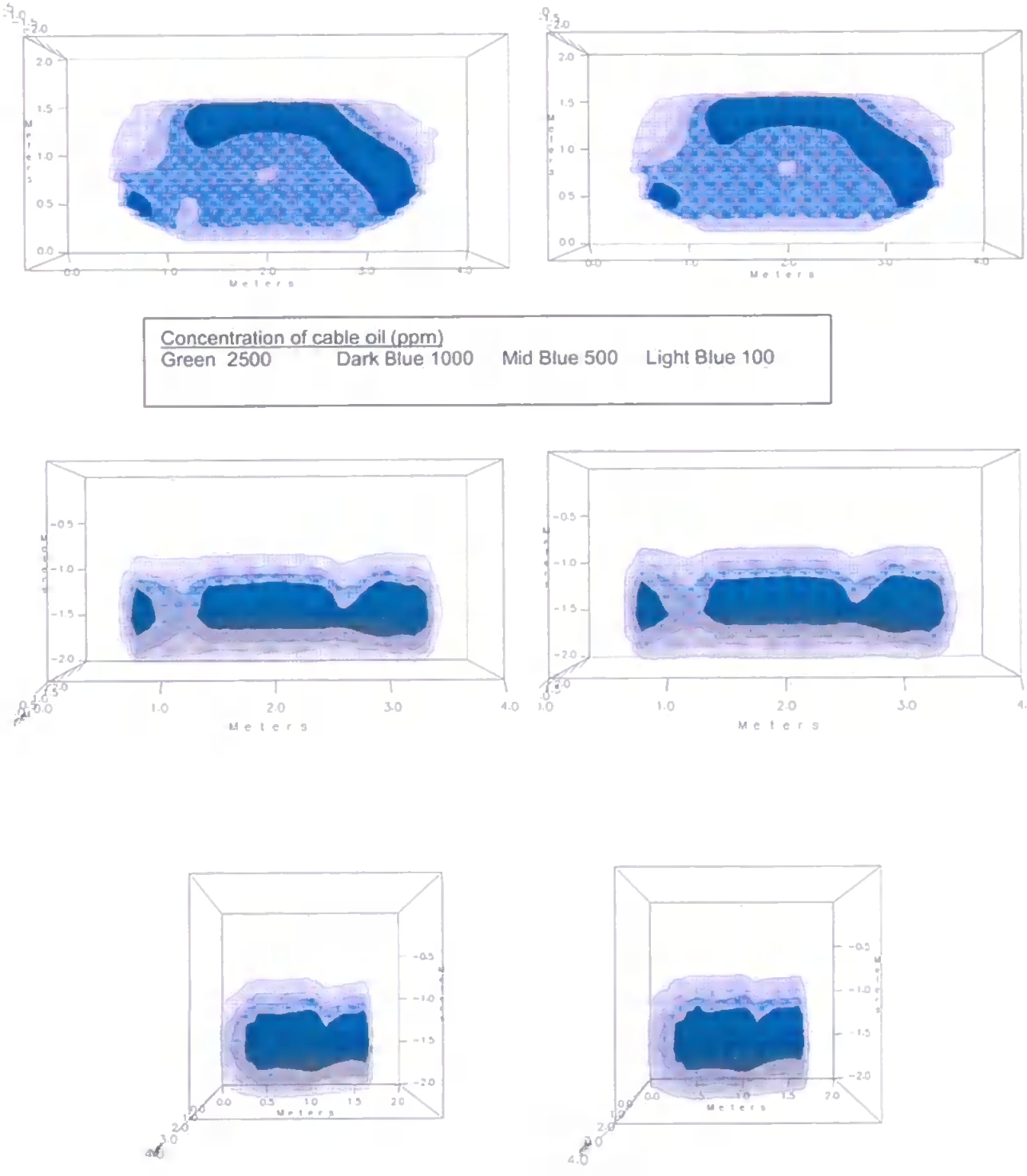

(g) Day 46, Actual and modelled oil migration for the Teign series soil.

Teign Series Soil

Actual and Modelled **Modelled**

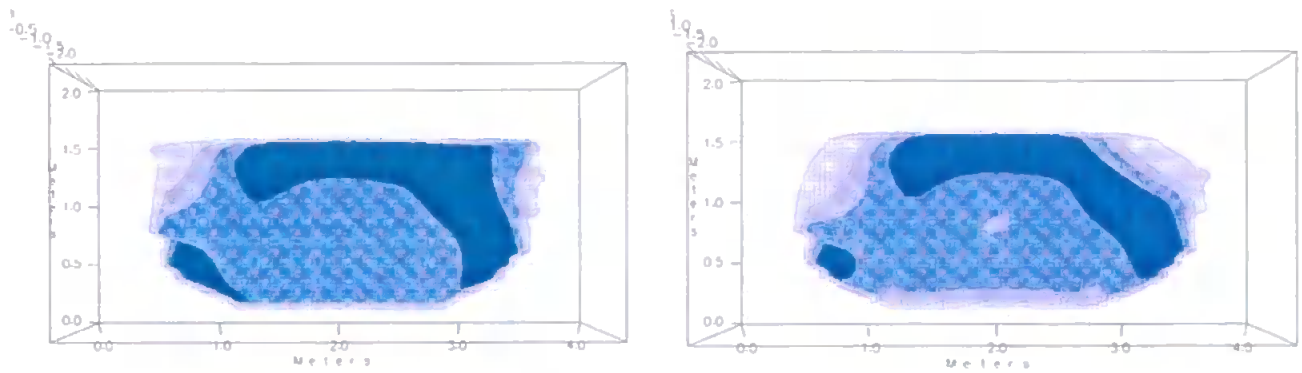

Concentration of cable oil (ppm)
Green 2500 Dark Blue 1000 Mid Blue 500 Light Blue 100

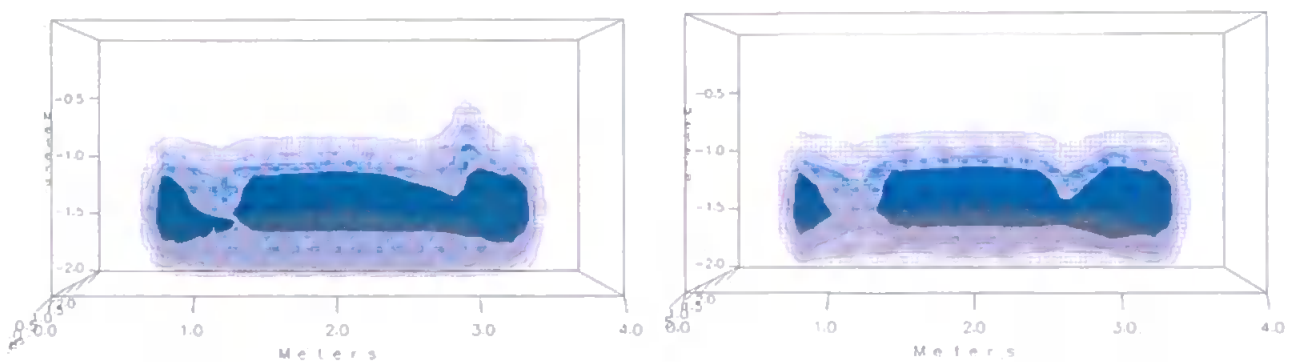

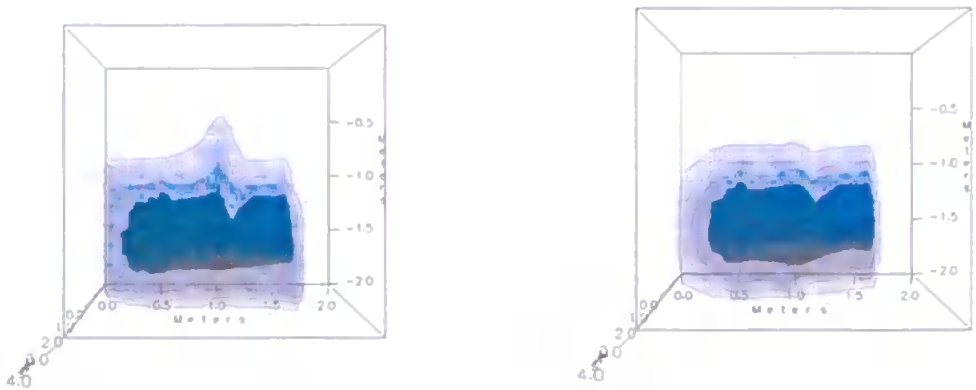

(h) Day 77, Actual and modelled cable oil migration for the Teign series soil.

As with the DeBathe soil interpolation it was possible to calculate the deviation between the experimentally derived concentrations and the interpolated ones. The quality of fit was once again measured by calculating the log RSD. Overall the interpolation fits the experimental data well. For the Teign soil the maximum log RSD value is 3.90, which suggests that the interpolation for the Teign soil is better than the DeBathe soil interpolation. As can be seen in Figure 7.21, there are no obvious trends in the log RSD value when plotted against the various parameters, i.e. height, distance, angle or day. However, there is a slight decrease in log RSD value with increasing height (from the point of injection).

An examination of the derived concentrations from the interpolated data set suggests that the interpolation slightly overestimates the extent of the cable oil plume. The interpolated data set also produces a smoother plume front, than the actual observations would suggest.

There are several broad conclusions that can be drawn from analysis of the Teign series oil migration study. Firstly, the oil plume appears to extend mainly, at or slightly below, the water table height, with little reaching the bottom of the pit. The main body of oil, in the form of a source glomus appears to split into secondary glomuses after 7 days, Figure 7.20d. The secondary glomuses are formed as a function only of the horizontal distance from the point of injection rather than depth, showing that lateral migration is occurring.

(a)

(b)

(c)

(d)

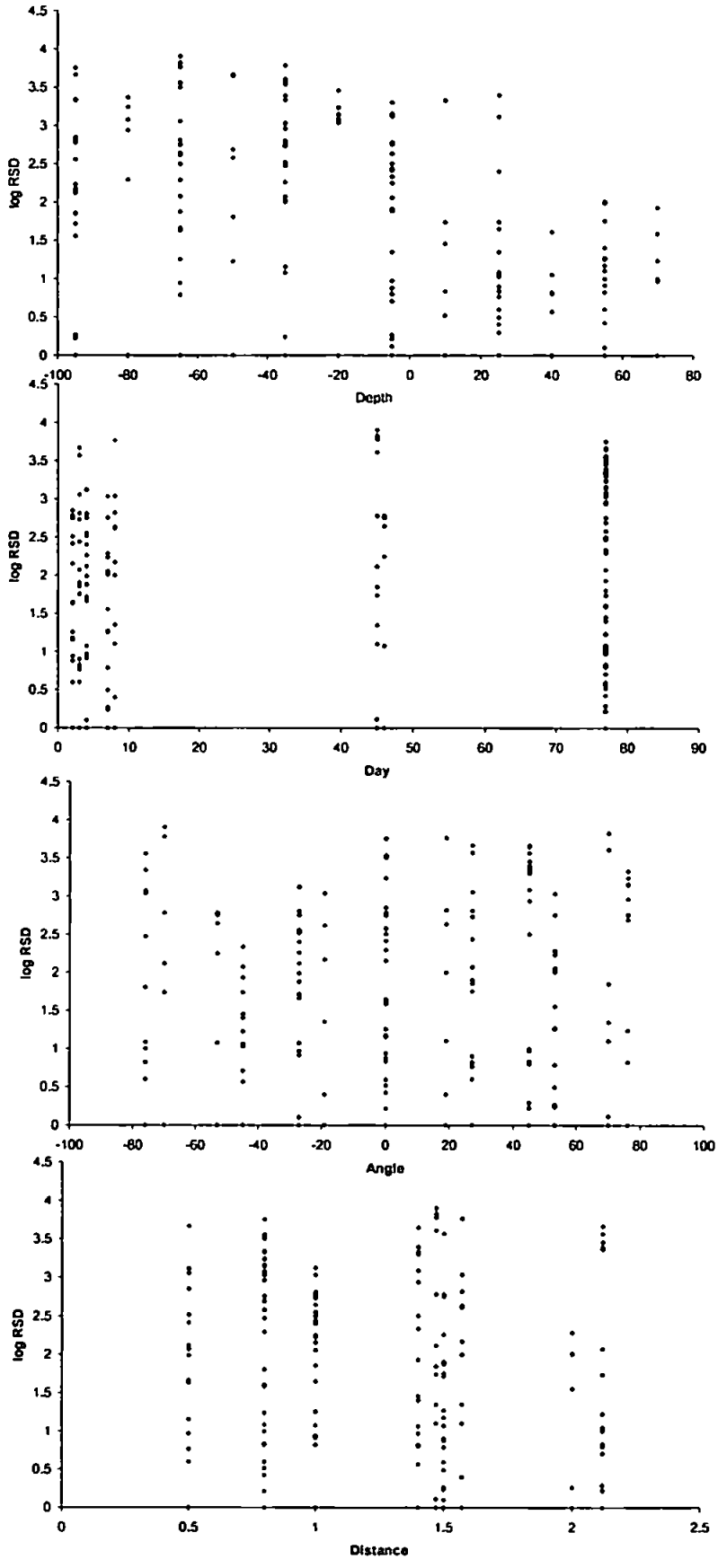

Figure 7.21 Graphs showing the log RSD in relation to (a) depth from the point of injection, (b) day, (c) the angle from the point of injection and (d) the distance from the point of injection.

Over time it is also noted that the oil has a tendency to migrate vertically down towards the bottom of the pit, Figure 7.20f, which can be explained in terms of a permanent decrease in the height of the water table. A temporary rise in the water table occurred around day 60, due to a period of rainfall, but did not appear to affect the overall migration of cable oil. A further observation from the data is that the highest concentrations of oil are found on the furthest edge of the plume, with respect to horizontal distance from the point of injection (top diagrams in Figure 7.20). This suggests that the oil is moving in a front away from the point of injection.

7.7 Discussion and Conclusions

It has been shown that the migration of cable oil occurs differently in the two types of repacked soil, and the shape of the oil plume is different. In the DeBathe soil the oil tends to migrate both laterally and vertically over time, whereas in the Teign series soil the oil tends to migrate only laterally, initially. The lateral extent of the oil plume is also greater in the Teign soil than for the DeBathe soil, compensating for the lack of vertical movement. Both soils experience a greater extent of oil migration over time, associated with an increase in the quantity of cable oil that has been added to the soil.

In the DeBathe soil, more oil migrates below the water table than in the Teign soil, with the majority of the oil remaining at the water table height in the Teign soil. It can also be shown that an increase in the height of the water table in the DeBathe soil causes some of the oil to migrate upwards in line with the rise in the water table. This is not reflected in the Teign soil data. However, this may be explained, at least in part, by the operational difficulties that were discussed in section 7.2.3.

Generally, it has been shown that there is symmetry in both pits. The plinth has a minimal impact on the migration of cable oil, although there is some evidence to suggest that the plinth increases the lateral extent of the migration in both soils. The data clearly shows

that the volume of cable oil injected into each pit has a major impact on the extent to which the oil migrates. This is a distinct effect in both soils. Movements in the water table do affect the oil plume, causing it to rise with the water table and fall when the water table is depressed.

Both pits had the same set of environmental conditions, to the extent that is possible in a field experiment, but the migration of the oil plume was significantly different. This indicates that the heterogeneities within the two soils are responsible for the differences in the pattern of oil migration. These heterogeneities can be shown in terms of soil structure, particle size distributions and water retention characteristics. These differences are, in part, characterised in the following chapter and used to understand the relationship between the soil characteristics and the migration of cable oil.

8. Overview

8.1 Introduction

There are five different aspects of the migration of oil through soil which have been discussed in this thesis, namely: (i) the fundamental theories in the literature, summarised by Dullien and subsequent research papers, (ii) the modelling of the behaviour of oil using Pore-Cor, (iii) the movement of oil in a 'one-dimensional' soil column, (iv) the migration of oil measured as a 'tomography' of a 0.5m soil block, and (v) the movement of oil over a scale of metres in the Cranfield pits.

These aspects range from pure theory to pure experiment, and cover a size range from pores of 0.02 μm to 2500 μm, and a sample length dimension from around 0.1 μm to several metres. There will inevitably be a range of observed behaviour, and a problem of upscaling. However, the broad range of size and approach make commonalities that emerge between the different scale experiments even more powerful. It is these commonalities which we now seek to identify, with respect to four aspects of oil behaviour, namely: (i) the distribution of oil in void space, (ii) the effect of void geometry on this distribution, (iii) the effect of oil loading on the distribution, and (iv) the effect of stationary and mobile water. The common picture that emerges will allow greater interpretation of other systems, or a predictive capability under other circumstances.

8.2 Distribution of Oil in the Void Space

There is general agreement in the literature about the way that oil distributes itself in porous media. Oil will normally enter a dry porous medium as a non-wetting fluid, by percolation, entering the largest and most accessible void features first. The oil therefore needs some driving force to make it intrude. In the laboratory experiments this can be an applied external pressure on the oil, and this force is also assumed in the modelling of the

oil percolation by Pore-Cor. In the pit, the only applied pressure was the transient pressure of the oil column in the injection tube.

At present, Pore-Cor can only simulate the intrusion of oil into a dry sample. In most natural systems however, the soil grains will have been wetted by water prior to the intrusion of oil. Therefore the oil will be intruding over a wetted surface and the characteristics will be different. This effect was emphasised in Figure 1.6, which is in contrast to the corresponding diagram in Dullian (1992), Figure 1.5, which mainly assumes the particles to be dry.

Pore-Cor is clearly an approximation to the experimental system studied. Despite this it has the advantage that it is based on a void network with the correct percolation characteristics, and therefore has a realistic size and positional distribution of pores and throats. Since this is also based on a realistic porosity, it can provide a worthwhile simulation of oil migration effects as discussed below.

The work reviewed by Dullien and subsequent publications provides a consensus on the way that oil distributes itself in a water wet, but partially saturated sample. There will be a volume of the sample in which the oil will be stationary and trapped. This will occur near to the point of injection, in the zone that we have named the 'source glomus'. The oil can move away from this region in two ways. Firstly, there will be a dissolved fraction. However, the distribution coefficient K_{od} (i.e. the partition coefficient normalised for organic carbon content) is low, see Table 1.2. As a result, very little oil will be moved by dissolution into the aqueous phase. However, under water flow conditions, the capillary and viscous forces exerted by the water will move some oil and the effects of this are discussed the Section 8.4 below.

8.3 *Effects of the Void Geometry on the Distribution of Oil*

Dullien makes some mention of the effects of void geometry on oil distribution, in terms of two-phase flow in capillaries with a diameter that changes as a step function with distance. Overall however, no theoretical consideration can cope with the sheer complexities of soil and sand structures. Pore-Cor is isotropic, and all pores are symmetrical cubes and all throats are cylinders with circular cross-sections. There are two ways of approaching this issue using Pore-Cor. Firstly, different void geometries in soil will cause different water retention characteristics. If these differing water retention curves are modelled by Pore-Cor, different Pore-Cor unit cells will result. Therefore the different geometries will be expressed as different Pore-Cor unit cell, although the Pore-Cor isotropy will mask the subtleties of the geometry effect.

Therefore we must turn to a second approach which is to observe how different void geometry in the different soil samples affects the oil distribution experiments. These phenomena have been observed for both the half-metre scale and pit experiments. Here we again encounter a difficulty, the very marked differences in the oil characteristics in the undisturbed DeBathe and repacked DeBathe at a half-meter scale suggest that the extent of soil packing must have an effect. The repacked soil having a substantial lower bulk density. The repacking density effects probably mask the void geometry effects.

The only comparable experiments are for repacked Teign and DeBathe at the half-metre scale and a similar comparison at the pit scale. The results show that under the lighter packing of the half-metre scale experiments, there was significant formation of multiple secondary glomuses within the DeBathe soil.

Work by Butts and Jensen (1996) showed that differences in the sand texture caused changes in the migration of oil. This phenomenon can be seen in the differences that have

Soil Type	Minimum Pore Size Plugged	Hydraulic Conductivity (milliDarcies)
DeBathe Repacked	338μm	2.298
Teign Repacked	250μm	1.058

Table 8.1 Table showing the reduced hydraulic conductivity with the associated pore plugged size, using the pit soil types, from reducing the percentage of pore volume by the calculated amount.

If these calculated hydraulic conductivities, Table 8.1, are compared against the typical hydraulic conductivities (from Chapter 2) it is possible to see a significant decrease in hydraulic conductivity. Observations of the pore structures, Figure 8.1 show that the decrease in hydraulic conductivity is significant, even though the relative number of pores that are oil filled (coloured purple) is low. This has the effect of reducing the amount of water that is able to flow through the sample.

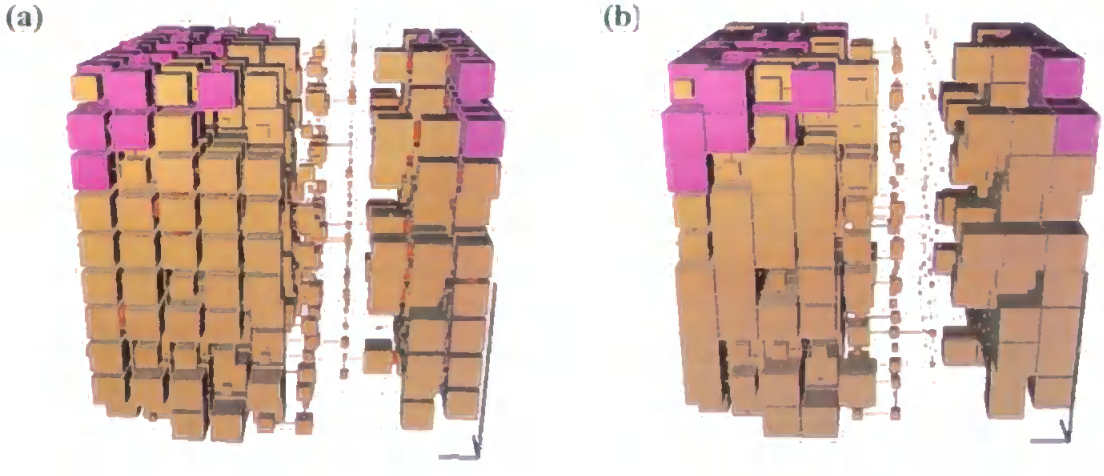

Figure 8.1 Pore-Cor soil simulated soil structures for (a) DeBathe repacked soil and (b) Teign repacked soil. Oil filled pores are coloured purple.

Joseph et al. (1992) undertook initial work on the impact of oil loading an the distribution of oil within soil. They showed a dependence of distance of oil movement on loading. We have shown in this work that this dependence occurs consistently over a wide range of scales, from the simulated pore-level to the experimental scale of several metres. However, the present work goes beyond that of Joseph *et al.* (1992) by providing a better quantification of the way in which this increased distance with loading is achieved.

occurred in the packing of the soil. The looser the packing density of the soil, the more fingering occurs causing the formation of multiple glomuses, as seen in Figure 5.18. Other researcheers such as Poulsen and Keuper (1992) found that heterogeneities within a porous structure will give rise to preferential flow of immiscible pollutants.

8.4 Effect of Oil Loading on the Distribution of Oil

It is clear from Figure 1.5 that under high loading of oil there is likely to be a quantity of the oil that is available for movement by the capillary and viscous force of the water. The oil will finger out from the source glomus to form secondary glomuses. This phenomona is clearly substantiated by Pore-Cor (Figure 2.16k) which shows the distribution of oil when the saturated hydraulic conductivity was reduced to zero by the oil.

It is also possible to use Pore-Cor to represent the amount of oil that is equivalent to that saturating a sample of soil located at a 50cm radius from the point of injection (for the purposes of this calculation the sand around the point of injection is ignored). It is feasible to estimate what percentage of pore volume is filled by a specific amount of cable oil, by estimating the pore volume for a specific soil. Using the soils in the pit, the specific pore volume of 50cm radius would be 160744 cm^{-3} for the DeBathe soil and 210487 cm^{-3} for the Teign soil. If it is assumed that 20 litres of oil is injected into this pore space, then it is possible to calculate the percentage of the pore volume with has been filled with oil. For the DeBathe soil the percentage of the pore volume filled with oil is 12.4% and for the Teign soil it is 9.5%.

Pore-Cor makes it possible to simulate the effect that the percentage of oil filled pores has on the soil structure and hydraulic conductivity. This is achieved in a similar fashion to the work described in Section 2.3. Pores were blocked (from largest to smallest) to the point at which the water retention decreases by the desired amount (i.e. 12.4% and 9.5%). Table 8.1 shows the associated void size and new hydraulic conductivity.

This better quantification was achieved using the glomus hypothesis. This clearly demonstrated the formation of a source glomus initially, and then a secondary glomus once sufficient loading is achieved.

8.5 Effects of Stationary and Mobile Water

As discussed above, stationary water will coat the particle of sand or soil, which will alter the contact angle between the water and the solid phase, probably reducing it and making the oil slightly more wetting. There is no exact theoretical structurally dependent approach to this phenomena. At a theoretical level it is normally approached by a phenomenical parameter expressing relative permeability as mentioned in Chapter 1. Hilfer has recently attempted to incorporate viscous and capillary effect within these coupling constants, but they are still a long way off structurally dependent relationships and hence have very little predictive capability.

Researchers such as Guigrad et al. (1996) and Aurelius and Brown (1987) have reported that the movement of a wetting front enhanced the movement and infiltration of immiscible chemicals. This has to some extent been shown by the one-dimensional study. Further evidence of this is given in Table 5.4. The chi-squared values suggest that there is a significant difference in the water flow rates before and after oil injection. This suggests that the addition of oil to a partially saturated sample affects the water flow distributions.

Pore-Cor does shed some light in this area because it gives predictions of saturated hydraulic conductivity in the presence of oil. The calculation above (Section 8.5), results in a ten fold decrease in hydraulic conductivity for an approximate 10% decrease in the pore volume available to flowing water. Unfortunately there is no way to quantify this in the pit experiments and this is now the subject of a planned research project.

To gain some semi-quantitative insight into the effect of water on oil migration, the glomus approach proves extremely useful. The data (Chapter 7) reveals that at long times after injection the simplicity of the glomus approach breaks down. It also breaks down when the water table is raised and passes through the glomus. In this instance a significant amount of oil is moved up by the capillary, viscous and buoyancy effects of the water. Overall the pit experiments showed that for sampling intervals at 0.5m spacing and one or more days apart, the two glomus approximation is a good one for the first seven days after the injection of oil, or in the real world in the first few days of a sub-terrain oil leak. The exact position of the secondary glomus cannot be predicted. In the DeBathe soil the secondary glomuses were below the point of injection and were not displaced horizontally away from the point of injection. In the Teign soil the displacement of the secondary glomus was horizontal not vertical. It is too early to say whether this substantial difference in migration behaviour was due to difference in packing or soil type. The DeBathe soil had a significant angle dependence i.e. it was not symmetrical about a central plane as shown in Figure 7.17c, but in the Teign soil there was no angle dependence.

Referring back to Pore-Cor and fundamental theory, we can conclude that the glomus positions should be symmetrical if the oil was perfectly homogeneously distributed and the saturation was also homogeneous. The extent to which the glomuses are not symmetrical suggests the extent of heterogeneity of the soil.

8.6 Conclusion

A unique feature of this work is the study of oil migration not only using a network model but also by experimentation over three sample size ranges. It can be seen from the previous discussion that a synthesis of the ideas gives a precise model of oil migration in the subsoil.

9. Conclusions and Future Work

9.1 Conclusions

The aim of this research has been to analyse the migration of oil pollutant through soil, which has been accomplished, for the first time, on a wide range of scales from pore- to field-level. This study significantly enhances the understanding of the flow of immiscible pollutants within soil, through experiments to define the spatial variability and extent of a contaminated area and the use of advanced modelling techniques to develop a comprehensive framework for the analysis of oil pollutant migration.

Relatively simple one–dimensional studies have shown that the quantity of cable oil is a critical factor in determining the migration of cable oil, in various sands. Permeability and porosity of the sample material are also important secondary factors. High permeability assists the migration of oil pollutants, whilst low permeability restricts pollutant migration. Soils with a high porosity allow the pollutant to migrate vertically under the influence of gravity, whereas soils with low porosity induce lateral oil migration, as the oil spreads from the point of injection.

The half metre scale experiments showed that the water flow velocity before and after oil injection had little effect on the overall pattern of water flow on any of the sand and soils studied. Greatest variation of flow occurred in the repacked soils. The overall water flows through these soils was consistent with previous findings that different random packings could cause variations in sample porosity and permeability.

These findings were then used in the design of the large scale experiments. The large scale study, located at Cranfield, was designed on the basis of being true to life in terms of leak rate, and incorporating the observations from the 1-D experiments to predict likely

behaviour. Symmetry of oil migration was noted from the point of oil injection in both soils. This series of experiments gave further evidence to support the finding that quantity of pollutant is a critical factor in determining the migration of cable oil. The effects of movements in the water table on the oil plume were also studied. Expectations that the oil would rise with an increase in the level of the water table were overturned, as significant quantities of oil remained below the water table when it was raised.

These studies have also observed that the repacking of soil, distorts the water retention characteristics and porosity of the soil. This causes different migration of cable oil to occur. Soils and sands with a high porosity will allow oil to migrate vertically under the influence of gravity, whereas soils with a low porosity will result in lateral oil migration, as the oil spreads from the point of injection.

Experimental data was used to establish modelling capabilities for the characterisation of pollutant migration. Modelling was undertaken at two levels. By using these two modelling approaches it has been possible to analyse the migration of cable oil in soil.

The first level of modelling consisted of the development of simple Gaussian equations based upon observations of oil glomuses. The glomus approach, which was newly developed in this work, can be compared to a fractal model, with the glomuses observed in each of the different scales studied. The glomus approach on the larger scale studies occur as numerous ganglia or capillary or viscous fingering is apparent at the pore scale.

The second stage of modelling involved the use of Pore-Cor to determine the pore scale movement of pollutants. This research suggested that, oil is often located in larger stagnant pores. Where greater concentration occurs, oil contaminates both larger and smaller pores, reducing permeability significantly

From the analysis of the water retention characteristics and Pore-Cor model output it was possible to suggest the pore scale movement of the cable oil within soil. This information suggests that during the early stages of pollutant migration oil is generally located in the larger stagnant pores, enabling smaller pores to continue to carry water. Consequently there is little impact on permeability. The repacking of soil results in less large pores being created, resulting in a lower ability to hold water and the formation of impenetrable barriers that the oil cannot vertically migrate down through, causing lateral flow to occur. In addition, Pore-Cor also realistically reproduces the capillary fingering of oil showing preferential flow occurring at pore level.

The Pore-Cor model has been able to successfully model the soil structure of the soils in this study. It has also modelled the permeability of these soils through the use of stochastic generations that closely match the experimental data. Pore-Cor has also been able to demonstrate the effect that oil has on the permeability of soil, with respect to trends in the permeability for three sample categories; sand, undisturbed soil and repacked soil.

9.2 Future Work

This study has developed a framework for the modelling of sub-surface pollutant migration through a range of porous media. Whilst the study strives to understand the processes at work and the impact of soil characteristics on pollutant migration, much work is required to develop a complete understanding of these processes which can be widely applied to a range of pollutants and soil types.

In the one-dimensional experiments work is required to further understand the impact of different soil types, pollutants and flow conditions. In particular, one-dimensional studies would benefit from comparisons between a wider range of materials, including undisturbed and repacked soils.

The half metre scale studies also require extension to cover these issues. In addition, a greater understanding of the different characteristics of *in situ* and repacked soil is required to understand the limitations of studies conducted on repacking.

For the three-dimensional field scale investigations, research is required to extend the framework developed in this study to a range of pollutants. In particular, research work must address whether the same patterns of pollution migration are observed for other immiscible pollutants and whether the Gaussian 'glomus' framework can usefully be applied and extended to remove the fitting parameters to further the understanding of the migration of these substances. Equally, the analysis must be applied to other soil types with the intention of producing a comprehensive model, which can be applied across the full range of soil types and common forms of immiscible pollutants. Ultimately, the ability to protect potable groundwater supplies from contamination depends on the development of a universally applicable model to determine pollutant migration.

At present automation of the rainfall simulator and grid lysimeter is taking place. This will allow for more detailed analysis of water flow rates to be carried out and also permit a wide range of pollutants and soil types to be studied. Greater use of the larger three – dimensional level would require a large financial investment, which may prohibit this. However, this study has shown the many benefits that such a large-scale experiment provides.

Pore-Cor also requires further development to model soil structures better. At present Pore-Cor attempts to model the four orders of magnitude difference of void size range found in soil into 100 void sizes, ideally this needs to be extended by a larger order of magnitude. Pore-Cor currently uses a simplified geometry, recent developments have been

concerned with changing the shape throats and increasing the permeability of the simulated structure. This model could be extended to simulate the effects of packing on soil structure, as well as the extension of the model to take into account the volume of absorption in addition to void size and pressure.

The ultimate aim is to be able to generate predictive capabilities, which would involve increasing the number of soil types studied. The predictive capabilities would use water retention curves and soil type to be able to generate predictions of pollutant flow, within the existing Pore-Cor framework. A research project which is currently underway aims to achieve some of these aims.

APPENDIX A DeBathe Repacked Interpolation

Sample	Angle	Distance	Height	Time	Concentration	Predicted	Actual or pred	log RSD
a	0	0.5	55	1	5.5	0.20	5.50	0.99
a	0	0.5	25	1	11	122.37	11.00	2.27
a	0	0.5	-5	1	4641.4	4632.32	4641.40	0.00
a	0	0.5	-35	1	10952.13	10953.41	10952.13	0.00
a	0	0.5	-65	1	1622.17	1617.79	1622.17	0.00
a	0	0.5	-95	1	166.17	14.92	166.17	2.40
b	0	1	55	1	7.67	0.00	7.67	1.19
b	0	1	25	1	7	0.38	7.00	1.07
b	0	1	-5	1	4.33	14.37	4.33	1.03
b	0	1	-35	1	3.67	33.97	3.67	1.69
b	0	1	-65	1	4	5.02	4.00	0.00
b	0	1	-95	1	4.33	0.05	4.33	0.92
c	0	1.5	55	1	4.67	0.00	4.67	0.97
c	0	1.5	25	1	2.67	0.00	2.67	0.73
c	0	1.5	-5	1	2	0.00	2.00	0.60
c	0	1.5	-35	1	2.33	0.00	2.33	0.67
c	0	1.5	-65	1	2.33	0.00	2.33	0.67
c	0	1.5	-95	1	3.67	0.00	3.67	0.87
d	27	0.5	55	1	10000000	0.20	0.20	n/a
d	27	0.5	25	1	10000000	122.37	122.37	n/a
d	27	0.5	-5	1	10000000	4632.32	4632.32	n/a
d	27	0.5	-35	1	10000000	10953.41	10953.41	n/a
d	27	0.5	-65	1	10000000	1617.79	1617.79	n/a
d	27	0.5	-95	1	10000000	14.92	14.92	n/a
e	27	1	55	1	10000000	0.00	0.00	n/a
e	27	1	25	1	10000000	0.38	0.38	n/a
e	27	1	-5	1	10000000	14.37	14.37	n/a
e	27	1	-35	1	10000000	33.97	33.97	n/a
e	27	1	-65	1	10000000	5.02	5.02	n/a
e	27	1	-95	1	10000000	0.05	0.05	n/a
f	27	1.5	55	1	10000000	0.00	0.00	n/a
f	27	1.5	25	1	10000000	0.00	0.00	n/a
f	27	1.5	-5	1	10000000	0.00	0.00	n/a
f	27	1.5	-35	1	10000000	0.00	0.00	n/a
f	27	1.5	-65	1	10000000	0.00	0.00	n/a
f	27	1.5	-95	1	10000000	0.00	0.00	n/a
g	-27	0.5	55	1	10000000	0.20	0.20	n/a
g	-27	0.5	25	1	10000000	122.37	122.37	n/a
g	-27	0.5	-5	1	10000000	4632.32	4632.32	n/a
g	-27	0.5	-35	1	10000000	10953.41	10953.41	n/a
g	-27	0.5	-65	1	10000000	1617.79	1617.79	n/a
g	-27	0.5	-95	1	10000000	14.92	14.92	n/a
h	-27	1	55	1	10000000	0.00	0.00	n/a
h	-27	1	25	1	10000000	0.38	0.38	n/a
h	-27	1	-5	1	10000000	14.37	14.37	n/a
h	-27	1	-35	1	10000000	33.97	33.97	n/a
h	-27	1	-65	1	10000000	5.02	5.02	n/a
h	-27	1	-95	1	10000000	0.05	0.05	n/a
i	-27	1.5	55	1	10000000	0.00	0.00	n/a
i	-27	1.5	25	1	10000000	0.00	0.00	n/a
i	-27	1.5	-5	1	10000000	0.00	0.00	n/a
i	-27	1.5	-35	1	10000000	0.00	0.00	n/a
i	-27	1.5	-65	1	10000000	0.00	0.00	n/a
i	-27	1.5	-95	1	10000000	0.00	0.00	n/a
j	53	0.5	55	1	10000000	0.20	0.20	n/a
j	53	0.5	25	1	10000000	122.37	122.37	n/a
j	53	0.5	-5	1	10000000	4632.32	4632.32	n/a
k	53	1	55	1	10000000	0.00	0.00	n/a
k	53	1	25	1	10000000	0.38	0.38	n/a
k	53	1	-5	1	10000000	14.37	14.37	n/a
k	53	1	-35	1	10000000	33.97	33.97	n/a
k	53	1	-65	1	10000000	5.02	5.02	n/a
k	53	1	-95	1	10000000	0.05	0.05	n/a
l	53	1.5	55	1	10000000	0.00	0.00	n/a
l	53	1.5	25	1	10000000	0.00	0.00	n/a
l	53	1.5	-5	1	10000000	0.00	0.00	n/a

l	53	1.5	-35	1	10000000	0.00	0.00	n/a
l	53	1.5	-65	1	10000000	0.00	0.00	n/a
l	53	1.5	-95	1	10000000	0.00	0.00	n/a
m	53	2	55	1	10000000	0.00	0.00	n/a
m	53	2	25	1	10000000	0.00	0.00	n/a
m	53	2	-5	1	10000000	0.00	0.00	n/a
m	53	2	-35	1	10000000	0.00	0.00	n/a
m	53	2	-65	1	10000000	0.00	0.00	n/a
m	53	2	-95	1	10000000	0.00	0.00	n/a
n	-70	1.47	55	1	10000000	0.00	0.00	n/a
n	-70	1.47	25	1	10000000	0.00	0.00	n/a
n	-70	1.47	-5	1	10000000	0.00	0.00	n/a
n	-70	1.47	-35	1	10000000	0.00	0.00	n/a
n	-70	1.47	-65	1	10000000	0.00	0.00	n/a
n	-70	1.47	-95	1	10000000	0.00	0.00	n/a
o	70	1.47	55	1	10000000	0.00	0.00	n/a
o	70	1.47	25	1	10000000	0.00	0.00	n/a
o	70	1.47	-5	1	10000000	0.00	0.00	n/a
o	70	1.47	-35	1	10000000	0.00	0.00	n/a
o	70	1.47	-65	1	10000000	0.00	0.00	n/a
p	-19	1.57	55	1	10000000	0.00	0.00	n/a
p	-19	1.57	25	1	10000000	0.00	0.00	n/a
p	-19	1.57	-5	1	10000000	0.00	0.00	n/a
p	-19	1.57	-35	1	10000000	0.00	0.00	n/a
p	-19	1.57	-65	1	10000000	0.00	0.00	n/a
p	-19	1.57	-95	1	10000000	0.00	0.00	n/a
q	19	1.57	55	1	10000000	0.00	0.00	n/a
q	19	1.57	25	1	10000000	0.00	0.00	n/a
q	19	1.57	-5	1	10000000	0.00	0.00	n/a
q	19	1.57	-35	1	10000000	0.00	0.00	n/a
q	19	1.57	-65	1	10000000	0.00	0.00	n/a
q	19	1.57	-95	1	10000000	0.00	0.00	n/a
r	76	0.8	70	1	10000000	0.00	0.00	n/a
r	76	0.8	55	1	10000000	0.01	0.01	n/a
r	76	0.8	40	1	10000000	0.35	0.35	n/a
r	76	0.8	25	1	10000000	6.07	6.07	n/a
r	76	0.8	10	1	10000000	52.83	52.83	n/a
r	76	0.8	-5	1	10000000	229.83	229.83	n/a
r	76	0.8	-20	1	10000000	499.84	499.84	n/a
r	76	0.8	-35	1	10000000	543.45	543.45	n/a
r	76	0.8	-50	1	10000000	295.39	295.39	n/a
r	76	0.8	-65	1	10000000	80.27	80.27	n/a
r	76	0.8	-80	1	10000000	10.90	10.90	n/a
r	76	0.8	-95	1	10000000	0.74	0.74	n/a
s	0	0.8	70	1	10000000	0.00	0.00	n/a
s	0	0.8	55	1	10000000	0.01	0.01	n/a
s	0	0.8	40	1	10000000	0.35	0.35	n/a
s	0	0.8	25	1	10000000	6.07	6.07	n/a
s	0	0.8	10	1	10000000	52.83	52.83	n/a
s	0	0.8	-5	1	10000000	229.83	229.83	n/a
s	0	0.8	-20	1	10000000	499.84	499.84	n/a
s	0	0.8	-35	1	10000000	543.45	543.45	n/a
s	0	0.8	-50	1	10000000	295.39	295.39	n/a
s	0	0.8	-65	1	10000000	80.27	80.27	n/a
s	0	0.8	-80	1	10000000	10.90	10.90	n/a
s	0	0.8	-95	1	10000000	0.74	0.74	n/a
t	-76	0.8	70	1	10000000	0.00	0.00	n/a
t	-76	0.8	55	1	10000000	0.01	0.01	n/a
t	-76	0.8	40	1	10000000	0.35	0.35	n/a
t	-76	0.8	25	1	10000000	6.07	6.07	n/a
t	-76	0.8	10	1	10000000	52.83	52.83	n/a
t	-76	0.8	-5	1	10000000	229.83	229.83	n/a
t	-76	0.8	-20	1	10000000	499.84	499.84	n/a
t	-76	0.8	-35	1	10000000	543.45	543.45	n/a
t	-76	0.8	-50	1	10000000	295.39	295.39	n/a
t	-76	0.8	-65	1	10000000	80.27	80.27	n/a
t	-76	0.8	-80	1	10000000	10.90	10.90	n/a
t	-76	0.8	-95	1	10000000	0.74	0.74	n/a
u	-45	2.12	70	1	10000000	0.00	0.00	n/a
u	-45	2.12	55	1	10000000	0.00	0.00	n/a
u	-45	2.12	40	1	10000000	0.00	0.00	n/a

u	-45	2.12	25	1	10000000	0.00	0.00	n/a
u	-45	2.12	10	1	10000000	0.00	0.00	n/a
u	-45	2.12	-5	1	10000000	0.00	0.00	n/a
u	-45	2.12	-20	1	10000000	0.00	0.00	n/a
u	-45	2.12	-35	1	10000000	0.00	0.00	n/a
u	-45	2.12	-50	1	10000000	0.00	0.00	n/a
u	-45	2.12	-65	1	10000000	0.00	0.00	n/a
u	-45	2.12	-80	1	10000000	0.00	0.00	n/a
u	45	2.12	-95	1	10000000	0.00	0.00	n/a
v	45	2.12	70	1	10000000	0.00	0.00	n/a
v	45	2.12	55	1	10000000	0.00	0.00	n/a
v	45	2.12	40	1	10000000	0.00	0.00	n/a
v	45	2.12	25	1	10000000	0.00	0.00	n/a
v	45	2.12	10	1	10000000	0.00	0.00	n/a
v	45	2.12	-5	1	10000000	0.00	0.00	n/a
v	45	2.12	-20	1	10000000	0.00	0.00	n/a
v	45	2.12	-35	1	10000000	0.00	0.00	n/a
v	45	2.12	-50	1	10000000	0.00	0.00	n/a
v	45	2.12	-65	1	10000000	0.00	0.00	n/a
v	45	2.12	-80	1	10000000	0.00	0.00	n/a
v	45	2.12	-95	1	10000000	0.00	0.00	n/a
w	-53	0.5	55	1	10000000	0.20	0.20	n/a
w	-53	0.5	25	1	10000000	122.37	122.37	n/a
w	-53	0.5	-5	1	10000000	4632.32	4632.32	n/a
x	-53	1	55	1	10000000	0.00	0.00	n/a
x	-53	1	25	1	10000000	0.38	0.38	n/a
x	-53	1	-5	1	10000000	14.37	14.37	n/a
x	-53	1	-35	1	10000000	33.97	33.97	n/a
x	-53	1	-65	1	10000000	5.02	5.02	n/a
x	-53	1	-95	1	10000000	0.05	0.05	n/a
y	-53	1.5	55	1	10000000	0.00	0.00	n/a
y	-53	1.5	25	1	10000000	0.00	0.00	n/a
y	-53	1.5	-5	1	10000000	0.00	0.00	n/a
y	-53	1.5	-35	1	10000000	0.00	0.00	n/a
y	-53	1.5	-65	1	10000000	0.00	0.00	n/a
y	-53	1.5	-95	1	10000000	0.00	0.00	n/a
bb	45	1.4	70	1	10000000	0.00	0.00	n/a
bb	45	1.4	55	1	10000000	0.00	0.00	n/a
bb	45	1.4	40	1	10000000	0.00	0.00	n/a
bb	45	1.4	25	1	10000000	0.00	0.00	n/a
bb	45	1.4	10	1	10000000	0.00	0.00	n/a
bb	45	1.4	-5	1	10000000	0.01	0.01	n/a
bb	45	1.4	-20	1	10000000	0.02	0.02	n/a
bb	45	1.4	-35	1	10000000	0.02	0.02	n/a
bb	45	1.4	-50	1	10000000	0.01	0.01	n/a
bb	45	1.4	-65	1	10000000	0.00	0.00	n/a
bb	45	1.4	-80	1	10000000	0.00	0.00	n/a
bb	45	1.4	-95	1	10000000	0.00	0.00	n/a
dd	-45	1.4	70	1	10000000	0.00	0.00	n/a
dd	-45	1.4	55	1	10000000	0.00	0.00	n/a
dd	-45	1.4	40	1	10000000	0.00	0.00	n/a
dd	-45	1.4	25	1	10000000	0.00	0.00	n/a
dd	-45	1.4	10	1	10000000	0.00	0.00	n/a
dd	-45	1.4	-5	1	10000000	0.01	0.01	n/a
dd	-45	1.4	-20	1	10000000	0.02	0.02	n/a
dd	-45	1.4	-35	1	10000000	0.02	0.02	n/a
dd	-45	1.4	-50	1	10000000	0.01	0.01	n/a
dd	-45	1.4	-65	1	10000000	0.00	0.00	n/a
dd	-45	1.4	-80	1	10000000	0.00	0.00	n/a
dd	-45	1.4	-95	1	10000000	0.00	0.00	n/a
a	0	0.5	55	2	10000000	0.73	0.73	n/a
a	0	0.5	25	2	10000000	798.40	798.40	n/a
a	0	0.5	-5	2	10000000	19838.57	19838.57	n/a
a	0	0.5	-35	2	10000000	11435.65	11435.65	n/a
a	0	0.5	-65	2	10000000	24603.59	24603.59	n/a
a	0	0.5	-95	2	10000000	3761.36	3761.36	n/a
b	0	1	55	2	10000000	0.00	0.00	n/a
b	0	1	25	2	10000000	0.16	0.16	n/a
b	0	1	-5	2	10000000	134.99	134.99	n/a
b	0	1	-35	2	10000000	2608.57	2608.57	n/a
b	0	1	-65	2	10000000	4660.18	4660.18	n/a

b	0	1	-95	2	10000000	556.83	556.83	n/a
c	0	1.5	55	2	10000000	0.00	0.00	n/a
c	0	1.5	25	2	10000000	0.00	0.00	n/a
c	0	1.5	-5	2	10000000	0.73	0.73	n/a
c	0	1.5	-35	2	10000000	46.17	46.17	n/a
c	0	1.5	-65	2	10000000	204.67	204.67	n/a
c	0	1.5	-95	2	10000000	23.86	23.86	n/a
d	27	0.5	55	2	1.67	14.41	1.67	1.31
d	27	0.5	25	2	145.25	4471.16	145.25	3.91
d	27	0.5	-5	2	17752.5	31442.50	17752.50	3.88
d	27	0.5	-35	2	5960.17	8063.60	5960.17	2.80
d	27	0.5	-65	2	21918	33675.19	21918.00	3.70
d	27	0.5	-95	2	956.5	611.10	956.50	2.18
e	27	1	55	2	70.33	0.00	70.33	2.15
e	27	1	25	2	16	2.91	16.00	1.26
e	27	1	-5	2	1105.33	691.86	1105.33	2.28
e	27	1	-35	2	2007.17	4171.25	2007.17	3.18
e	27	1	-65	2	630.67	5340.91	630.67	3.87
e	27	1	-95	2	43	89.96	43.00	1.52
f	27	1.5	55	2	3.67	0.00	3.67	0.87
f	27	1.5	25	2	9	0.01	9.00	1.25
f	27	1.5	-5	2	3	5.50	3.00	0.17
f	27	1.5	-35	2	11	113.52	11.00	2.23
f	27	1.5	-65	2	4.5	233.69	4.50	2.64
f	27	1.5	-95	2	2.5	3.89	2.50	0.00
g	-27	0.5	55	2	10000000	0.02	0.02	n/a
g	-27	0.5	25	2	10000000	93.60	93.60	n/a
g	-27	0.5	-5	2	10000000	8218.19	8218.19	n/a
g	-27	0.5	-35	2	10000000	16366.61	16366.61	n/a
g	-27	0.5	-65	2	10000000	9459.36	9459.36	n/a
g	-27	0.5	-95	2	10000000	11358.48	11358.48	n/a
h	-27	1	55	2	10000000	0.00	0.00	n/a
h	-27	1	25	2	10000000	0.01	0.01	n/a
h	-27	1	-5	2	10000000	17.29	17.29	n/a
h	-27	1	-35	2	10000000	1165.23	1165.23	n/a
h	-27	1	-65	2	10000000	3040.74	3040.74	n/a
h	-27	1	-95	2	10000000	1709.98	1709.98	n/a
i	-27	1.5	55	2	10000000	0.00	0.00	n/a
i	-27	1.5	25	2	10000000	0.00	0.00	n/a
i	-27	1.5	-5	2	10000000	0.06	0.06	n/a
i	-27	1.5	-35	2	10000000	13.73	13.73	n/a
l	-27	1.5	-65	2	10000000	118.16	118.16	n/a
l	-27	1.5	-95	2	10000000	73.63	73.63	n/a
j	53	0.5	55	2	10000000	14.41	14.41	n/a
j	53	0.5	25	2	10000000	4471.16	4471.16	n/a
j	53	0.5	-5	2	10000000	31442.50	31442.50	n/a
k	53	1	55	2	10000000	0.00	0.00	n/a
k	53	1	25	2	10000000	2.91	2.91	n/a
k	53	1	-5	2	10000000	691.86	691.86	n/a
k	53	1	-35	2	10000000	4171.25	4171.25	n/a
k	53	1	-65	2	10000000	5340.91	5340.91	n/a
k	53	1	-95	2	10000000	89.96	89.96	n/a
l	53	1.5	55	2	10000000	0.00	0.00	n/a
l	53	1.5	25	2	10000000	0.01	0.01	n/a
l	53	1.5	-5	2	10000000	5.50	5.50	n/a
l	53	1.5	-35	2	10000000	113.52	113.52	n/a
l	53	1.5	-65	2	10000000	233.69	233.69	n/a
l	53	1.5	-95	2	10000000	3.89	3.89	n/a
m	53	2	55	2	10000000	0.00	0.00	n/a
m	53	2	25	2	10000000	0.00	0.00	n/a
m	53	2	-5	2	10000000	0.02	0.02	n/a
m	53	2	-35	2	10000000	0.75	0.75	n/a
m	53	2	-65	2	10000000	2.56	2.56	n/a
m	53	2	-95	2	10000000	0.05	0.05	n/a
n	-70	1.47	55	2	10000000	0.00	0.00	n/a
n	-70	1.47	25	2	10000000	0.00	0.00	n/a
n	-70	1.47	-5	2	10000000	0.09	0.09	n/a
n	-70	1.47	-35	2	10000000	18.47	18.47	n/a
n	-70	1.47	-65	2	10000000	150.27	150.27	n/a
n	-70	1.47	-95	2	10000000	92.34	92.34	n/a
o	70	1.47	55	2	10000000	0.00	0.00	n/a

o	70	1.47	25	2	10000000	0.01	0.01	n/a
o	70	1.47	-5	2	10000000	7.51	7.51	n/a
o	70	1.47	-35	2	10000000	147.10	147.10	n/a
o	70	1.47	-65	2	10000000	293.31	293.31	n/a
p	-19	1.57	55	2	10000000	0.00	0.00	n/a
p	-19	1.57	25	2	10000000	0.00	0.00	n/a
p	-19	1.57	-5	2	10000000	0.03	0.03	n/a
p	-19	1.57	-35	2	10000000	6.77	6.77	n/a
p	-19	1.57	-65	2	10000000	66.09	66.09	n/a
p	-19	1.57	-95	2	10000000	42.60	42.60	n/a
q	19	1.57	55	2	10000000	0.00	0.00	n/a
q	19	1.57	25	2	10000000	0.00	0.00	n/a
q	19	1.57	-5	2	10000000	2.62	2.62	n/a
q	19	1.57	-35	2	10000000	60.83	60.83	n/a
q	19	1.57	-65	2	10000000	134.87	134.87	n/a
q	19	1.57	-95	2	10000000	2.27	2.27	n/a
r	76	0.8	70	2	10000000	0.00	0.00	n/a
r	76	0.8	55	2	10000000	0.01	0.01	n/a
r	76	0.8	40	2	10000000	0.98	0.98	n/a
r	76	0.8	25	2	10000000	40.38	40.38	n/a
r	76	0.8	10	2	10000000	643.76	643.76	n/a
r	76	0.8	-5	2	10000000	3982.01	3982.01	n/a
r	76	0.8	-20	2	10000000	9586.84	9586.84	n/a
r	76	0.8	-35	2	10000000	10017.91	10017.91	n/a
r	76	0.8	-50	2	10000000	11493.11	11493.11	n/a
r	76	0.8	-65	2	10000000	12788.35	12788.35	n/a
r	76	0.8	-80	2	10000000	3728.63	3728.63	n/a
r	76	0.8	-95	2	10000000	224.53	224.53	n/a
s	0	0.8	70	2	10000000	0.00	0.00	n/a
s	0	0.8	55	2	10000000	0.00	0.00	n/a
s	0	0.8	40	2	10000000	0.04	0.04	n/a
s	0	0.8	25	2	10000000	2.99	2.99	n/a
s	0	0.8	10	2	10000000	89.61	89.61	n/a
s	0	0.8	-5	2	10000000	1041.89	1041.89	n/a
s	0	0.8	-20	2	10000000	4701.28	4701.28	n/a
s	0	0.8	-35	2	10000000	8323.98	8323.98	n/a
s	0	0.8	-50	2	10000000	7655.78	7655.78	n/a
s	0	0.8	-65	2	10000000	10439.39	10439.39	n/a
s	0	0.8	-80	2	10000000	7984.82	7984.82	n/a
s	0	0.8	-95	2	10000000	1384.75	1384.75	n/a
t	-76	0.8	70	2	10000000	0.00	0.00	n/a
t	-76	0.8	55	2	10000000	0.00	0.00	n/a
t	-76	0.8	40	2	10000000	0.00	0.00	n/a
t	-76	0.8	25	2	10000000	0.15	0.15	n/a
t	-76	0.8	10	2	10000000	8.19	8.19	n/a
t	-76	0.8	-5	2	10000000	178.99	178.99	n/a
t	-76	0.8	-20	2	10000000	1517.90	1517.90	n/a
t	-76	0.8	-35	2	10000000	4998.63	4998.63	n/a
t	-76	0.8	-50	2	10000000	6630.16	6630.16	n/a
t	-76	0.8	-65	2	10000000	6356.15	6356.15	n/a
t	-76	0.8	-80	2	10000000	8736.13	8736.13	n/a
t	-76	0.8	-95	2	10000000	4208.64	4208.64	n/a
u	-45	2.12	70	2	10000000	0.00	0.00	n/a
u	-45	2.12	55	2	10000000	0.00	0.00	n/a
u	-45	2.12	40	2	10000000	0.00	0.00	n/a
u	-45	2.12	25	2	10000000	0.00	0.00	n/a
u	-45	2.12	10	2	10000000	0.00	0.00	n/a
u	-45	2.12	-5	2	10000000	0.00	0.00	n/a
u	-45	2.12	-20	2	10000000	0.00	0.00	n/a
u	-45	2.12	-35	2	10000000	0.01	0.01	n/a
u	-45	2.12	-50	2	10000000	0.07	0.07	n/a
u	-45	2.12	-65	2	10000000	0.27	0.27	n/a
u	-45	2.12	-80	2	10000000	0.49	0.49	n/a
u	45	2.12	-95	2	10000000	0.01	0.01	n/a
v	45	2.12	70	2	10000000	0.00	0.00	n/a
v	45	2.12	55	2	10000000	0.00	0.00	n/a
v	45	2.12	40	2	10000000	0.00	0.00	n/a
v	45	2.12	25	2	10000000	0.00	0.00	n/a
v	45	2.12	10	2	10000000	0.00	0.00	n/a
v	45	2.12	-5	2	10000000	0.00	0.00	n/a
v	45	2.12	-20	2	10000000	0.04	0.04	n/a

v	45	2.12	-35	2	10000000	0.19	0.19	n/a
v	45	2.12	-50	2	10000000	0.59	0.59	n/a
v	45	2.12	-65	2	10000000	0.71	0.71	n/a
v	45	2.12	-80	2	10000000	0.20	0.20	n/a
v	45	2.12	-95	2	10000000	0.01	0.01	n/a
w	-53	0.5	55	2	10000000	0.02	0.02	n/a
w	-53	0.5	25	2	10000000	93.60	93.60	n/a
w	-53	0.5	-5	2	10000000	8218.19	8218.19	n/a
x	-53	1	55	2	10000000	0.00	0.00	n/a
x	-53	1	25	2	10000000	0.01	0.01	n/a
x	-53	1	-5	2	10000000	17.29	17.29	n/a
x	-53	1	-35	2	10000000	1165.23	1165.23	n/a
x	-53	1	-65	2	10000000	3040.74	3040.74	n/a
x	-53	1	-95	2	10000000	1709.98	1709.98	n/a
y	-53	1.5	55	2	10000000	0.00	0.00	n/a
y	-53	1.5	25	2	10000000	0.00	0.00	n/a
y	-53	1.5	-5	2	10000000	0.06	0.06	n/a
y	-53	1.5	-35	2	10000000	13.73	13.73	n/a
y	-53	1.5	-65	2	10000000	118.16	118.16	n/a
y	-53	1.5	-95	2	10000000	73.63	73.63	n/a
bb	45	1.4	70	2	10000000	0.00	0.00	n/a
bb	45	1.4	55	2	10000000	0.00	0.00	n/a
bb	45	1.4	40	2	10000000	0.00	0.00	n/a
bb	45	1.4	25	2	10000000	0.02	0.02	n/a
bb	45	1.4	10	2	10000000	0.97	0.97	n/a
bb	45	1.4	-5	2	10000000	15.38	15.38	n/a
bb	45	1.4	-20	2	10000000	95.79	95.79	n/a
bb	45	1.4	-35	2	10000000	264.07	264.07	n/a
bb	45	1.4	-50	2	10000000	487.41	487.41	n/a
bb	45	1.4	-65	2	10000000	488.79	488.79	n/a
bb	45	1.4	-80	2	10000000	134.60	134.60	n/a
bb	45	1.4	-95	2	10000000	8.07	8.07	n/a
dd	-45	1.4	70	2	10000000	0.00	0.00	n/a
dd	-45	1.4	55	2	10000000	0.00	0.00	n/a
dd	-45	1.4	40	2	10000000	0.00	0.00	n/a
dd	-45	1.4	25	2	10000000	0.00	0.00	n/a
dd	-45	1.4	10	2	10000000	0.00	0.00	n/a
dd	-45	1.4	-5	2	10000000	0.20	0.20	n/a
dd	-45	1.4	-20	2	10000000	4.28	4.28	n/a
dd	-45	1.4	-35	2	10000000	36.30	36.30	n/a
dd	-45	1.4	-50	2	10000000	127.06	127.06	n/a
dd	-45	1.4	-65	2	10000000	257.89	257.89	n/a
dd	-45	1.4	-80	2	10000000	346.63	346.63	n/a
dd	-45	1.4	-95	2	10000000	153.66	153.66	n/a
a	0	0.5	55	3	10000000	1.00	1.00	n/a
a	0	0.5	25	3	10000000	988.18	988.18	n/a
a	0	0.5	-5	3	10000000	22324.52	22324.52	n/a
a	0	0.5	-35	3	10000000	11879.15	11879.15	n/a
a	0	0.5	-65	3	10000000	25579.93	25579.93	n/a
a	0	0.5	-95	3	10000000	3497.91	3497.91	n/a
b	0	1	55	3	10000000	0.00	0.00	n/a
b	0	1	25	3	10000000	0.22	0.22	n/a
b	0	1	-5	3	10000000	162.62	162.62	n/a
b	0	1	-35	3	10000000	2838.77	2838.77	n/a
b	0	1	-65	3	10000000	4878.11	4878.11	n/a
b	0	1	-95	3	10000000	531.57	531.57	n/a
c	0	1.5	55	3	10000000	0.00	0.00	n/a
c	0	1.5	25	3	10000000	0.00	0.00	n/a
c	0	1.5	-5	3	10000000	0.86	0.86	n/a
c	0	1.5	-35	3	10000000	49.54	49.54	n/a
c	0	1.5	-65	3	10000000	218.25	218.25	n/a
c	0	1.5	-95	3	10000000	23.59	23.59	n/a
d	27	0.5	55	3	10000000	19.05	19.05	n/a
d	27	0.5	25	3	10000000	5358.71	5358.71	n/a
d	27	0.5	-5	3	10000000	34308.59	34308.59	n/a
d	27	0.5	-35	3	10000000	8982.75	8982.75	n/a
d	27	0.5	-65	3	10000000	32732.20	32732.20	n/a
d	27	0.5	-95	3	10000000	581.87	581.87	n/a
e	27	1	55	3	10000000	0.00	0.00	n/a
e	27	1	25	3	10000000	3.78	3.78	n/a
e	27	1	-5	3	10000000	803.66	803.66	n/a

e	27	1	-35	3	10000000	4485.64	4485.64	n/a
e	27	1	-65	3	10000000	5311.13	5311.13	n/a
e	27	1	-95	3	10000000	87.91	87.91	n/a
f	27	1.5	55	3	10000000	0.00	0.00	n/a
f	27	1.5	25	3	10000000	0.01	0.01	n/a
f	27	1.5	-5	3	10000000	6.25	6.25	n/a
f	27	1.5	-35	3	10000000	122.16	122.16	n/a
f	27	1.5	-65	3	10000000	239.43	239.43	n/a
f	27	1.5	-95	3	10000000	3.92	3.92	n/a
g	-27	0.5	55	3	0	0.03	0.00	0.00
g	-27	0.5	25	3	531.83	119.69	531.83	2.72
g	-27	0.5	-5	3	182.17	9541.90	182.17	4.26
g	-27	0.5	-35	3	10611.75	17332.36	10611.75	3.51
g	-27	0.5	-65	3	16989.25	10724.72	16989.25	3.45
g	-27	0.5	-95	3	4129.83	10635.84	4129.83	3.76
h	-27	1	55	3	73	0.00	73.00	2.16
h	-27	1	25	3	30.67	0.01	30.67	1.79
h	-27	1	-5	3	2190.67	21.62	2190.67	3.63
h	-27	1	-35	3	4318	1306.65	4318.00	3.51
h	-27	1	-65	3	7397.5	3282.83	7397.50	3.50
h	-27	1	-95	3	257.25	1643.00	257.25	3.31
i	-27	1.5	55	3	14.67	0.00	14.67	1.47
i	-27	1.5	25	3	13.67	0.00	13.67	1.44
i	-27	1.5	-5	3	7	0.08	7.00	1.13
i	-27	1.5	-35	3	2	15.08	2.00	1.30
i	-27	1.5	-65	3	2.33	128.68	2.33	2.39
i	-27	1.5	-95	3	1.67	73.26	1.67	2.14
j	53	0.5	55	3	10000000	19.05	19.05	n/a
j	53	0.5	25	3	10000000	5358.71	5358.71	n/a
j	53	0.5	-5	3	10000000	34308.59	34308.59	n/a
k	53	1	55	3	10000000	0.00	0.00	n/a
k	53	1	25	3	10000000	3.78	3.78	n/a
k	53	1	-5	3	10000000	803.66	803.66	n/a
k	53	1	-35	3	10000000	4485.64	4485.64	n/a
k	53	1	-65	3	10000000	5311.13	5311.13	n/a
k	53	1	-95	3	10000000	87.91	87.91	n/a
l	53	1.5	55	3	10000000	0.00	0.00	n/a
l	53	1.5	25	3	10000000	0.01	0.01	n/a
l	53	1.5	-5	3	10000000	6.25	6.25	n/a
l	53	1.5	-35	3	10000000	122.16	122.16	n/a
l	53	1.5	-65	3	10000000	239.43	239.43	n/a
l	53	1.5	-95	3	10000000	3.92	3.92	n/a
m	53	2	55	3	10000000	0.00	0.00	n/a
m	53	2	25	3	10000000	0.00	0.00	n/a
m	53	2	-5	3	10000000	0.02	0.02	n/a
m	53	2	-35	3	10000000	0.82	0.82	n/a
m	53	2	-65	3	10000000	2.75	2.75	n/a
m	53	2	-95	3	10000000	0.05	0.05	n/a
n	-70	1.47	55	3	10000000	0.00	0.00	n/a
n	-70	1.47	25	3	10000000	0.00	0.00	n/a
n	-70	1.47	-5	3	10000000	0.11	0.11	n/a
n	-70	1.47	-35	3	10000000	20.32	20.32	n/a
n	-70	1.47	-65	3	10000000	163.45	163.45	n/a
n	-70	1.47	-95	3	10000000	91.66	91.66	n/a
o	70	1.47	55	3	10000000	0.00	0.00	n/a
o	70	1.47	25	3	10000000	0.01	0.01	n/a
o	70	1.47	-5	3	10000000	8.56	8.56	n/a
o	70	1.47	-35	3	10000000	158.30	158.30	n/a
o	70	1.47	-65	3	10000000	299.88	299.88	n/a
p	-19	1.57	55	3	10000000	0.00	0.00	n/a
p	-19	1.57	25	3	10000000	0.00	0.00	n/a
p	-19	1.57	-5	3	10000000	0.03	0.03	n/a
p	-19	1.57	-35	3	10000000	7.39	7.39	n/a
p	-19	1.57	-65	3	10000000	72.20	72.20	n/a
p	-19	1.57	-95	3	10000000	42.63	42.63	n/a
q	19	1.57	55	3	10000000	0.00	0.00	n/a
q	19	1.57	25	3	10000000	0.00	0.00	n/a
q	19	1.57	-5	3	10000000	2.96	2.96	n/a
q	19	1.57	-35	3	10000000	65.47	65.47	n/a
q	19	1.57	-65	3	10000000	138.91	138.91	n/a
q	19	1.57	-95	3	10000000	2.29	2.29	n/a

r	76	0.8	70	3	10000000	0.00	0.00	n/a
r	76	0.8	55	3	10000000	0.01	0.01	n/a
r	76	0.8	40	3	10000000	1.33	1.33	n/a
r	76	0.8	25	3	10000000	51.68	51.68	n/a
r	76	0.8	10	3	10000000	780.61	780.61	n/a
r	76	0.8	-5	3	10000000	4580.20	4580.20	n/a
r	76	0.8	-20	3	10000000	10488.10	10488.10	n/a
r	76	0.8	-35	3	10000000	10718.60	10718.60	n/a
r	76	0.8	-50	3	10000000	12316.42	12316.42	n/a
r	76	0.8	-65	3	10000000	12590.52	12590.52	n/a
r	76	0.8	-80	3	10000000	3515.37	3515.37	n/a
r	76	0.8	-95	3	10000000	216.83	216.83	n/a
s	0	0.8	70	3	10000000	0.00	0.00	n/a
s	0	0.8	55	3	10000000	0.00	0.00	n/a
s	0	0.8	40	3	10000000	0.05	0.05	n/a
s	0	0.8	25	3	10000000	3.97	3.97	n/a
s	0	0.8	10	3	10000000	112.62	112.62	n/a
s	0	0.8	-5	3	10000000	1241.19	1241.19	n/a
s	0	0.8	-20	3	10000000	5314.94	5314.94	n/a
s	0	0.8	-35	3	10000000	8982.72	8982.72	n/a
s	0	0.8	-50	3	10000000	8261.87	8261.87	n/a
s	0	0.8	-65	3	10000000	10893.72	10893.72	n/a
s	0	0.8	-80	3	10000000	7693.20	7693.20	n/a
s	0	0.8	-95	3	10000000	1306.09	1306.09	n/a
t	-76	0.8	70	3	10000000	0.00	0.00	n/a
t	-76	0.8	55	3	10000000	0.00	0.00	n/a
t	-76	0.8	40	3	10000000	0.00	0.00	n/a
t	-76	0.8	25	3	10000000	0.20	0.20	n/a
t	-76	0.8	10	3	10000000	10.67	10.67	n/a
t	-76	0.8	-5	3	10000000	220.95	220.95	n/a
t	-76	0.8	-20	3	10000000	1776.69	1776.69	n/a
t	-76	0.8	-35	3	10000000	5556.49	5556.49	n/a
t	-76	0.8	-50	3	10000000	7093.13	7093.13	n/a
t	-76	0.8	-65	3	10000000	6894.11	6894.11	n/a
t	-76	0.8	-80	3	10000000	8841.64	8841.64	n/a
t	-76	0.8	-95	3	10000000	3996.34	3996.34	n/a
u	-45	2.12	70	3	10000000	0.00	0.00	n/a
u	-45	2.12	55	3	10000000	0.00	0.00	n/a
u	-45	2.12	40	3	10000000	0.00	0.00	n/a
u	-45	2.12	25	3	10000000	0.00	0.00	n/a
u	-45	2.12	10	3	10000000	0.00	0.00	n/a
u	-45	2.12	-5	3	10000000	0.00	0.00	n/a
u	-45	2.12	-20	3	10000000	0.00	0.00	n/a
u	-45	2.12	-35	3	10000000	0.01	0.01	n/a
u	-45	2.12	-50	3	10000000	0.08	0.08	n/a
u	-45	2.12	-65	3	10000000	0.31	0.31	n/a
u	-45	2.12	-80	3	10000000	0.54	0.54	n/a
u	45	2.12	-95	3	10000000	0.01	0.01	n/a
v	45	2.12	70	3	10000000	0.00	0.00	n/a
v	45	2.12	55	3	10000000	0.00	0.00	n/a
v	45	2.12	40	3	10000000	0.00	0.00	n/a
v	45	2.12	25	3	10000000	0.00	0.00	n/a
v	45	2.12	10	3	10000000	0.00	0.00	n/a
v	45	2.12	-5	3	10000000	0.00	0.00	n/a
v	45	2.12	-20	3	10000000	0.04	0.04	n/a
v	45	2.12	-35	3	10000000	0.20	0.20	n/a
v	45	2.12	-50	3	10000000	0.68	0.68	n/a
v	45	2.12	-65	3	10000000	0.78	0.78	n/a
v	45	2.12	-80	3	10000000	0.22	0.22	n/a
v	45	2.12	-95	3	10000000	0.01	0.01	n/a
w	-53	0.5	55	3	10000000	0.03	0.03	n/a
w	-53	0.5	25	3	10000000	119.69	119.69	n/a
w	-53	0.5	-5	3	10000000	9541.90	9541.90	n/a
x	-53	1	55	3	10000000	0.00	0.00	n/a
x	-53	1	25	3	10000000	0.01	0.01	n/a
x	-53	1	-5	3	10000000	21.62	21.62	n/a
x	-53	1	-35	3	10000000	1306.65	1306.65	n/a
x	-53	1	-65	3	10000000	3282.83	3282.83	n/a
x	-53	1	-95	3	10000000	1643.00	1643.00	n/a
y	-53	1.5	55	3	10000000	0.00	0.00	n/a
y	-53	1.5	25	3	10000000	0.00	0.00	n/a

y	-53	1.5	-5	3	10000000	0.08	0.08	n/a
y	-53	1.5	-35	3	10000000	15.08	15.08	n/a
y	-53	1.5	-65	3	10000000	128.68	128.68	n/a
y	-53	1.5	-95	3	10000000	73.26	73.26	n/a
bb	45	1.4	70	3	10000000	0.00	0.00	n/a
bb	45	1.4	55	3	10000000	0.00	0.00	n/a
bb	45	1.4	40	3	10000000	0.00	0.00	n/a
bb	45	1.4	25	3	10000000	0.03	0.03	n/a
bb	45	1.4	10	3	10000000	1.17	1.17	n/a
bb	45	1.4	-5	3	10000000	17.63	17.63	n/a
bb	45	1.4	-20	3	10000000	104.44	104.44	n/a
bb	45	1.4	-35	3	10000000	284.24	284.24	n/a
bb	45	1.4	-50	3	10000000	525.36	525.36	n/a
bb	45	1.4	-65	3	10000000	497.36	497.36	n/a
bb	45	1.4	-80	3	10000000	132.04	132.04	n/a
bb	45	1.4	-95	3	10000000	8.08	8.08	n/a
dd	-45	1.4	70	3	10000000	0.00	0.00	n/a
dd	-45	1.4	55	3	10000000	0.00	0.00	n/a
dd	-45	1.4	40	3	10000000	0.00	0.00	n/a
dd	-45	1.4	25	3	10000000	0.00	0.00	n/a
dd	-45	1.4	10	3	10000000	0.00	0.00	n/a
dd	-45	1.4	-5	3	10000000	0.24	0.24	n/a
dd	-45	1.4	-20	3	10000000	5.00	5.00	n/a
dd	-45	1.4	-35	3	10000000	40.17	40.17	n/a
dd	-45	1.4	-50	3	10000000	136.45	136.45	n/a
dd	-45	1.4	-65	3	10000000	279.89	279.89	n/a
dd	-45	1.4	-80	3	10000000	360.14	360.14	n/a
dd	-45	1.4	-95	3	10000000	151.71	151.71	n/a
a	0	0.5	55	7	10000000	3.12	3.12	n/a
a	0	0.5	25	7	10000000	2088.64	2088.64	n/a
a	0	0.5	-5	7	10000000	32307.87	32307.87	n/a
a	0	0.5	-35	7	10000000	13115.42	13115.42	n/a
a	0	0.5	-65	7	10000000	27429.64	27429.64	n/a
a	0	0.5	-95	7	10000000	2653.73	2653.73	n/a
b	0	1	55	7	10000000	0.00	0.00	n/a
b	0	1	25	7	10000000	0.63	0.63	n/a
b	0	1	-5	7	10000000	303.32	303.32	n/a
b	0	1	-35	7	10000000	3626.28	3626.28	n/a
b	0	1	-65	7	10000000	5396.38	5396.38	n/a
b	0	1	-95	7	10000000	445.06	445.06	n/a
c	0	1.5	55	7	10000000	0.00	0.00	n/a
c	0	1.5	25	7	10000000	0.00	0.00	n/a
c	0	1.5	-5	7	10000000	1.45	1.45	n/a
c	0	1.5	-35	7	10000000	63.28	63.28	n/a
c	0	1.5	-65	7	10000000	267.34	267.34	n/a
c	0	1.5	-95	7	10000000	22.77	22.77	n/a
d	27	0.5	55	7	10000000	52.29	52.29	n/a
d	27	0.5	25	7	10000000	9965.03	9965.03	n/a
d	27	0.5	-5	7	10000000	43932.02	43932.02	n/a
d	27	0.5	-35	7	10000000	13563.80	13563.80	n/a
d	27	0.5	-65	7	10000000	28209.03	28209.03	n/a
d	27	0.5	-95	7	10000000	484.25	484.25	n/a
e	27	1	55	7	10000000	0.00	0.00	n/a
e	27	1	25	7	10000000	9.47	9.47	n/a
e	27	1	-5	7	10000000	1298.21	1298.21	n/a
e	27	1	-35	7	10000000	5606.11	5606.11	n/a
e	27	1	-65	7	10000000	4974.60	4974.60	n/a
e	27	1	-95	7	10000000	80.78	80.78	n/a
f	27	1.5	55	7	10000000	0.00	0.00	n/a
f	27	1.5	25	7	10000000	0.02	0.02	n/a
f	27	1.5	-5	7	10000000	9.16	9.16	n/a
f	27	1.5	-35	7	10000000	165.16	165.16	n/a
f	27	1.5	-65	7	10000000	254.50	254.50	n/a
f	27	1.5	-95	7	10000000	4.13	4.13	n/a
g	-27	0.5	55	7	10000000	0.12	0.12	n/a
g	-27	0.5	25	7	10000000	288.06	288.06	n/a
g	-27	0.5	-5	7	10000000	15639.30	15639.30	n/a
g	-27	0.5	-35	7	10000000	19786.43	19786.43	n/a
g	-27	0.5	-65	7	10000000	15443.70	15443.70	n/a
g	-27	0.5	-95	7	10000000	8163.72	8163.72	n/a
h	-27	1	55	7	10000000	0.00	0.00	n/a

h	-27	1	25	7	10000000	0.03	0.03	n/a
h	-27	1	-5	7	10000000	46.70	46.70	n/a
h	-27	1	-35	7	10000000	1845.54	1845.54	n/a
h	-27	1	-65	7	10000000	4107.10	4107.10	n/a
h	-27	1	-95	7	10000000	1387.50	1387.50	n/a
i	-27	1.5	55	7	10000000	0.00	0.00	n/a
i	-27	1.5	25	7	10000000	0.00	0.00	n/a
i	-27	1.5	-5	7	10000000	0.15	0.15	n/a
i	-27	1.5	-35	7	10000000	19.83	19.83	n/a
i	-27	1.5	-65	7	10000000	176.01	176.01	n/a
i	-27	1.5	-95	7	10000000	71.15	71.15	n/a
j	53	0.5	55	7	0	52.29	0.00	2.02
j	53	0.5	25	7	91.49	9965.03	91.49	4.29
j	53	0.5	-5	7	35917.25	43932.02	35917.25	3.21
k	53	1	55	7	24.33	0.00	24.33	1.69
k	53	1	25	7	2	9.47	2.00	0.99
k	53	1	-5	7	10804.38	1298.21	10804.38	4.17
k	53	1	-35	7	5659.33	5606.11	5659.33	0.00
k	53	1	-65	7	5027.33	4974.60	5027.33	0.00
k	53	1	-95	7	420.67	80.78	420.67	2.66
l	53	1.5	55	7	3.67	0.00	3.67	0.87
l	53	1.5	25	7	2	0.02	2.00	0.59
l	53	1.5	-5	7	100.4	9.16	100.40	2.18
l	53	1.5	-35	7	1067.4	165.16	1067.40	3.12
l	53	1.5	-65	7	254	254.50	254.00	0.00
l	53	1.5	-95	7	97	4.13	97.00	2.23
m	53	2	55	7	3	0.00	3.00	0.78
m	53	2	25	7	1.67	0.00	1.67	0.52
m	53	2	-5	7	3.5	0.02	3.50	0.84
m	53	2	-35	7	2	1.50	2.00	0.00
m	53	2	-65	7	4.67	3.68	4.67	0.00
m	53	2	-95	7	0	0.06	0.00	0.00
n	-70	1.47	55	7	10000000	0.00	0.00	n/a
n	-70	1.47	25	7	10000000	0.00	0.00	n/a
n	-70	1.47	-5	7	10000000	0.22	0.22	n/a
n	-70	1.47	-35	7	10000000	26.93	26.93	n/a
n	-70	1.47	-65	7	10000000	221.35	221.35	n/a
n	-70	1.47	-95	7	10000000	88.10	88.10	n/a
o	70	1.47	55	7	10000000	0.00	0.00	n/a
o	70	1.47	25	7	10000000	0.03	0.03	n/a
o	70	1.47	-5	7	10000000	12.69	12.69	n/a
o	70	1.47	-35	7	10000000	212.19	212.19	n/a
o	70	1.47	-65	7	10000000	315.60	315.60	n/a
p	-19	1.57	55	7	10000000	0.00	0.00	n/a
p	-19	1.57	25	7	10000000	0.00	0.00	n/a
p	-19	1.57	-5	7	10000000	0.07	0.07	n/a
p	-19	1.57	-35	7	10000000	9.56	9.56	n/a
p	-19	1.57	-65	7	10000000	101.37	101.37	n/a
p	-19	1.57	-95	7	10000000	42.46	42.46	n/a
q	19	1.57	55	7	10000000	0.00	0.00	n/a
q	19	1.57	25	7	10000000	0.01	0.01	n/a
q	19	1.57	-5	7	10000000	4.22	4.22	n/a
q	19	1.57	-35	7	10000000	90.62	90.62	n/a
q	19	1.57	-65	7	10000000	151.35	151.35	n/a
q	19	1.57	-95	7	10000000	2.47	2.47	n/a
r	76	0.8	70	7	10000000	0.00	0.00	n/a
r	76	0.8	55	7	10000000	0.05	0.05	n/a
r	76	0.8	40	7	10000000	3.95	3.95	n/a
r	76	0.8	25	7	10000000	123.40	123.40	n/a
r	76	0.8	10	7	10000000	1504.46	1504.46	n/a
r	76	0.8	-5	7	10000000	7159.07	7159.07	n/a
r	76	0.8	-20	7	10000000	13550.33	13550.33	n/a
r	76	0.8	-35	7	10000000	13158.13	13158.13	n/a
r	76	0.8	-50	7	10000000	14743.09	14743.09	n/a
r	76	0.8	-65	7	10000000	11373.05	11373.05	n/a
r	76	0.8	-80	7	10000000	2791.89	2791.89	n/a
r	76	0.8	-95	7	10000000	190.42	190.42	n/a
s	0	0.8	70	7	10000000	0.00	0.00	n/a
s	0	0.8	55	7	10000000	0.00	0.00	n/a
s	0	0.8	40	7	10000000	0.19	0.19	n/a
s	0	0.8	25	7	10000000	10.96	10.96	n/a

s	0	0.8	10	7	10000000	250.26	250.26	n/a
s	0	0.8	-5	7	10000000	2229.35	2229.35	n/a
s	0	0.8	-20	7	10000000	7763.96	7763.96	n/a
s	0	0.8	-35	7	10000000	11100.73	11100.73	n/a
s	0	0.8	-50	7	10000000	10448.88	10448.88	n/a
s	0	0.8	-65	7	10000000	11877.58	11877.58	n/a
s	0	0.8	-80	7	10000000	6497.02	6497.02	n/a
s	0	0.8	-95	7	10000000	1045.19	1045.19	n/a
t	-76	0.8	70	7	10000000	0.00	0.00	n/a
t	-76	0.8	55	7	10000000	0.00	0.00	n/a
t	-76	0.8	40	7	10000000	0.01	0.01	n/a
t	-76	0.8	25	7	10000000	0.64	0.64	n/a
t	-76	0.8	10	7	10000000	27.39	27.39	n/a
t	-76	0.8	-5	7	10000000	457.14	457.14	n/a
t	-76	0.8	-20	7	10000000	2975.73	2975.73	n/a
t	-76	0.8	-35	7	10000000	7608.49	7608.49	n/a
t	-76	0.8	-50	7	10000000	8594.69	8594.69	n/a
t	-76	0.8	-65	7	10000000	8725.44	8725.44	n/a
t	-76	0.8	-80	7	10000000	8721.08	8721.08	n/a
t	-76	0.8	-95	7	10000000	3231.86	3231.86	n/a
u	-45	2.12	70	7	10000000	0.00	0.00	n/a
u	-45	2.12	55	7	10000000	0.00	0.00	n/a
u	-45	2.12	40	7	10000000	0.00	0.00	n/a
u	-45	2.12	25	7	10000000	0.00	0.00	n/a
u	-45	2.12	10	7	10000000	0.00	0.00	n/a
u	-45	2.12	-5	7	10000000	0.00	0.00	n/a
u	-45	2.12	-20	7	10000000	0.00	0.00	n/a
u	-45	2.12	-35	7	10000000	0.02	0.02	n/a
u	-45	2.12	-50	7	10000000	0.15	0.15	n/a
u	-45	2.12	-65	7	10000000	0.62	0.62	n/a
u	-45	2.12	-80	7	10000000	0.84	0.84	n/a
u	45	2.12	-95	7	10000000	0.02	0.02	n/a
v	45	2.12	70	7	10000000	0.00	0.00	n/a
v	45	2.12	55	7	10000000	0.00	0.00	n/a
v	45	2.12	40	7	10000000	0.00	0.00	n/a
v	45	2.12	25	7	10000000	0.00	0.00	n/a
v	45	2.12	10	7	10000000	0.00	0.00	n/a
v	45	2.12	-5	7	10000000	0.00	0.00	n/a
v	45	2.12	-20	7	10000000	0.06	0.06	n/a
v	45	2.12	-35	7	10000000	0.42	0.42	n/a
v	45	2.12	-50	7	10000000	1.25	1.25	n/a
v	45	2.12	-65	7	10000000	1.11	1.11	n/a
v	45	2.12	-80	7	10000000	0.28	0.28	n/a
v	45	2.12	-95	7	10000000	0.02	0.02	n/a
w	-53	0.5	55	7	10000000	0.12	0.12	n/a
w	-53	0.5	25	7	10000000	288.06	288.06	n/a
w	-53	0.5	-5	7	10000000	15639.30	15639.30	n/a
x	-53	1	55	7	10000000	0.00	0.00	n/a
x	-53	1	25	7	10000000	0.03	0.03	n/a
x	-53	1	-5	7	10000000	46.70	46.70	n/a
x	-53	1	-35	7	10000000	1845.54	1845.54	n/a
x	-53	1	-65	7	10000000	4107.10	4107.10	n/a
x	-53	1	-95	7	10000000	1387.50	1387.50	n/a
y	-53	1.5	55	7	10000000	0.00	0.00	n/a
y	-53	1.5	25	7	10000000	0.00	0.00	n/a
y	-53	1.5	-5	7	10000000	0.15	0.15	n/a
y	-53	1.5	-35	7	10000000	19.83	19.83	n/a
y	-53	1.5	-65	7	10000000	176.01	176.01	n/a
y	-53	1.5	-95	7	10000000	71.15	71.15	n/a
bb	45	1.4	70	7	10000000	0.00	0.00	n/a
bb	45	1.4	55	7	10000000	0.00	0.00	n/a
bb	45	1.4	40	7	10000000	0.00	0.00	n/a
bb	45	1.4	25	7	10000000	0.07	0.07	n/a
bb	45	1.4	10	7	10000000	2.22	2.22	n/a
bb	45	1.4	-5	7	10000000	26.74	26.74	n/a
bb	45	1.4	-20	7	10000000	135.40	135.40	n/a
bb	45	1.4	-35	7	10000000	374.55	374.55	n/a
bb	45	1.4	-50	7	10000000	667.49	667.49	n/a
bb	45	1.4	-65	7	10000000	512.18	512.18	n/a
bb	45	1.4	-80	7	10000000	122.26	122.26	n/a
bb	45	1.4	-95	7	10000000	8.24	8.24	n/a

dd	-45	1.4	70	7	10000000	0.00	0.00	n/a
dd	-45	1.4	55	7	10000000	0.00	0.00	n/a
dd	-45	1.4	40	7	10000000	0.00	0.00	n/a
dd	-45	1.4	25	7	10000000	0.00	0.00	n/a
dd	-45	1.4	10	7	10000000	0.01	0.01	n/a
dd	-45	1.4	-5	7	10000000	0.50	0.50	n/a
dd	-45	1.4	-20	7	10000000	8.14	8.14	n/a
dd	-45	1.4	-35	7	10000000	54.09	54.09	n/a
dd	-45	1.4	-50	7	10000000	175.69	175.69	n/a
dd	-45	1.4	-65	7	10000000	371.28	371.28	n/a
dd	-45	1.4	-80	7	10000000	397.45	397.45	n/a
dd	-45	1.4	-95	7	10000000	142.54	142.54	n/a
a	0	0.5	55	10	10000000	6.76	6.76	n/a
a	0	0.5	25	10	10000000	3369.28	3369.28	n/a
a	0	0.5	-5	10	10000000	39313.66	39313.66	n/a
a	0	0.5	-35	10	10000000	13982.87	13982.87	n/a
a	0	0.5	-65	10	10000000	27021.08	27021.08	n/a
a	0	0.5	-95	10	10000000	2186.81	2186.81	n/a
b	0	1	55	10	10000000	0.00	0.00	n/a
b	0	1	25	10	10000000	1.27	1.27	n/a
b	0	1	-5	10	10000000	437.56	437.56	n/a
b	0	1	-35	10	10000000	4100.30	4100.30	n/a
b	0	1	-65	10	10000000	5471.56	5471.56	n/a
b	0	1	-95	10	10000000	392.99	392.99	n/a
c	0	1.5	55	10	10000000	0.00	0.00	n/a
c	0	1.5	25	10	10000000	0.00	0.00	n/a
c	0	1.5	-5	10	10000000	1.92	1.92	n/a
c	0	1.5	-35	10	10000000	79.65	79.65	n/a
c	0	1.5	-65	10	10000000	299.05	299.05	n/a
c	0	1.5	-95	10	10000000	22.42	22.42	n/a
d	27	0.5	55	10	10000000	102.48	102.48	n/a
d	27	0.5	25	10	10000000	14613.39	14613.39	n/a
d	27	0.5	-5	10	10000000	48846.03	48846.03	n/a
d	27	0.5	-35	10	10000000	17666.44	17666.44	n/a
d	27	0.5	-65	10	10000000	24592.01	24592.01	n/a
d	27	0.5	-95	10	10000000	426.57	426.57	n/a
e	27	1	55	10	10000000	0.00	0.00	n/a
e	27	1	25	10	10000000	17.01	17.01	n/a
e	27	1	-5	10	10000000	1688.62	1688.62	n/a
e	27	1	-35	10	10000000	6332.97	6332.97	n/a
e	27	1	-65	10	10000000	4593.51	4593.51	n/a
e	27	1	-95	10	10000000	76.35	76.35	n/a
f	27	1.5	55	10	10000000	0.00	0.00	n/a
f	27	1.5	25	10	10000000	0.03	0.03	n/a
f	27	1.5	-5	10	10000000	11.29	11.29	n/a
f	27	1.5	-35	10	10000000	214.61	214.61	n/a
f	27	1.5	-65	10	10000000	260.34	260.34	n/a
f	27	1.5	-95	10	10000000	4.35	4.35	n/a
g	-27	0.5	55	10	10000000	0.29	0.29	n/a
g	-27	0.5	25	10	10000000	511.84	511.84	n/a
g	-27	0.5	-5	10	10000000	20876.94	20876.94	n/a
g	-27	0.5	-35	10	10000000	20385.03	20385.03	n/a
g	-27	0.5	-65	10	10000000	18114.95	18114.95	n/a
g	-27	0.5	-95	10	10000000	6704.23	6704.23	n/a
h	-27	1	55	10	10000000	0.00	0.00	n/a
h	-27	1	25	10	10000000	0.06	0.06	n/a
h	-27	1	-5	10	10000000	75.10	75.10	n/a
h	-27	1	-35	10	10000000	2196.52	2196.52	n/a
h	-27	1	-65	10	10000000	4546.54	4546.54	n/a
h	-27	1	-95	10	10000000	1217.30	1217.30	n/a
i	-27	1.5	55	10	10000000	0.00	0.00	n/a
i	-27	1.5	25	10	10000000	0.00	0.00	n/a
i	-27	1.5	-5	10	10000000	0.22	0.22	n/a
i	-27	1.5	-35	10	10000000	23.93	23.93	n/a
i	-27	1.5	-65	10	10000000	217.55	217.55	n/a
i	-27	1.5	-95	10	10000000	69.46	69.46	n/a
j	53	0.5	55	10	10000000	102.48	102.48	n/a
j	53	0.5	25	10	10000000	14613.39	14613.39	n/a
j	53	0.5	-5	10	10000000	48846.03	48846.03	n/a
k	53	1	55	10	10000000	0.00	0.00	n/a
k	53	1	25	10	10000000	17.01	17.01	n/a

k	53	1	-5	10	10000000	1688.62	1688.62	n/a
k	53	1	-35	10	10000000	6332.97	6332.97	n/a
k	53	1	-65	10	10000000	4593.51	4593.51	n/a
k	53	1	-95	10	10000000	76.35	76.35	n/a
l	53	1.5	55	10	10000000	0.00	0.00	n/a
l	53	1.5	25	10	10000000	0.03	0.03	n/a
l	53	1.5	-5	10	10000000	11.29	11.29	n/a
l	53	1.5	-35	10	10000000	214.61	214.61	n/a
l	53	1.5	-65	10	10000000	260.34	260.34	n/a
l	53	1.5	-95	10	10000000	4.35	4.35	n/a
m	53	2	55	10	10000000	0.00	0.00	n/a
m	53	2	25	10	10000000	0.00	0.00	n/a
m	53	2	-5	10	10000000	0.03	0.03	n/a
m	53	2	-35	10	10000000	2.73	2.73	n/a
m	53	2	-65	10	10000000	4.51	4.51	n/a
m	53	2	-95	10	10000000	0.08	0.08	n/a
n	-70	1.47	55	10	1	0.00	1.00	0.30
n	-70	1.47	25	10	0	0.00	0.00	0.00
n	-70	1.47	-5	10	2441.67	0.32	2441.67	3.69
n	-70	1.47	-35	10	3468.83	32.35	3468.83	3.83
n	-70	1.47	-65	10	1832.5	270.60	1832.50	3.37
n	-70	1.47	-95	10	285.8	85.31	285.80	2.34
o	70	1.47	55	10	0	0.00	0.00	0.00
o	70	1.47	25	10	2.33	0.05	2.33	0.64
o	70	1.47	-5	10	6536.14	15.69	6536.14	4.11
o	70	1.47	-35	10	1006.8	271.77	1006.80	2.93
o	70	1.47	-65	10	615.4	320.15	615.40	2.27
p	-19	1.57	55	10	11	0.00	11.00	1.34
p	-19	1.57	25	10	1	0.00	1.00	0.30
p	-19	1.57	-5	10	568.6	0.09	568.60	3.06
p	-19	1.57	-35	10	3678.75	11.73	3678.75	3.86
p	-19	1.57	-65	10	2882.5	128.81	2882.50	3.70
p	-19	1.57	-95	10	163.5	42.30	163.50	2.15
q	19	1.57	55	10	3.67	0.00	3.67	0.87
q	19	1.57	25	10	2	0.01	2.00	0.59
q	19	1.57	-5	10	3536.75	5.16	3536.75	3.85
q	19	1.57	-35	10	3239	122.22	3239.00	3.76
q	19	1.57	-65	10	589.5	158.05	589.50	2.70
q	19	1.57	-95	10	288	2.65	288.00	2.75
r	76	0.8	70	10	10000000	0.00	0.00	n/a
r	76	0.8	55	10	10000000	0.12	0.12	n/a
r	76	0.8	40	10	10000000	8.11	8.11	n/a
r	76	0.8	25	10	10000000	215.41	215.41	n/a
r	76	0.8	10	10	10000000	2239.40	2239.40	n/a
r	76	0.8	-5	10	10000000	9133.89	9133.89	n/a
r	76	0.8	-20	10	10000000	15223.49	15223.49	n/a
r	76	0.8	-35	10	10000000	14657.02	14657.02	n/a
r	76	0.8	-50	10	10000000	15619.90	15619.90	n/a
r	76	0.8	-65	10	10000000	10239.67	10239.67	n/a
r	76	0.8	-80	10	10000000	2364.02	2364.02	n/a
r	76	0.8	-95	10	10000000	174.16	174.16	n/a
s	0	0.8	70	10	10000000	0.00	0.00	n/a
s	0	0.8	55	10	10000000	0.00	0.00	n/a
s	0	0.8	40	10	10000000	0.43	0.43	n/a
s	0	0.8	25	10	10000000	21.31	21.31	n/a
s	0	0.8	10	10	10000000	414.12	414.12	n/a
s	0	0.8	-5	10	10000000	3149.45	3149.45	n/a
s	0	0.8	-20	10	10000000	9440.52	9440.52	n/a
s	0	0.8	-35	10	10000000	12209.83	12209.83	n/a
s	0	0.8	-50	10	10000000	11759.28	11759.28	n/a
s	0	0.8	-65	10	10000000	11878.04	11878.04	n/a
s	0	0.8	-80	10	10000000	5647.27	5647.27	n/a
s	0	0.8	-95	10	10000000	893.93	893.93	n/a
t	-76	0.8	70	10	10000000	0.00	0.00	n/a
t	-76	0.8	55	10	10000000	0.00	0.00	n/a
t	-76	0.8	40	10	10000000	0.01	0.01	n/a
t	-76	0.8	25	10	10000000	1.39	1.39	n/a
t	-76	0.8	10	10	10000000	50.47	50.47	n/a
t	-76	0.8	-5	10	10000000	717.31	717.31	n/a
t	-76	0.8	-20	10	10000000	3992.64	3992.64	n/a
t	-76	0.8	-35	10	10000000	8855.94	8855.94	n/a

t	-76	0.8	-50	10	10000000	9437.82	9437.82	n/a
t	-76	0.8	-65	10	10000000	9662.50	9662.50	n/a
t	-76	0.8	-80	10	10000000	8238.25	8238.25	n/a
t	-76	0.8	-95	10	10000000	2751.62	2751.62	n/a
u	-45	2.12	70	10	10000000	0.00	0.00	n/a
u	-45	2.12	55	10	10000000	0.00	0.00	n/a
u	-45	2.12	40	10	10000000	0.00	0.00	n/a
u	-45	2.12	25	10	10000000	0.00	0.00	n/a
u	-45	2.12	10	10	10000000	0.00	0.00	n/a
u	-45	2.12	-5	10	10000000	0.00	0.00	n/a
u	-45	2.12	-20	10	10000000	0.00	0.00	n/a
u	-45	2.12	-35	10	10000000	0.03	0.03	n/a
u	-45	2.12	-50	10	10000000	0.32	0.32	n/a
u	-45	2.12	-65	10	10000000	1.05	1.05	n/a
u	-45	2.12	-80	10	10000000	1.14	1.14	n/a
u	45	2.12	-95	10	10000000	0.02	0.02	n/a
v	45	2.12	70	10	10000000	0.00	0.00	n/a
v	45	2.12	55	10	10000000	0.00	0.00	n/a
v	45	2.12	40	10	10000000	0.00	0.00	n/a
v	45	2.12	25	10	10000000	0.00	0.00	n/a
v	45	2.12	10	10	10000000	0.00	0.00	n/a
v	45	2.12	-5	10	10000000	0.01	0.01	n/a
v	45	2.12	-20	10	10000000	0.13	0.13	n/a
v	45	2.12	-35	10	10000000	0.85	0.85	n/a
v	45	2.12	-50	10	10000000	1.95	1.95	n/a
v	45	2.12	-65	10	10000000	1.44	1.44	n/a
v	45	2.12	-80	10	10000000	0.34	0.34	n/a
v	45	2.12	-95	10	10000000	0.02	0.02	n/a
w	-53	0.5	55	10	10000000	0.29	0.29	n/a
w	-53	0.5	25	10	10000000	511.84	511.84	n/a
w	-53	0.5	-5	10	10000000	20876.94	20876.94	n/a
x	-53	1	55	10	10000000	0.00	0.00	n/a
x	-53	1	25	10	10000000	0.06	0.06	n/a
x	-53	1	-5	10	10000000	75.10	75.10	n/a
x	-53	1	-35	10	10000000	2196.52	2196.52	n/a
x	-53	1	-65	10	10000000	4546.54	4546.54	n/a
x	-53	1	-95	10	10000000	1217.30	1217.30	n/a
y	-53	1.5	55	10	10000000	0.00	0.00	n/a
y	-53	1.5	25	10	10000000	0.00	0.00	n/a
y	-53	1.5	-5	10	10000000	0.22	0.22	n/a
y	-53	1.5	-35	10	10000000	23.93	23.93	n/a
y	-53	1.5	-65	10	10000000	217.55	217.55	n/a
y	-53	1.5	-95	10	10000000	69.46	69.46	n/a
bb	45	1.4	70	10	10000000	0.00	0.00	n/a
bb	45	1.4	55	10	10000000	0.00	0.00	n/a
bb	45	1.4	40	10	10000000	0.00	0.00	n/a
bb	45	1.4	25	10	10000000	0.12	0.12	n/a
bb	45	1.4	10	10	10000000	3.19	3.19	n/a
bb	45	1.4	-5	10	10000000	33.39	33.39	n/a
bb	45	1.4	-20	10	10000000	161.58	161.58	n/a
bb	45	1.4	-35	10	10000000	465.43	465.43	n/a
bb	45	1.4	-50	10	10000000	762.70	762.70	n/a
bb	45	1.4	-65	10	10000000	510.13	510.13	n/a
bb	45	1.4	-80	10	10000000	115.91	115.91	n/a
bb	45	1.4	-95	10	10000000	8.47	8.47	n/a
dd	-45	1.4	70	10	10000000	0.00	0.00	n/a
dd	-45	1.4	55	10	10000000	0.00	0.00	n/a
dd	-45	1.4	40	10	10000000	0.00	0.00	n/a
dd	-45	1.4	25	10	10000000	0.00	0.00	n/a
dd	-45	1.4	10	10	10000000	0.02	0.02	n/a
dd	-45	1.4	-5	10	10000000	0.75	0.75	n/a
dd	-45	1.4	-20	10	10000000	10.58	10.58	n/a
dd	-45	1.4	-35	10	10000000	64.53	64.53	n/a
dd	-45	1.4	-50	10	10000000	216.38	216.38	n/a
dd	-45	1.4	-65	10	10000000	443.34	443.34	n/a
dd	-45	1.4	-80	10	10000000	412.12	412.12	n/a
dd	-45	1.4	-95	10	10000000	135.54	135.54	n/a
a	0	0.5	55	63	10000000	4769.65	4769.65	n/a
a	0	0.5	25	63	10000000	19519.52	19519.52	n/a
a	0	0.5	-5	63	10000000	10414.26	10414.26	n/a
a	0	0.5	-35	63	10000000	6883.51	6883.51	n/a

a	0	0.5	-65	63	10000000	1699.55	1699.55	n/a
a	0	0.5	-95	63	10000000	131.40	131.40	n/a
b	0	1	55	63	10000000	169.36	169.36	n/a
b	0	1	25	63	10000000	1366.60	1366.60	n/a
b	0	1	-5	63	10000000	3447.88	3447.88	n/a
b	0	1	-35	63	10000000	2721.85	2721.85	n/a
b	0	1	-65	63	10000000	672.52	672.52	n/a
b	0	1	-95	63	10000000	52.00	52.00	n/a
c	0	1.5	55	63	10000000	36.12	36.12	n/a
c	0	1.5	25	63	10000000	291.30	291.30	n/a
c	0	1.5	-5	63	10000000	735.15	735.15	n/a
c	0	1.5	-35	63	10000000	580.52	580.52	n/a
c	0	1.5	-65	63	10000000	143.44	143.44	n/a
c	0	1.5	-95	63	10000000	11.09	11.09	n/a
d	27	0.5	55	63	10000000	13787.56	13787.56	n/a
d	27	0.5	25	63	10000000	20957.18	20957.18	n/a
d	27	0.5	-5	63	10000000	12003.71	12003.71	n/a
d	27	0.5	-35	63	10000000	6188.22	6188.22	n/a
d	27	0.5	-65	63	10000000	1037.98	1037.98	n/a
d	27	0.5	-95	63	10000000	54.48	54.48	n/a
e	27	1	55	63	10000000	486.99	486.99	n/a
e	27	1	25	63	10000000	2667.48	2667.48	n/a
e	27	1	-5	63	10000000	4568.05	4568.05	n/a
e	27	1	-35	63	10000000	2448.56	2448.56	n/a
e	27	1	-65	63	10000000	410.74	410.74	n/a
e	27	1	-95	63	10000000	21.56	21.56	n/a
f	27	1.5	55	63	10000000	103.84	103.84	n/a
f	27	1.5	25	63	10000000	568.58	568.58	n/a
f	27	1.5	-5	63	10000000	974.15	974.15	n/a
f	27	1.5	-35	63	10000000	522.24	522.24	n/a
f	27	1.5	-65	63	10000000	87.60	87.60	n/a
f	27	1.5	-95	63	10000000	4.60	4.60	n/a
g	-27	0.5	55	63	10000000	1142.40	1142.40	n/a
g	-27	0.5	25	63	10000000	13788.65	13788.65	n/a
g	-27	0.5	-5	63	10000000	10016.86	10016.86	n/a
g	-27	0.5	-35	63	10000000	6762.02	6762.02	n/a
g	-27	0.5	-65	63	10000000	2445.76	2445.76	n/a
g	-27	0.5	-95	63	10000000	278.53	278.53	n/a
h	-27	1	55	63	10000000	51.77	51.77	n/a
h	-27	1	25	63	10000000	615.26	615.26	n/a
h	-27	1	-5	63	10000000	2287.28	2287.28	n/a
h	-27	1	-35	63	10000000	2659.27	2659.27	n/a
h	-27	1	-65	63	10000000	967.80	967.80	n/a
h	-27	1	-95	63	10000000	110.22	110.22	n/a
i	-27	1.5	55	63	10000000	11.04	11.04	n/a
i	-27	1.5	25	63	10000000	131.17	131.17	n/a
i	-27	1.5	-5	63	10000000	487.60	487.60	n/a
i	-27	1.5	-35	63	10000000	567.15	567.15	n/a
i	-27	1.5	-65	63	10000000	206.42	206.42	n/a
i	-27	1.5	-95	63	10000000	23.51	23.51	n/a
j	53	0.5	55	63	10000000	13787.56	13787.56	n/a
j	53	0.5	25	63	10000000	20957.18	20957.18	n/a
j	53	0.5	-5	63	10000000	12003.71	12003.71	n/a
k	53	1	55	63	10000000	486.99	486.99	n/a
k	53	1	25	63	10000000	2667.48	2667.48	n/a
k	53	1	-5	63	10000000	4568.05	4568.05	n/a
k	53	1	-35	63	10000000	2448.56	2448.56	n/a
k	53	1	-65	63	10000000	410.74	410.74	n/a
k	53	1	-95	63	10000000	21.56	21.56	n/a
l	53	1.5	55	63	10000000	103.84	103.84	n/a
l	53	1.5	25	63	10000000	568.58	568.58	n/a
l	53	1.5	-5	63	10000000	974.15	974.15	n/a
l	53	1.5	-35	63	10000000	522.24	522.24	n/a
l	53	1.5	-65	63	10000000	87.60	87.60	n/a
l	53	1.5	-95	63	10000000	4.60	4.60	n/a
m	53	2	55	63	10000000	11.94	11.94	n/a
m	53	2	25	63	10000000	65.36	65.36	n/a
m	53	2	-5	63	10000000	111.99	111.99	n/a
m	53	2	-35	63	10000000	60.04	60.04	n/a
m	53	2	-65	63	10000000	10.07	10.07	n/a
m	53	2	-95	63	10000000	0.53	0.53	n/a

n	-70	1.47	55	63	10000000	12.33	12.33	n/a
n	-70	1.47	25	63	10000000	146.44	146.44	n/a
n	-70	1.47	-5	63	10000000	544.37	544.37	n/a
n	-70	1.47	-35	63	10000000	633.18	633.18	n/a
n	-70	1.47	-65	63	10000000	230.45	230.45	n/a
n	-70	1.47	-95	63	10000000	26.24	26.24	n/a
o	70	1.47	55	63	10000000	115.93	115.93	n/a
o	70	1.47	25	63	10000000	634.78	634.78	n/a
o	70	1.47	-5	63	10000000	1087.57	1087.57	n/a
o	70	1.47	-35	63	10000000	583.04	583.04	n/a
o	70	1.47	-65	63	10000000	97.80	97.80	n/a
p	-19	1.57	55	63	10000000	8.47	8.47	n/a
p	-19	1.57	25	63	10000000	100.57	100.57	n/a
p	-19	1.57	-5	63	10000000	373.85	373.85	n/a
p	-19	1.57	-35	63	10000000	434.84	434.84	n/a
p	-19	1.57	-65	63	10000000	158.26	158.26	n/a
p	-19	1.57	-95	63	10000000	18.02	18.02	n/a
q	19	1.57	55	63	10000000	79.62	79.62	n/a
q	19	1.57	25	63	10000000	435.94	435.94	n/a
q	19	1.57	-5	63	10000000	746.89	746.89	n/a
q	19	1.57	-35	63	10000000	400.41	400.41	n/a
q	19	1.57	-65	63	10000000	67.17	67.17	n/a
q	19	1.57	-95	63	10000000	3.53	3.53	n/a
r	76	0.8	70	63	2	212.03	2.00	2.62
r	76	0.8	55	63	0	780.87	0.00	3.19
r	76	0.8	40	63	2	2146.40	2.00	3.63
r	76	0.8	25	63	1	4320.35	1.00	3.94
r	76	0.8	10	63	2	6412.89	2.00	4.11
r	76	0.8	-5	63	6195	7162.23	6195.00	2.15
r	76	0.8	-20	63	6293	6038.54	6293.00	1.02
r	76	0.8	-35	63	1197	3821.16	1197.00	3.44
r	76	0.8	-50	63	1359	1809.55	1359.00	2.11
r	76	0.8	-65	63	661	640.95	661.00	0.00
r	76	0.8	-80	63	1183	169.80	1183.00	3.18
r	76	0.8	-95	63	214	33.64	214.00	2.42
s	0	0.8	70	63	7	60.39	7.00	1.93
s	0	0.8	55	63	2	268.13	2.00	2.72
s	0	0.8	40	63	5	897.86	5.00	3.25
s	0	0.8	25	63	0	2227.40	0.00	3.65
s	0	0.8	10	63	47	4041.35	47.00	3.89
s	0	0.8	-5	63	2250	5447.02	2250.00	3.42
s	0	0.8	-20	63	3344	5541.98	3344.00	3.04
s	0	0.8	-35	63	60	4248.74	60.00	3.91
s	0	0.8	-50	63	2424	2441.32	2424.00	0.00
s	0	0.8	-65	63	1045	1049.46	1045.00	0.00
s	0	0.8	-80	63	559	337.42	559.00	2.04
s	0	0.8	-95	63	594	81.14	594.00	2.89
t	-76	0.8	70	63	4	15.17	4.00	1.11
t	-76	0.8	55	63	843	81.26	843.00	3.10
t	-76	0.8	40	63	4171	328.68	4171.00	3.82
t	-76	0.8	25	63	1730	998.50	1730.00	2.59
t	-76	0.8	10	63	3465	2231.75	3465.00	2.73
t	-76	0.8	-5	63	2049	3657.64	2049.00	2.96
t	-76	0.8	-20	63	2828	4485.19	2828.00	2.88
t	-76	0.8	-35	63	5535	4155.54	5535.00	2.59
t	-76	0.8	-50	63	5420	2895.06	5420.00	3.19
t	-76	0.8	-65	63	8261	1510.25	8261.00	3.97
t	-76	0.8	-80	63	10347	589.32	10347.00	4.24
t	-76	0.8	-95	63	6867	171.99	6867.00	4.11
u	-45	2.12	70	63	14	0.13	14.00	1.44
u	-45	2.12	55	63	37	0.69	37.00	1.84
u	-45	2.12	40	63	23	2.75	23.00	1.50
u	-45	2.12	25	63	4	8.18	4.00	0.46
u	-45	2.12	10	63	7	18.25	7.00	1.00
u	-45	2.12	-5	63	42	30.42	42.00	0.57
u	-45	2.12	-20	63	320	37.94	320.00	2.65
u	-45	2.12	-35	63	163	35.39	163.00	2.22
u	-45	2.12	-50	63	366	24.68	366.00	2.78
u	-45	2.12	-65	63	150	12.88	150.00	2.36
u	-45	2.12	-80	63	114	5.03	114.00	2.30
u	45	2.12	-95	63	263	0.29	263.00	2.72

v	45	2.12	70	63	3	1.79	3.00	0.00
v	45	2.12	55	63	19	6.48	19.00	1.09
v	45	2.12	40	63	32	17.53	32.00	0.93
v	45	2.12	25	63	10	35.48	10.00	1.46
v	45	2.12	10	63	8	53.69	8.00	1.83
v	45	2.12	-5	63	340	60.78	340.00	2.59
v	45	2.12	-20	63	128	51.46	128.00	1.81
v	45	2.12	-35	63	11	32.58	11.00	1.33
v	45	2.12	-50	63	41	15.43	41.00	1.36
v	45	2.12	-65	63	51	5.47	51.00	1.87
v	45	2.12	-80	63	63	1.45	63.00	2.07
v	45	2.12	-95	63	454	0.29	454.00	2.96
w	-53	0.5	55	63	1229	1142.40	1229.00	0.80
w	-53	0.5	25	63	1608	13788.65	1608.00	4.28
w	-53	0.5	-5	63	6911	10016.86	6911.00	3.06
x	-53	1	55	63	74	51.77	74.00	0.90
x	-53	1	25	63	91	615.26	91.00	2.89
x	-53	1	-5	63	1417	2287.28	1417.00	2.61
x	-53	1	-35	63	1290	2659.27	1290.00	2.98
x	-53	1	-65	63	1301	967.80	1301.00	1.99
x	-53	1	-95	63	852	110.22	852.00	3.06
y	-53	1.5	55	63	4	11.04	4.00	0.82
y	-53	1.5	25	63	2	131.17	2.00	2.40
y	-53	1.5	-5	63	96	487.60	96.00	2.72
y	-53	1.5	-35	63	5259	567.15	5259.00	3.88
y	-53	1.5	-65	63	161	206.42	161.00	1.05
y	-53	1.5	-95	63	484	23.51	484.00	2.92
bb	45	1.4	70	63	10000000	41.08	41.08	n/a
bb	45	1.4	55	63	10000000	148.61	148.61	n/a
bb	45	1.4	40	63	10000000	402.10	402.10	n/a
bb	45	1.4	25	63	10000000	813.72	813.72	n/a
bb	45	1.4	10	63	10000000	1231.59	1231.59	n/a
bb	45	1.4	-5	63	10000000	1394.14	1394.14	n/a
bb	45	1.4	-20	63	10000000	1180.33	1180.33	n/a
bb	45	1.4	-35	63	10000000	747.39	747.39	n/a
bb	45	1.4	-50	63	10000000	353.96	353.96	n/a
bb	45	1.4	-65	63	10000000	125.37	125.37	n/a
bb	45	1.4	-80	63	10000000	33.21	33.21	n/a
bb	45	1.4	-95	63	10000000	6.58	6.58	n/a
dd	-45	1.4	70	63	10000000	2.97	2.97	n/a
dd	-45	1.4	55	63	10000000	15.80	15.80	n/a
dd	-45	1.4	40	63	10000000	62.98	62.98	n/a
dd	-45	1.4	25	63	10000000	187.72	187.72	n/a
dd	-45	1.4	10	63	10000000	418.51	418.51	n/a
dd	-45	1.4	-5	63	10000000	697.82	697.82	n/a
dd	-45	1.4	-20	63	10000000	870.23	870.23	n/a
dd	-45	1.4	-35	63	10000000	811.67	811.67	n/a
dd	-45	1.4	-50	63	10000000	566.21	566.21	n/a
dd	-45	1.4	-65	63	10000000	295.41	295.41	n/a
dd	-45	1.4	-80	63	10000000	115.27	115.27	n/a
dd	-45	1.4	-95	63	10000000	33.64	33.64	n/a
a	0	0.5	55	65	10000000	4589.67	4589.67	n/a
a	0	0.5	25	65	10000000	16206.77	16206.77	n/a
a	0	0.5	-5	65	10000000	9121.93	9121.93	n/a
a	0	0.5	-35	65	10000000	5930.99	5930.99	n/a
a	0	0.5	-65	65	10000000	1437.25	1437.25	n/a
a	0	0.5	-95	65	10000000	113.77	113.77	n/a
b	0	1	55	65	10000000	203.12	203.12	n/a
b	0	1	25	65	10000000	1415.13	1415.13	n/a
b	0	1	-5	65	10000000	3218.00	3218.00	n/a
b	0	1	-35	65	10000000	2389.30	2389.30	n/a
b	0	1	-65	65	10000000	579.28	579.28	n/a
b	0	1	-95	65	10000000	45.86	45.86	n/a
c	0	1.5	55	65	10000000	44.67	44.67	n/a
c	0	1.5	25	65	10000000	311.13	311.13	n/a
c	0	1.5	-5	65	10000000	707.61	707.61	n/a
c	0	1.5	-35	65	10000000	525.45	525.45	n/a
c	0	1.5	-65	65	10000000	127.39	127.39	n/a
c	0	1.5	-95	65	10000000	10.08	10.08	n/a
d	27	0.5	55	65	10000000	12512.47	12512.47	n/a
d	27	0.5	25	65	10000000	17204.65	17204.65	n/a

d	27	0.5	-5	65	10000000	10607.17	10607.17	n/a
d	27	0.5	-35	65	10000000	5274.58	5274.58	n/a
d	27	0.5	-65	65	10000000	880.55	880.55	n/a
d	27	0.5	-95	65	10000000	48.00	48.00	n/a
e	27	1	55	65	10000000	553.53	553.53	n/a
e	27	1	25	65	10000000	2655.40	2655.40	n/a
e	27	1	-5	65	10000000	4157.69	4157.69	n/a
e	27	1	-35	65	10000000	2125.82	2125.82	n/a
e	27	1	-65	65	10000000	354.90	354.90	n/a
e	27	1	-95	65	10000000	19.35	19.35	n/a
f	27	1.5	55	65	10000000	121.72	121.72	n/a
f	27	1.5	25	65	10000000	583.82	583.82	n/a
f	27	1.5	-5	65	10000000	914.30	914.30	n/a
f	27	1.5	-35	65	10000000	467.51	467.51	n/a
f	27	1.5	-65	65	10000000	78.05	78.05	n/a
f	27	1.5	-95	65	10000000	4.25	4.25	n/a
g	-27	0.5	55	65	10000000	1173.97	1173.97	n/a
g	-27	0.5	25	65	10000000	11890.81	11890.81	n/a
g	-27	0.5	-5	65	10000000	8449.69	8449.69	n/a
g	-27	0.5	-35	65	10000000	5908.85	5908.85	n/a
g	-27	0.5	-65	65	10000000	2071.59	2071.59	n/a
g	-27	0.5	-95	65	10000000	238.15	238.15	n/a
h	-27	1	55	65	10000000	65.82	65.82	n/a
h	-27	1	25	65	10000000	665.92	665.92	n/a
h	-27	1	-5	65	10000000	2199.45	2199.45	n/a
h	-27	1	-35	65	10000000	2371.41	2371.41	n/a
h	-27	1	-65	65	10000000	834.95	834.95	n/a
h	-27	1	-95	65	10000000	95.99	95.99	n/a
i	-27	1.5	55	65	10000000	14.47	14.47	n/a
i	-27	1.5	25	65	10000000	146.42	146.42	n/a
i	-27	1.5	-5	65	10000000	483.60	483.60	n/a
i	-27	1.5	-35	65	10000000	521.51	521.51	n/a
i	-27	1.5	-65	65	10000000	183.62	183.62	n/a
i	-27	1.5	-95	65	10000000	21.11	21.11	n/a
j	53	0.5	55	65	10000000	12512.47	12512.47	n/a
j	53	0.5	25	65	10000000	17204.65	17204.65	n/a
j	53	0.5	-5	65	10000000	10607.17	10607.17	n/a
k	53	1	55	65	10000000	553.53	553.53	n/a
k	53	1	25	65	10000000	2655.40	2655.40	n/a
k	53	1	-5	65	10000000	4157.69	4157.69	n/a
k	53	1	-35	65	10000000	2125.82	2125.82	n/a
k	53	1	-65	65	10000000	354.90	354.90	n/a
k	53	1	-95	65	10000000	19.35	19.35	n/a
l	53	1.5	55	65	10000000	121.72	121.72	n/a
l	53	1.5	25	65	10000000	583.82	583.82	n/a
l	53	1.5	-5	65	10000000	914.30	914.30	n/a
l	53	1.5	-35	65	10000000	467.51	467.51	n/a
l	53	1.5	-65	65	10000000	78.05	78.05	n/a
l	53	1.5	-95	65	10000000	4.25	4.25	n/a
m	53	2	55	65	10000000	14.61	14.61	n/a
m	53	2	25	65	10000000	70.06	70.06	n/a
m	53	2	-5	65	10000000	109.71	109.71	n/a
m	53	2	-35	65	10000000	56.10	56.10	n/a
m	53	2	-65	65	10000000	9.37	9.37	n/a
m	53	2	-95	65	10000000	0.51	0.51	n/a
n	-70	1.47	55	65	10000000	16.12	16.12	n/a
n	-70	1.47	25	65	10000000	163.11	163.11	n/a
n	-70	1.47	-5	65	10000000	538.73	538.73	n/a
n	-70	1.47	-35	65	10000000	580.96	580.96	n/a
n	-70	1.47	-65	65	10000000	204.55	204.55	n/a
n	-70	1.47	-95	65	10000000	23.52	23.52	n/a
o	70	1.47	55	65	10000000	135.59	135.59	n/a
o	70	1.47	25	65	10000000	650.38	650.38	n/a
o	70	1.47	-5	65	10000000	1018.53	1018.53	n/a
o	70	1.47	-35	65	10000000	520.80	520.80	n/a
o	70	1.47	-65	65	10000000	86.95	86.95	n/a
p	-19	1.57	55	65	10000000	11.16	11.16	n/a
p	-19	1.57	25	65	10000000	112.86	112.86	n/a
p	-19	1.57	-5	65	10000000	372.74	372.74	n/a
p	-19	1.57	-35	65	10000000	401.96	401.96	n/a
p	-19	1.57	-65	65	10000000	141.53	141.53	n/a

p	-19	1.57	-95	65	10000000	16.27	16.27	n/a
q	19	1.57	55	65	10000000	93.82	93.82	n/a
q	19	1.57	25	65	10000000	449.99	449.99	n/a
q	19	1.57	-5	65	10000000	704.71	704.71	n/a
q	19	1.57	-35	65	10000000	360.34	360.34	n/a
q	19	1.57	-65	65	10000000	60.16	60.16	n/a
q	19	1.57	-95	65	10000000	3.28	3.28	n/a
r	76	0.8	70	65	10000000	258.44	258.44	n/a
r	76	0.8	55	65	10000000	870.62	870.62	n/a
r	76	0.8	40	65	10000000	2213.03	2213.03	n/a
r	76	0.8	25	65	10000000	4196.98	4196.98	n/a
r	76	0.8	10	65	10000000	5970.39	5970.39	n/a
r	76	0.8	-5	65	10000000	6447.04	6447.04	n/a
r	76	0.8	-20	65	10000000	5290.79	5290.79	n/a
r	76	0.8	-35	65	10000000	3288.26	3288.26	n/a
r	76	0.8	-50	65	10000000	1545.29	1545.29	n/a
r	76	0.8	-65	65	10000000	548.96	548.96	n/a
r	76	0.8	-80	65	10000000	147.41	147.41	n/a
r	76	0.8	-95	65	10000000	29.92	29.92	n/a
s	0	0.8	70	65	10000000	78.40	78.40	n/a
s	0	0.8	55	65	10000000	317.01	317.01	n/a
s	0	0.8	40	65	10000000	973.67	973.67	n/a
s	0	0.8	25	65	10000000	2246.30	2246.30	n/a
s	0	0.8	10	65	10000000	3865.01	3865.01	n/a
s	0	0.8	-5	65	10000000	5011.01	5011.01	n/a
s	0	0.8	-20	65	10000000	4939.72	4939.72	n/a
s	0	0.8	-35	65	10000000	3696.28	3696.28	n/a
s	0	0.8	-50	65	10000000	2093.03	2093.03	n/a
s	0	0.8	-65	65	10000000	896.02	896.02	n/a
s	0	0.8	-80	65	10000000	289.96	289.96	n/a
s	0	0.8	-95	65	10000000	70.93	70.93	n/a
t	-76	0.8	70	65	10000000	21.05	21.05	n/a
t	-76	0.8	55	65	10000000	102.18	102.18	n/a
t	-76	0.8	40	65	10000000	377.20	377.20	n/a
t	-76	0.8	25	65	10000000	1054.82	1054.82	n/a
t	-76	0.8	10	65	10000000	2206.52	2206.52	n/a
t	-76	0.8	-5	65	10000000	3449.25	3449.25	n/a
t	-76	0.8	-20	65	10000000	4080.15	4080.15	n/a
t	-76	0.8	-35	65	10000000	3670.63	3670.63	n/a
t	-76	0.8	-50	65	10000000	2503.51	2503.51	n/a
t	-76	0.8	-65	65	10000000	1291.48	1291.48	n/a
t	-76	0.8	-80	65	10000000	503.65	503.65	n/a
t	-76	0.8	-95	65	10000000	148.47	148.47	n/a
u	-45	2.12	70	65	10000000	0.20	0.20	n/a
u	-45	2.12	55	65	10000000	0.95	0.95	n/a
u	-45	2.12	40	65	10000000	3.49	3.49	n/a
u	-45	2.12	25	65	10000000	9.65	9.65	n/a
u	-45	2.12	10	65	10000000	20.18	20.18	n/a
u	-45	2.12	-5	65	10000000	31.88	31.88	n/a
u	-45	2.12	-20	65	10000000	38.08	38.08	n/a
u	-45	2.12	-35	65	10000000	34.38	34.38	n/a
u	-45	2.12	-50	65	10000000	23.46	23.46	n/a
u	-45	2.12	-65	65	10000000	12.10	12.10	n/a
u	-45	2.12	-80	65	10000000	4.72	4.72	n/a
u	45	2.12	-95	65	10000000	0.28	0.28	n/a
v	45	2.12	70	65	10000000	2.41	2.41	n/a
v	45	2.12	55	65	10000000	8.02	8.02	n/a
v	45	2.12	40	65	10000000	20.21	20.21	n/a
v	45	2.12	25	65	10000000	38.49	38.49	n/a
v	45	2.12	10	65	10000000	55.39	55.39	n/a
v	45	2.12	-5	65	10000000	60.27	60.27	n/a
v	45	2.12	-20	65	10000000	49.57	49.57	n/a
v	45	2.12	-35	65	10000000	30.82	30.82	n/a
v	45	2.12	-50	65	10000000	14.48	14.48	n/a
v	45	2.12	-65	65	10000000	5.15	5.15	n/a
v	45	2.12	-80	65	10000000	1.38	1.38	n/a
v	45	2.12	-95	65	10000000	0.28	0.28	n/a
w	-53	0.5	55	65	10000000	1173.97	1173.97	n/a
w	-53	0.5	25	65	10000000	11890.81	11890.81	n/a
w	-53	0.5	-5	65	10000000	8449.69	8449.69	n/a
x	-53	1	55	65	10000000	65.82	65.82	n/a

x	-53	1	25	65	10000000	665.92	665.92	n/a
x	-53	1	-5	65	10000000	2199.45	2199.45	n/a
x	-53	1	-35	65	10000000	2371.41	2371.41	n/a
x	-53	1	-65	65	10000000	834.95	834.95	n/a
x	-53	1	-95	65	10000000	95.99	95.99	n/a
y	-53	1.5	55	65	10000000	14.47	14.47	n/a
y	-53	1.5	25	65	10000000	146.42	146.42	n/a
y	-53	1.5	-5	65	10000000	483.60	483.60	n/a
y	-53	1.5	-35	65	10000000	521.51	521.51	n/a
y	-53	1.5	-65	65	10000000	183.62	183.62	n/a
y	-53	1.5	-95	65	10000000	21.11	21.11	n/a
bb	45	1.4	70	65	0	51.90	0.00	2.02
bb	45	1.4	55	65	541	172.96	541.00	2.58
bb	45	1.4	40	65	1090	435.69	1090.00	2.75
bb	45	1.4	25	65	409.67	829.61	409.67	2.45
bb	45	1.4	10	65	965.5	1194.11	965.50	1.68
bb	45	1.4	-5	65	2053.33	1299.23	2053.33	2.53
bb	45	1.4	-20	65	2329	1068.56	2329.00	2.97
bb	45	1.4	-35	65	1964.75	664.33	1964.75	3.11
bb	45	1.4	-50	65	726.83	312.20	726.83	2.52
bb	45	1.4	-65	65	118.4	110.91	118.40	0.00
bb	45	1.4	-80	65	213.75	29.78	213.75	2.44
bb	45	1.4	-95	65	1082.6	6.05	1082.60	3.33
dd	-45	1.4	70	65	8	4.25	8.00	0.36
dd	-45	1.4	55	65	5	20.57	5.00	1.28
dd	-45	1.4	40	65	2	75.24	2.00	2.14
dd	-45	1.4	25	65	2.5	208.06	2.50	2.60
dd	-45	1.4	10	65	51	434.92	51.00	2.78
dd	-45	1.4	-5	65	6166.33	687.20	6166.33	3.94
dd	-45	1.4	-20	65	904.6	820.79	904.60	0.91
dd	-45	1.4	-35	65	628.83	741.06	628.83	1.26
dd	-45	1.4	-50	65	645	505.77	645.00	1.53
dd	-45	1.4	-65	65	730	260.92	730.00	2.65
dd	-45	1.4	-80	65	875.75	101.75	875.75	3.09
dd	-45	1.4	-95	65	611.2	30.00	611.20	3.02

APPENDIX B Teign Repacked Interpolation

Sample	Angle	Distance	Height	Time	Concentration	Predicted	Actual or Pred	log RSD
AA	0	0.5	55	2	0.00	0.000	0.00	0
AA	0	0.5	25	2	0.00	0.192	0.00	0
AA	0	0.5	-5	2	1314.25	790.837	1314.25	2.415449401
AA	0	0.5	-35	2	12489.67	12070.083	12489.67	1.156443632
AA	0	0.5	-65	2	521.17	681.027	521.17	1.628535456
AA	0	0.5	-95	2	355.17	0.142	355.17	2.850941059
BB	0	1	55	2	9.00	0.000	9.00	1.255272499
BB	0	1	25	2	22.50	0.050	22.50	1.650305291
BB	0	1	-5	2	17.67	207.198	17.67	2.504471464
BB	0	1	-35	2	4638.33	3162.347	4638.33	2.747062412
BB	0	1	-65	2	220.25	178.428	220.25	0.943214126
BB	0	1	-95	2	71.50	0.037	71.50	2.154657795
CC	0	1.5	55	2	7.50	0.000	7.50	1.176091258
CC	0	1.5	25	2	2.00	0.005	2.00	0.598551154
CC	0	1.5	-5	2	11.00	22.227	11.00	0.880079256
CC	0	1.5	-35	2	12.67	339.241	12.67	2.782565197
DD	27	0.5	55	2	10000000	0.000	0.00	n/a
DD	27	0.5	25	2	10000000	0.192	0.19	n/a
DD	27	0.5	-5	2	10000000	790.837	790.84	n/a
DD	27	0.5	-35	2	10000000	12070.083	12070.08	n/a
DD	27	0.5	-65	2	10000000	681.027	681.03	n/a
DD	27	0.5	-95	2	10000000	0.142	0.14	n/a
EE	27	1	55	2	10000000	0.000	0.00	n/a
EE	27	1	25	2	10000000	0.050	0.05	n/a
EE	27	1	-5	2	10000000	207.198	207.20	n/a
EE	27	1	-35	2	10000000	3162.347	3162.35	n/a
EE	27	1	-65	2	10000000	178.428	178.43	n/a
FF	27	1	-95	2	10000000	0.037	0.04	n/a
FF	27	1.5	55	2	10000000	0.000	0.00	n/a
FF	27	1.5	25	2	10000000	0.005	0.01	n/a
FF	27	1.5	-5	2	10000000	22.227	22.23	n/a
FF	27	1.5	-35	2	10000000	339.241	339.24	n/a
GG	-27	0.5	55	2	10000000	0.000	0.00	n/a
GG	-27	0.5	25	2	10000000	0.192	0.19	n/a
GG	-27	0.5	-5	2	10000000	790.837	790.84	n/a
GG	-27	0.5	-35	2	10000000	12070.083	12070.08	n/a
GG	-27	0.5	-65	2	10000000	681.027	681.03	n/a
GG	-27	0.5	-95	2	10000000	0.142	0.14	n/a
HH	-27	1	55	2	10000000	0.000	0.00	n/a
HH	-27	1	25	2	10000000	0.050	0.05	n/a
HH	-27	1	-5	2	10000000	207.198	207.20	n/a
HH	-27	1	-35	2	10000000	3162.347	3162.35	n/a
HH	-27	1	-65	2	10000000	178.428	178.43	n/a
HH	-27	1	-95	2	10000000	0.037	0.04	n/a
II	-27	1.5	55	2	10000000	0.000	0.00	n/a
II	-27	1.5	25	2	10000000	0.005	0.01	n/a
II	-27	1.5	-5	2	10000000	22.227	22.23	n/a
II	-27	1.5	-35	2	10000000	339.241	339.24	n/a
II	-27	1.5	-65	2	10000000	19.141	19.14	n/a
II	-27	1.5	-95	2	10000000	0.004	0.00	n/a
JJ	53	0.5	55	2	10000000	0.000	0.00	n/a
JJ	53	0.5	25	2	10000000	0.192	0.19	n/a
KK	53	1	55	2	10000000	0.000	0.00	n/a
KK	53	1	25	2	10000000	0.050	0.05	n/a
KK	53	1	-5	2	10000000	207.198	207.20	n/a
KK	53	1	-35	2	10000000	3162.347	3162.35	n/a
KK	53	1	-65	2	10000000	178.428	178.43	n/a
KK	53	1	-95	2	10000000	0.037	0.04	n/a
LL	53	1.5	55	2	10000000	0.000	0.00	n/a
LL	53	1.5	25	2	10000000	0.005	0.01	n/a
LL	53	1.5	-5	2	10000000	22.227	22.23	n/a
LL	53	1.5	-35	2	10000000	339.241	339.24	n/a
LL	53	1.5	-65	2	10000000	19.141	19.14	n/a
LL	53	1.5	-95	2	10000000	0.004	0.00	n/a
MM	53	2	55	2	10000000	0.000	0.00	n/a
MM	53	2	25	2	10000000	0.000	0.00	n/a
MM	53	2	-5	2	10000000	0.976	0.98	n/a

MM	53	2	-35	2	10000000	14.901	14.90	n/a
MM	53	2	-65	2	10000000	0.841	0.84	n/a
MM	53	2	-95	2	10000000	0.000	0.00	n/a
PP	-19	1.57	55	2	10000000	0.000	0.00	n/a
PP	-19	1.57	25	2	10000000	0.004	0.00	n/a
PP	-19	1.57	-5	2	10000000	15.143	15.14	n/a
PP	-19	1.57	-35	2	10000000	231.117	231.12	n/a
PP	-19	1.57	-65	2	10000000	13.040	13.04	n/a
PP	-19	1.57	-95	2	10000000	0.003	0.00	n/a
QQ	19	1.57	55	2	10000000	0.000	0.00	n/a
QQ	19	1.57	25	2	10000000	0.004	0.00	n/a
QQ	19	1.57	-5	2	10000000	15.143	15.14	n/a
QQ	19	1.57	-35	2	10000000	231.117	231.12	n/a
QQ	19	1.57	-65	2	10000000	13.040	13.04	n/a
QQ	19	1.57	-95	2	10000000	0.003	0.00	n/a
NN	-70	1.47	55	2	10000000	0.000	0.00	n/a
NN	-70	1.47	25	2	10000000	0.006	0.01	n/a
NN	-70	1.47	-5	2	10000000	26.061	26.06	n/a
NN	-70	1.47	-35	2	10000000	397.754	397.75	n/a
NN	-70	1.47	-65	2	10000000	22.442	22.44	n/a
NN	-70	1.47	-95	2	10000000	0.005	0.00	n/a
OO	70	1.47	55	2	10000000	0.000	0.00	n/a
OO	70	1.47	25	2	10000000	0.006	0.01	n/a
OO	70	1.47	-5	2	10000000	26.061	26.06	n/a
OO	70	1.47	-35	2	10000000	397.754	397.75	n/a
OO	70	1.47	-65	2	10000000	22.442	22.44	n/a
OO	70	1.47	-95	2	10000000	0.005	0.00	n/a
WW	-53	0.5	55	2	10000000	0.000	0.00	n/a
WW	-53	0.5	25	2	10000000	0.192	0.19	n/a
XX	-53	1	55	2	10000000	0.000	0.00	n/a
XX	-53	1	25	2	10000000	0.050	0.05	n/a
XX	-53	1	-5	2	10000000	207.198	207.20	n/a
XX	-53	1	-35	2	10000000	3162.347	3162.35	n/a
XX	-53	1	-65	2	10000000	178.428	178.43	n/a
XX	-53	1	-95	2	10000000	0.037	0.04	n/a
YY	-53	1.5	55	2	10000000	0.000	0.00	n/a
YY	-53	1.5	25	2	10000000	0.005	0.01	n/a
YY	-53	1.5	-5	2	10000000	22.227	22.23	n/a
RR	76	0.8	70	2	10000000	0.000	0.00	n/a
RR	76	0.8	55	2	10000000	0.000	0.00	n/a
RR	76	0.8	40	2	10000000	0.000	0.00	n/a
RR	76	0.8	25	2	10000000	0.095	0.10	n/a
RR	76	0.8	10	2	10000000	12.352	12.35	n/a
RR	76	0.8	-5	2	10000000	394.096	394.10	n/a
RR	76	0.8	-20	2	10000000	3100.526	3100.53	n/a
RR	76	0.8	-35	2	10000000	6014.864	6014.86	n/a
RR	76	0.8	-50	2	10000000	2877.226	2877.23	n/a
RR	76	0.8	-65	2	10000000	339.375	339.37	n/a
RR	76	0.8	-80	2	10000000	9.871	9.87	n/a
RR	76	0.8	-95	2	10000000	0.071	0.07	n/a
SS	0	0.8	70	2	10000000	0.000	0.00	n/a
SS	0	0.8	55	2	10000000	0.000	0.00	n/a
SS	0	0.8	40	2	10000000	0.000	0.00	n/a
SS	0	0.8	25	2	10000000	0.095	0.10	n/a
SS	0	0.8	10	2	10000000	12.352	12.35	n/a
SS	0	0.8	-5	2	10000000	394.096	394.10	n/a
SS	0	0.8	-20	2	10000000	3100.526	3100.53	n/a
SS	0	0.8	-35	2	10000000	6014.864	6014.86	n/a
SS	0	0.8	-50	2	10000000	2877.226	2877.23	n/a
SS	0	0.8	-65	2	10000000	339.375	339.37	n/a
SS	0	0.8	-80	2	10000000	9.871	9.87	n/a
SS	0	0.8	-95	2	10000000	0.071	0.07	n/a
TT	-76	0.8	70	2	10000000	0.000	0.00	n/a
TT	-76	0.8	55	2	10000000	0.000	0.00	n/a
TT	-76	0.8	40	2	10000000	0.000	0.00	n/a
TT	-76	0.8	25	2	10000000	0.095	0.10	n/a
TT	-76	0.8	10	2	10000000	12.352	12.35	n/a
TT	-76	0.8	-5	2	10000000	394.096	394.10	n/a
TT	-76	0.8	-20	2	10000000	3100.526	3100.53	n/a
TT	-76	0.8	-35	2	10000000	6014.864	6014.86	n/a
TT	-76	0.8	-50	2	10000000	2877.226	2877.23	n/a

TT	-76	0.8	-65	2	10000000	339.375	339.37	n/a
TT	-76	0.8	-80	2	10000000	9.871	9.87	n/a
TT	-76	0.8	-95	2	10000000	0.071	0.07	n/a
UU	-45	2.12	70	2	10000000	0.000	0.00	n/a
UU	-45	2.12	55	2	10000000	0.000	0.00	n/a
UU	-45	2.12	40	2	10000000	0.000	0.00	n/a
UU	-45	2.12	25	2	10000000	0.000	0.00	n/a
UU	-45	2.12	10	2	10000000	0.013	0.01	n/a
UU	-45	2.12	-5	2	10000000	0.404	0.40	n/a
UU	-45	2.12	-20	2	10000000	3.177	3.18	n/a
UU	-45	2.12	-35	2	10000000	6.162	6.16	n/a
UU	-45	2.12	-50	2	10000000	2.948	2.95	n/a
UU	-45	2.12	-65	2	10000000	0.348	0.35	n/a
VV	45	2.12	-95	2	10000000	0.000	0.00	n/a
VV	45	2.12	70	2	10000000	0.000	0.00	n/a
VV	45	2.12	55	2	10000000	0.000	0.00	n/a
VV	45	2.12	40	2	10000000	0.000	0.00	n/a
VV	45	2.12	25	2	10000000	0.000	0.00	n/a
VV	45	2.12	10	2	10000000	0.013	0.01	n/a
VV	45	2.12	-5	2	10000000	0.404	0.40	n/a
VV	45	2.12	-20	2	10000000	3.177	3.18	n/a
VV	45	2.12	-35	2	10000000	6.162	6.16	n/a
VV	45	2.12	-50	2	10000000	2.948	2.95	n/a
VV	45	2.12	-65	2	10000000	0.348	0.35	n/a
VV	45	2.12	-80	2	10000000	0.010	0.01	n/a
ββ	45	1.4	70	2	10000000	0.000	0.00	n/a
ββ	45	1.4	55	2	10000000	0.000	0.00	n/a
ββ	45	1.4	40	2	10000000	0.000	0.00	n/a
ββ	45	1.4	25	2	10000000	0.009	0.01	n/a
ββ	45	1.4	10	2	10000000	1.169	1.17	n/a
ββ	45	1.4	-5	2	10000000	37.309	37.31	n/a
ββ	45	1.4	-20	2	10000000	293.523	293.52	n/a
ββ	45	1.4	-35	2	10000000	569.420	569.42	n/a
ββ	45	1.4	-50	2	10000000	272.383	272.38	n/a
ββ	45	1.4	-65	2	10000000	32.128	32.13	n/a
ββ	45	1.4	-80	2	10000000	0.934	0.93	n/a
δδ	45	1.4	-95	2	10000000	0.007	0.01	n/a
δδ	-45	1.4	70	2	10000000	0.000	0.00	n/a
δδ	-45	1.4	55	2	10000000	0.000	0.00	n/a
δδ	-45	1.4	40	2	10000000	0.000	0.00	n/a
δδ	-45	1.4	25	2	10000000	0.009	0.01	n/a
δδ	-45	1.4	10	2	10000000	1.169	1.17	n/a
δδ	-45	1.4	-5	2	10000000	37.309	37.31	n/a
AA	0	0.5	55	3	10000000	0.000	0.00	n/a
AA	0	0.5	25	3	10000000	0.027	0.03	n/a
AA	0	0.5	-5	3	10000000	296.161	296.16	n/a
AA	0	0.5	-35	3	10000000	11984.387	11984.39	n/a
AA	0	0.5	-65	3	10000000	1792.812	1792.81	n/a
AA	0	0.5	-95	3	10000000	0.991	0.99	n/a
BB	0	1	55	3	10000000	0.000	0.00	n/a
BB	0	1	25	3	10000000	0.013	0.01	n/a
BB	0	1	-5	3	10000000	147.562	147.56	n/a
BB	0	1	-35	3	10000000	5971.227	5971.23	n/a
BB	0	1	-65	3	10000000	893.269	893.27	n/a
BB	0	1	-95	3	10000000	0.494	0.49	n/a
CC	0	1.5	55	3	10000000	0.000	0.00	n/a
CC	0	1.5	25	3	10000000	0.004	0.00	n/a
CC	0	1.5	-5	3	10000000	46.208	46.21	n/a
CC	0	1.5	-35	3	10000000	1869.863	1869.86	n/a
DD	27	0.5	55	3	2.00	0.000	2.00	0.602059985
DD	27	0.5	25	3	3.00	0.027	3.00	0.766382838
DD	27	0.5	-5	3	313.00	296.161	313.00	0
DD	27	0.5	-35	3	10826.83	11984.387	10826.83	2.069963953
DD	27	0.5	-65	3	3533.50	1792.812	3533.50	3.056045248
DD	27	0.5	-95	3	2318.33	0.991	2318.33	3.665648632
EE	27	1	55	3	3.33	0.000	3.33	0.823908739
EE	27	1	25	3	0.00	0.013	0.00	0
EE	27	1	-5	3	3.67	147.562	3.67	2.437489917
EE	27	1	-35	3	7907.33	5971.227	7907.33	2.732544206
EE	27	1	-65	3	276.83	893.269	276.83	2.812582112
FF	27	1	-95	3	37.33	0.494	37.33	1.855847597

FF	27	1.5	55	3	28.33	0.000	28.33	1.753327667
FF	27	1.5	25	3	4.00	0.004	4.00	0.901714725
FF	27	1.5	-5	3	2.00	46.208	2.00	1.908917294
FF	27	1.5	-35	3	1.50	1869.863	1.50	3.571794423
GG	-27	0.5	55	3	10000000	0.000	0.00	n/a
GG	-27	0.5	25	3	10000000	0.027	0.03	n/a
GG	-27	0.5	-5	3	10000000	296.161	296.16	n/a
GG	-27	0.5	-35	3	10000000	11984.387	11984.39	n/a
GG	-27	0.5	-65	3	10000000	1792.812	1792.81	n/a
GG	-27	0.5	-95	3	10000000	0.991	0.99	n/a
HH	-27	1	55	3	10000000	0.000	0.00	n/a
HH	-27	1	25	3	10000000	0.013	0.01	n/a
HH	-27	1	-5	3	10000000	147.562	147.56	n/a
HH	-27	1	-35	3	10000000	5971.227	5971.23	n/a
HH	-27	1	-65	3	10000000	893.269	893.27	n/a
HH	-27	1	-95	3	10000000	0.494	0.49	n/a
II	-27	1.5	55	3	10000000	0.000	0.00	n/a
II	-27	1.5	25	3	10000000	0.004	0.00	n/a
II	-27	1.5	-5	3	10000000	46.208	46.21	n/a
II	-27	1.5	-35	3	10000000	1869.863	1869.86	n/a
II	-27	1.5	-65	3	10000000	279.723	279.72	n/a
II	-27	1.5	-95	3	10000000	0.155	0.15	n/a
JJ	53	0.5	55	3	10000000	0.000	0.00	n/a
JJ	53	0.5	25	3	10000000	0.027	0.03	n/a
KK	53	1	55	3	10000000	0.000	0.00	n/a
KK	53	1	25	3	10000000	0.013	0.01	n/a
KK	53	1	-5	3	10000000	147.562	147.56	n/a
KK	53	1	-35	3	10000000	5971.227	5971.23	n/a
KK	53	1	-65	3	10000000	893.269	893.27	n/a
KK	53	1	-95	3	10000000	0.494	0.49	n/a
LL	53	1.5	55	3	10000000	0.000	0.00	n/a
LL	53	1.5	25	3	10000000	0.004	0.00	n/a
LL	53	1.5	-5	3	10000000	46.208	46.21	n/a
LL	53	1.5	-35	3	10000000	1869.863	1869.86	n/a
LL	53	1.5	-65	3	10000000	279.723	279.72	n/a
LL	53	1.5	-95	3	10000000	0.155	0.15	n/a
MM	53	2	55	3	10000000	0.000	0.00	n/a
MM	53	2	25	3	10000000	0.001	0.00	n/a
MM	53	2	-5	3	10000000	9.094	9.09	n/a
MM	53	2	-35	3	10000000	368.006	368.01	n/a
MM	53	2	-65	3	10000000	55.052	55.05	n/a
MM	53	2	-95	3	10000000	0.030	0.03	n/a
PP	-19	1.57	55	3	10000000	0.000	0.00	n/a
PP	-19	1.57	25	3	10000000	0.003	0.00	n/a
PP	-19	1.57	-5	3	10000000	37.847	37.85	n/a
PP	-19	1.57	-35	3	10000000	1531.505	1531.51	n/a
PP	-19	1.57	-65	3	10000000	229.106	229.11	n/a
PP	-19	1.57	-95	3	10000000	0.127	0.13	n/a
QQ	19	1.57	55	3	10000000	0.000	0.00	n/a
QQ	19	1.57	25	3	10000000	0.003	0.00	n/a
QQ	19	1.57	-5	3	10000000	37.847	37.85	n/a
QQ	19	1.57	-35	3	10000000	1531.505	1531.51	n/a
QQ	19	1.57	-65	3	10000000	229.106	229.11	n/a
QQ	19	1.57	-95	3	10000000	0.127	0.13	n/a
NN	-70	1.47	55	3	10000000	0.000	0.00	n/a
NN	-70	1.47	25	3	10000000	0.005	0.00	n/a
NN	-70	1.47	-5	3	10000000	50.195	50.20	n/a
NN	-70	1.47	-35	3	10000000	2031.201	2031.20	n/a
NN	-70	1.47	-65	3	10000000	303.859	303.86	n/a
NN	-70	1.47	-95	3	10000000	0.168	0.17	n/a
OO	70	1.47	55	3	10000000	0.000	0.00	n/a
OO	70	1.47	25	3	10000000	0.005	0.00	n/a
OO	70	1.47	-5	3	10000000	50.195	50.20	n/a
OO	70	1.47	-35	3	10000000	2031.201	2031.20	n/a
OO	70	1.47	-65	3	10000000	303.859	303.86	n/a
OO	70	1.47	-95	3	10000000	0.168	0.17	n/a
WW	-53	0.5	55	3	10000000	0.000	0.00	n/a
WW	-53	0.5	25	3	10000000	0.027	0.03	n/a
XX	-53	1	55	3	10000000	0.000	0.00	n/a
XX	-53	1	25	3	10000000	0.013	0.01	n/a
XX	-53	1	-5	3	10000000	147.562	147.56	n/a

XX	-53	1	-35	3	10000000	5971.227	5971.23	n/a
XX	-53	1	-65	3	10000000	893.269	893.27	n/a
XX	-53	1	-95	3	10000000	0.494	0.49	n/a
YY	-53	1.5	55	3	10000000	0.000	0.00	n/a
YY	-53	1.5	25	3	10000000	0.004	0.00	n/a
YY	-53	1.5	-5	3	10000000	46.208	46.21	n/a
RR	76	0.8	70	3	10000000	0.000	0.00	n/a
RR	76	0.8	55	3	10000000	0.000	0.00	n/a
RR	76	0.8	40	3	10000000	0.000	0.00	n/a
RR	76	0.8	25	3	10000000	0.019	0.02	n/a
RR	76	0.8	10	3	10000000	3.968	3.97	n/a
RR	76	0.8	-5	3	10000000	206.158	206.16	n/a
RR	76	0.8	-20	3	10000000	2640.983	2640.98	n/a
RR	76	0.8	-35	3	10000000	8342.355	8342.35	n/a
RR	76	0.8	-50	3	10000000	6497.844	6497.84	n/a
RR	76	0.8	-65	3	10000000	1247.980	1247.98	n/a
RR	76	0.8	-80	3	10000000	59.102	59.10	n/a
RR	76	0.8	-95	3	10000000	0.690	0.69	n/a
SS	0	0.8	70	3	10000000	0.000	0.00	n/a
SS	0	0.8	55	3	10000000	0.000	0.00	n/a
SS	0	0.8	40	3	10000000	0.000	0.00	n/a
SS	0	0.8	25	3	10000000	0.019	0.02	n/a
SS	0	0.8	10	3	10000000	3.968	3.97	n/a
SS	0	0.8	-5	3	10000000	206.158	206.16	n/a
SS	0	0.8	-20	3	10000000	2640.983	2640.98	n/a
SS	0	0.8	-35	3	10000000	8342.355	8342.35	n/a
SS	0	0.8	-50	3	10000000	6497.844	6497.84	n/a
SS	0	0.8	-65	3	10000000	1247.980	1247.98	n/a
SS	0	0.8	-80	3	10000000	59.102	59.10	n/a
SS	0	0.8	-95	3	10000000	0.690	0.69	n/a
TT	-76	0.8	70	3	10000000	0.000	0.00	n/a
TT	-76	0.8	55	3	10000000	0.000	0.00	n/a
TT	-76	0.8	40	3	10000000	0.000	0.00	n/a
TT	-76	0.8	25	3	10000000	0.019	0.02	n/a
TT	-76	0.8	10	3	10000000	3.968	3.97	n/a
TT	-76	0.8	-5	3	10000000	206.158	206.16	n/a
TT	-76	0.8	-20	3	10000000	2640.983	2640.98	n/a
TT	-76	0.8	-35	3	10000000	8342.355	8342.35	n/a
TT	-76	0.8	-50	3	10000000	6497.844	6497.84	n/a
TT	-76	0.8	-65	3	10000000	1247.980	1247.98	n/a
TT	-76	0.8	-80	3	10000000	59.102	59.10	n/a
TT	-76	0.8	-95	3	10000000	0.690	0.69	n/a
UU	-45	2.12	70	3	10000000	0.000	0.00	n/a
UU	-45	2.12	55	3	10000000	0.000	0.00	n/a
UU	-45	2.12	40	3	10000000	0.000	0.00	n/a
UU	-45	2.12	25	3	10000000	0.001	0.00	n/a
UU	-45	2.12	10	3	10000000	0.111	0.11	n/a
UU	-45	2.12	-5	3	10000000	5.745	5.75	n/a
UU	-45	2.12	-20	3	10000000	73.602	73.60	n/a
UU	-45	2.12	-35	3	10000000	232.494	232.49	n/a
UU	-45	2.12	-50	3	10000000	181.089	181.09	n/a
UU	-45	2.12	-65	3	10000000	34.780	34.78	n/a
VV	45	2.12	-95	3	10000000	0.019	0.02	n/a
VV	45	2.12	70	3	10000000	0.000	0.00	n/a
VV	45	2.12	55	3	10000000	0.000	0.00	n/a
VV	45	2.12	40	3	10000000	0.000	0.00	n/a
VV	45	2.12	25	3	10000000	0.001	0.00	n/a
VV	45	2.12	10	3	10000000	0.111	0.11	n/a
VV	45	2.12	-5	3	10000000	5.745	5.75	n/a
VV	45	2.12	-20	3	10000000	73.602	73.60	n/a
VV	45	2.12	-35	3	10000000	232.494	232.49	n/a
VV	45	2.12	-50	3	10000000	181.089	181.09	n/a
VV	45	2.12	-65	3	10000000	34.780	34.78	n/a
VV	45	2.12	-80	3	10000000	1.647	1.65	n/a
ββ	45	1.4	70	3	10000000	0.000	0.00	n/a
ββ	45	1.4	55	3	10000000	0.000	0.00	n/a
ββ	45	1.4	40	3	10000000	0.000	0.00	n/a
ββ	45	1.4	25	3	10000000	0.006	0.01	n/a
ββ	45	1.4	10	3	10000000	1.164	1.16	n/a
ββ	45	1.4	-5	3	10000000	60.493	60.49	n/a
ββ	45	1.4	-20	3	10000000	774.950	774.95	n/a

ββ	45	1.4	-35	3	10000000	2447.917	2447.92	n/a
ββ	45	1.4	-50	3	10000000	1906.678	1906.68	n/a
ββ	45	1.4	-65	3	10000000	366.198	366.20	n/a
ββ	45	1.4	-80	3	10000000	17.342	17.34	n/a
δδ	45	1.4	-95	3	10000000	0.203	0.20	n/a
δδ	-45	1.4	70	3	10000000	0.000	0.00	n/a
δδ	-45	1.4	55	3	10000000	0.000	0.00	n/a
δδ	-45	1.4	40	3	10000000	0.000	0.00	n/a
δδ	-45	1.4	25	3	10000000	0.006	0.01	n/a
δδ	-45	1.4	10	3	10000000	1.164	1.16	n/a
δδ	-45	1.4	-5	3	10000000	60.493	60.49	n/a
AA	0	0.5	55	4	10000000	48.655	48.65	n/a
AA	0	0.5	25	4	10000000	652.557	652.56	n/a
AA	0	0.5	-5	4	10000000	3502.591	3502.59	n/a
AA	0	0.5	-35	4	10000000	7523.805	7523.80	n/a
AA	0	0.5	-65	4	10000000	6467.894	6467.89	n/a
AA	0	0.5	-95	4	10000000	2225.182	2225.18	n/a
BB	0	1	55	4	10000000	9.545	9.54	n/a
BB	0	1	25	4	10000000	128.017	128.02	n/a
BB	0	1	-5	4	10000000	687.130	687.13	n/a
BB	0	1	-35	4	10000000	1476.002	1476.00	n/a
BB	0	1	-65	4	10000000	1268.856	1268.86	n/a
BB	0	1	-95	4	10000000	436.531	436.53	n/a
CC	0	1.5	55	4	10000000	0.632	0.63	n/a
CC	0	1.5	25	4	10000000	8.479	8.48	n/a
CC	0	1.5	-5	4	10000000	45.512	45.51	n/a
CC	0	1.5	-35	4	10000000	97.762	97.76	n/a
DD	27	0.5	55	4	10000000	48.655	48.65	n/a
DD	27	0.5	25	4	10000000	652.557	652.56	n/a
DD	27	0.5	-5	4	10000000	3502.591	3502.59	n/a
DD	27	0.5	-35	4	10000000	7523.805	7523.80	n/a
DD	27	0.5	-65	4	10000000	6467.894	6467.89	n/a
DD	27	0.5	-95	4	10000000	2225.182	2225.18	n/a
EE	27	1	55	4	10000000	9.545	9.54	n/a
EE	27	1	25	4	10000000	128.017	128.02	n/a
EE	27	1	-5	4	10000000	687.130	687.13	n/a
EE	27	1	-35	4	10000000	1476.002	1476.00	n/a
EE	27	1	-65	4	10000000	1268.856	1268.86	n/a
FF	27	1	-95	4	10000000	436.531	436.53	n/a
FF	27	1.5	55	4	10000000	0.632	0.63	n/a
FF	27	1.5	25	4	10000000	8.479	8.48	n/a
FF	27	1.5	-5	4	10000000	45.512	45.51	n/a
FF	27	1.5	-35	4	10000000	97.762	97.76	n/a
GG	-27	0.5	55	4	0.00	48.655	0.00	1.988155244
GG	-27	0.5	25	4	0.00	652.557	0.00	3.115648689
GG	-27	0.5	-5	4	3686.33	3502.591	3686.33	0.97278367
GG	-27	0.5	-35	4	6030.67	7523.805	6030.67	2.517147359
GG	-27	0.5	-65	4	5933.67	6467.894	5933.67	1.663005895
GG	-27	0.5	-95	4	1716.50	2225.182	1716.50	2.118241528
HH	-27	1	55	4	2.50	9.545	2.50	0.915982986
HH	-27	1	25	4	1.00	128.017	1.00	2.398107357
HH	-27	1	-5	4	7.67	687.130	7.67	3.1235044
HH	-27	1	-35	4	649.33	1476.002	649.33	2.808265798
HH	-27	1	-65	4	553.67	1268.856	553.67	2.749199384
HH	-27	1	-95	4	933.50	436.531	933.50	2.556958135
II	-27	1.5	55	4	0.00	0.632	0.00	0.101887343
II	-27	1.5	25	4	1.00	8.479	1.00	1.071962992
II	-27	1.5	-5	4	2.67	45.512	2.67	1.881977113
II	-27	1.5	-35	4	2.33	97.762	2.33	2.259973382
II	-27	1.5	-65	4	21.33	84.042	21.33	1.87294356
II	-27	1.5	-95	4	1.00	28.913	1.00	1.716788058
JJ	53	0.5	55	4	10000000	48.655	48.65	n/a
JJ	53	0.5	25	4	10000000	652.557	652.56	n/a
KK	53	1	55	4	10000000	9.545	9.54	n/a
KK	53	1	25	4	10000000	128.017	128.02	n/a
KK	53	1	-5	4	10000000	687.130	687.13	n/a
KK	53	1	-35	4	10000000	1476.002	1476.00	n/a
KK	53	1	-65	4	10000000	1268.856	1268.86	n/a
KK	53	1	-95	4	10000000	436.531	436.53	n/a
LL	53	1.5	55	4	10000000	0.632	0.63	n/a
LL	53	1.5	25	4	10000000	8.479	8.48	n/a

LL	53	1.5	-5	4	10000000	45.512	45.51	n/a
LL	53	1.5	-35	4	10000000	97.762	97.76	n/a
LL	53	1.5	-65	4	10000000	84.042	84.04	n/a
LL	53	1.5	-95	4	10000000	28.913	28.91	n/a
MM	53	2	55	4	10000000	0.014	0.01	n/a
MM	53	2	25	4	10000000	0.190	0.19	n/a
MM	53	2	-5	4	10000000	1.018	1.02	n/a
MM	53	2	-35	4	10000000	2.186	2.19	n/a
MM	53	2	-65	4	10000000	1.879	1.88	n/a
MM	53	2	-95	4	10000000	0.647	0.65	n/a
PP	-19	1.57	55	4	10000000	0.396	0.40	n/a
PP	-19	1.57	25	4	10000000	5.317	5.32	n/a
PP	-19	1.57	-5	4	10000000	28.539	28.54	n/a
PP	-19	1.57	-35	4	10000000	61.304	61.30	n/a
PP	-19	1.57	-65	4	10000000	52.701	52.70	n/a
PP	-19	1.57	-95	4	10000000	18.131	18.13	n/a
QQ	19	1.57	55	4	10000000	0.396	0.40	n/a
QQ	19	1.57	25	4	10000000	5.317	5.32	n/a
QQ	19	1.57	-5	4	10000000	28.539	28.54	n/a
QQ	19	1.57	-35	4	10000000	61.304	61.30	n/a
QQ	19	1.57	-65	4	10000000	52.701	52.70	n/a
QQ	19	1.57	-95	4	10000000	18.131	18.13	n/a
NN	-70	1.47	55	4	10000000	0.767	0.77	n/a
NN	-70	1.47	25	4	10000000	10.289	10.29	n/a
NN	-70	1.47	-5	4	10000000	55.227	55.23	n/a
NN	-70	1.47	-35	4	10000000	118.632	118.63	n/a
NN	-70	1.47	-65	4	10000000	101.983	101.98	n/a
NN	-70	1.47	-95	4	10000000	35.086	35.09	n/a
OO	70	1.47	55	4	10000000	0.767	0.77	n/a
OO	70	1.47	25	4	10000000	10.289	10.29	n/a
OO	70	1.47	-5	4	10000000	55.227	55.23	n/a
OO	70	1.47	-35	4	10000000	118.632	118.63	n/a
OO	70	1.47	-65	4	10000000	101.983	101.98	n/a
OO	70	1.47	-95	4	10000000	35.086	35.09	n/a
WW	-53	0.5	55	4	10000000	48.655	48.65	n/a
WW	-53	0.5	25	4	10000000	652.557	652.56	n/a
XX	-53	1	55	4	10000000	9.545	9.54	n/a
XX	-53	1	25	4	10000000	128.017	128.02	n/a
XX	-53	1	-5	4	10000000	687.130	687.13	n/a
XX	-53	1	-35	4	10000000	1476.002	1476.00	n/a
XX	-53	1	-65	4	10000000	1268.856	1268.86	n/a
XX	-53	1	-95	4	10000000	436.531	436.53	n/a
YY	-53	1.5	55	4	10000000	0.632	0.63	n/a
YY	-53	1.5	25	4	10000000	8.479	8.48	n/a
YY	-53	1.5	-5	4	10000000	45.512	45.51	n/a
RR	76	0.8	70	4	10000000	4.040	4.04	n/a
RR	76	0.8	55	4	10000000	20.859	20.86	n/a
RR	76	0.8	40	4	10000000	85.657	85.66	n/a
RR	76	0.8	25	4	10000000	279.767	279.77	n/a
RR	76	0.8	10	4	10000000	726.770	726.77	n/a
RR	76	0.8	-5	4	10000000	1501.645	1501.64	n/a
RR	76	0.8	-20	4	10000000	2467.781	2467.78	n/a
RR	76	0.8	-35	4	10000000	3225.635	3225.64	n/a
RR	76	0.8	-50	4	10000000	3353.461	3353.46	n/a
RR	76	0.8	-65	4	10000000	2772.941	2772.94	n/a
RR	76	0.8	-80	4	10000000	1823.717	1823.72	n/a
RR	76	0.8	-95	4	10000000	953.989	953.99	n/a
SS	0	0.8	70	4	10000000	4.040	4.04	n/a
SS	0	0.8	55	4	10000000	20.859	20.86	n/a
SS	0	0.8	40	4	10000000	85.657	85.66	n/a
SS	0	0.8	25	4	10000000	279.767	279.77	n/a
SS	0	0.8	10	4	10000000	726.770	726.77	n/a
SS	0	0.8	-5	4	10000000	1501.645	1501.64	n/a
SS	0	0.8	-20	4	10000000	2467.781	2467.78	n/a
SS	0	0.8	-35	4	10000000	3225.635	3225.64	n/a
SS	0	0.8	-50	4	10000000	3353.461	3353.46	n/a
SS	0	0.8	-65	4	10000000	2772.941	2772.94	n/a
SS	0	0.8	-80	4	10000000	1823.717	1823.72	n/a
SS	0	0.8	-95	4	10000000	953.989	953.99	n/a
TT	-76	0.8	70	4	10000000	4.040	4.04	n/a
TT	-76	0.8	55	4	10000000	20.859	20.86	n/a

TT	-76	0.8	40	4	10000000	85.657	85.66	n/a
TT	-76	0.8	25	4	10000000	279.767	279.77	n/a
TT	-76	0.8	10	4	10000000	726.770	726.77	n/a
TT	-76	0.8	-5	4	10000000	1501.645	1501.64	n/a
TT	-76	0.8	-20	4	10000000	2467.781	2467.78	n/a
TT	-76	0.8	-35	4	10000000	3225.635	3225.64	n/a
TT	-76	0.8	-50	4	10000000	3353.461	3353.46	n/a
TT	-76	0.8	-65	4	10000000	2772.941	2772.94	n/a
TT	-76	0.8	-80	4	10000000	1823.717	1823.72	n/a
TT	-76	0.8	-95	4	10000000	953.989	953.99	n/a
UU	-45	2.12	70	4	10000000	0.001	0.00	n/a
UU	-45	2.12	55	4	10000000	0.005	0.00	n/a
UU	-45	2.12	40	4	10000000	0.020	0.02	n/a
UU	-45	2.12	25	4	10000000	0.065	0.06	n/a
UU	-45	2.12	10	4	10000000	0.168	0.17	n/a
UU	-45	2.12	-5	4	10000000	0.348	0.35	n/a
UU	-45	2.12	-20	4	10000000	0.572	0.57	n/a
UU	-45	2.12	-35	4	10000000	0.747	0.75	n/a
UU	-45	2.12	-50	4	10000000	0.777	0.78	n/a
UU	-45	2.12	-65	4	10000000	0.642	0.64	n/a
VV	45	2.12	-95	4	10000000	0.221	0.22	n/a
VV	45	2.12	70	4	10000000	0.001	0.00	n/a
VV	45	2.12	55	4	10000000	0.005	0.00	n/a
VV	45	2.12	40	4	10000000	0.020	0.02	n/a
VV	45	2.12	25	4	10000000	0.065	0.06	n/a
VV	45	2.12	10	4	10000000	0.168	0.17	n/a
VV	45	2.12	-5	4	10000000	0.348	0.35	n/a
VV	45	2.12	-20	4	10000000	0.572	0.57	n/a
VV	45	2.12	-35	4	10000000	0.747	0.75	n/a
VV	45	2.12	-50	4	10000000	0.777	0.78	n/a
VV	45	2.12	-65	4	10000000	0.642	0.64	n/a
VV	45	2.12	-80	4	10000000	0.422	0.42	n/a
ββ	45	1.4	70	4	10000000	0.230	0.23	n/a
ββ	45	1.4	55	4	10000000	1.187	1.19	n/a
ββ	45	1.4	40	4	10000000	4.873	4.87	n/a
ββ	45	1.4	25	4	10000000	15.917	15.92	n/a
ββ	45	1.4	10	4	10000000	41.349	41.35	n/a
ββ	45	1.4	-5	4	10000000	85.434	85.43	n/a
ββ	45	1.4	-20	4	10000000	140.401	140.40	n/a
ββ	45	1.4	-35	4	10000000	183.518	183.52	n/a
ββ	45	1.4	-50	4	10000000	190.790	190.79	n/a
ββ	45	1.4	-65	4	10000000	157.763	157.76	n/a
ββ	45	1.4	-80	4	10000000	103.758	103.76	n/a
δδ	45	1.4	-95	4	10000000	54.276	54.28	n/a
δδ	-45	1.4	70	4	10000000	0.230	0.23	n/a
δδ	-45	1.4	55	4	10000000	1.187	1.19	n/a
δδ	-45	1.4	40	4	10000000	4.873	4.87	n/a
δδ	-45	1.4	25	4	10000000	15.917	15.92	n/a
δδ	-45	1.4	10	4	10000000	41.349	41.35	n/a
δδ	-45	1.4	-5	4	10000000	85.434	85.43	n/a
AA	0	0.5	55	7	10000000	0.000	0.00	n/a
AA	0	0.5	25	7	10000000	0.258	0.26	n/a
AA	0	0.5	-5	7	10000000	52.357	52.36	n/a
AA	0	0.5	-35	7	10000000	1115.814	1115.81	n/a
AA	0	0.5	-65	7	10000000	2495.848	2495.85	n/a
AA	0	0.5	-95	7	10000000	585.963	585.96	n/a
BB	0	1	55	7	10000000	0.000	0.00	n/a
BB	0	1	25	7	10000000	0.307	0.31	n/a
BB	0	1	-5	7	10000000	56.599	56.60	n/a
BB	0	1	-35	7	10000000	956.548	956.55	n/a
BB	0	1	-65	7	10000000	1499.861	1499.86	n/a
BB	0	1	-95	7	10000000	223.966	223.97	n/a
CC	0	1.5	55	7	10000000	0.001	0.00	n/a
CC	0	1.5	25	7	10000000	1.561	1.56	n/a
CC	0	1.5	-5	7	10000000	285.259	285.26	n/a
CC	0	1.5	-35	7	10000000	4711.652	4711.65	n/a
DD	27	0.5	55	7	10000000	0.000	0.00	n/a
DD	27	0.5	25	7	10000000	0.258	0.26	n/a
DD	27	0.5	-5	7	10000000	52.357	52.36	n/a
DD	27	0.5	-35	7	10000000	1115.814	1115.81	n/a
DD	27	0.5	-65	7	10000000	2495.848	2495.85	n/a

DD	27	0.5	-95	7	10000000	585.963	585.96	n/a
EE	27	1	55	7	10000000	0.000	0.00	n/a
EE	27	1	25	7	10000000	0.307	0.31	n/a
EE	27	1	-5	7	10000000	56.599	56.60	n/a
EE	27	1	-35	7	10000000	956.548	956.55	n/a
EE	27	1	-65	7	10000000	1499.861	1499.86	n/a
FF	27	1	-95	7	10000000	223.966	223.97	n/a
FF	27	1.5	55	7	10000000	0.001	0.00	n/a
FF	27	1.5	25	7	10000000	1.561	1.56	n/a
FF	27	1.5	-5	7	10000000	285.259	285.26	n/a
FF	27	1.5	-35	7	10000000	4711.652	4711.65	n/a
GG	-27	0.5	55	7	10000000	0.000	0.00	n/a
GG	-27	0.5	25	7	10000000	0.258	0.26	n/a
GG	-27	0.5	-5	7	10000000	52.357	52.36	n/a
GG	-27	0.5	-35	7	10000000	1115.814	1115.81	n/a
GG	-27	0.5	-65	7	10000000	2495.848	2495.85	n/a
GG	-27	0.5	-95	7	10000000	585.963	585.96	n/a
HH	-27	1	55	7	10000000	0.000	0.00	n/a
HH	-27	1	25	7	10000000	0.307	0.31	n/a
HH	-27	1	-5	7	10000000	56.599	56.60	n/a
HH	-27	1	-35	7	10000000	956.548	956.55	n/a
HH	-27	1	-65	7	10000000	1499.861	1499.86	n/a
HH	-27	1	-95	7	10000000	223.966	223.97	n/a
II	-27	1.5	55	7	10000000	0.001	0.00	n/a
II	-27	1.5	25	7	10000000	1.561	1.56	n/a
II	-27	1.5	-5	7	10000000	285.259	285.26	n/a
II	-27	1.5	-35	7	10000000	4711.652	4711.65	n/a
II	-27	1.5	-65	7	10000000	7034.519	7034.52	n/a
II	-27	1.5	-95	7	10000000	949.453	949.45	n/a
JJ	53	0.5	55	7	0.00	0.000	0.00	0
JJ	53	0.5	25	7	0.00	0.258	0.00	0
KK	53	1	55	7	0.00	0.000	0.00	0
KK	53	1	25	7	0.00	0.307	0.00	0
KK	53	1	-5	7	0.00	56.599	0.00	2.053838368
KK	53	1	-35	7	2280.33	956.548	2280.33	3.034538399
KK	53	1	-65	7	1668.00	1499.861	1668.00	1.251600275
KK	53	1	-95	7	467.17	223.966	467.17	2.233396225
LL	53	1.5	55	7	9.33	0.001	9.33	1.270958986
LL	53	1.5	25	7	0.00	1.561	0.00	0.494442734
LL	53	1.5	-5	7	0.00	285.259	0.00	2.756268986
LL	53	1.5	-35	7	4802.33	4711.652	4802.33	0.237705397
LL	53	1.5	-65	7	7244.00	7034.519	7244.00	0.788637079
LL	53	1.5	-95	7	991.83	949.453	991.83	0.267262169
MM	53	2	55	7	50.67	0.000	50.67	2.005751954
MM	53	2	25	7	0.00	0.030	0.00	0
MM	53	2	-5	7	2.67	5.392	2.67	0.265611456
MM	53	2	-35	7	15.33	89.055	15.33	2.017567276
MM	53	2	-65	7	13.67	132.940	13.67	2.287964286
MM	53	2	-95	7	0.00	17.937	0.00	1.554787555
PP	-19	1.57	55	7	10000000	0.001	0.00	n/a
PP	-19	1.57	25	7	10000000	1.260	1.26	n/a
PP	-19	1.57	-5	7	10000000	230.213	230.21	n/a
PP	-19	1.57	-35	7	10000000	3802.347	3802.35	n/a
PP	-19	1.57	-65	7	10000000	5676.543	5676.54	n/a
PP	-19	1.57	-95	7	10000000	766.052	766.05	n/a
QQ	19	1.57	55	7	10000000	0.001	0.00	n/a
QQ	19	1.57	25	7	10000000	1.260	1.26	n/a
QQ	19	1.57	-5	7	10000000	230.213	230.21	n/a
QQ	19	1.57	-35	7	10000000	3802.347	3802.35	n/a
QQ	19	1.57	-65	7	10000000	5676.543	5676.54	n/a
QQ	19	1.57	-95	7	10000000	766.052	766.05	n/a
NN	-70	1.47	55	7	10000000	0.001	0.00	n/a
NN	-70	1.47	25	7	10000000	1.654	1.65	n/a
NN	-70	1.47	-5	7	10000000	302.261	302.26	n/a
NN	-70	1.47	-35	7	10000000	4992.581	4992.58	n/a
NN	-70	1.47	-65	7	10000000	7454.286	7454.29	n/a
NN	-70	1.47	-95	7	10000000	1006.211	1006.21	n/a
OO	70	1.47	55	7	10000000	0.001	0.00	n/a
OO	70	1.47	25	7	10000000	1.654	1.65	n/a
OO	70	1.47	-5	7	10000000	302.261	302.26	n/a
OO	70	1.47	-35	7	10000000	4992.581	4992.58	n/a

OO	70	1.47	-65	7	10000000	7454.286	7454.29	n/a
OO	70	1.47	-95	7	10000000	1006.211	1006.21	n/a
WW	-53	0.5	55	7	10000000	0.000	0.00	n/a
WW	-53	0.5	25	7	10000000	0.258	0.26	n/a
XX	-53	1	55	7	10000000	0.000	0.00	n/a
XX	-53	1	25	7	10000000	0.307	0.31	n/a
XX	-53	1	-5	7	10000000	56.599	56.60	n/a
XX	-53	1	-35	7	10000000	956.548	956.55	n/a
XX	-53	1	-65	7	10000000	1499.861	1499.86	n/a
XX	-53	1	-95	7	10000000	223.966	223.97	n/a
YY	-53	1.5	55	7	10000000	0.001	0.00	n/a
YY	-53	1.5	25	7	10000000	1.561	1.56	n/a
YY	-53	1.5	-5	7	10000000	285.259	285.26	n/a
RR	76	0.8	70	7	10000000	0.000	0.00	n/a
RR	76	0.8	55	7	10000000	0.000	0.00	n/a
RR	76	0.8	40	7	10000000	0.003	0.00	n/a
RR	76	0.8	25	7	10000000	0.102	0.10	n/a
RR	76	0.8	10	7	10000000	1.903	1.90	n/a
RR	76	0.8	-5	7	10000000	20.063	20.06	n/a
RR	76	0.8	-20	7	10000000	119.371	119.37	n/a
RR	76	0.8	-35	7	10000000	401.762	401.76	n/a
RR	76	0.8	-50	7	10000000	766.896	766.90	n/a
RR	76	0.8	-65	7	10000000	832.516	832.52	n/a
RR	76	0.8	-80	7	10000000	515.275	515.27	n/a
RR	76	0.8	-95	7	10000000	182.203	182.20	n/a
SS	0	0.8	70	7	10000000	0.000	0.00	n/a
SS	0	0.8	55	7	10000000	0.000	0.00	n/a
SS	0	0.8	40	7	10000000	0.003	0.00	n/a
SS	0	0.8	25	7	10000000	0.102	0.10	n/a
SS	0	0.8	10	7	10000000	1.903	1.90	n/a
SS	0	0.8	-5	7	10000000	20.063	20.06	n/a
SS	0	0.8	-20	7	10000000	119.371	119.37	n/a
SS	0	0.8	-35	7	10000000	401.762	401.76	n/a
SS	0	0.8	-50	7	10000000	766.896	766.90	n/a
SS	0	0.8	-65	7	10000000	832.516	832.52	n/a
SS	0	0.8	-80	7	10000000	515.275	515.27	n/a
SS	0	0.8	-95	7	10000000	182.203	182.20	n/a
TT	-76	0.8	70	7	10000000	0.000	0.00	n/a
TT	-76	0.8	55	7	10000000	0.000	0.00	n/a
TT	-76	0.8	40	7	10000000	0.003	0.00	n/a
TT	-76	0.8	25	7	10000000	0.102	0.10	n/a
TT	-76	0.8	10	7	10000000	1.903	1.90	n/a
TT	-76	0.8	-5	7	10000000	20.063	20.06	n/a
TT	-76	0.8	-20	7	10000000	119.371	119.37	n/a
TT	-76	0.8	-35	7	10000000	401.762	401.76	n/a
TT	-76	0.8	-50	7	10000000	766.896	766.90	n/a
TT	-76	0.8	-65	7	10000000	832.516	832.52	n/a
TT	-76	0.8	-80	7	10000000	515.275	515.27	n/a
TT	-76	0.8	-95	7	10000000	182.203	182.20	n/a
UU	-45	2.12	70	7	10000000	0.000	0.00	n/a
UU	-45	2.12	55	7	10000000	0.000	0.00	n/a
UU	-45	2.12	40	7	10000000	0.000	0.00	n/a
UU	-45	2.12	25	7	10000000	0.005	0.00	n/a
UU	-45	2.12	10	7	10000000	0.089	0.09	n/a
UU	-45	2.12	-5	7	10000000	0.895	0.89	n/a
UU	-45	2.12	-20	7	10000000	4.912	4.91	n/a
UU	-45	2.12	-35	7	10000000	14.781	14.78	n/a
UU	-45	2.12	-50	7	10000000	24.389	24.39	n/a
UU	-45	2.12	-65	7	10000000	22.065	22.07	n/a
VV	45	2.12	-95	7	10000000	2.977	2.98	n/a
VV	45	2.12	70	7	10000000	0.000	0.00	n/a
VV	45	2.12	55	7	10000000	0.000	0.00	n/a
VV	45	2.12	40	7	10000000	0.000	0.00	n/a
VV	45	2.12	25	7	10000000	0.005	0.00	n/a
VV	45	2.12	10	7	10000000	0.089	0.09	n/a
VV	45	2.12	-5	7	10000000	0.895	0.89	n/a
VV	45	2.12	-20	7	10000000	4.912	4.91	n/a
VV	45	2.12	-35	7	10000000	14.781	14.78	n/a
VV	45	2.12	-50	7	10000000	24.389	24.39	n/a
VV	45	2.12	-65	7	10000000	22.065	22.07	n/a
VV	45	2.12	-80	7	10000000	10.946	10.95	n/a

ββ	45	1.4	70	7	10000000	0.000	0.00	n/a
ββ	45	1.4	55	7	10000000	0.001	0.00	n/a
ββ	45	1.4	40	7	10000000	0.053	0.05	n/a
ββ	45	1.4	25	7	10000000	1.749	1.75	n/a
ββ	45	1.4	10	7	10000000	31.930	31.93	n/a
ββ	45	1.4	-5	7	10000000	319.618	319.62	n/a
ββ	45	1.4	-20	7	10000000	1754.290	1754.29	n/a
ββ	45	1.4	-35	7	10000000	5279.702	5279.70	n/a
ββ	45	1.4	-50	7	10000000	8712.878	8712.88	n/a
ββ	45	1.4	-65	7	10000000	7884.397	7884.40	n/a
ββ	45	1.4	-80	7	10000000	3912.434	3912.43	n/a
δδ	45	1.4	-95	7	10000000	1064.695	1064.70	n/a
δδ	-45	1.4	70	7	10000000	0.000	0.00	n/a
δδ	-45	1.4	55	7	10000000	0.001	0.00	n/a
δδ	-45	1.4	40	7	10000000	0.053	0.05	n/a
δδ	-45	1.4	25	7	10000000	1.749	1.75	n/a
δδ	-45	1.4	10	7	10000000	31.930	31.93	n/a
δδ	-45	1.4	-5	7	10000000	319.618	319.62	n/a
AA	0	0.5	55	8	10000000	0.000	0.00	n/a
AA	0	0.5	25	8	10000000	0.221	0.22	n/a
AA	0	0.5	-5	8	10000000	49.001	49.00	n/a
AA	0	0.5	-35	8	10000000	1072.667	1072.67	n/a
AA	0	0.5	-65	8	10000000	2319.957	2319.96	n/a
AA	0	0.5	-95	8	10000000	495.745	495.74	n/a
BB	0	1	55	8	10000000	0.000	0.00	n/a
BB	0	1	25	8	10000000	0.304	0.30	n/a
BB	0	1	-5	8	10000000	56.245	56.25	n/a
BB	0	1	-35	8	10000000	951.436	951.44	n/a
BB	0	1	-65	8	10000000	1481.645	1481.64	n/a
BB	0	1	-95	8	10000000	215.511	215.51	n/a
CC	0	1.5	55	8	10000000	0.001	0.00	n/a
CC	0	1.5	25	8	10000000	1.561	1.56	n/a
CC	0	1.5	-5	8	10000000	285.251	285.25	n/a
CC	0	1.5	-35	8	10000000	4711.527	4711.53	n/a
DD	27	0.5	55	8	10000000	0.000	0.00	n/a
DD	27	0.5	25	8	10000000	0.221	0.22	n/a
DD	27	0.5	-5	8	10000000	49.001	49.00	n/a
DD	27	0.5	-35	8	10000000	1072.667	1072.67	n/a
DD	27	0.5	-65	8	10000000	2319.957	2319.96	n/a
DD	27	0.5	-95	8	10000000	495.745	495.74	n/a
EE	27	1	55	8	10000000	0.000	0.00	n/a
EE	27	1	25	8	10000000	0.304	0.30	n/a
EE	27	1	-5	8	10000000	56.245	56.25	n/a
EE	27	1	-35	8	10000000	951.436	951.44	n/a
EE	27	1	-65	8	10000000	1481.645	1481.64	n/a
FF	27	1	-95	8	10000000	215.511	215.51	n/a
FF	27	1.5	55	8	10000000	0.001	0.00	n/a
FF	27	1.5	25	8	10000000	1.561	1.56	n/a
FF	27	1.5	-5	8	10000000	285.251	285.25	n/a
FF	27	1.5	-35	8	10000000	4711.527	4711.53	n/a
GG	-27	0.5	55	8	10000000	0.000	0.00	n/a
GG	-27	0.5	25	8	10000000	0.221	0.22	n/a
GG	-27	0.5	-5	8	10000000	49.001	49.00	n/a
GG	-27	0.5	-35	8	10000000	1072.667	1072.67	n/a
GG	-27	0.5	-65	8	10000000	2319.957	2319.96	n/a
GG	-27	0.5	-95	8	10000000	495.745	495.74	n/a
HH	-27	1	55	8	10000000	0.000	0.00	n/a
HH	-27	1	25	8	10000000	0.304	0.30	n/a
HH	-27	1	-5	8	10000000	56.245	56.25	n/a
HH	-27	1	-35	8	10000000	951.436	951.44	n/a
HH	-27	1	-65	8	10000000	1481.645	1481.64	n/a
HH	-27	1	-95	8	10000000	215.511	215.51	n/a
II	-27	1.5	55	8	10000000	0.001	0.00	n/a
II	-27	1.5	25	8	10000000	1.561	1.56	n/a
II	-27	1.5	-5	8	10000000	285.251	285.25	n/a
II	-27	1.5	-35	8	10000000	4711.527	4711.53	n/a
II	-27	1.5	-65	8	10000000	7034.127	7034.13	n/a
II	-27	1.5	-95	8	10000000	949.292	949.29	n/a
JJ	53	0.5	55	8	10000000	0.000	0.00	n/a
JJ	53	0.5	25	8	10000000	0.221	0.22	n/a
KK	53	1	55	8	10000000	0.000	0.00	n/a

KK	53	1	25	8	10000000	0.304	0.30	n/a
KK	53	1	-5	8	10000000	56.245	56.25	n/a
KK	53	1	-35	8	10000000	951.436	951.44	n/a
KK	53	1	-65	8	10000000	1481.645	1481.64	n/a
KK	53	1	-95	8	10000000	215.511	215.51	n/a
LL	53	1.5	55	8	10000000	0.001	0.00	n/a
LL	53	1.5	25	8	10000000	1.561	1.56	n/a
LL	53	1.5	-5	8	10000000	285.251	285.25	n/a
LL	53	1.5	-35	8	10000000	4711.527	4711.53	n/a
LL	53	1.5	-65	8	10000000	7034.127	7034.13	n/a
LL	53	1.5	-95	8	10000000	949.292	949.29	n/a
MM	53	2	55	8	10000000	0.000	0.00	n/a
MM	53	2	25	8	10000000	0.030	0.03	n/a
MM	53	2	-5	8	10000000	5.392	5.39	n/a
MM	53	2	-35	8	10000000	89.054	89.05	n/a
MM	53	2	-65	8	10000000	132.939	132.94	n/a
MM	53	2	-95	8	10000000	17.937	17.94	n/a
PP	-19	1.57	55	8	0.00	0.001	0.00	0
PP	-19	1.57	25	8	0.00	1.260	0.00	0.401327348
PP	-19	1.57	-5	8	163.75	230.209	163.75	1.350692196
PP	-19	1.57	-35	8	2025.33	3802.282	2025.33	3.034888932
PP	-19	1.57	-65	8	4244.67	5676.342	4244.67	2.616163036
PP	-19	1.57	-95	8	464.17	765.971	464.17	2.17052724
QQ	19	1.57	55	8	6.33	0.001	6.33	1.102534155
QQ	19	1.57	25	8	0.00	1.260	0.00	0.401327348
QQ	19	1.57	-5	8	5.00	230.209	5.00	2.634748489
QQ	19	1.57	-35	8	4446.33	3802.282	4446.33	2.002489742
QQ	19	1.57	-65	8	1199.20	5676.342	1199.20	3.765724744
QQ	19	1.57	-95	8	1661.33	765.971	1661.33	2.819903396
NN	-70	1.47	55	8	10000000	0.001	0.00	n/a
NN	-70	1.47	25	8	10000000	1.654	1.65	n/a
NN	-70	1.47	-5	8	10000000	302.251	302.25	n/a
NN	-70	1.47	-35	8	10000000	4992.417	4992.42	n/a
NN	-70	1.47	-65	8	10000000	7453.770	7453.77	n/a
NN	-70	1.47	-95	8	10000000	1005.998	1006.00	n/a
OO	70	1.47	55	8	10000000	0.001	0.00	n/a
OO	70	1.47	25	8	10000000	1.654	1.65	n/a
OO	70	1.47	-5	8	10000000	302.251	302.25	n/a
OO	70	1.47	-35	8	10000000	4992.417	4992.42	n/a
OO	70	1.47	-65	8	10000000	7453.770	7453.77	n/a
OO	70	1.47	-95	8	10000000	1005.998	1006.00	n/a
WW	-53	0.5	55	8	10000000	0.000	0.00	n/a
WW	-53	0.5	25	8	10000000	0.221	0.22	n/a
XX	-53	1	55	8	10000000	0.000	0.00	n/a
XX	-53	1	25	8	10000000	0.304	0.30	n/a
XX	-53	1	-5	8	10000000	56.245	56.25	n/a
XX	-53	1	-35	8	10000000	951.436	951.44	n/a
XX	-53	1	-65	8	10000000	1481.645	1481.64	n/a
XX	-53	1	-95	8	10000000	215.511	215.51	n/a
YY	-53	1.5	55	8	10000000	0.001	0.00	n/a
YY	-53	1.5	25	8	10000000	1.561	1.56	n/a
YY	-53	1.5	-5	8	10000000	285.251	285.25	n/a
RR	76	0.8	70	8	10000000	0.000	0.00	n/a
RR	76	0.8	55	8	10000000	0.000	0.00	n/a
RR	76	0.8	40	8	10000000	0.003	0.00	n/a
RR	76	0.8	25	8	10000000	0.091	0.09	n/a
RR	76	0.8	10	8	10000000	1.761	1.76	n/a
RR	76	0.8	-5	8	10000000	19.016	19.02	n/a
RR	76	0.8	-20	8	10000000	114.734	114.73	n/a
RR	76	0.8	-35	8	10000000	387.349	387.35	n/a
RR	76	0.8	-50	8	10000000	732.868	732.87	n/a
RR	76	0.8	-65	8	10000000	778.190	778.19	n/a
RR	76	0.8	-80	8	10000000	464.330	464.33	n/a
RR	76	0.8	-95	8	10000000	155.836	155.84	n/a
SS	0	0.8	70	8	10000000	0.000	0.00	n/a
SS	0	0.8	55	8	10000000	0.000	0.00	n/a
SS	0	0.8	40	8	10000000	0.003	0.00	n/a
SS	0	0.8	25	8	10000000	0.091	0.09	n/a
SS	0	0.8	10	8	10000000	1.761	1.76	n/a
SS	0	0.8	-5	8	10000000	19.016	19.02	n/a
SS	0	0.8	-20	8	10000000	114.734	114.73	n/a

SS	0	0.8	-35	8	10000000	387.349	387.35	n/a
SS	0	0.8	-50	8	10000000	732.868	732.87	n/a
SS	0	0.8	-65	8	10000000	778.190	778.19	n/a
SS	0	0.8	-80	8	10000000	464.330	464.33	n/a
SS	0	0.8	-95	8	10000000	155.836	155.84	n/a
TT	-76	0.8	70	8	10000000	0.000	0.00	n/a
TT	-76	0.8	55	8	10000000	0.000	0.00	n/a
TT	-76	0.8	40	8	10000000	0.003	0.00	n/a
TT	-76	0.8	25	8	10000000	0.091	0.09	n/a
TT	-76	0.8	10	8	10000000	1.761	1.76	n/a
TT	-76	0.8	-5	8	10000000	19.016	19.02	n/a
TT	-76	0.8	-20	8	10000000	114.734	114.73	n/a
TT	-76	0.8	-35	8	10000000	387.349	387.35	n/a
TT	-76	0.8	-50	8	10000000	732.868	732.87	n/a
TT	-76	0.8	-65	8	10000000	778.190	778.19	n/a
TT	-76	0.8	-80	8	10000000	464.330	464.33	n/a
TT	-76	0.8	-95	8	10000000	155.836	155.84	n/a
UU	-45	2.12	70	8	10000000	0.000	0.00	n/a
UU	-45	2.12	55	8	10000000	0.000	0.00	n/a
UU	-45	2.12	40	8	10000000	0.000	0.00	n/a
UU	-45	2.12	25	8	10000000	0.005	0.00	n/a
UU	-45	2.12	10	8	10000000	0.089	0.09	n/a
UU	-45	2.12	-5	8	10000000	0.895	0.89	n/a
UU	-45	2.12	-20	8	10000000	4.912	4.91	n/a
UU	-45	2.12	-35	8	10000000	14.781	14.78	n/a
UU	-45	2.12	-50	8	10000000	24.389	24.39	n/a
UU	-45	2.12	-65	8	10000000	22.065	22.06	n/a
VV	45	2.12	-95	8	10000000	2.977	2.98	n/a
VV	45	2.12	70	8	10000000	0.000	0.00	n/a
VV	45	2.12	55	8	10000000	0.000	0.00	n/a
VV	45	2.12	40	8	10000000	0.000	0.00	n/a
VV	45	2.12	25	8	10000000	0.005	0.00	n/a
VV	45	2.12	10	8	10000000	0.089	0.09	n/a
VV	45	2.12	-5	8	10000000	0.895	0.89	n/a
VV	45	2.12	-20	8	10000000	4.912	4.91	n/a
VV	45	2.12	-35	8	10000000	14.781	14.78	n/a
VV	45	2.12	-50	8	10000000	24.389	24.39	n/a
VV	45	2.12	-65	8	10000000	22.065	22.06	n/a
VV	45	2.12	-80	8	10000000	10.945	10.95	n/a
ββ	45	1.4	70	8	10000000	0.000	0.00	n/a
ββ	45	1.4	55	8	10000000	0.001	0.00	n/a
ββ	45	1.4	40	8	10000000	0.053	0.05	n/a
ββ	45	1.4	25	8	10000000	1.749	1.75	n/a
ββ	45	1.4	10	8	10000000	31.927	31.93	n/a
ββ	45	1.4	-5	8	10000000	319.599	319.60	n/a
ββ	45	1.4	-20	8	10000000	1754.197	1754.20	n/a
ββ	45	1.4	-35	8	10000000	5279.403	5279.40	n/a
ββ	45	1.4	-50	8	10000000	8712.213	8712.21	n/a
ββ	45	1.4	-65	8	10000000	7883.437	7883.44	n/a
ββ	45	1.4	-80	8	10000000	3911.606	3911.61	n/a
δδ	45	1.4	-95	8	10000000	1064.291	1064.29	n/a
δδ	-45	1.4	70	8	10000000	0.000	0.00	n/a
δδ	-45	1.4	55	8	10000000	0.001	0.00	n/a
δδ	-45	1.4	40	8	10000000	0.053	0.05	n/a
δδ	-45	1.4	25	8	10000000	1.749	1.75	n/a
δδ	-45	1.4	10	8	10000000	31.927	31.93	n/a
δδ	-45	1.4	-5	8	10000000	319.599	319.60	n/a
AA	0	0.5	55	45	10000000	0.000	0.00	n/a
AA	0	0.5	25	45	10000000	0.201	0.20	n/a
AA	0	0.5	-5	45	10000000	47.040	47.04	n/a
AA	0	0.5	-35	45	10000000	1062.165	1062.17	n/a
AA	0	0.5	-65	45	10000000	2315.120	2315.12	n/a
AA	0	0.5	-95	45	10000000	487.098	487.10	n/a
BB	0	1	55	45	10000000	0.000	0.00	n/a
BB	0	1	25	45	10000000	0.302	0.30	n/a
BB	0	1	-5	45	10000000	56.057	56.06	n/a
BB	0	1	-35	45	10000000	950.060	950.06	n/a
BB	0	1	-65	45	10000000	1480.188	1480.19	n/a
BB	0	1	-95	45	10000000	214.552	214.55	n/a
CC	0	1.5	55	45	10000000	0.001	0.00	n/a
CC	0	1.5	25	45	10000000	1.561	1.56	n/a

CC	0	1.5	-5	45	10000000	285.247	285.25	n/a
CC	0	1.5	-35	45	10000000	4711.491	4711.49	n/a
DD	27	0.5	55	45	10000000	0.000	0.00	n/a
DD	27	0.5	25	45	10000000	0.201	0.20	n/a
DD	27	0.5	-5	45	10000000	47.040	47.04	n/a
DD	27	0.5	-35	45	10000000	1062.165	1062.17	n/a
DD	27	0.5	-65	45	10000000	2315.120	2315.12	n/a
DD	27	0.5	-95	45	10000000	487.098	487.10	n/a
EE	27	1	55	45	10000000	0.000	0.00	n/a
EE	27	1	25	45	10000000	0.302	0.30	n/a
EE	27	1	-5	45	10000000	56.057	56.06	n/a
EE	27	1	-35	45	10000000	950.060	950.06	n/a
EE	27	1	-65	45	10000000	1480.188	1480.19	n/a
FF	27	1	-95	45	10000000	214.552	214.55	n/a
FF	27	1.5	55	45	10000000	0.001	0.00	n/a
FF	27	1.5	25	45	10000000	1.561	1.56	n/a
FF	27	1.5	-5	45	10000000	285.247	285.25	n/a
FF	27	1.5	-35	45	10000000	4711.491	4711.49	n/a
GG	-27	0.5	55	45	10000000	0.000	0.00	n/a
GG	-27	0.5	25	45	10000000	0.201	0.20	n/a
GG	-27	0.5	-5	45	10000000	47.040	47.04	n/a
GG	-27	0.5	-35	45	10000000	1062.165	1062.17	n/a
GG	-27	0.5	-65	45	10000000	2315.120	2315.12	n/a
GG	-27	0.5	-95	45	10000000	487.098	487.10	n/a
HH	-27	1	55	45	10000000	0.000	0.00	n/a
HH	-27	1	25	45	10000000	0.302	0.30	n/a
HH	-27	1	-5	45	10000000	56.057	56.06	n/a
HH	-27	1	-35	45	10000000	950.060	950.06	n/a
HH	-27	1	-65	45	10000000	1480.188	1480.19	n/a
HH	-27	1	-95	45	10000000	214.552	214.55	n/a
II	-27	1.5	55	45	10000000	0.001	0.00	n/a
II	-27	1.5	25	45	10000000	1.561	1.56	n/a
II	-27	1.5	-5	45	10000000	285.247	285.25	n/a
II	-27	1.5	-35	45	10000000	4711.491	4711.49	n/a
II	-27	1.5	-65	45	10000000	7034.074	7034.07	n/a
II	-27	1.5	-95	45	10000000	949.270	949.27	n/a
JJ	53	0.5	55	45	10000000	0.000	0.00	n/a
JJ	53	0.5	25	45	10000000	0.201	0.20	n/a
KK	53	1	55	45	10000000	0.000	0.00	n/a
KK	53	1	25	45	10000000	0.302	0.30	n/a
KK	53	1	-5	45	10000000	56.057	56.06	n/a
KK	53	1	-35	45	10000000	950.060	950.06	n/a
KK	53	1	-65	45	10000000	1480.188	1480.19	n/a
KK	53	1	-95	45	10000000	214.552	214.55	n/a
LL	53	1.5	55	45	10000000	0.001	0.00	n/a
LL	53	1.5	25	45	10000000	1.561	1.56	n/a
LL	53	1.5	-5	45	10000000	285.247	285.25	n/a
LL	53	1.5	-35	45	10000000	4711.491	4711.49	n/a
LL	53	1.5	-65	45	10000000	7034.074	7034.07	n/a
LL	53	1.5	-95	45	10000000	949.270	949.27	n/a
MM	53	2	55	45	10000000	0.000	0.00	n/a
MM	53	2	25	45	10000000	0.030	0.03	n/a
MM	53	2	-5	45	10000000	5.392	5.39	n/a
MM	53	2	-35	45	10000000	89.054	89.05	n/a
MM	53	2	-65	45	10000000	132.938	132.94	n/a
MM	53	2	-95	45	10000000	17.937	17.94	n/a
PP	-19	1.57	55	45	10000000	0.001	0.00	n/a
PP	-19	1.57	25	45	10000000	1.260	1.26	n/a
PP	-19	1.57	-5	45	10000000	230.208	230.21	n/a
PP	-19	1.57	-35	45	10000000	3802.263	3802.26	n/a
PP	-19	1.57	-65	45	10000000	5676.313	5676.31	n/a
PP	-19	1.57	-95	45	10000000	765.960	765.96	n/a
QQ	19	1.57	55	45	10000000	0.001	0.00	n/a
QQ	19	1.57	25	45	10000000	1.260	1.26	n/a
QQ	19	1.57	-5	45	10000000	230.208	230.21	n/a
QQ	19	1.57	-35	45	10000000	3802.263	3802.26	n/a
QQ	19	1.57	-65	45	10000000	5676.313	5676.31	n/a
QQ	19	1.57	-95	45	10000000	765.960	765.96	n/a
NN	-70	1.47	55	45	0.00	0.001	0.00	0
NN	-70	1.47	25	45	32.00	1.654	32.00	1.738198961
NN	-70	1.47	-5	45	0.00	302.246	0.00	2.781390282

NN	-70	1.47	-35	45	800.83	4992.371	800.83	3.782857837
NN	-70	1.47	-65	45	1464.67	7453.702	1464.67	3.905458368
NN	-70	1.47	-95	45	673.33	1005.969	673.33	2.119838245
OO	70	1.47	55	45	6.33	0.001	6.33	1.102494053
OO	70	1.47	25	45	15.50	1.654	15.50	1.349319073
OO	70	1.47	-5	45	282.75	302.246	282.75	0.113759738
OO	70	1.47	-35	45	1390.40	4992.371	1390.40	3.60910108
OO	70	1.47	-65	45	1881.25	7453.702	1881.25	3.823010627
OO	70	1.47	-95	45	756.17	1005.969	756.17	1.850182965
WW	-53	0.5	55	45	10000000	0.000	0.00	n/a
WW	-53	0.5	25	45	10000000	0.201	0.20	n/a
XX	-53	1	55	45	10000000	0.000	0.00	n/a
XX	-53	1	25	45	10000000	0.302	0.30	n/a
XX	-53	1	-5	45	10000000	56.057	56.06	n/a
XX	-53	1	-35	45	10000000	950.060	950.06	n/a
XX	-53	1	-65	45	10000000	1480.188	1480.19	n/a
XX	-53	1	-95	45	10000000	214.552	214.55	n/a
YY	-53	1.5	55	45	10000000	0.001	0.00	n/a
YY	-53	1.5	25	45	10000000	1.561	1.56	n/a
YY	-53	1.5	-5	45	10000000	285.247	285.25	n/a
RR	76	0.8	70	45	10000000	0.000	0.00	n/a
RR	76	0.8	55	45	10000000	0.000	0.00	n/a
RR	76	0.8	40	45	10000000	0.002	0.00	n/a
RR	76	0.8	25	45	10000000	0.085	0.09	n/a
RR	76	0.8	10	45	10000000	1.681	1.68	n/a
RR	76	0.8	-5	45	10000000	18.435	18.43	n/a
RR	76	0.8	-20	45	10000000	112.615	112.61	n/a
RR	76	0.8	-35	45	10000000	383.615	383.62	n/a
RR	76	0.8	-50	45	10000000	729.473	729.47	n/a
RR	76	0.8	-65	45	10000000	775.074	775.07	n/a
RR	76	0.8	-80	45	10000000	460.489	460.49	n/a
RR	76	0.8	-95	45	10000000	153.058	153.06	n/a
SS	0	0.8	70	45	10000000	0.000	0.00	n/a
SS	0	0.8	55	45	10000000	0.000	0.00	n/a
SS	0	0.8	40	45	10000000	0.002	0.00	n/a
SS	0	0.8	25	45	10000000	0.085	0.09	n/a
SS	0	0.8	10	45	10000000	1.681	1.68	n/a
SS	0	0.8	-5	45	10000000	18.435	18.43	n/a
SS	0	0.8	-20	45	10000000	112.615	112.61	n/a
SS	0	0.8	-35	45	10000000	383.615	383.62	n/a
SS	0	0.8	-50	45	10000000	729.473	729.47	n/a
SS	0	0.8	-65	45	10000000	775.074	775.07	n/a
SS	0	0.8	-80	45	10000000	460.489	460.49	n/a
SS	0	0.8	-95	45	10000000	153.058	153.06	n/a
TT	-76	0.8	70	45	10000000	0.000	0.00	n/a
TT	-76	0.8	55	45	10000000	0.000	0.00	n/a
TT	-76	0.8	40	45	10000000	0.002	0.00	n/a
TT	-76	0.8	25	45	10000000	0.085	0.09	n/a
TT	-76	0.8	10	45	10000000	1.681	1.68	n/a
TT	-76	0.8	-5	45	10000000	18.435	18.43	n/a
TT	-76	0.8	-20	45	10000000	112.615	112.61	n/a
TT	-76	0.8	-35	45	10000000	383.615	383.62	n/a
TT	-76	0.8	-50	45	10000000	729.473	729.47	n/a
TT	-76	0.8	-65	45	10000000	775.074	775.07	n/a
TT	-76	0.8	-80	45	10000000	460.489	460.49	n/a
TT	-76	0.8	-95	45	10000000	153.058	153.06	n/a
UU	-45	2.12	70	45	10000000	0.000	0.00	n/a
UU	-45	2.12	55	45	10000000	0.000	0.00	n/a
UU	-45	2.12	40	45	10000000	0.000	0.00	n/a
UU	-45	2.12	25	45	10000000	0.005	0.00	n/a
UU	-45	2.12	10	45	10000000	0.089	0.09	n/a
UU	-45	2.12	-5	45	10000000	0.895	0.89	n/a
UU	-45	2.12	-20	45	10000000	4.912	4.91	n/a
UU	-45	2.12	-35	45	10000000	14.781	14.78	n/a
UU	-45	2.12	-50	45	10000000	24.389	24.39	n/a
UU	-45	2.12	-65	45	10000000	22.065	22.06	n/a
VV	45	2.12	-95	45	10000000	2.977	2.98	n/a
VV	45	2.12	70	45	10000000	0.000	0.00	n/a
VV	45	2.12	55	45	10000000	0.000	0.00	n/a
VV	45	2.12	40	45	10000000	0.000	0.00	n/a
VV	45	2.12	25	45	10000000	0.005	0.00	n/a

VV	45	2.12	10	45	10000000	0.089	0.09	n/a
VV	45	2.12	-5	45	10000000	0.895	0.89	n/a
VV	45	2.12	-20	45	10000000	4.912	4.91	n/a
VV	45	2.12	-35	45	10000000	14.781	14.78	n/a
VV	45	2.12	-50	45	10000000	24.389	24.39	n/a
VV	45	2.12	-65	45	10000000	22.065	22.06	n/a
VV	45	2.12	-80	45	10000000	10.945	10.95	n/a
ββ	45	1.4	70	45	10000000	0.000	0.00	n/a
ββ	45	1.4	55	45	10000000	0.001	0.00	n/a
ββ	45	1.4	40	45	10000000	0.053	0.05	n/a
ββ	45	1.4	25	45	10000000	1.749	1.75	n/a
ββ	45	1.4	10	45	10000000	31.926	31.93	n/a
ββ	45	1.4	-5	45	10000000	319.590	319.59	n/a
ββ	45	1.4	-20	45	10000000	1754.159	1754.16	n/a
ββ	45	1.4	-35	45	10000000	5279.318	5279.32	n/a
ββ	45	1.4	-50	45	10000000	8712.097	8712.10	n/a
ββ	45	1.4	-65	45	10000000	7883.318	7883.32	n/a
ββ	45	1.4	-80	45	10000000	3911.507	3911.51	n/a
δδ	45	1.4	-95	45	10000000	1064.238	1064.24	n/a
δδ	-45	1.4	70	45	10000000	0.000	0.00	n/a
δδ	-45	1.4	55	45	10000000	0.001	0.00	n/a
δδ	-45	1.4	40	45	10000000	0.053	0.05	n/a
δδ	-45	1.4	25	45	10000000	1.749	1.75	n/a
δδ	-45	1.4	10	45	10000000	31.926	31.93	n/a
δδ	-45	1.4	-5	45	10000000	319.590	319.59	n/a
AA	0	0.5	55	46	10000000	0.000	0.00	n/a
AA	0	0.5	25	46	10000000	0.201	0.20	n/a
AA	0	0.5	-5	46	10000000	47.040	47.04	n/a
AA	0	0.5	-35	46	10000000	1062.165	1062.17	n/a
AA	0	0.5	-65	46	10000000	2315.120	2315.12	n/a
AA	0	0.5	-95	46	10000000	487.098	487.10	n/a
BB	0	1	55	46	10000000	0.000	0.00	n/a
BB	0	1	25	46	10000000	0.302	0.30	n/a
BB	0	1	-5	46	10000000	56.057	56.06	n/a
BB	0	1	-35	46	10000000	950.060	950.06	n/a
BB	0	1	-65	46	10000000	1480.188	1480.19	n/a
BB	0	1	-95	46	10000000	214.552	214.55	n/a
CC	0	1.5	55	46	10000000	0.001	0.00	n/a
CC	0	1.5	25	46	10000000	1.561	1.56	n/a
CC	0	1.5	-5	46	10000000	285.247	285.25	n/a
CC	0	1.5	-35	46	10000000	4711.491	4711.49	n/a
DD	27	0.5	55	46	10000000	0.000	0.00	n/a
DD	27	0.5	25	46	10000000	0.201	0.20	n/a
DD	27	0.5	-5	46	10000000	47.040	47.04	n/a
DD	27	0.5	-35	46	10000000	1062.165	1062.17	n/a
DD	27	0.5	-65	46	10000000	2315.120	2315.12	n/a
DD	27	0.5	-95	46	10000000	487.098	487.10	n/a
EE	27	1	55	46	10000000	0.000	0.00	n/a
EE	27	1	25	46	10000000	0.302	0.30	n/a
EE	27	1	-5	46	10000000	56.057	56.06	n/a
EE	27	1	-35	46	10000000	950.060	950.06	n/a
EE	27	1	-65	46	10000000	1480.188	1480.19	n/a
FF	27	1	-95	46	10000000	214.552	214.55	n/a
FF	27	1.5	55	46	10000000	0.001	0.00	n/a
FF	27	1.5	25	46	10000000	1.561	1.56	n/a
FF	27	1.5	-5	46	10000000	285.247	285.25	n/a
FF	27	1.5	-35	46	10000000	4711.491	4711.49	n/a
GG	-27	0.5	55	46	10000000	0.000	0.00	n/a
GG	-27	0.5	25	46	10000000	0.201	0.20	n/a
GG	-27	0.5	-5	46	10000000	47.040	47.04	n/a
GG	-27	0.5	-35	46	10000000	1062.165	1062.17	n/a
GG	-27	0.5	-65	46	10000000	2315.120	2315.12	n/a
GG	-27	0.5	-95	46	10000000	487.098	487.10	n/a
HH	-27	1	55	46	10000000	0.000	0.00	n/a
HH	-27	1	25	46	10000000	0.302	0.30	n/a
HH	-27	1	-5	46	10000000	56.057	56.06	n/a
HH	-27	1	-35	46	10000000	950.060	950.06	n/a
HH	-27	1	-65	46	10000000	1480.188	1480.19	n/a
HH	-27	1	-95	46	10000000	214.552	214.55	n/a
II	-27	1.5	55	46	10000000	0.001	0.00	n/a
II	-27	1.5	25	46	10000000	1.561	1.56	n/a

II	-27	1.5	-5	46	10000000	285.247	285.25	n/a
II	-27	1.5	-35	46	10000000	4711.491	4711.49	n/a
II	-27	1.5	-65	46	10000000	7034.074	7034.07	n/a
II	-27	1.5	-95	46	10000000	949.270	949.27	n/a
JJ	53	0.5	55	46	10000000	0.000	0.00	n/a
JJ	53	0.5	25	46	10000000	0.201	0.20	n/a
KK	53	1	55	46	10000000	0.000	0.00	n/a
KK	53	1	25	46	10000000	0.302	0.30	n/a
KK	53	1	-5	46	10000000	56.057	56.06	n/a
KK	53	1	-35	46	10000000	950.060	950.06	n/a
KK	53	1	-65	46	10000000	1480.188	1480.19	n/a
KK	53	1	-95	46	10000000	214.552	214.55	n/a
LL	53	1.5	55	46	10000000	0.001	0.00	n/a
LL	53	1.5	25	46	10000000	1.561	1.56	n/a
LL	53	1.5	-5	46	10000000	285.247	285.25	n/a
LL	53	1.5	-35	46	10000000	4711.491	4711.49	n/a
LL	53	1.5	-65	46	10000000	7034.074	7034.07	n/a
LL	53	1.5	-95	46	10000000	949.270	949.27	n/a
MM	53	2	55	46	10000000	0.000	0.00	n/a
MM	53	2	25	46	10000000	0.030	0.03	n/a
MM	53	2	-5	46	10000000	5.392	5.39	n/a
MM	53	2	-35	46	10000000	89.054	89.05	n/a
MM	53	2	-65	46	10000000	132.938	132.94	n/a
MM	53	2	-95	46	10000000	17.937	17.94	n/a
PP	-19	1.57	55	46	10000000	0.001	0.00	n/a
PP	-19	1.57	25	46	10000000	1.260	1.26	n/a
PP	-19	1.57	-5	46	10000000	230.208	230.21	n/a
PP	-19	1.57	-35	46	10000000	3802.263	3802.26	n/a
PP	-19	1.57	-65	46	10000000	5676.313	5676.31	n/a
PP	-19	1.57	-95	46	10000000	765.960	765.96	n/a
QQ	19	1.57	55	46	10000000	0.001	0.00	n/a
QQ	19	1.57	25	46	10000000	1.260	1.26	n/a
QQ	19	1.57	-5	46	10000000	230.208	230.21	n/a
QQ	19	1.57	-35	46	10000000	3802.263	3802.26	n/a
QQ	19	1.57	-65	46	10000000	5676.313	5676.31	n/a
QQ	19	1.57	-95	46	10000000	765.960	765.96	n/a
NN	-70	1.47	55	46	10000000	0.001	0.00	n/a
NN	-70	1.47	25	46	10000000	1.654	1.65	n/a
NN	-70	1.47	-5	46	10000000	302.246	302.25	n/a
NN	-70	1.47	-35	46	10000000	4992.371	4992.37	n/a
NN	-70	1.47	-65	46	10000000	7453.702	7453.70	n/a
NN	-70	1.47	-95	46	10000000	1005.969	1005.97	n/a
OO	70	1.47	55	46	10000000	0.001	0.00	n/a
OO	70	1.47	25	46	10000000	1.654	1.65	n/a
OO	70	1.47	-5	46	10000000	302.246	302.25	n/a
OO	70	1.47	-35	46	10000000	4992.371	4992.37	n/a
OO	70	1.47	-65	46	10000000	7453.702	7453.70	n/a
OO	70	1.47	-95	46	10000000	1005.969	1005.97	n/a
WW	-53	0.5	55	46	0.00	0.000	0.00	0
WW	-53	0.5	25	46	0.00	0.201	0.00	0
XX	-53	1	55	46	0.00	0.000	0.00	0
XX	-53	1	25	46	0.00	0.302	0.00	0
XX	-53	1	-5	46	209.20	56.057	209.20	2.24755978
XX	-53	1	-35	46	1059.83	950.060	1059.83	1.078852156
XX	-53	1	-65	46	774.00	1480.188	774.00	2.645880522
XX	-53	1	-95	46	756.17	214.552	756.17	2.781316552
YY	-53	1.5	55	46	0.00	0.001	0.00	0
YY	-53	1.5	25	46	1.00	1.561	1.00	0
YY	-53	1.5	-5	46	0.00	285.247	0.00	2.756251553
RR	76	0.8	70	46	10000000	0.000	0.00	n/a
RR	76	0.8	55	46	10000000	0.000	0.00	n/a
RR	76	0.8	40	46	10000000	0.002	0.00	n/a
RR	76	0.8	25	46	10000000	0.085	0.09	n/a
RR	76	0.8	10	46	10000000	1.681	1.68	n/a
RR	76	0.8	-5	46	10000000	18.435	18.43	n/a
RR	76	0.8	-20	46	10000000	112.615	112.61	n/a
RR	76	0.8	-35	46	10000000	383.615	383.62	n/a
RR	76	0.8	-50	46	10000000	729.473	729.47	n/a
RR	76	0.8	-65	46	10000000	775.074	775.07	n/a
RR	76	0.8	-80	46	10000000	460.489	460.49	n/a
RR	76	0.8	-95	46	10000000	153.058	153.06	n/a

SS	0	0.8	70	46	10000000	0.000	0.00	n/a
SS	0	0.8	55	46	10000000	0.000	0.00	n/a
SS	0	0.8	40	46	10000000	0.002	0.00	n/a
SS	0	0.8	25	46	10000000	0.085	0.09	n/a
SS	0	0.8	10	46	10000000	1.681	1.68	n/a
SS	0	0.8	-5	46	10000000	18.435	18.43	n/a
SS	0	0.8	-20	46	10000000	112.615	112.61	n/a
SS	0	0.8	-35	46	10000000	383.615	383.62	n/a
SS	0	0.8	-50	46	10000000	729.473	729.47	n/a
SS	0	0.8	-65	46	10000000	775.074	775.07	n/a
SS	0	0.8	-80	46	10000000	460.489	460.49	n/a
SS	0	0.8	-95	46	10000000	153.058	153.06	n/a
TT	-76	0.8	70	46	10000000	0.000	0.00	n/a
TT	-76	0.8	55	46	10000000	0.000	0.00	n/a
TT	-76	0.8	40	46	10000000	0.002	0.00	n/a
TT	-76	0.8	25	46	10000000	0.085	0.09	n/a
TT	-76	0.8	10	46	10000000	1.681	1.68	n/a
TT	-76	0.8	-5	46	10000000	18.435	18.43	n/a
TT	-76	0.8	-20	46	10000000	112.615	112.61	n/a
TT	-76	0.8	-35	46	10000000	383.615	383.62	n/a
TT	-76	0.8	-50	46	10000000	729.473	729.47	n/a
TT	-76	0.8	-65	46	10000000	775.074	775.07	n/a
TT	-76	0.8	-80	46	10000000	460.489	460.49	n/a
TT	-76	0.8	-95	46	10000000	153.058	153.06	n/a
UU	-45	2.12	70	46	10000000	0.000	0.00	n/a
UU	-45	2.12	55	46	10000000	0.000	0.00	n/a
UU	-45	2.12	40	46	10000000	0.000	0.00	n/a
UU	-45	2.12	25	46	10000000	0.005	0.00	n/a
UU	-45	2.12	10	46	10000000	0.089	0.09	n/a
UU	-45	2.12	-5	46	10000000	0.895	0.89	n/a
UU	-45	2.12	-20	46	10000000	4.912	4.91	n/a
UU	-45	2.12	-35	46	10000000	14.781	14.78	n/a
UU	-45	2.12	-50	46	10000000	24.389	24.39	n/a
UU	-45	2.12	-65	46	10000000	22.065	22.06	n/a
VV	45	2.12	-95	46	10000000	2.977	2.98	n/a
VV	45	2.12	70	46	10000000	0.000	0.00	n/a
VV	45	2.12	55	46	10000000	0.000	0.00	n/a
VV	45	2.12	40	46	10000000	0.000	0.00	n/a
VV	45	2.12	25	46	10000000	0.005	0.00	n/a
VV	45	2.12	10	46	10000000	0.089	0.09	n/a
VV	45	2.12	-5	46	10000000	0.895	0.89	n/a
VV	45	2.12	-20	46	10000000	4.912	4.91	n/a
VV	45	2.12	-35	46	10000000	14.781	14.78	n/a
VV	45	2.12	-50	46	10000000	24.389	24.39	n/a
VV	45	2.12	-65	46	10000000	22.065	22.06	n/a
VV	45	2.12	-80	46	10000000	10.945	10.95	n/a
ββ	45	1.4	70	46	10000000	0.000	0.00	n/a
ββ	45	1.4	55	46	10000000	0.001	0.00	n/a
ββ	45	1.4	40	46	10000000	0.053	0.05	n/a
ββ	45	1.4	25	46	10000000	1.749	1.75	n/a
ββ	45	1.4	10	46	10000000	31.926	31.93	n/a
ββ	45	1.4	-5	46	10000000	319.590	319.59	n/a
ββ	45	1.4	-20	46	10000000	1754.159	1754.16	n/a
ββ	45	1.4	-35	46	10000000	5279.318	5279.32	n/a
ββ	45	1.4	-50	46	10000000	8712.097	8712.10	n/a
ββ	45	1.4	-65	46	10000000	7883.318	7883.32	n/a
ββ	45	1.4	-80	46	10000000	3911.507	3911.51	n/a
δδ	45	1.4	-95	46	10000000	1064.238	1064.24	n/a
δδ	-45	1.4	70	46	10000000	0.000	0.00	n/a
δδ	-45	1.4	55	46	10000000	0.001	0.00	n/a
δδ	-45	1.4	40	46	10000000	0.053	0.05	n/a
δδ	-45	1.4	25	46	10000000	1.749	1.75	n/a
δδ	-45	1.4	10	46	10000000	31.926	31.93	n/a
δδ	-45	1.4	-5	46	10000000	319.590	319.59	n/a
AA	0	0.5	55	77	10000000	0.000	0.00	n/a
AA	0	0.5	25	77	10000000	0.201	0.20	n/a
AA	0	0.5	-5	77	10000000	47.040	47.04	n/a
AA	0	0.5	-35	77	10000000	1062.165	1062.17	n/a
AA	0	0.5	-65	77	10000000	2315.120	2315.12	n/a
AA	0	0.5	-95	77	10000000	487.098	487.10	n/a
BB	0	1	55	77	10000000	0.000	0.00	n/a

BB	0	1	25	77	10000000	0.302	0.30	n/a
BB	0	1	-5	77	10000000	56.057	56.06	n/a
BB	0	1	-35	77	10000000	950.060	950.06	n/a
BB	0	1	-65	77	10000000	1480.188	1480.19	n/a
BB	0	1	-95	77	10000000	214.552	214.55	n/a
CC	0	1.5	55	77	10000000	0.001	0.00	n/a
CC	0	1.5	25	77	10000000	1.561	1.56	n/a
CC	0	1.5	-5	77	10000000	285.247	285.25	n/a
CC	0	1.5	-35	77	10000000	4711.491	4711.49	n/a
DD	27	0.5	55	77	10000000	0.000	0.00	n/a
DD	27	0.5	25	77	10000000	0.201	0.20	n/a
DD	27	0.5	-5	77	10000000	47.040	47.04	n/a
DD	27	0.5	-35	77	10000000	1062.165	1062.17	n/a
DD	27	0.5	-65	77	10000000	2315.120	2315.12	n/a
DD	27	0.5	-95	77	10000000	487.098	487.10	n/a
EE	27	1	55	77	10000000	0.000	0.00	n/a
EE	27	1	25	77	10000000	0.302	0.30	n/a
EE	27	1	-5	77	10000000	56.057	56.06	n/a
EE	27	1	-35	77	10000000	950.060	950.06	n/a
EE	27	1	-65	77	10000000	1480.188	1480.19	n/a
FF	27	1	-95	77	10000000	214.552	214.55	n/a
FF	27	1.5	55	77	10000000	0.001	0.00	n/a
FF	27	1.5	25	77	10000000	1.561	1.56	n/a
FF	27	1.5	-5	77	10000000	285.247	285.25	n/a
FF	27	1.5	-35	77	10000000	4711.491	4711.49	n/a
GG	-27	0.5	55	77	10000000	0.000	0.00	n/a
GG	-27	0.5	25	77	10000000	0.201	0.20	n/a
GG	-27	0.5	-5	77	10000000	47.040	47.04	n/a
GG	-27	0.5	-35	77	10000000	1062.165	1062.17	n/a
GG	-27	0.5	-65	77	10000000	2315.120	2315.12	n/a
GG	-27	0.5	-95	77	10000000	487.098	487.10	n/a
HH	-27	1	55	77	10000000	0.000	0.00	n/a
HH	-27	1	25	77	10000000	0.302	0.30	n/a
HH	-27	1	-5	77	10000000	56.057	56.06	n/a
HH	-27	1	-35	77	10000000	950.060	950.06	n/a
HH	-27	1	-65	77	10000000	1480.188	1480.19	n/a
HH	-27	1	-95	77	10000000	214.552	214.55	n/a
II	-27	1.5	55	77	10000000	0.001	0.00	n/a
II	-27	1.5	25	77	10000000	1.561	1.56	n/a
II	-27	1.5	-5	77	10000000	285.247	285.25	n/a
II	-27	1.5	-35	77	10000000	4711.491	4711.49	n/a
II	-27	1.5	-65	77	10000000	7034.074	7034.07	n/a
II	-27	1.5	-95	77	10000000	949.270	949.27	n/a
JJ	53	0.5	55	77	10000000	0.000	0.00	n/a
JJ	53	0.5	25	77	10000000	0.201	0.20	n/a
KK	53	1	55	77	10000000	0.000	0.00	n/a
KK	53	1	25	77	10000000	0.302	0.30	n/a
KK	53	1	-5	77	10000000	56.057	56.06	n/a
KK	53	1	-35	77	10000000	950.060	950.06	n/a
KK	53	1	-65	77	10000000	1480.188	1480.19	n/a
KK	53	1	-95	77	10000000	214.552	214.55	n/a
LL	53	1.5	55	77	10000000	0.001	0.00	n/a
LL	53	1.5	25	77	10000000	1.561	1.56	n/a
LL	53	1.5	-5	77	10000000	285.247	285.25	n/a
LL	53	1.5	-35	77	10000000	4711.491	4711.49	n/a
LL	53	1.5	-65	77	10000000	7034.074	7034.07	n/a
LL	53	1.5	-95	77	10000000	949.270	949.27	n/a
MM	53	2	55	77	10000000	0.000	0.00	n/a
MM	53	2	25	77	10000000	0.030	0.03	n/a
MM	53	2	-5	77	10000000	5.392	5.39	n/a
MM	53	2	-35	77	10000000	89.054	89.05	n/a
MM	53	2	-65	77	10000000	132.938	132.94	n/a
MM	53	2	-95	77	10000000	17.937	17.94	n/a
PP	-19	1.57	55	77	10000000	0.001	0.00	n/a
PP	-19	1.57	25	77	10000000	1.260	1.26	n/a
PP	-19	1.57	-5	77	10000000	230.208	230.21	n/a
PP	-19	1.57	-35	77	10000000	3802.263	3802.26	n/a
PP	-19	1.57	-65	77	10000000	5676.313	5676.31	n/a
PP	-19	1.57	-95	77	10000000	765.960	765.96	n/a
QQ	19	1.57	55	77	10000000	0.001	0.00	n/a
QQ	19	1.57	25	77	10000000	1.260	1.26	n/a

QQ	19	1.57	-5	77	10000000	230.208	230.21	n/a
QQ	19	1.57	-35	77	10000000	3802.263	3802.26	n/a
QQ	19	1.57	-65	77	10000000	5676.313	5676.31	n/a
QQ	19	1.57	-95	77	10000000	765.960	765.96	n/a
NN	-70	1.47	55	77	10000000	0.001	0.00	n/a
NN	-70	1.47	25	77	10000000	1.654	1.65	n/a
NN	-70	1.47	-5	77	10000000	302.246	302.25	n/a
NN	-70	1.47	-35	77	10000000	4992.371	4992.37	n/a
NN	-70	1.47	-65	77	10000000	7453.702	7453.70	n/a
NN	-70	1.47	-95	77	10000000	1005.969	1005.97	n/a
OO	70	1.47	55	77	10000000	0.001	0.00	n/a
OO	70	1.47	25	77	10000000	1.654	1.65	n/a
OO	70	1.47	-5	77	10000000	302.246	302.25	n/a
OO	70	1.47	-35	77	10000000	4992.371	4992.37	n/a
OO	70	1.47	-65	77	10000000	7453.702	7453.70	n/a
OO	70	1.47	-95	77	10000000	1005.969	1005.97	n/a
WW	-53	0.5	55	77	10000000	0.000	0.00	n/a
WW	-53	0.5	25	77	10000000	0.201	0.20	n/a
XX	-53	1	55	77	10000000	0.000	0.00	n/a
XX	-53	1	25	77	10000000	0.302	0.30	n/a
XX	-53	1	-5	77	10000000	56.057	56.06	n/a
XX	-53	1	-35	77	10000000	950.060	950.06	n/a
XX	-53	1	-65	77	10000000	1480.188	1480.19	n/a
XX	-53	1	-95	77	10000000	214.552	214.55	n/a
YY	-53	1.5	55	77	10000000	0.001	0.00	n/a
YY	-53	1.5	25	77	10000000	1.561	1.56	n/a
YY	-53	1.5	-5	77	10000000	285.247	285.25	n/a
RR	76	0.8	70	77	8.67	0.000	8.67	1.23888204
RR	76	0.8	55	77	3.33	0.000	3.33	0.823894047
RR	76	0.8	40	77	0.33	0.002	0.33	0
RR	76	0.8	25	77	0.00	0.085	0.00	0
RR	76	0.8	10	77	2.00	1.681	2.00	0
RR	76	0.8	-5	77	771.67	18.435	771.67	3.157204547
RR	76	0.8	-20	77	989.83	112.615	989.83	3.144887258
RR	76	0.8	-35	77	1247.67	383.615	1247.67	2.961579834
RR	76	0.8	-50	77	1462.17	729.473	1462.17	2.690105167
RR	76	0.8	-65	77	1600.67	775.074	1600.67	2.758762093
RR	76	0.8	-80	77	1893.17	460.489	1893.17	3.241584178
RR	76	0.8	-95	77	1470.83	153.058	1470.83	3.330155647
SS	0	0.8	70	77	19.33	0.000	19.33	1.587336713
SS	0	0.8	55	77	1.33	0.000	1.33	0.425931997
SS	0	0.8	40	77	20.33	0.002	20.33	1.609084607
SS	0	0.8	25	77	3.67	0.085	3.67	0.834885408
SS	0	0.8	10	77	5.00	1.681	5.00	0.518270626
SS	0	0.8	-5	77	13.33	18.435	13.33	0.21442392
SS	0	0.8	-20	77	1155.17	112.615	1155.17	3.234180794
SS	0	0.8	-35	77	2674.00	383.615	2674.00	3.535463918
SS	0	0.8	-50	77	1359.33	729.473	1359.33	2.579619705
SS	0	0.8	-65	77	3324.17	775.074	3324.17	3.501097637
SS	0	0.8	-80	77	814.50	460.489	814.50	2.293557521
SS	0	0.8	-95	77	3263.75	153.058	3263.75	3.753123387
TT	-76	0.8	70	77	5.00	0.000	5.00	0.999999915
TT	-76	0.8	55	77	2.00	0.000	2.00	0.602035501
TT	-76	0.8	40	77	3.33	0.002	3.33	0.822969435
TT	-76	0.8	25	77	6.33	0.085	6.33	1.085083801
TT	-76	0.8	10	77	1.67	1.681	1.67	0
TT	-76	0.8	-5	77	17.33	18.435	17.33	0
TT	-76	0.8	-20	77	827.50	112.615	827.50	3.036321514
TT	-76	0.8	-35	77	803.50	383.615	803.50	2.472796715
TT	-76	0.8	-50	77	962.33	729.473	962.33	1.806868791
TT	-76	0.8	-65	77	3577.67	775.074	3577.67	3.557386991
TT	-76	0.8	-80	77	1558.00	460.489	1558.00	3.076821534
TT	-76	0.8	-95	77	1503.83	153.058	1503.83	3.342902083
UU	-45	2.12	70	77	0.00	0.000	0.00	0
UU	-45	2.12	55	77	0.00	0.000	0.00	0
UU	-45	2.12	40	77	5.67	0.000	5.67	1.054323842
UU	-45	2.12	25	77	5.33	0.005	5.33	1.026832127
UU	-45	2.12	10	77	27.67	0.089	27.67	1.738774167
UU	-45	2.12	-5	77	4.67	0.895	4.67	0.708910522
UU	-45	2.12	-20	77	5.67	4.912	5.67	0
UU	-45	2.12	-35	77	15.67	14.781	15.67	0

UU	-45	2.12	-50	77	49.33	24.389	49.33	1.2273877
UU	-45	2.12	-65	77	111.33	22.065	111.33	2.077277695
VV	45	2.12	-95	77	5.67	2.977	5.67	0.22369375
VV	45	2.12	70	77	5.00	0.000	5.00	0.999999994
VV	45	2.12	55	77	5.00	0.000	5.00	0.999999369
VV	45	2.12	40	77	0.00	0.000	0.00	0
VV	45	2.12	25	77	1.00	0.005	1.00	0.294643864
VV	45	2.12	10	77	3.67	0.089	3.67	0.833396723
VV	45	2.12	-5	77	5.33	0.895	5.33	0.801114227
VV	45	2.12	-20	77	1449.00	4.912	1449.00	3.457679422
VV	45	2.12	-35	77	1272.50	14.781	1272.50	3.390523987
VV	45	2.12	-50	77	2396.17	24.389	2396.17	3.667263045
VV	45	2.12	-65	77	1894.17	22.065	1894.17	3.563241015
VV	45	2.12	-80	77	1194.00	10.945	1194.00	3.366072155
ββ	45	1.4	70	77	4.67	0.000	4.67	0.970034596
ββ	45	1.4	55	77	3.33	0.001	3.33	0.823570665
ββ	45	1.4	40	77	3.33	0.053	3.33	0.803324388
ββ	45	1.4	25	77	1250.67	1.749	1250.67	3.396349383
ββ	45	1.4	10	77	1156.83	31.926	1156.83	3.32816941
ββ	45	1.4	-5	77	1768.33	319.590	1768.33	3.303298625
ββ	45	1.4	-20	77	3550.40	1754.159	3550.40	3.085109768
ββ	45	1.4	-35	77	2411.67	5279.318	2411.67	3.330100639
ββ	45	1.4	-50	77	3496.20	8712.097	3496.20	3.649032975
ββ	45	1.4	-65	77	6379.33	7883.318	6379.33	2.50131647
ββ	45	1.4	-80	77	2271.17	3911.507	2271.17	2.939721678
δδ	45	1.4	-95	77	0.00	1064.238	0.00	3.328068595
δδ	-45	1.4	70	77	42.67	0.000	42.67	1.931118472
δδ	-45	1.4	55	77	12.67	0.001	12.67	1.403603373
δδ	-45	1.4	40	77	2.00	0.053	2.00	0.56768776
δδ	-45	1.4	25	77	10.00	1.749	10.00	1.064077911
δδ	-45	1.4	10	77	8.00	31.926	8.00	1.457517569
δδ	-45	1.4	-5	77	642.00	319.590	642.00	2.334858138

Reference List

Abdul, A. S. and Gibson, T. L. (1991), Laboratory Studies of Surfactant-Enhanced Washing of Polychlorinated Biphenyl From Sandy Material, *Environmental Science and Technology*, **25**, pp 665-671

Acher, A. J., Boderie, P., and Yaron, B. (1989), Soil Pollution by Petroleum Products I. Multiphase Migratin of Kerosene Components in Soil Components, *Journal Of Contaminant Hydrology*, **4**, pp 333-345

Ahuja, R. K., Kodialam, M., Mishra, A. K., and Orlin, J. B. (1997), Computational Investigations of Maximum Flow Algorithms, *European Journal Of Operational Research*, **97**, pp 509-542

American Public Health Association (1975), Standard Methods for the Examination of Water and Wastewater,

Andreini, M. S. and Steenhuis, T. S. (1990), Preferential Paths of Flow Under Conventional and Conservation Tillage, *Geoderma*, **46**, pp 85-102

Ang, C. C. and Abdul, A. S. (1991), Aqueous Surfactant Washing of Residual Oil Contamination From Sandy Soil, *Ground Water Monitoring Review*, **11**, pp 121-127

Archie, G. E. (1952), Classification of Carbonate Reservoir Rocks and Petrophysical Considerations, *Bulletin of the American Association of Petroleum Geologists*, **36**, pp 278-298

Archie, G. E. (1942), Electrical Resistivity Log as an Aid in Determining Some Reservoir Characteristics, *Petroleum Technology*, 55

Aurelius, M. W. and Brown, K. W. (1987), Fate of Spilled Xylene As Influenced by Soil Moisture Content, *Water Air And Soil Pollution*, 23-31

Baker, R. S. and Hillel, D. (1990), Laboratory Tests of Fingering During Infiltration into Layered Soils, *Soil Science Society Of America Journal*, **54**, pp 20-30

Bartoli, F., Bird, N. R. A., Gomendy, V., Vivier, H., and Niquet, S. (1999), The Relation Between Silty Soil Structures and Their Mercury Porosimetry Curve Counterparts: Fractals and Percolation, *European Journal of Soil Science*, **50**, pp 9-22

Beven, K. and Germann, P. (1982), Macropores and Water Flow in Soil, *Water Resources Research*, **18**, pp 1311-1325

Birks, J. B. (1974), An Introduction to Liquid Scintillation Counting, Boch-Light Laboratories Limited,

Brooks, R. H. and Corey, A. T. (1964), Hydraulic Properties of Porous Media, Civil Engineering Department, Colorado State University, Fort Collins, pp 1-

Bowman, B. T., Brunke, R. R., Reynolds, W. D., and Wall, G. J. (1994), Rainfall Simulator Grid Lysimeter System for Solute Transport Studies Using Large, Intact Soil Blocks, *Journal Of Environmental Quality*, **23**, pp 815-822

Buchter, B., Hinz, C., Flury, M., and Flühler, H. (1995), Heterogeneous Flow and Solute Transport in an Unsaturated Stony Soil Monolith, *Soil Science Society Of America Journal*, **59** , pp 14-21

Butts, M. B. and Jensen, K. H. (1996), Effective Parameters for Multiphase Flow in Layered Soil, *Journal Of Hydrology*, **183**, pp 101-116

Cary, J. W., Mcbride, J. F., and Simmons, C. S. (1989), Observations of Water and Oil Infiltration into Soil - Some Simulation Challenges, *Water Resources Research*, **25**, pp 73-80

Cassel, D. K. and Klute, A. (1986), Water Potential: Tensiometry, Methods of Soil Analysis: Part One, American Society of Agronomy & Soil Science Society of America, Madison, pp 563-596

Celia, M. A., Reeves, P. C., and Ferrand, L. A. (1995), Recent Advances in Pore Scale Models for Multiphase Flow in Porous- Media, *Reviews of Geophysics*, **33**, pp 1049-1057

Cheston, A. Bioremediation of Joint Bays. 1997. Cranfield University, Institute of Bioscience and Technology.

Chevalier, L. R. and Peterson, J. (1999), Literature Review of 2D Laboratory Experiments in NAPL Flow, Transport and Remediation, *Journal of Soil Contamination*, **8**, pp 149-167

Chow, V. T. and Harbaugh, T. E. (1965), Raindrop Production for Laboratory Watershed Experiments, *Journal of Geophysical Research*, **70**, pp 6111-6119

Chu, S. T. (1994), Capillary-Tube Infiltration-Model With Brooks-Corey Parameters, *Transactions of the American Society of Agricultural Engineering*, **37**, pp 1205-1208

Cousin, I., Levitz, P., and Bruand, A. (1996), Three-Dimensional Analysis of a Loamy-Clay Soil Using Pore and Solid Chord Distributions, *European Journal of Soil Science*, **47**, pp 439-452

Davis, J. L. and Annan, A. P. (1977), Electromagnetic Detection of Soil Moisture: Progress Report I., *Canadian Journal of Remote Sensing*, **3**, pp 76-86

Davis, J. L. and Chudobiak, W. J. (1975), In-Situ Meter for Measuring Relative Permittivity of Soils., *Geological Survey of Canada*, **75-1**, pp 75-79

Dawe, R. A., Wheat, M. R., and Binder M.S. (1992), Experimental Investigation of Capillary Pressure Effects on Immiscible Displacements in Lensed and Layered Porous Media., *Transport in Porous Media*, **7**, pp 83-101

Dekker, L. W. and Ritsema, C. J. (1994), How Water Moves in a Water Repellent Sandy Soil 1. Potential and Actual Water Repellency, *Water Resources Research*, **30**, pp 2507-2517

Dexter, A. R. (1995), Heterogeneity of Unsaturated, Gravitational Flow of Water Through Beds of Large Particles, *Water Resources Research*, **29**, pp 1859-1862

Dowd, J. F. and Williams, A. G. (1989), Calibration and Use of Pressure Transducers in Soil Hydrology, *Hydrological Processes*, **3**, pp 43-49

Dullien, F.A.L. (1998), Capillary Effects and Multiphase Flow in Porous Media, *Journal of Porous Media*, **1**, pp 1-29.

Dullien, F.A.L. (1992), Porous Media : Fluid Transport and Pore Structure, Academic Press, New York.

Faust, C. R. (1985), Transport of Immiscible Fluids Within and Below the Unsaturated Zone :A Numerical Model, *Water Resources Research*, **21**, pp 587-596

Faust, C. R., Guswa, J. H., and Mercer, J. W. (1989), Simulation of Three Dimensional Immiscible Fluids Within and Below the Unsaturated Zone, *Water Resources Research*, **25**, pp 2449-2464

Ferrand, L. A., Milly, P. C. D., and Pinder, G. F. (1986), Dual-Gamma Attenuation for the Determination of Porous Medium Saturation With Respect to Three Fluids, *Water Resources Research*, **22**, pp 1657-1663

Flury, M., Flühler, H., Jury, W. A., and Leuenberger, J. (1994), Susceptibility of Soils to Preferential Flow of Water: A Field Study, *Water Resources Research*, **30**, pp 1945-1954

Fu, M., Chen G., Davies, D. K., Sutton, S. J., and Patel, D. (2000), Use of Fluorometry in the Determination of DDB Contamination in Soils From Underground Oil-Filled Power Cable Leaks.

Gane, P. A. C., Kettle, J. P., Matthews, G. P., and Ridgway, C. J. (1995), Void Space Structure of Compressible Polymer Spheres and Consolidated Calcium Carbonate Paper-Coating Formulations, *Industrial and Engineering Chemistry Research*, **35**, pp 1753-1764

Garboczi, E. J. (1990), Permeability, Diffusivity and Microstructural Parameters: A Critical Review, *Cement and Concrete Research*, **20**, pp 591-601

Gardner, C. M. K., Bell, J. P., Cooper, J. D., Dean, T. J., and Hodnett, M. G. (1991), Soil Water Content, *Soil Analysis: Pysical Methods*, Marcel Decker, New York, pp 1-73

Ghodrati, M. and Jury, W. A. (1990), A Field Study Using Dyes to Characterise Preferential Flow of Water, *Soil Science Society Of America Journal*, **54**, pp 1558-1563

Gledhill, W. E., Saeger, V. W., and Trehy, M. L. (1991), An Aquatic Environmental Safety Assessment of Linear Alkyl Benzene, *Environmental Toxicology and Chemistry*, **10**, pp 169-178

Guigard, S., Stiver, W. H., and Zytner, R. G. (1996), The Infiltration and Movement of Immiscible Chemicals in Unsaturated Soil, *Environmental Technology*, **17**, pp 1123-1130

Haines, W. B. (1927), Studies in the Physical Properties of Soils. IV. A Further Contribution to the Theory of Capillary Phenomena in Soil, *Journal of Agricultural Science*, **17**, pp 264-290

Harwell, J. H. (1991), Factors Affecting Surfactant Performance in Groundwater Remediation Applications, *Preceedings of Symposium on Transport and Remediation of Subsurface Contaminants*, 124-132

Hatfield, K., Ziegler, J., and Burris, D. R. (1993), Transport in Porous-Media Containing Residual Hydrocarbon .2. Experiments, *Journal Of Environmental Engineering-Asce*, **119**, pp 559-575

Hendrickx, J. M. H., Dekker, L. W., and Boersma, O. H. (1993), Unstable Wetting Fronts in Water Repellent Field Soils, *Journal Of Environmental Quality*, **22**, pp 109-118

Hignett, C. T., Gusli, S., Cass, A., and Besz, W. (1995), An Automated Laboratory Rainfall Simulation System With Controlled Rainfall Intensity, Raindrop Energy and Soil Drainage, *Soil Technology*, **8**, pp 31-42

Hilfer, R. (1998), Macroscopic Equations of Motion for Two-Phase Flow in Porous Media, *Physical Review E*, **58**, pp 2090-2096.

Holden, N. M., Dowd, J. F., Williams, A. G., and Scholefield, D. (1995), Computer Control for Investigating Water and Chemical Transport in a Large Isolated Soil Block, *Computers and Electronics in Agriculture*, **12**, pp 225-236

Host-Madsen, J. and Hogh Jensen, K. (1992), Laboratory and Numerical Investigations of Immiscible Multiphase Flow in Soil, *Journal Of Hydrology*, **135**, pp 13-52

Illangasekare, T. H., Armbruster, E. J., and Yates, D. N. (1995a), Non-Aqueous-Phase Fluids in Heterogeneous Aquifers-Experimental Study, *ASCE, Journal of Environmental Engineering Division*, **121**, pp 571-579

Illangasekare, T. H., Armbruster, E. J., and Yates, D. N. (1995b), Non-Aqueous-Phase Fluids in Heterogeneous Aquifers - Experimental Study, *Journal Of Environmental Engineering-Asce*, **121**, pp 571-579

Joseph, A. T., Grenney, W. T., and Stevens, D. K. (1994), Oil Migration Through Unsaturated Soils and Its Effect on the Vadose Zone Interactive Processes (VIP) Model Output, *Water Science and Technology*, **30**, pp 39-51

Keuper, B. H., Abbott, W., and Farquhar, G. R. (1989), Experimental Observations of Multiphase Flow in Heterogeneous Porous Media, *Journal Of Contaminant Hydrology*, **5**, pp 83-95

Klute, A. (1986), Water Retention: Laboratory Methods, Methods of Soil Analysis: Part One, American Society of Agronomy & Soil Science Society of America, Madison, pp 635-662

Kosugi, K. (1994), Three-Parameter Lognormal Distribution Model for Soil-Water Retention, *Water Resources Research*, **30**, pp 891-901

Kung, K.-J. S. (1990a), Preferential Flow in a Sandy Vadose Zone: 2. Mechanism and Implications, *Geoderma*, **46**, pp 59-71

Kung, K.-J. S. (1990b), Preferential Flow in a Sandy Vadose; 1. Field Observation, *Geoderma*, **46**, pp 51-58

Ledieu, J., de Ridder, P., de Clerk, P., and Dautrebande, S. (1986), A Method of Measuring Soil Moisture by TDR, *Journal Of Hydrology*, **88**, pp 319-328

Lenormand, R., Touboul, E., and Zarcone, C. (1988), Numerical Models and Experiments on Immiscible Displacements in Porous Media, *Journal of Fluid Mechanics*, **189**, pp 165-187

Letniowski, F. W. Numerical methods for NAPL groundwater contamination in three dimensions. 1-98. 1989. Master of Math. Thesis, University of Waterloo, Waterloo, Ont.

Leverett, M. C. (1941), Capillary Behaviour in Porous Solids, *Transaction of the American Institute of Mining and Metallogy Engineering*, **142**, pp 152-169

Lowry, M. I. and Miller, C. T. (1995), Pore-Scale Modelling of Nonwetting-Phase Residual in Porous-Media, *Water Resources Research*, **31**, pp 455-473

Mason, G. and Morrow, N. R. (1994), Effect of Contact Angle on Capillary Displacement Curvatures in Pore Throats Formed by Spheres, *Journal of Colloid and Interface Science*, **168**, pp 130-141

Mathews, T. J. and Matthews, G. P. (1999), Discriminatory Water and Tracer Flow in Homogeneous Repacked Sand, *Water Resources Research*, **submitted**, pp

Matthews, G. P., Moss, A. K., and Ridgway, C. J. (1995), The Effects of Correlated Networks on Mercury Intrusion Simulations and Permeabilities of Sandstone and Other Porous Media, *Powder Technology*, **83**, pp 61-77

Matthews, G. P., Moss, A. K., Spearing, M. C., and Voland, F. (1993), Network Calculation of Mercury Intrusion and Absolute Permeability in Sandstone and Other Porous Media, *Powder Technology*, **76**, pp 95-107

Matthews, G. P., Ridgway, C. J., and Spearing, M. C. (1995), Void Space Modeling of Mercury Intrusion Hysteresis in Sandstone, Paper Coating, and Other Porous Media, *Journal of Colloid and Interface Science*, **171**, pp 8-27

Mercer, J. W. and Cohen, R. M. (1990), A Review of Immiscible Fluids in the Subsurface: Properties, Models, Characterisation and Remediation, *Journal Of Contaminant Hydrology*, **6**, pp 107-163

Miyazaki, T. (1993), Water Flow In Soils, Marcel Dekker,

Moscou, L. and Lub, S. (1981), Practical Use of Mercury Porosimetry in the Study of Porous Solids, *Powder Technology*, **29**, pp 45-52

Mualem, Y. and Friedman, S. P. (1991), Theoretical Prediction of Electrical Conductivity in Saturated and Unsaturated Soil, *Water Resources Research*, **27**, pp 2771-2777

Nichols, J. A. The Environmental Impact of Cable Oils. 1996. Cranfield University, Institute of Bioscience and Technology.

Osborne, M. and Sykes, J. (1986), Numerical Modelling of Immiscible Organic Transport at the Hyde Park Landfill, *Water Resources Research*, **22**, pp 25-33

Pantazidou, M. and Sitar, N. (1993), Emplacement of Nonaqueous Liquids in the Vadose Zone, *Water Resources Research*, **29**, pp 705-722

Parker, J.C., Katyal, A.K., Kaluarachchi, J.J., Lenhard, R.J., Johnson, T.J., Jayaraman, K., Unlu, K., and Zhu, J.L. (1991), Modelling multiphase organic chemical transport in soils and groundwater,

Parker, J. C., Lenhard, R. J., and Kuppusamy, T. (1987), A Parametric Model for Constitutive Properties Governing Multiphase Flow in Porous Media, *Water Resources Research*, **23**, pp 618-624

Peat, D. M. W., Matthews, G. P., Worsfold, P. J., and Jarvis, S. C. (2000), Simulation of Water Retention and Hydraulic Conductivity in Soil Using a Three-Dimensional Network, *European Journal of Soil Science*, **51**, pp in press-

Pennell, K. D., Pope, G. A., and Abriola, L. M. (1996), Influence of Viscous and Buoyancy Forces on the Mobilization of Residual Tetrachloroethylene During Surfactant Flushing, *Environmental Science & Technology*, **30**, pp 1328-1335

Perrier, E., Mullon, C., Rieu, M., and de Marsily, G. (1995), Computer Construction of Fractal Soil Structures - Simulation of Their Hydraulic and Shrinkage Properties, *Water Resources Research*, **31**, pp 2927-2943

Phillips, R. E., Quisenberry, V. L., and Zeleznik, J. M. (1995), Water and Solute Movement in an Undisturbed, Macroporous Column - Extraction Pressure Effects, *Soil Science Society Of America Journal*, **59**, pp 707-712

Pinder, G. F. and Abriola, L. M. (1986), On the Simulation of Non Aqueous Phase Organic Compounds, *Water Resources Research*, **22**, pp 109-119

Porter, K. E. (1968a), Liquid Flow in Packed Columns 1. The Rivulet Model, *Transactions of Institution of Chemical Engineers*, **46**, pp 69-73

Porter, K. E., Barnet, V. D., and Templeman, J. J. (1968b), Liquid Flow in Packed Columns 2. The Spread of Liquid Over Random Packings, *Transactions of Institution of Chemical Engineers*, **46**, pp 74-85

Porter, K. E. (1989), An Overview of Formation Damage, *Journal of Petroleum Technology*, 780-786

Poulsen, M. M. and Keuper, B. H. (1992), A Field Experiment to Study the Behaviour of Tetrachloroethylene in Unsaturated Porous Media, *Environmental Science and Technology*, **26**, pp 889-895

Priddle, M. W. and Macquarrie, K. B. (1994), Dissolution of Creosote in Groundwater - an Experimental and Modelling Investigation, *Journal Of Contaminant Hydrology*, **15**, pp 27-56

Raats, P. A. C. (1973), Unstable Wetting Fronts in Uniform and Nonuniform Soils, *Soil Science Society Of America Journal*, **37**, pp 681-685

Rajaram, H., Ferrand, L. A., and Celia, M. A. (1997), Prediction of Relative Permeabilities for Unconsolidated Soils Using Pore-Scale Network Models, *Water Resources Research*, **33**, pp 43-52

Reible, D. D., Illangasekare, T. H., Doshi, D. V., and Malhiet, M. E. (1990), Infiltration of Immiscible Contaminants in the Unsaturated Zone., *Ground Water*, **28**, pp 685-692

Renshaw, C. E., Zynda, G. D., and Fountain, J. C. (1997), Permeability Reductions Induced by Sorption of Surfactant, *Water Resources Research*, **33**, pp 371-378

Ridley, A. M. and Brady, K. C. (1997), The Development of an Improved Tensiometer for the Measurement of Soil Suction, Transport Research Laboratory,

Ritsema, C. J. and Dekker, L. W. (1994), How Water Moves in a Water Repellent Sandy Soil 2. Dynamics of Fingered Flow, *Water Resources Research*, **30**, pp 2519-2531

Romkens, M. J. M., Glenn, L. F., Nelson, D. W., and Roth, C. B. (1975), A Laboratory Rainfall Simulator for Infiltration and Soil Detachment Studies., *Soil Science Society of America Proceedings*, **39**, pp 158-160

Roth, K., Schulin, R., Fluhler, H., and Attinger, W. (1990), Calibrationof Time Domain Reflectometry for Water Content Measurement Using a Composite Dielectric Approach, *Water Resources Research*, **26**, pp 2267-2273

Schiegg, H. O. (1979), Verdrabgungs-Simulation Dreier Nicht Mischbarer Fluide in Poroser Matrix. Mitt. Versuchanst., *Wasserbau Hydrol.Glaziol.*, **40**,

Schiegg, H.O. (1990), Laboratory setup and results of experiments on two dimensional multiphase flow in porous media, US Department of Energy, Report DE-AC06-76RLO1830, pp 1-423

Schlicting, H. (1979), Boundary layer theory, McGraw-Hill, New York

Schroth, M., Istok, J. D., Ahearn, S. J., and Selker, J. S. (1995), Geometry and Position of Light Nonaqueous-Phase Liquid Lenses in Water-Wetted Porous-Media, *Journal Of Contaminant Hydrology*, **19**, pp 269-287

Schwille, F. (1967), Petroleum Contamination of the Subsoil - A Hydrological Problem, the Migration of Hydrocarbons in a Water Bearing Stratum, The Joint Problems of the Oil and Water Industries, American Elsevier, New York, pp 23-54

Schwille, F. (1988), Dense Chlorinated Solvents in Porous and Fractured Media: Model Experiments,

Simmons, C. S., McBride, J. F., Cary, J. W., and Lenhard, R. J. (1992), Organic Liquid Infiltration into Unsaturated Porous Media, Subsurface Contamination by Immiscible Fluids, Balkema, Rotterdam, pp 213-219

Smith, K. A. and Mullins, C. E. Soil Analysis: Physical Methods. 45-55. 1991. New York, Marcel Dekker Inc.

Stannard, D. I. (1992), Tensiometers - Theory, Construction and Use, *Geotechnical Testing Journal*, **15**, pp 48-58

Swisher, R. D., Kaeble, E. F., and Liu, S. K. (1961), Capillary Gas Chromatography of Phenyl Dodecane Alkylation and Isomeration Mixtures, *Journal of Organic Chemistry*, **26**, pp 4066-

Templeton, C. (1954), A Study of Displacements in Microscopic Capillaries, *Petroleum Transactions AIME*, **201**, pp 162-168

Thomson, N. R., Graham, D. N., and Farquhar, G. R. (1992), One Dimensional Immiscible Displacement Experiments, *Journal Of Contaminant Hydrology*, **10**, pp 197-223

Thompson, A.H., Katz, A.J., and Raschke, R.A. (1987), Estimation of Absolute Permeability From Capillary Pressure Measurements, 62nd Annual Technical Conference and Exhibition of the Society of Petroleum Engineers, pp 475-481

Topp, G. C. and Davis, J. L. (1985), Measurement of Soil-Water Content Using Time-Domain Reflectrometry (TDR) - A Field-Evaluation, *Soil Science Society Of America Journal*, **49**, pp 19-24

Topp, G. C., Davis, J. L., and Annan, A. P. (1980), Electromagnetic Determination of Soil Water Content: Measurements in Coaxial Transmission Lines, *Water Resources Research*, **16**, pp 574-582

Tsakiroglou, C. D. and Payatakes, A. C. (1991), Effects of Pore-Size Correlations on Mercury Porosimetry Curves, *Journal of Colloid and Interface Science*, **146**, pp 479-494

Tsakiroglou, C. D. and Payatakes, A. C. (1993), Pore-Wall Roughness As a Fractal Surface and Theoretical Simulation of Mercury Intrusion Retraction in Porous-Media, *Journal of Colloid and Interface Science*, **159**, pp 287-301

Tyler, S. W. and Wheatcraft, S. W. (1990), Fractal Processes in Soil-Water Retention, *Water Resources Research*, **26**, pp 1047-1054

van Geel, P. L. and Sykes, J. F. (1994), Laboratory and Model Simulations of a LNAPL Spill in a Variably Saturated Sand. I. Laboratory Experiments and Image Analysis Techniques., *Journal Of Contaminant Hydrology*, **17**, pp 1-25

van Geel, P. L. and Sykes, J. F. (1997), The Importance of Fluid Entrapment, Saturation Hysteresis and Residual Saturation on the Distributions of a Lighter-Than-Water Non-Aqueous Phase Liquid in a Variably Saturated Sand Medium., *Journal Of Contaminant Hydrology*, **25**, pp 249-270

van Genuchten, M. Th. (1980), A Closed Form Equation for Predicting the Hydraulic Conductivity of Unsaturated Soils, *Soil Science Society Of America Journal*, **44**, pp 892-898

Whalley, W. R. (1993), Considerations on the Use of Time-Domain Reflectometry (TDR) for Measuring Soil Water Content, *Journal of Soil Science*, **44**, pp 1-9

Zalidis, G. C., Annable, M. D., Wallace, R. B., Hayden, N. J., and Voice, T. C. (1991), A Laboratory Method for Studying the Aqueous Phase Transport of Dissolved Constituents From Residually Held NAPL in Unsaturated Soil Columns, *Journal Of Contaminant Hydrology*, **8**, pp 143-156

Zegelin, S. J., White, I., and Jenkins, D. R. (1989), Improved Field Probes for Soil Water Content and Electrical Conductivity Measurement Using Time-Domain Reflectometry, *Water Resources Research*, **25**, pp 2367-2376

Zhou, D. and Blunt, M. (1997), Effect of Spreading Coefficient on the Distribution of Light Non-Aqueous Phase Liquid in the Subsurface, *Journal Of Contaminant Hydrology*, **25**, pp 1-19